Rheinland-Pfälzische Technische Universität Kaiserslautern Landau

Investigation of membrane proteins involved in c-di-GMP signalling in *P. aeruginosa* with focus on the phosphodiesterase NbdA

vom Fachbereich Biologie

der Rheinland-Pfälzischen Technischen Universität Kaiserslautern-Landau

zur Verleihung des akademischen Grades Dr. rer. nat. genehmigte

Dissertation

von

Anna Scherhag, M.Sc., geb. in Koblenz

Mündliche Prüfung: 17.05.2024

Dekan:	Prof. Dr. Stefan Kins
Promotionskommissionsvorsitzender:	Prof. Dr. Stefan Kins
Berichterstattende:	PD Dr. Susanne Zehner
	Prof. Dr. Matthias Hahn

D 386

Table of contents

Danksagung

An dieser Stelle möchte ich mich bei PD Dr. Susanne Zehner für ihre ausgezeichnete Betreuung bedanken. Ich danke ihr für ihren Einsatz, hilfreiche Anregungen, konstruktive Kritik, und dass sie sich stets Zeit für meine Fragen und Probleme genommen hat. Weiterhin möchte ich mich bei Prof. Dr. Frankenberg-Dinkel für die Möglichkeit, unter ihrer Aufsicht diese Arbeit zu verfassen und die zahlreichen Ratschläge bedanken. Herrn Prof. Dr. Matthias Hahn danke ich für die Übernahme der Zweitkorrektur. Ich danke Prof. Dr. Stefan Kins für die Übernahme des Vorsitz der Prüfungskommission.

Weiterhin möchte ich mich bei Dr. Markus Räschle für die Beratung und die fachliche Unterstützung im Umgang mit massenspektrometrischen Daten bedanken.

Außerdem danke ich Prof. Dr. Elke Richling, Dr. Simone Stegmüller und Hanna Becker für die Zusammenarbeit zur Identifizierung und Quantifizierung von Nukleotiden. Jürgen Seehase möchte ich für die AFM Bilder sowie die ausführlichen Erklärungen zur Messmethode danken.

Maya Shasha Bruderer und Urs Jenal von der Universität Basel danke ich für die freundliche Bereitstellung des Phagen DMS3*vir*. Außerdem danke ich Matthias Koch von der Texas A&M University für die Bereitstellung einiger Plasmide.

Ich möchte mich außerdem bei Dr. Eugenio Pérez Patallo und David Glück für die Unterstützung im Umgang mit Polymeren bedanken. Michael Tope Agbadola danke ich für die Unterstützung beim Durchführen der SEC. Außerdem danke ich Prof. Dr. Mühlhaus und Dr. Bennedict Venn für die Zusammenarbeit und Beratung zur Auswertung der Proteom Daten. Ich danke Miriam Haak für die Unterstützung beim Klonieren einiger Konstrukte.

Weiterhin danke ich der Deutschen Forschungsgemeinschaft (DFG) für die finanzielle Förderung dieser Arbeit innerhalb des SPP 1879. Der Forschungsinitiative (FI) des Landes Rheinland-Pfalz danke ich ebenfalls für finanzielle Förderung innerhalb des BioComp Projektes.

Ich danke der gesamten Abteilung Mikrobiologie für die angenehme Arbeitsatmosphäre, die ständige Hilfsbereitschaft und die nette Aufnahme in das Team. Danke besonders Christina, Nora, Federica, Thomas und Lo, für viele lustige Stunden im Labor, in der Hühnerleiter, aber auch viel Spaß außerhalb der Arbeit. Ich bedanke mich auch bei dem ehemaligen Mitarbeitern der Abteilung Mikrobiolgie für viele hilfreiche Tipps und das freundliche Klima. Besonders möchte ich dabei meinen fachlichen Vorgängerinnen Martina Rüger und Katrin Gerbracht danken. Außerdem möchte ich mich bei all denjenigen bedanken, die mich während des Studiums begleitet und motiviert haben. Ein besonderer Dank gilt meinen Eltern, die mich immer unterstützt und mir dieses Studium ermöglicht haben, meiner Familie und meinen Freunden.

Publikation

Scherhag, A., Räschle, M., Unbehend, N., Venn, B., Glück, D., Mühlhaus, T., Keller, S., Pérez Patallo, E., Zehner, S., Frankenberg-Dinkel, N. (2023) „Characterization of a soluble library of the *Pseudomonas aeruginosa* PAO1 membrane proteome with emphasis on c-di-GMP turnover enzymes" *microlife*, Volume 4, uqad028. DOI: https://doi.org/10.1093/femsml/uqad028.

Abstract
Studies of protein–protein interactions in membranes are very important to fully understand the biological function of a cell. The extraction of proteins from the native membrane environment is a critical step in the preparation of membrane proteins that might affect the stability of protein complexes. In this work, we used the amphiphilic diisobutylene/maleic acid copolymer to extract the membrane proteome of the opportunistic pathogen *Pseudomonas aeruginosa*, thereby creating a soluble membrane-protein library within a native-like lipid-bilayer environment. Size fractionation of nanodisc-embedded proteins and subsequent mass spectrometry enabled the identification of 3358 proteins. The native membrane-protein library showed a very good overall coverage compared to previous proteome data. The pattern of size fractionation indicated that protein complexes were preserved in the library. More than 20 previously described complexes, e.g. the SecYEG and Pili complexes, were identified and analyzed for coelution. Although the mass-spectrometric dataset alone did not reveal new protein complexes, combining pulldown assays with mass spectrometry was successful in identifying new protein interactions in the native membrane-protein library. Thus, we identified several candidate proteins for interactions with the membrane phosphodiesterase NbdA, a member of the c-di-GMP network. We confirmed the candidate proteins CzcR, PA4200, SadC, and PilB as novel interaction partners of NbdA using the bacterial adenylate cyclase two-hybrid assay. Taken together, this work demonstrates the usefulness of the native membrane-protein library of *P. aeruginosa* for the investigation of protein interactions and membrane-protein complexes. Data are available via ProteomeXchange with identifiers PXD039702 and PXD039700.

Die folgenden Abschnitte dieser Arbeit entahlten Daten, Beschreibungen und Auswertungen, die im Rahmen von Scherhag *et al.*, 2023 bereits veröffentlicht wurden:

1 Introduction: 1.1, 1.1.1, 1.1.2, 1.1.3, 1.2.2, 1.2.3, 1.3.1, 1.3.2, 1.3.3, 1.4.1, 1.5
2 Material and Methods: 2.3.1, 2.3.7, 2.4.1, 2.4.2, 2.4.3, 2.4.4, 2.4.6, 2.4.8, 2.4.12, 2.4.13, 2.4.14, 2.4.15, 2.4.16, 2.7.3, 2.7.4
3 Results: 3.1, 3.1.2, 3.1.3, 3.1.4, 3.1.5, 3.1.6, 3.1.7, 3.2, 3.2.1, 3.2.2
4 Discussion: 4.1, 4.1.1, 4.1.2, 4.1.3, 4.1.4, 4.2.5
5 Sumary
Appendix

Beiträge zur Publikation

Scherhag, A., Räschle, M., Unbehend, N., Venn, B., Glück, D., Mühlhaus, T., Keller, S., Pérez Patallo, E., Zehner, S., Frankenberg-Dinkel, N. (2023) „Characterization of a soluble library of the *Pseudomonas aeruginosa* PAO1 membrane proteome with emphasis on c-di-GMP turnover enzymes" *microlife*, Volume 4, uqad028. DOI: https://doi.org/10.1093/femsml/uqad028.

Scherhag, A.: Planung der Versuche, Probenvorbereitung der Complexom und NbdA-Pull-down Proben, Durchführung der BACTH Interaktionstests mit Ausnahme der Interaktion von NbdA und PilB und der Positivkontrolle, Auswertung, Interpretation und Darstellung der Daten, Anfertigung der Abbildungen und Tabellen, Schreiben des Manuskripts (Draft)

Räschle M.: Beratung zum Versuchsaufbau, Bereitstellung von Protokollen und Material zur Probenvorbereitung für die Massenspektroskopie (MS), Messung der Proben mittels MS, Auswertung der MS Daten in MaxQuant und Perseus (Protein Identifizierung, IBAQ-Werte, Berechnung von FC und *p*-value (Pulldown), Darstellung der Ergebnisse des Pulldown in einem Volcano plot)

Unbehend N.: Bachelorstudent unter Anweisungen von A. Scherhag. Klonierung von pUT18-pilB, Durchführung des BACTH Tests für die Interaktion von NbdA mit PilB, inklusive Negativkontrollen und Positivkontrolle mit Leucine zipper

Venn, B: Unterstützung bei der Auswertung der Daten des Complexoms, Interpretation der Ergebnisse insbesondere nach Clusteranalyse und Correlationsanalyse

Glück, D.: Unterstützung bei Konzeption und Planung des Complexoms Versuchs

Mühlhaus, T: Unterstützung bei der Auswertung der Daten des Complexoms

Keller, S.: Unterstützung bei Konzeption und Planung des Complexoms Versuchs, Bereitstellung der Polymere

Perez-Patallo E.: Unterstützung bei SEC, Expertise im Umgang mit Polymeren

Zehner, S.: Betreuung der Doktorarbeit, Unterstützung bei Planung der Versuche, Auswertung und Interpretation der Daten, Konzeption und Planung des Manuskripts, Überarbeitung des Manuskripts

Frankenberg-Dinkel, N.: Unterstützung bei Planung der Versuche und Auswertung, Überarbeitung des Manuskripts

Abbreviations

2‘3’c-di-GMP	(2‘,5‘)-(3‘,5‘)-cyclic diguanosine monophosphate
3D	three dimensional
aa	amino acids
ABC	ammonium bicarbonate
ACC	average correlation coefficient
AFM	atomic force microscopy
Amp	ampicillin
APS	ammonium persulfate
AU	absorption units
B2H	bacterial adenylate cyclase two hybrid
BCIP	5-bromo-4-chloro-3-indolyl phosphate
BIFC	bimolecular fluorescence complementation
BLUF	sensors of blue light using FAD
BSA	bovine serum albumin
Cache	calcium channels and chemotaxis receptor
cAMP	cyclic adenosine monophosphate
CAP	catabolite activator protein
c-di-GMP	bis-(3‘,5’)-cyclic diguanosine monophosphate
cf.	*conferatur*, latin for confer, compare to
Chase	cyclases/histidine kinases associated sensing extracellular
cGAMP	(3‘,5’)-cyclic guanosine monophosphate-adenosine monophosphate
cGMP	cyclic guanosine monophosphate
CLSM	confocal laser scanning microscopy
COG	clusters of ortholog groups
co-IP	co-immunoprecipitation
Da	dalton
DDM	dodecyl ß-D-maltoside
DGC	diguanylate cyclase
DIBMA	diisobutylene/maleic acid
DMSO	dimethyl sulfoxide
DNA	desoxyribonucleic acid
dNTP	dephosphorylated nucleotide triphosphate
EDTA	ethylene diamine tetraacetic acid
Em_{λ}	emission at λ (nm)
EPS	extracellular polymeric substances
Ex_{λ}	excitation at λ (nm)
FAD	flavin adenine dinucleotide
FDR	false discovery rate
FRET	Förster resonance energy transfer
FU	fluorescence units
GAPES	gamma-proteobacterial periplasmic sensory
gDNA	genomic DNA
Gm	gentamycin
GMP	guanosine monophosphate
GTP	guanosine triphosphate

HCl	hydrochloric acid
IBAQ	intensity based absolute quantification
IPTG	isopropyl β-D-thiogalactopyranoside
Kan	kanamycin
kb	kilobases
kDa	kilodalton
LFQ	label free quantification
LLOQ	lower limit of quantification
LOD	limit of detection
LOQ	limit of quantification
m/z	mass to charge ratio
MASE	membrane-associated sensor
MOI	multiplicity of infection, ratio of agent to infection targets
MS	mass spectrometry
MSP	membrane scaffold protein
MW	molecular weight
MWCO	molecular weigth cut off
NBT	nitro blue tetrazolium chloride
NMR	nuclear magnetic resonance
NO	nitric oxide
OD	optical density
ORF	open reading frame
PAS	Per-Arnt-Sim
PBS	phosphate buffered saline
PCR	polymerase chain reaction
PDE	phosphodiesterase
PFU	plaque forming units
ppGpp	guanosine tetraphosphate
pGpG	5'-phosphoguanylyl-3',5'-guanosine
pI	isoelectric point
PIA	Pseudomonas isolation agar
PVDF	polyvinyliden fluoride
RNA	ribonucleic acid
rpm	rotations per minute
RT	room temperature
SDS	sodium dodecyl sulfate
PAGE	polyacrylamide gel electrophoresis
SEC	size exclusion chromatography
SMA	styrene maleic acid
STING	stimulator of interferon genes
Str	streptomycin
T2SS	type II secretion system
T4P	type IV pili
T6SS	typeVI secretion system
TAE	Tris - acetic acid - EDTA
TBS	Tris buffered saline
TEM	transmission electron microscopy
TEMED	tetramethylethylenediamine
Tet	teracycline

TM	transmembrane
Tris	tris(hydroxymethyl)aminomethane
ULOQ	upper limit of quantification
v/v	volume per volume
w/v	weight per volume
x g	times gravitational acceleration or g force (9.81 m/s^2)
ε	extinction coefficient
λ	wavelength (nm)

1 Introduction

1.1 Membranes and membrane proteins

The presence of membranes is a prerequisite for life. Bacterial membranes provide a diffusion barrier to the environment while still being able to perceive the surroundings. To carry out these functions, bacterial cell membranes are dynamic, fluid lipid bilayers that consist of a heterogeneous matrix of lipids and lipid-soluble proteins. The membrane proteins integrated into the two-dimensional fluid are the bridge between the aqueous compartments that are separated by the membrane. Membrane proteins serve many crucial functions for the cell such as transport of molecules, energy storage, sensing of environmental signals, motility, or cellular defence. Many of them interact with other proteins to fulfil their biological function (Carlson *et al.*, 2019).

1.1.1 Solubilisation methods

Membrane proteins adapt their native conformation in the bipolar environment of the membrane as they are in contact with both the non-polar and the polar phases in an intact cell. Thereby, the lipid environment not only stabilizes the proteins but also affects their folding, structure, and function (Thoma *et al.*, 2020). The membrane integrity is therefore crucial for membrane proteins and formation of complexes (Guérin *et al.*, 2020; Sachs *et al.*, 2006). So far, just a few proteins have been investigated in their native membranes, e. g. the structure of bacteriorhodopsin from halobacteria (Henderson *et al.*, 1975; Müller *et al.*, 2007). However, handling of native membranes is often challenging, and depends on high abundance of the protein of interest with little contaminants. Investigation of membrane proteins often requires the proteins to be extracted from the membranes. To achieve this, a variety of solubilisation methods are commonly used. During the solubilisation process, the original cell membrane is disrupted in order to extract the proteins. Hydrophobic areas of the proteins get covered by substances that possess similar properties as the phospholipids: a hydrophilic part to keep the protein in aqueous solution, and a hydrophobic part that covers the lipid-soluble part of the proteins. The most frequent approach for membrane protein investigation is the solubilisation of the host membranes into detergent micelles (Thoma *et al.*, 2020). A detergent is an amphipathic molecule, containing a hydrophilic head and a hydrophobic tail. Due to their structure the detergents self-assemble to micelles in aqueous solutions. In the solubilisation process with detergents, the lipid bilayer is destabilised and fragmentated, followed by the dissolution of proteins and lipids into mixed micelles (**Fig. 1.1**) (Lichtenberg *et al.*, 1983). The mixed micelles contain either protein-detergent, lipid-detergent, or protein-lipid-detergent. Solubilisation of proteins with detergents is widely used, as is applicable to various downstream processes, such as protein purification with chromatographic methods, protein refolding, blue native gel electrophoresis, single-particle cryo-EM or NMR. Thereby also protein complexes have been investigated successfully after detergent solubilisation (Heide *et al.*, 2012; Van Strien *et al.*, 2019; Walian *et al.*, 2012). Detergent micelles are also the starting point of further membrane protein stabilisation methods. For example,

especially for cryo-EM investigation, detergent-solubilised membrane proteins are subsequently treated with amphipols. These amphipols are small amphipathic polymers with a high affinity to the hydrophobic regions, thereby remaining associated to the membrane proteins even at low concentrations. This eliminates the micelle problem in cryo-EM, where free micelles interfere with the background and ice-thickness (Autzen *et al.*, 2019). However, in the process of protein solubilization the native lipid environment of the membrane protein is replaced by the detergent. This treatment often comes along with a significant loss of stability (Jodaitis *et al.*, 2021; Yang *et al.*, 2014) since lipid molecules were shown to modulate the oligomerization of membrane-protein complexes (Sobti *et al.*, 2020; Sun *et al.*, 2018). Reconstitution of the membrane proteins into other membrane mimetics such as bicelles, membrane scaffold protein (MSP) nanodiscs, peptidiscs or liposomes can improve stability and pave the way for more detailed studies (**Fig. 1.1**) (Carlson *et al.*, 2019; Thoma *et al.*, 2020).

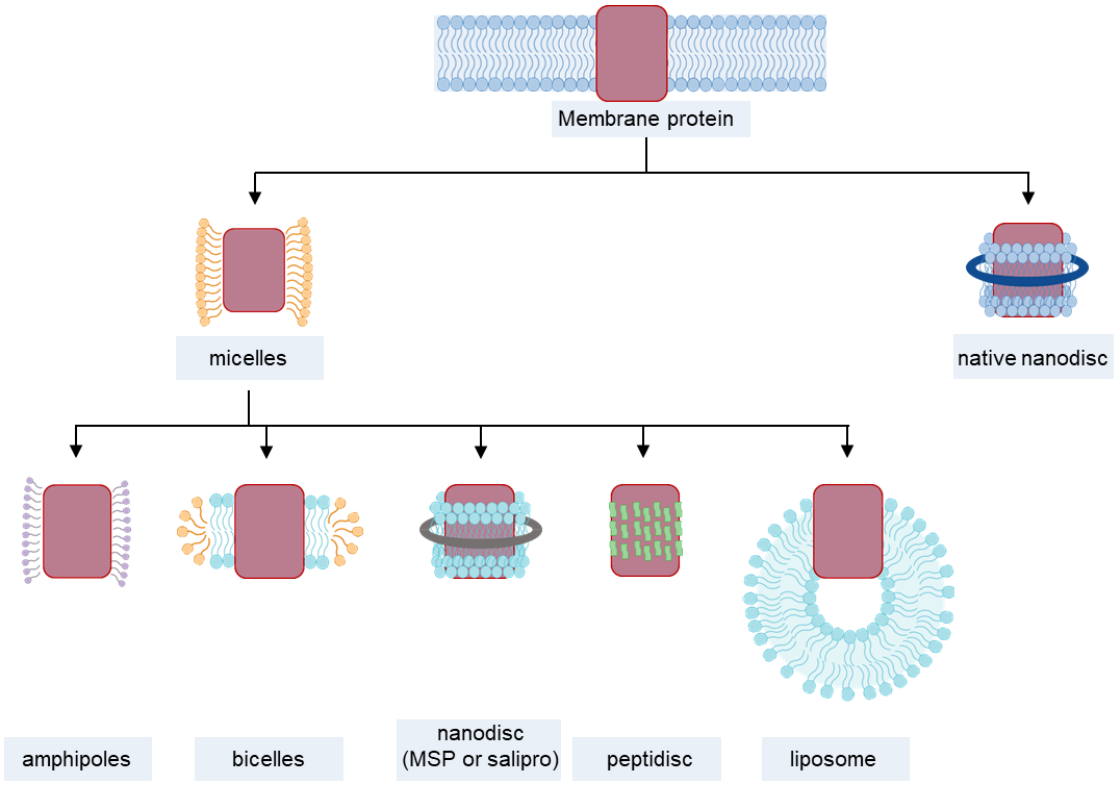

Fig. 1.1 Methods for solubilisation and stabilisation of membrane proteins in aqueous solution. Detergent solubilisation (orange) is a frequently used solubilisation method resulting in mixed micelles. Starting from there, proteins can be further stabilised by amphipols (violet), reconstituted in bicelles (blue and orange), nanodiscs (grey), peptidiscs (green), or liposomes (blue). Some polymers extract membrane proteins directly into native nanodiscs (dark blue).

One example for a membrane mimetic are bicelles or bilayered micelles. The bicelles contain phospholipids, that are surrounded by detergent or short-chained lipids (Majeed *et al.*, 2021; Vold *et al.*, 1997). They are usually formed by addition of phospholipids to detergent-solubilised membrane proteins. Alternatively, they can be assembled by addition of detergents to preformed

proteoliposomes. Bicelles exhibit structural variability, often resulting in proteins adopting a functional state (Majeed *et al.*, 2021; Thoma *et al.*, 2020).

Another frequently used membrane mimetic system are membrane scaffold proteins (MSP). Thereby the membrane proteins reside in a disc-like structure composed of phospholipids, that is stabilised by the MSP (Bayburt *et al.*, 2002). Reconstitution of detergent-solubilised proteins is achieved by addition of solubilised phospholipids and the membrane scaffold protein. Self-assembly of the nanodisc is driven by detergent removal, resulting in lipid bilayer embedded proteins with a helical belt consisting of the MSP (Denisov *et al.*, 2004; Rasmussen *et al.*, 2011). Similarly, nanodiscs can be formed by the saposin-lipoprotein (Salipro) system (Autzen *et al.*, 2019). The saposin protein family consists of small amphipathic helical glycoproteins and is known for its lipid binding properties and modulation of lipid membranes (Ahn *et al.*, 2003; Bruhn, 2005). The resulting saposin-lipoprotein nanoparticles self-assemble and adjust to the size of the incorporated protein (Frauenfeld *et al.*, 2016). In a comparable approach, detergent-solubilised membrane proteins were reconstituted in so-called peptidiscs. Thereby short bi-helical peptides stabilise the membrane proteins in aqueous solutions. In contrast to the reconstitution with MSPs or Salipro system, no additional lipids are added (Carlson *et al.*, 2018).

Alternatively, membrane proteins can also be reconstituted into liposomes. Liposomes are self-assembling vesicles of artificial lipid bilayers. Membrane protein insertion into liposomes is mediated by detergent removal either for preformed liposomes or a mixture of micelles containing detergent-solubilised lipids that self-assemble to liposomes in the process (Jesorka *et al.*, 2008; Thoma *et al.*, 2020). Liposomes resemble native membranes in terms of permeability and flexibility, and protein complexes could be reconstituted in functional state (Eytan, 1982). In addition, liposomes are frequently used in biological sciences e. g. in drug delivery, immunosensing or as nanotube vesicle networks (Jesorka *et al.*, 2008). Limiting factors for the application of liposomes are orientation of the inserted proteins and liposome stability towards hydrolysis (Jesorka *et al.*, 2008; Tunuguntla *et al.*, 2013).

By reconstituting the membrane proteins into detergent-free scaffolds, the exposure of the extracted proteins to detergent is strongly reduced. The result is improved stability of membrane proteins and protein complexes, which can also positively affect activity (Alami *et al.*, 2007; Bayburt *et al.*, 2006). However, an initial extraction of the membrane proteins by detergents is still required. In contrast, amphiphilic copolymers can directly extract proteins from membranes together with their lipid environment by forming “native nanodiscs” (Dörr *et al.*, 2014; Knowles *et al.*, 2009; Oluwole *et al.*, 2017). Several membrane proteins, e. g., rhomboid proteases and bacteriorhodopsin as well as protein complexes, e. g., the SecYEG/SecDF/YajC/YidC complex have been successfully extracted from native membranes and showed enhanced stability (Barniol-Xicota *et al.*, 2018; Komar *et al.*, 2016; Swainsbury *et al.*, 2014; Ueta *et al.*, 2020). However, high charge densities in certain polymers can

result in nonspecific interactions with charged lipids or proteins, interfering with further analytical methods like electrophoresis or enzymatic activity (Glueck *et al.*, 2022; Pollock *et al.*, 2022).
In conclusion, there are currently numerous solubilisation methods available for the investigation of membrane proteins, each having their own benefits and challenges.

1.1.2 Investigation of membrane protein-protein interactions

Many membrane proteins interact with other proteins to fulfil their biological function (Carlson *et al.*, 2019). Frequently, membrane integrity is crucial for the formation and function of these complexes (Guérin *et al.*, 2020; Sachs *et al.*, 2006). With the elucidation of large membrane-protein complexes, the understanding of cellular processes has significantly advanced (Komar *et al.*, 2016). However, the dynamics and interaction of membrane proteins is still intriguing, since not all protein interactions are stable for *in vitro* elucidation. Techniques for the investigation of protein-protein interactions *in vivo* include, for example, bacterial adenylate cyclase two hybrid (B2H) assay, split-ubiquitin system, or bimolecular fluorescence complementation (BIFC). Thereby, a reporter protein is split in two subunits that are each fused to one target protein. Interaction of the two target proteins leads to a complementation of the reporter proteins, which can be detected either directly by fluorescence, or indirectly through reporter gene expression. Similarly, in Förster resonance energy transfer (FRET), energy transfer from one fluorophore to another results in fluorescence of the latter. In super resolution microscopy, interactions can be resolved at the single-molecule level (King *et al.*, 2016; Sydor *et al.*, 2015). The mentioned techniques are furthermore applicable for high throughput screening of novel interaction partner candidates to one target protein (Meiresonne *et al.*, 2019; Miller *et al.*, 2015; Ouellette *et al.*, 2017; Sowa *et al.*, 2020). Nonetheless, these methods prevalently require overexpression of the target protein to enable the detection, labelling of the target protein or non-native environments (e. g. *E. coli* in the B2H analysis). A pulldown approach or co-immunoprecipitation (co-IP) is another method to investigate interaction partners of a target protein. The assay is performed *ex vivo*, thereby membrane proteins need to be solubilised first. The protein of interest is then bound to column material or beads via either an affinity tag or by antigen-antibody interactions. Cross-linking is frequently used to stabilise protein complexes and detect weak or transient interactions (Pertl-Obermeyer *et al.*, 2020). Possible interaction partners are either identified by mass spectrometry (MS), or interaction with a previous determined possible interactor is confirmed by immunodetection. Emergence of large-scale approaches led to the discipline of complexomics and computational modelling of interactomic networks (Xing *et al.*, 2016). All (membrane) proteins are thereby screened for interaction in a comprehensive, global, and untargeted manner. A commonly used method is complexome profiling by blue native gel electrophoresis coupled to MS (Wessels *et al.*, 2009). Thereby, membrane proteins are solubilised with detergents, complexes are separated by native gel electrophoresis, and proteins are identified in MS. This method was first established for the investigation of mitochondrial membrane complexes, but also bacterial complexes were identified successfully (de Almeida *et al.*, 2016; Versantvoort *et al.*, 2019; Wessels

et al., 2009). An alternative separation method for solubilised membrane proteins is size exclusion chromatography (SEC) which was also used in combination with native polymer nanodiscs or peptidiscs to record membrane protein complexes (Carlson *et al.*, 2019; Glueck *et al.*, 2022). Cross-link mass spectrometry (XL-MS) is another approach to study global protein-protein interactions. Thereby, proteins are reacted with cross-linking reagents that physically connect closely spaced amino acid residues through the formation of covalent bonds. The cross-linked proteins are then digested, and peptides are analysed by MS. The method is capable to simultaneously uncover protein-protein interactions, and their physical interaction contacts (Sinz, 2010; Yu *et al.*, 2018). Moreover, the method can provide structural information about proteins and protein complexes (Chen *et al.*, 2010; Piersimoni *et al.*, 2022; Yu *et al.*, 2018). Membrane protein interactions have been extensively studied in the past using an ever-expanding range of sophisticated techniques.

1.1.3 Functions of bacterial membrane proteins

About one third of all proteins in a cell are membrane proteins (Granseth *et al.*, 2005). The majority of membrane proteins contain α-helical transmembrane structures, whereas a β-barrel structure is mainly found in outer membrane proteins of Gram-negative bacteria (Hedin *et al.*, 2011; Xie *et al.*, 2008). Integration of membrane proteins into the lipid bilayer is mediated prevalently by the SEC-SRP translocation system. Thereby the signal recognition particle (SRP) recognises and interacts with the unfolded target protein and delivers it to the Sec translocon (Valent *et al.*, 1998). In contrast, the twin arginine translocation (Tat) system transports fully folded proteins, that often contain metal cofactors (Lee *et al.*, 2006). Membrane proteins have a multitude of essential roles for the cell, including molecule transportation across the membrane, energy storage, and environmental signal detection (Hedin *et al.*, 2011). Albeit some molecules like gases can pass the lipid bilayer without a transport system, the transport of molecules, metabolites, and larger molecules such as RNA or DNA through the membranes is facilitated by diverse channels and transporters (**Fig. 1.2**) (Padan, 2009). Thereby, cells ingest nutrients, discard unwanted or toxic compounds, secrete virulence factors, take up DNA for homologous recombination, or secrete adhesion factors for surface attachment (Costa *et al.*, 2015; Mitra *et al.*, 2016).

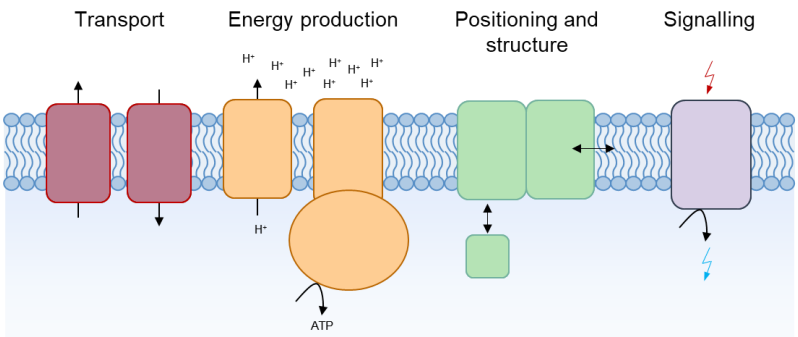

Fig. 1.2 Examples for functions of membrane proteins in bacteria. Membrane proteins can facilitate transport of specific or unspecific molecules across the membrane (red), be involved in energy production through generation of a gradient (yellow), provide structure to shape the cell or position proteins (green), and perceive or transmit signals (violet).

Additionally, membrane proteins are involved in energy storage and energy production. A common mechanism is the generation of a gradient across a bacterial membrane, that in turn fuels either ATP synthesis or a direct output (e. g. flagella rotation in *E. coli*) (Gabel *et al.*, 2003). Many members of the respiratory chain, the citrate cycle, or the light reaction in photosynthesis of cyanobacteria and plants are therefore membrane integrated proteins. Besides, membrane integration of proteins also facilitates protein positioning which can also be crucial for the function, e. g. during cell division (Laloux *et al.*, 2014; Mitra *et al.*, 2016). Further, membrane proteins are involved in maintaining the shape of the cell or controlling the lipid composition e. g. penicillin-binding proteins (PBPs) or membrane bound shape determinants like products of the *mre* locus in *E. coli* (Cabeen *et al.*, 2005; Hedin *et al.*, 2011). Moreover, membrane proteins are frequently involved in sensing and signalling, where an external signal is perceived by a membrane protein which results in a cellular response in the cytoplasm. Alternatively, a signal can also be transduced from the cytoplasm to the outside of the cell (Newell *et al.*, 2011). Many proteins involved in sensing carry N-terminal sensory domains, that are membrane integrated or extracellular. Examples for common signal transduction systems are two-component systems, second messenger, or chemosensory systems.

1.2 The second messenger c-di-GMP

The signalling via second messengers is a universal biochemical process in bacteria, archaea and eukaryotes, where a primary signal is transduced into an intracellular chemical signal molecule (second messenger). In general, a control module for second messenger signalling consists of four elements: two enzymes that synthesize and degrade the messenger molecule, and an effector that can bind the messenger. Binding of the messenger to an effector leads to its direct interaction with a target, the fourth component, that generates the cellular output (Hengge, 2009). The first described second messenger was cAMP, that regulates carbon utilisation in bacteria or glycogen breakdown in humans (Assmann, 1995; Gomelsky, 2011). Since then, a variety of other second messengers were described, e. g. Ca^{2+} (McCormack *et al.*, 1986), NO (Kerwin *et al.*, 1995), CO (Broillet *et al.*, 1996), as well as nucleotides like cGMP, ppGpp and c-di-GMP (Gomelsky, 2011).

The molecule bis-(3’5’)-cyclic-di-guanosine monophosphate (c-di-GMP) is a bacterial second messenger that controls various processes such as bacterial cell cycle progression, motility, biofilm formation, or virulence (Hengge, 2009). Since its first description in 1987 as a regulator of cellulose synthesis in *Acetobacter xylinum* it became one of the most studied second messengers in bacteria (Ross *et al.*, 1987; Sondermann *et al.*, 2012). Considering c-di-GMP is also found in clinically relevant bacteria but not in humans or higher eukaryotes, it is also a target for the fight against bacterial infections (Foletti *et al.*, 2018; Karaolis *et al.*, 2005; Sintim *et al.*, 2010). The molecule was furthermore described to be a promising adjuvant in cancer treatment and vaccination as it triggers innate immune response in humans by activating the STING pathway (Wang *et al.*, 2015b; Zhang *et al.*, 2023).

1.2.1 Synthesis and degradation of c-di-GMP

Intracellular levels of the second messenger c-di-GMP in bacteria are mainly determined by two classes of enzymes: diguanylate cyclases (DGCs) that synthesize the messenger and phosphodiesterases (PDEs) that degrade it. DGCs possess a GGDEF domain, whereas PDEs possess an EAL or HD-GYP domain (**Fig. 1.3**) (Hengge, 2009; Römling *et al.*, 2005). These domains are named after their characteristic amino acid motifs (Römling *et al.*, 2005). One c-di-GMP molecule is synthesized by DGCs using two guanosine triphosphate (GTP) molecules. The catalysis requires dimerization of two DGCs, with one GTP bound to each protein. The reaction is initiated by the deprotonation of the 3'OH groups that provoke a nucleophilic attack on the α-phosphate. A conserved lysine stabilises the charge of the emerging phosphoryl transition state and the departing pyrophosphate group (Chan *et al.*, 2004). PDEs degrade c-di-GMP to 5'phosphoguanyl-(3'-5')-guanosine (pGpG) or two molecules of guanosine monophosphate (GMP) (Römling *et al.*, 2005). Thereby in EAL domains the phosphate-sugar bond is broken presumably by a nucleophilic attack of a catalytic hydroxide ion. The reaction requires one or two metal ions (often Mg^{2+} or Mn^{2+}) to coordinate the hydroxide ion as well as the substrate c-di-GMP at the phosphate-oxygen bond (Tchigvintsev *et al.*, 2010). HD-GYP domains are presumed to have a more flexible 3D structure of the active site, thereby occasional enabling hydrolysis of cGAMP (Wright *et al.*, 2020). They contain two or three metal ions (often Fe^{2+} ions) that are presumed to coordinate the activating hydroxide ion as well as the substrate's phosphate oxygens to assist bond breakage and transition state stabilisation (Lovering *et al.*, 2011; Miner *et al.*, 2016; Wigren *et al.*, 2014). Additionally, the active centre was shown to bind pGpG with higher affinity than c-di-GMP (Galperin *et al.*, 2022; Stelitano *et al.*, 2013).

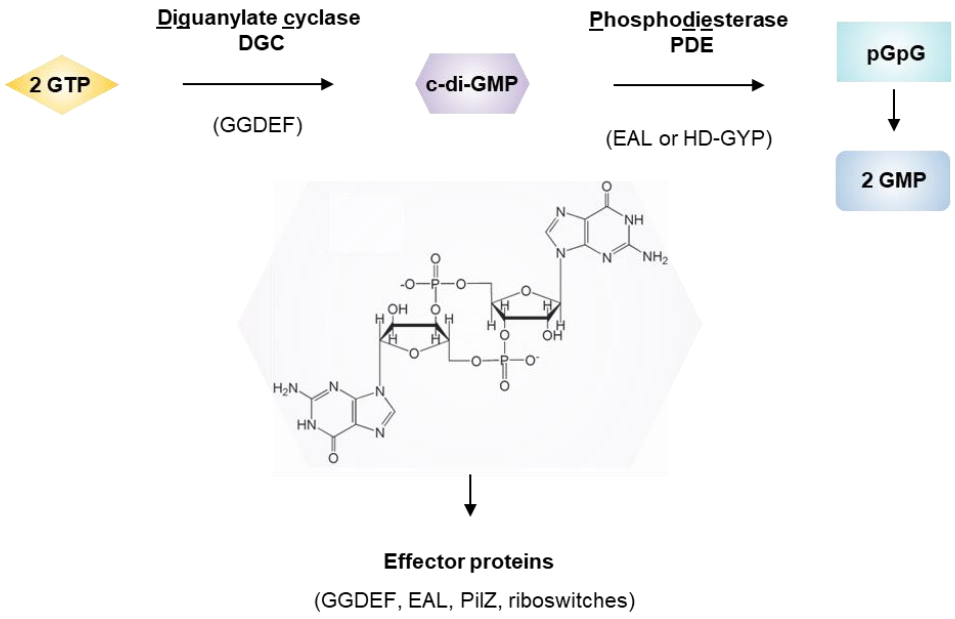

Fig. 1.3 Enzymes involved in synthesis and degradation of c-di-GMP. The second messenger c-di-GMP is synthesized by DGCs containing a GGDEF motif and degraded by PDEs that harbour an EAL motif. Intracellular c-di-GMP levels are recognised by effector proteins, that bind c-di-GMP and lead to a cellular output. Figure modified from Hengge, 2009.

In the cellular environment, the level of c-di-GMP is detected by effectors that have the ability to bind c-di-GMP. The c-di-GMP synthesizing GGDEF domains often harbour an allosteric binding site for c-di-GMP with a conserved RxxD motiv, indicating product inhibition (Christen *et al.*, 2006, Schirmer *et al.*, 2009). Moreover, several (inactive) EAL domains were shown to bind c-di-GMP and function as effectors (Hengge, 2016; Newell *et al.*, 2011; Newell *et al.*, 2009). PilZ domains, in addition to GGDEF and EAL domains, are another known binding domain for c-di-GMP (Amikam *et al.*, 2006). Members of this domain show overall low sequence similarity except for two conserved motifs RxxxR and D/NxSxxG, that are involved in nucleotide binding (Benach *et al.*, 2007). The three-dimensional conformation of c-di-GMP also contributes to its binding to diverse effectors, as the molecule exists in various conformations, including a stacked or elongated form (Egli *et al.*, 1990; Krasteva *et al.*, 2012; Zhang *et al.*, 2006). In addition to proteins, RNA can also act as a c-di-GMP effector. Known binding motives are the GEMM motif or the pseudoknot in riboswitches (Smith *et al.*, 2011; Sudarsan *et al.*, 2008). Binding of c-di-GMP to an effector triggers a specific output that is mediated via various mechanisms like transcriptional (de-) activation, DNA binding, conformational changes, localisation, protein-protein interaction, or altered enzymatic activity (Boyd *et al.*, 2012; Steiner *et al.*, 2013). Thereby c-di-GMP levels control a wide range of phenotypic outputs like biofilm formation, motility, virulence, and cell cycle progression.

1.2.2 Impact of c-di-GMP signalling on bacterial phenotypes

In general, c-di-GMP levels in bacteria control the transition from free-swimming cells to a sessile lifestyle. Thereby high intracellular levels of the messenger stimulate the production of adhesins and extracellular polymeric substances (EPS) for biofilm formation while inhibiting motility (**Fig. 1.4**) (Hengge, 2009). This applies to many bacterial species such as *Pseudomonas aeruginosa*, *Escherichia coli*, *Vibrio cholerae* (Tischler *et al.*, 2004), *Salmonella enterica* serovar Typhimurium (Ahmad *et al.*, 2011), and some cyanobacteria (Enomoto *et al.*, 2023). The mechanisms by which c-di-GMP levels are translated into global but defined and consistent outcomes are subject of ongoing studies. In *P. aeruginosa*, the transcription factor FleQ is considered the master regulator for the motile-sessile lifestyle switch, which senses the messenger molecule and inhibits expression of flagellar biosynthesis genes while promoting expression of EPS biosynthesis genes (Arora *et al.*, 1997; Hickman *et al.*, 2008). Also, the first cellular output discovered for c-di-GMP was the regulation of cellulose synthesis in *A. xylinum*. Cellulose is an EPS and also a matrix component in biofilms (Morgan *et al.*, 2014; Ross *et al.*, 1987; Zogaj *et al.*, 2003). In *E. coli*, c-di-GMP regulates among other factors the transcription of *csgD*, the master regulator for biofilm formation and curli fimbriae (Lindenberg *et al.*, 2013; Ogasawara *et al.*, 2010). In *S. enterica* serovar Typhimurium CsgD regulates biofilm formation through cellulose expression while inhibiting pro-inflammatory response. Thereby c-di-GMP also controls virulence and infection (Lamprokostopoulou *et al.*, 2010). Motility is frequently inhibited by high c-di-GMP levels, as shown in *E. coli* where the underlying mechanism has already been described. Upon binding of c-di-GMP to the effector YcgR, the protein binds to the

flagellar motor thereby decreasing the swimming speed via MotA (Boehm *et al.*, 2010) and inhibiting clockwise (CW) rotation via FliG (Fang *et al.*, 2010). A YcgR homolog (named YpfA, later renamed to DgrA) was also found in *Bacillus subtilis* to inhibit motility at elevated c-di-GMP levels via MotA (Gao *et al.*, 2013). Nonetheless, signalling is not always consistent between species, as for example high c-di-GMP level promote type IV pili (T4P) assembly in *Clostridium difficile* (Bordeleau *et al.*, 2015), while inhibiting them in *Myxococcus xanthus* (Skotnicka *et al.*, 2015), whereas *P. aeruginosa* forms T4P over a broad range of c-di-GMP levels (Jain *et al.*, 2012).

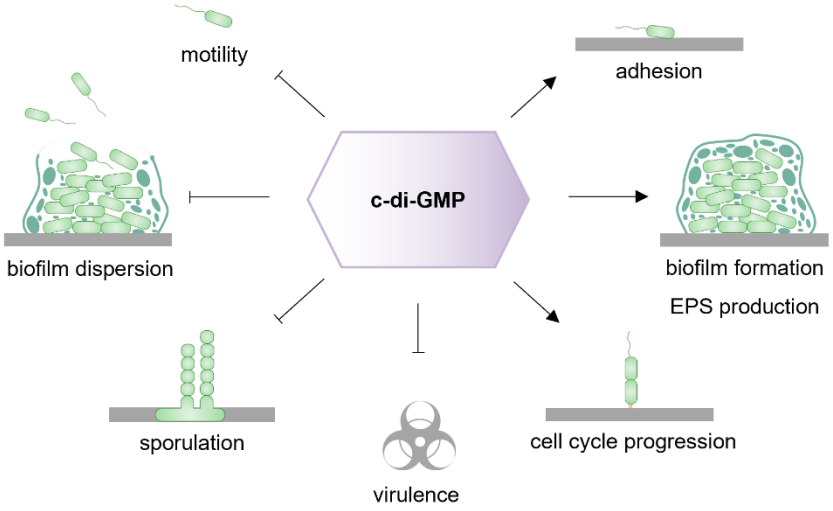

Fig. 1.4 Phenotypic outputs regulated by c-di-GMP. Low intracellular levels of c-di-GMP are associated with biofilm dispersion, motility, virulence, or sporulation. In contrast, high levels are related to cellular adhesion, biofilm formation, cell cycle progression, or vegetative growth.

Furthermore, cell division and cell cycle progression are regulated by c-di-GMP. It was shown for *Caulobacter crescentus*, *Shewanella oneidensis* and *P. aeruginosa*, that cells can undergo asymmetric cell division resulting in heterologous c-di-GMP levels in daughter cells (Christen *et al.*, 2010; Rick *et al.*, 2022). *C. crescentus* employs a bimodal lifestyle where swarmer cells transition to a stalked cell before cell division. Enhanced c-di-GMP levels promote the stalk formation and are mainly mediated by the DGC PleD (Abel *et al.*, 2013; Aldridge *et al.*, 2003; Duerig *et al.*, 2009). In addition, c-di-GMP regulates G1 to S-phase transition via the replication initiation inhibitor CtrA and the c-di-GMP effector PopA (Duerig *et al.*, 2009). Moreover, c-di-GMP was shown to arrest growth by changing the metabolic flow, presumably contributing to antibiotic tolerance and persister formation (Hwang *et al.*, 2023). In streptomycetes, c-di-GMP signalling is involved in the regulation of sporulation (Bush *et al.*, 2015). At high levels of c-di-GMP, the messenger binds to BldD, the master regulator for sporulation, which in turn represses expression of ~170 sporulation genes by directly inhibiting expression of key sporulation regulators, thereby promoting vegetative growth. As antibiotic synthesis is also developmentally regulated in streptomyces, c-di-GMP signalling also has an indirect effect on antibiotic biosynthesis (Bush *et al.*, 2015).

1.2.3 Modulation of the c-di-GMP levels in bacteria: Global and local c-di-GMP signalling

Many bacterial genomes encode for numerous GGDEF, EAL and/or HD-GYP domain containing proteins. Usually, Gram-negative bacteria encode more GGDEF/EAL/HD-GYP domain containing proteins than Gram-positive bacteria (Hengge, 2009). The large number of these proteins in a single organism is raising the question for their biological function and regulation. Transcriptional and post-transcriptional control of gene expression results in temporal distribution, albeit it was shown that multiple enzymes with the same activity are present at the same time in the cell (Hou *et al.*, 2023; Motta *et al.*, 2020, Sommerfeldt *et al.*, 2009). Deletion of different DGCs or PDEs leads to distinct phenotypes, although mutants have comparable intracellular c-di-GMP levels (Kulasakara *et al.*, 2006; Merritt *et al.*, 2010; Sarenko *et al.*, 2017). A possible explanation is the formation of global and local pools of c-di-GMP, that act parallel and lead to defined outputs (**Fig. 1.5**) (Hengge, 2016). The current model suggests a spatial distribution of involved proteins in so-called supermodules, where c-di-GMP producing and degrading proteins are close to their effector proteins, thereby generating multiple local pools of the second messenger (Hengge, 2021; Junkermeier *et al.*, 2023; Sarenko *et al.*, 2017). Global c-di-GMP levels are mainly controlled by a master PDE and effectors that are activated at different c-di-GMP levels by their specific binding affinities (K_D).

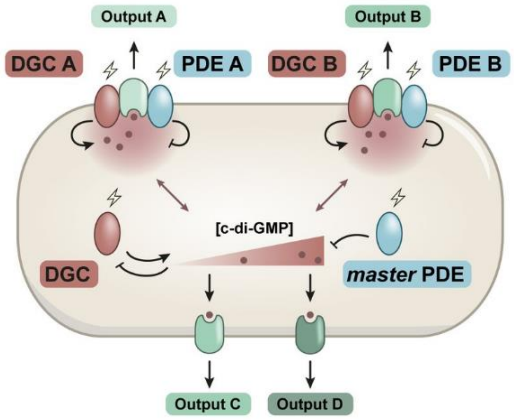

Fig. 1.5 Principle of global and local c-di-GMP signalling. Global c-di-GMP level is influenced by a master PDE and DGC. Specific effectors recognize the global c-di-GMP level. Local signalling units consisting of a DGC, a PDE and a specific effector target exist in parallel. The proteins are further regulated by signal recognition (indicated by bolts) often through N-terminal sensor domains. Figure extracted from Junkermeier *et al.*, 2023 (Permission by Oxford University Press, Licence Number: 5714650863127).

For this model, the localisation and interaction of proteins involved in signalling is important. Membrane localisation might facilitate local signalling. For the model organisms *B. subtilis*, *V. cholerae*, *P. aeruginosa*, *S. oneidensis*, *E. coli*, and *S. enterica* more than half of the c-di-GMP modulating proteins are predicted membrane proteins (Pfam database). Membrane localisation might also enable heterologous c-di-GMP levels of cells in a population. Thereby, some DGCs/PDEs localize to one cell pole. After cell division this localization results in an asymmetric distribution of the DGC/PDE proteins in cells of a population, thus generating different intracellular c-di-GMP levels

(Christen *et al.*, 2010; Laventie *et al.*, 2019; Rick *et al.*, 2022). The investigation of membrane protein dynamics is thereby important for the understanding of the signalling networks.

The activity of the c-di-GMP modulating enzymes is furthermore adjusted by linked sensor domains. Based on the complexity scheme, most signal transduction proteins can be classified into one-component, two-component and chemosensory systems (Randall *et al.*, 2022). In a one-component system, signal input domains are directly linked to the output domain, in this case GGDEF, EAL or HD-GYP domains. A variety of other signal input domains are fused to GGDEF/EAL or HD-GYP domain proteins, for example GAF, PAS, Chase, MASE, MHYT, CSS, GAPES, BLUF, or Cache domains, and multiple perceived signals were described, like light, temperature, sugars, nucleotides, gases, or amino acids (reviewed in Randall *et al.*, 2022). The most abundant sensory domain for GGDEF/EAL/HD-GYP domain proteins is the well-studied PAS domain (Dayton *et al.*, 2020; Randall *et al.*, 2022) that is frequently able to bind heme-cofactors or small ligands (Monson *et al.*, 1992; Pellequer *et al.*, 1998). Examples for signals perceived by PAS domains that directly influence activity were oxygen (RbdA in *P. aeruginosa*), redox stress (YfiN in *E. coli*), temperature (TdcA in *P. aeruginosa*), light (SL2 in *Synecococcus elongatus*) phenazines, or lipids (RmcA in *P. aeruginosa*) (Almblad *et al.*, 2021; An *et al.*, 2010; Cao *et al.*, 2010; Giardina *et al.*, 2013; Okegbe *et al.*, 2017). Notably, some GGDEF/EAL/HD-GYP proteins contain more than one signal input domain, therefore being able to integrate multiple signals. In contrast, in two-component sensory systems, signal perception and output are carried out by two individual proteins. Instead of a signal input domain, GGDEF/EAL/HD-GYP domain proteins harbor a N-terminal receiver domain. Signal perception is carried out by a senor kinase, that phosphorylates the receiver domain upon activation. In turn, this phosphorylation alters the activity, as it was shown for the DGC PleD from *C. crescentus* or the PDE RocR from *P. aeruginosa* (Christen *et al.*, 2005; Kuchma *et al.*, 2005, Chen *et al.*, 2012). The more complex chemosensory systems consist of at least six components. The first described chemosensory system was the flagella motility regulating system in *E. coli*, which consist of the methylating chemotaxis protein (McpA), a histidine kinase (CheA), coupling protein (CheW), methyltransferase (CheR), methylesterase (CheB) and response regulator (CheY) (Hazelbauer, 1988). In *P. aeruginosa*, the homologous chemosensory Wsp-system involved in surface sensing is interlinked with c-di-GMP signalling. Activation of the systems results in a phosphorylation of the DGC WspR, thereby regulating its activity (Hickman *et al.*, 2005).

In summary, signal inputs of c-di-GMP regulating enzymes are diverse and the perceived signal of GGDEF/EAL/HD-GYP domain proteins are often not yet identified. In most bacteria, c-di-GMP signalling requires a complex regulatory network with temporal and spatial distribution of involved proteins to generate a specific response.

1.3 *Pseudomonas aeruginosa* as a model organism

1.3.1 Lifestyle and clinical relevance of the bacterium *P. aeruginosa*

Pseudomonas aeruginosa is a Gram-negative, rod-shaped, monotrichous flagellated bacterium that belongs to the genus Gammaproteobacteria (Murray *et al.*, 1990; Stanier *et al.*, 1966). The cell size is between 1-5 µm long and 0.5-1 µm wide. *P. aeruginosa* possesses a large genome of ~6.3 million base pairs and 5570 predicted ORFs, which has been completely sequenced (Stover *et al.*, 2000). The bacterium is highly adaptive to various growth conditions, as it can metabolise a wide range of carbons and sugar derivatives, fatty acids, aliphatic and circular amino acids, alcohols, polyalcohols, and glycols for energy production. It is further capable of anaerobic respiration by using nitrate instead of oxygen as a terminal electron acceptor (Stanier *et al.*, 1966). Additionally, the organism can survive a broad temperature range between 4 °C and 42 °C (Diggle *et al.*, 2020). Therefore, *P. aeruginosa* is ubiquitous in the environment in water and soil especially in locations with high human activity like wastewater or pesticide-contaminated soil. Moreover, the bacterium can also infect plants, animals, and humans as an opportunistic pathogen (Crone *et al.*, 2020). People with a weakened immune system, such as cancer patients or patients in intensive care units, are particularly affected by infections with this germ. Thereby, *P. aeruginosa* colonises burn wounds, the lower respiratory tract, catheters, or implants. Also, patients with cystic fibrosis often suffer from chronic infections by *P. aeruginosa* (Donlan *et al.*, 2002; Rasamiravaka *et al.*, 2015; Stover *et al.*, 2000). Treatment of these infections represent a particular challenge as the bacterium shows high intrinsic and mutational antibiotic resistances (Hancock *et al.*, 2000) e. g. by efflux systems or antibiotic-inactivating enzymes like ß-lactamases. In addition, the bacterium can form stable biofilms which goes along with an increased tolerance against antibiotics (also called adaptive antibiotic resistance) (Pang *et al.*, 2019; Rasamiravaka *et al.*, 2015). Novel therapeutic strategies to combat *P. aeruginosa* infections such as quorum sensing inhibition, phage therapy, novel antibiotics including antimicrobial peptides, nanoparticles, or iron chelation are in high demand (Chatterjee *et al.*, 2016; Pang *et al.*, 2019; Spagnolo *et al.*, 2021).

In research, *P. aeruginosa* became a model organism for the investigation of infection and biofilm formation, maintenance, and dispersion. The most commonly used strain is PAO1, which originated from a wound isolate from Australia in 1954 (Holloway, 1955). Notably, strains in different laboratories exhibit phenotypic and genomic variation, which impedes consistency of experiments across research teams (Chandler *et al.*, 2019; Diggle *et al.*, 2020; Klockgether *et al.*, 2010).

1.3.2 Biofilm formation in *P. aeruginosa*

Bacterial biofilms are structured consortia of surface-attached communities that are enclosed in a matrix of self-produced extracellular polymeric substances (EPS) (Flemming *et al.*, 2016). They are also referred to as “city of microbes”, where bacteria actively shape their microenvironment to more favourable conditions (Hengge, 2020; Watnick *et al.*, 2000). Biofilms are of clinical relevance since cells in a biofilm are better protected from antibiotics and the host's immune system.

The process of biofilm formation can be segmented into three different phases (**Fig. 1.6**) (Sauer *et al.*, 2022). Initially, planktonic *P. aeruginosa* cells encounter a surface, where they temporarily attach themselves to (Kuchma *et al.*, 2007). Then, the cells adhere irreversibly to the surface along their longitudinal axis. Alternatively, after their initial temporary attachment, the cells move along the surface through twitching or swarming motility (Ha *et al.*, 2015). Following attachment, the biofilm matures through the production of exopolysaccharides with *P. aeruginosa* primarily using Pel, Psl and alginate (Ha *et al.*, 2015). Additionally, the extracellular matrix of biofilms comprises proteins, nucleic acids, and lipids (Sutherland, 2001). As the biofilm matures, macrocolonies with a complex three-dimensional structure and a thickness of approximately 100 µm are formed (Sauer *et al.*, 2002). Dispersion of biofilms is induced by various environmental factors such as glutamate concentration, presence of the gas NO, and nutrient availability (Barraud *et al.*, 2006; Sauer *et al.*, 2004). Upon dispersion, free-swimming planktonic cells are released in the surrounding, able to colonise new habitats (Ha *et al.*, 2015).

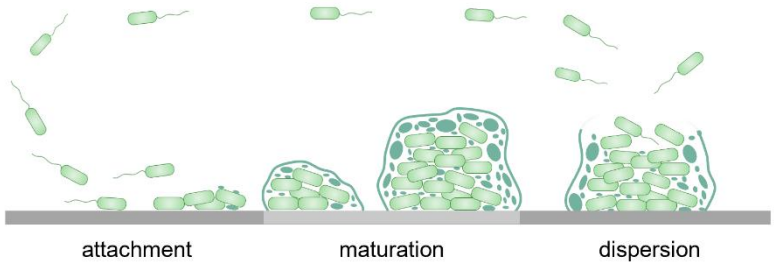

Fig. 1.6 Biofilm formation in *P. aeruginosa*. Biofilm formation comprises three phases: attachment to a surface, maturation of the biofilm, and dispersion (Sauer *et al.*, 2022). The process is regulated by various factors, e. g. quorum sensing or c-di-GMP signalling. Figure adapted from Rasamiravaka *et al.*, 2015.

To decide whether it is appropriate to form a biofilm, cells must be able to sense their environment, e. g. nutrient availability or surface properties and react accordingly. Thereby, sensor proteins are of particular importance. The formation of biofilms is tightly controlled in *P. aeruginosa*, e. g. by the intracellular concentration of the nucleotide second messenger c-di-GMP (Ha *et al.*, 2015). *P. aeruginosa* cells within a biofilm contain up to 10 times more c-di-GMP than their planktonic counterparts (Roy *et al.*, 2012).

1.3.3 Modulation of the c-di-GMP network in *P. aeruginosa*

In *P. aeruginosa*, c-di-GMP regulates various cellular processes via a complex signalling network. More than 40 proteins are potentially involved in synthesizing or degrading c-di-GMP. The strain PAO1 encodes 18 GGDEF, 5 EAL, 16 GGDEF-EAL, and 3 HD-GYP domain containing proteins. In addition, there are more than 15 c-di-GMP specific effectors described, that regulate diverse cellular outputs (Banerjee *et al.*, 2021; Valentini *et al.*, 2016a). For instance, c-di-GMP specific effectors were demonstrated to modulate EPS synthesis (FleQ, PelD), flagella-mediated motility (FlgZ, MapZ) or type IV pili mediated motility (FimX, PilZ) in *P. aeruginosa* (Arora *et al.*, 1997;

Hickman *et al.*, 2008; Whitfield *et al.*, 2020; Baker *et al.*, 2016; Xu *et al.*, 2016; Amikam *et al.*, 2006; Guzzo *et al.*, 2009).

The redundant enzyme activities of GGDEF/EAL/HD-GYP domain containing proteins are tightly regulated on transcriptional and posttranslational levels, e. g. by temporal and spatial distribution of proteins, as well as specialized sensory or regulatory domains and protein-protein interactions (see section 1.2.3) (Ha *et al.*, 2015; Schirmer, 2016). It was directly shown in *P. aeruginosa*, that even at similar intracellular c-di-GMP levels deletion of single DGC or PDE genes result in diverse phenotypic outputs, thereby supporting the model for the local signalling network (Merritt *et al.*, 2010). Moreover, some GGDEF/EAL domain containing proteins were shown to act as c-di-GMP sensors themselves, e. g. LapD (Newell *et al.*, 2009). The c-di-GMP signalling network is also interlinked with other networks, e. g. quorum sensing systems, various two-component systems (e. g. HsbD/HsbA, or SiaD/SiaC), and chemosensory pathways (Wsp, Pil-Chp) (Armbruster *et al.*, 2019; Chen *et al.*, 2020; Chen *et al.*, 2021; Hickman *et al.*, 2005; Valentini *et al.*, 2016b). Notably, the majority of c-di-GMP producing or degrading proteins are predicted to be located in the inner membrane.

1.4 The Phosphodiesterase NbdA

1.4.1 Domain structure and activity

One example of a membrane integrated tandem phosphodiesterase in *P. aeruginosa* is NbdA (NO-induced biofilm dispersion locus A) (Li *et al.*, 2013) with the locus tag PA3311 in PAO1. The gene is found in Gammaproteobacteria, particularly of the *P. aeruginosa* group (94 %), but is also occasional found in *P. fluorescence*, *Acinetobacter baumannii* or unclassified *Pseudomonas* sp. (NCBI database, protein blast, max difference 0.85). The protein comprises three domains: an N-terminal MHYT domain consisting of seven transmembrane helices in the cytoplasmic membrane, followed by a GGDEF domain and an EAL domain in the cytosol (**Fig. 1.7**). The GGDEF domain of NbdA harbours an AGDEF motif instead of the canonical GGDEF motif, therefore the protein exhibits no DGC activity (Li *et al.*, 2013). NbdA contains the conserved RxxD motif or I-site, that is an autoinhibitory site for product inhibition in several GGDEF domain containing proteins (An *et al.*, 2010; Christen *et al.*, 2006). The C-terminal EAL domain of NbdA was shown to possess PDE activity, thereby converting c-di-GMP to pGpG (Li *et al.*, 2013; Rüger, 2019). The function of the MHYT domain is still unknown, but it was postulated to bind and sense diatomic gases such as NO, CO, or O_2 (Galperin *et al.*, 2001).

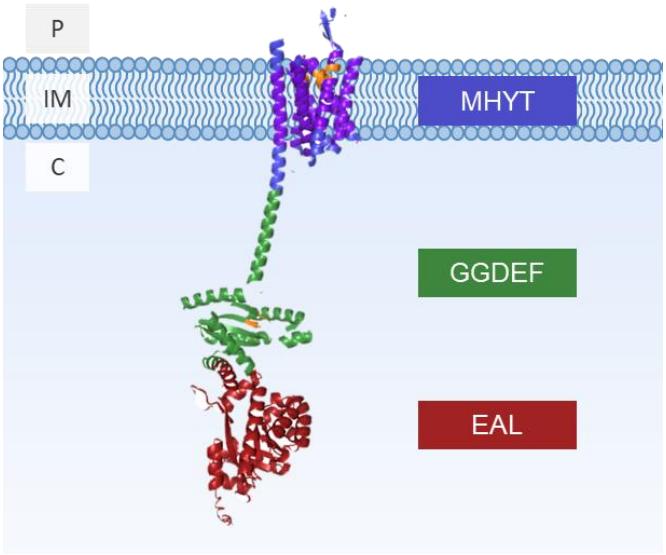

Fig. 1.7 Domain structure of NbdA. N-terminal membrane integrated MHYT domain depicted in blue, the GGDEF domain with an imperfect AGDEF motif coloured green, the C-terminal EAL domain in red. Predicted transmembrane regions in the MHYT domain are coloured violet. Conserved amino acid motives of the domains are shown in orange. 3D structure of NbdA predicted with alpha fold. P = periplasm, IM = inner membrane, C = cytoplasm.

1.4.2 The MHYT domain

Genes encoding MHYT domain containing proteins are found in various bacteria and fungi (Galperin *et al.*, 2001). The MHYT domain consists of six transmembrane (TM) regions, connected by short loops rich in charged amino acid residues. One MHYT domain subunit is characterised by two transmembrane regions, with the conserved MHYT motif facing the outer site of the cytoplasmic membrane (Galperin *et al.*, 2001). Conserved Met, Tyr, and His residues indicate copper binding, therefore the domain is suggested to be involved in sensing diatomic gases, like NO, CO, or O_2 (Galperin *et al.*, 2001). In most organisms, the MHYT domain is coupled to a GGDEF and EAL domain but may also pair with histidine kinase domains, DNA binding domains, or be stand-alone MHYT domain proteins (Galperin *et al.*, 2001).

One example for an MHYT domain protein is CC0091 from *C. crescentus*. CC0091 is an active PDE *in vitro*. The protein is probably an antagonist of DGC PleD regulating holdfast formation. Deletion of CC0091 leads to 25 % higher surface attachment, premature holdfast formation and increased cell aggregation. Overexpression of CC0091 has a similar phenotype to deletion of *pleD* in terms of holdfast formation while cells show increased swarming and improper flagellar shedding. Thus, CC0091 is thought to fine-tune holdfast formation together with PleD, presumably via c-di-GMP signals (Levi *et al.*, 2006). Another protein with an MHYT domain is DgcW (former YkoW) in *B. subtilis* (Bedrunka *et al.*, 2017) with the domain structure: MHYT-PAS-GGDEF-EAL. DgcW has a DGC activity *in vitro* and is localised at distinct sites in the membrane (Bedrunka *et al.*, 2017). Effectors and functions of this protein are not known. Deletion of *dgcW* had no effect on growth, biofilm formation, and motility. DgcW is part of the SigD regulon and is co-expressed with chemotaxis genes (Nicolas *et al.*, 2012).

The proteins CoxC and CoxH from *Oligotropha carboxydovorans* consist of a MHYT domain coupled to an HTH/LytTR domain. The C-terminal LytTR domain is a DNA-binding domain often found in response regulators (Nikolskaya *et al.*, 2002). CoxC and CoxH flank the operon of CO-dehydrogenase in *O. carboxydovorans*. Therefore, it is assumed that they are responsible for the regulation of the *cox* genes (Kerby *et al.*, 2008) or are involved in the anchoring of CO-dehydrogenase in the membrane (Hille *et al.*, 2014). Another characterized protein with an MHYT domain is CdgB from *Azospirillum baldaniorum* Sp245. The MHYT domain is linked to a PAS, GGDEF, and EAL domain. The protein localises to the cell pole, which is dependent on the presence of the MHYT domain. CdgB is probably a dual function enzyme with a primary PDE activity, while under certain conditions the protein can act as a DGC. Deletion of CdgB leads to reduced biofilm formation and EPS accumulation. It is therefore hypothesized that the protein is involved in regulating the motile-sessile lifestyle switch in response to environmental signals (Viruega-Góngora *et al.*, 2022).

In *P. aeruginosa*, in addition to NbdA there is another MHYT domain containing protein. The protein MucR also exhibits a MHYT-GGDEF-EAL domain structure, with seven TM regions (Hay *et al.*, 2009). It is thought to be a positive regulator of alginate biosynthesis, by exerting DGC activity. Produced c-di-GMP can be sensed locally by the PilZ domain protein Alg44, that activates alginate biosynthesis (Hay *et al.*, 2009). Protein variants either with impaired GGDEF or EAL motif showed no increase in alginate yield, indicating that both DGC and PDE activity of MucR are required for alginate production (Wang *et al.*, 2015a). Addition of nitrate (KNO_3) reduced the alginate production in a *mucR*-dependent manner. The His residue of the second MHYT motif was crucial for this effect, suggesting a role of this motif in nitrate perception. Nitrate can be utilized as an alternative electron acceptor in denitrification. However, it cannot be clearly established whether MucR senses nitrate directly, the metabolic intermediate NO, and/or changes in redox potential (Wang *et al.*, 2015a).

1.4.3 Possible functions of NbdA

NbdA was first described to induce biofilm dispersion in response to NO presumably via PDE activity (Li *et al.*, 2013). However, in subsequent studies neither a role of NbdA in NO dependent biofilm dispersion nor a regulatory effect of NO on the PDE activity of NbdA was found (Rüger, 2019; Zemke *et al.*, 2020). Transcription of *nbdA* is upregulated by RpoS, a transcription factor for stationary phase and stress response in bacteria (Gerbracht, 2021; Potvin *et al.*, 2008). Furthermore, transcription is inhibited by AmrZ, a transcription factor regulating diverse outputs often associated with motility or virulence (Gerbracht, 2021; Jones *et al.*, 2014) (**Fig. 1.8**).

Deletion of *nbdA* had no effect on c-di-GMP related phenotypes as biofilm formation, swimming, swarming, or twitching motility (Rüger, 2019). Global c-di-GMP levels were also not altered in a *nbdA* deletion strain indicating a local function (Rüger, 2019; Xin *et al.*, 2019). NbdA is able to act as a PDE *in vitro* and in a heterologous host (Li *et al.*, 2013; Rüger, 2019). The regulation of activity is not yet fully understood, but there are indications that iron and heme stimulate the PDE activity of NbdA *in vitro* (Agbadaola, 2023). Overexpression of *nbdA* leads to unexpected phenotypes in PAO1.

While reduced biofilm formation and pellicle formation could be directly linked to the PDE activity, overexpression also resulted in reduced swimming and twitching motility. In addition, overexpression of *nbdA* was demonstrated to lead to growth impairment on solid media and an elongated cell morphology. These phenotypes were related to the presence of the membrane anchored MHYT domain (Gerbracht, 2021; Rehner, 2020; Rüger, 2019).

NbdA was further found to regulate the flagellar motor switch in PAO1 together with the PDEs DipA and RbdA (Xin *et al.*, 2019) (**Fig. 1.8**). The PDE activity is thereby crucial for this effect since the output is mediated by the c-di-GMP effector MapZ. The three PDEs are presumed to be located at the cell pole in the MCPs-constituted chemoreceptor array (Xin *et al.*, 2019). MapZ was previously shown to interact with the chemotaxis methyltransferase CheR1, thus regulating methylation of chemoreceptors and flagellar motor switching (Xu *et al.*, 2016).

Further, NbdA was shown to stimulate rhamnolipid synthesis under prolonged fermentation in the strain KT1115. This phenotype was also directly linked to the PDE activity of NbdA, however the effector was not identified (Liu *et al.*, 2022a).

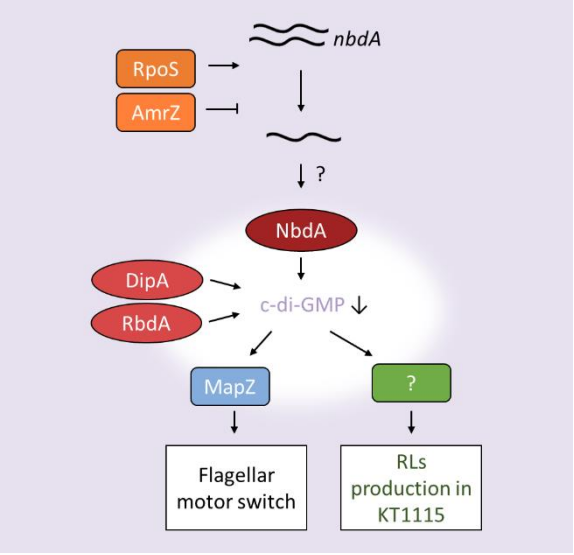

Fig. 1.8 Possible functions of NbdA. Expression of *nbdA* is activated by the stationary phase transcription factor RpoS and inhibited by AmrZ. An additional translational or post-translational regulation of NbdA is proposed (Gerbracht, 2021). In PAO1, NbdA controls together with the PDEs DipA and RbdA a local c-di-GMP pool that influences the MapZ mediated flagella motor switch (Xin *et al.*, 2019). In KT1115, local decrease in c-di-GMP triggers rhamnolipids (RLs) production via an unknown effector (Liu *et al.*, 2022a).

1.5 Objectives of this work

Membrane proteins have a multitude of essential roles for the cell, including molecule transportation across the membrane, energy storage, and environmental signal detection. The membrane proteins often require interaction partners to conduct the intended function in the cell. In particular, for signalling with the second messenger c-di-GMP, protein-protein interactions are considered crucial. Also, in *P. aeruginosa* - a model organism for biofilm formation and infection - several important

signalling proteins as well as the majority of c-di-GMP synthesizing or degrading enzymes are membrane proteins. In the first part of this thesis, membrane proteins in *P. aeruginosa* PAO1 should be investigated in a global approach. Thereby, the membrane proteins are to be solubilised with the rather new technique of the formation of native nanodiscs by using amphiphilic polymers. A native membrane-protein library ought to be created representing the membrane proteome of *P. aeruginosa* PAO1. The library should be characterized by testing for reproducible and stable extraction of membrane proteins, coverage of the membrane proteome, and the capability to detect protein-protein interactions within a lipid-bilayer environment as well as membrane-bound protein complexes. In addition, membrane-associated proteins involved in c-di-GMP signalling and their interaction partners are aimed to be investigated in more detail. To this end, targeted approaches for described protein complexes as well as global analyses should be carried out.

In the second part of the thesis, the membrane-integrated phosphodiesterase NbdA should be investigated for its role in the c-di-GMP network. The current model for c-di-GMP signalling suggests the organisation of local signalling supermodules alongside global factors for specific functions in the cell. It was previously suggested that NbdA rather has a local function than acting on global scale. Therefore, the protein NbdA should be tested for protein-protein interaction partners in *P. aeruginosa* by a pulldown assay following mass spectrometry for novel candidate identification, and by bacterial adenylate cyclase two hybrid (B2H) assay for candidate verification. Moreover, the influence of NbdA on the global c-di-GMP level ought to be measured. Therefore, a markerless deletion mutant and overexpression strains are to be tested. To find out more about the role of the individual domains of NbdA, also global c-di-GMP levels of strains overproducing protein variants should be assayed. In previous studies a possible role of the MHYT domain in cell elongation as well as growth on solid media was observed. To further test for the specificity of these observations, other MHYT domain containing proteins ought to be investigated for similar phenotypes in *P. aeruginosa*. Since previous studies suggested an influence of NbdA overexpression on T4P, also pili formation should be examined in a phage assay and by atomic force microscopy (AFM). Further, to determine whether NbdA is located at the piliated pole, the co-localisation of NbdA with pili components should be tested by confocal laser scanning microscopy (CLSM).

2 Material and methods

2.1 Equipment and materiales

2.1.1 Equipment

Designation, identifier and manufacturer of the utilised devices and lab equipment are listed in Table 2.1. If applicable, the corresponding software was also specified.

Table 2.1: Equipment

Instrument	Name	Company
Agarose gel documentation	GelDoc, Gel IX imaging Darkbox Gel IX Imager Exview HAD CCDTM Camera UV Transilluminator ultra bright 312 nm	Intas
Agarose gel electrophoresis chamber	EasyPhor Mini ComPhor L Mini	Biozym Bioplastics BV
Agarose gel electrophoresis power supply	Electrophoresis Power Supply EPS 301	Amersham pharmacia biotech
	Electrophoresis Power Supply EPS 601	Amersham pharmacia biotech
Atomic force microscope	JPK Nanowizard 3, NanoScience SFM Axio Observer A.1 JPK Acoustic enclosure box	Bruker Zeiss Bruker
Autoklav	VX 150	Systec
Blotting system	SemiDry Blot Trans-Blot® SD	BioRad
Centrifuge	Sorvall Lynx6000 Rotor: F9-6x1000 LEX T29-8x50	ThermoScientific
Electroporation device	MicroPulser Electroporator	BioRad
Fluorescence spectrometer	FP-8300	Jasco
Freeze and dry machine	LSC plus	Christ
HPLC system	Series 1100 Degaser G1322A BinPump G1312A ALS G1330A ALS G1329A ColComp G1316A G1314A Column: Gemini-NX 250 x 4.60 mm Software: Agilent Chem Station	Hewlett Packard Phenomenex Agilent Technologies
Incubation shaker	Innova 2300 Innova® 44 Rocker 3D basic	New Brunswick Scientific New Brunswick Scientific IKA
Incubator	B2600 Kelvitron t B28	Heraeus instruments Heraeus instruments Binder
Light cabinet for pictures	syncroScopy	Synoptics
Magnetic stirer	MR3001 MR2000 MR-Hei-Mix L MR-Hei-Standard	Heidolph Heidolph Heidolph Heidolph

Mass spectrometer	Q Exactive HF™ Mass Spectrometer	Thermo Fisher Scientific
	uHPLC system: EASY-nLC 1200	Thermo Fisher Scientific
	Column: reverse phase 50 cm 75 µm diameter	New Objective
	Material: 1.8 µm ReproSil-Pur 120 C18-AQ particles	Dr. Maisch GmbH
	QTrap 5500 tandem mass spectrometer	AB Sciex,
	HPLC: Agilent 1290	
	binary pump (G4220A), column oven (TCC G1316C) autosampler (G4226A) thermostat (G1330B)	Agilent Technologies
	column: Luna C8, 150x3 mm, 3 µm, reversed phase	Phenomenex,
	TripleTOF® 6600 system	Sciex
	ExionLCTM AD System	Sciex
	Column: Synergi 4 u polar RP 100 × 2 mm	Phenomenex
Microscope	LSM 880, AxioObserver	Zeiss
	Objective: Plan-Apochromat 63x / 1.4 oil DIC M27	
	Software: ZEN 2.3 black, version 14.0.27.201	
Nanodrop	NanoDrop Lite Spectrophotometer	Thermo Scientific
pH meter	PB 11	Sartorius
	pH 50 + DHS	Dostmann Electronic
Photometer	Ultrospec 500 pro	Amersham Biosciences
Plate reader	Infinite® F200 PRO	Tecan
	FLUOstar Omega	BMG Labtech
Refractometer	Abbemat 500	Anton Paar
Rotational vacuum concentrator	RVC 2-25 CD plus	Christ
Scale	Research R300 S	Sartorius
	ATILON	Acculab Sartorius group
	Europe 4000 AR	Giberini
	RS-232	Kern & Sohn GmbH
SDS-PAGE chamber	Mini-PROTEAN Tetra Vertical Electrophoresis Cell	BioRad
	Mini-PROTEAN	BioRad
SDS-PAGE Power supply	PowerPac HC	BioRad
	PowerPac 300	BioRad
Size exclusion chromatography system	Äkta Purifier 10 system	GE Healthcare
	Column: Superose 6 Increase GL 10/300	
Sonicator	Sonoplus	Bandelin
	Electronic UW 220	Bandelin
Sterile bench	Antares	Biohit
Tabletop centrifuge	Centrifuge 5810R	Eppendorf
	Rotor: A-4-62	
	Centrifuge 5415D	Eppendorf
	Rotor: F45-24-11	
	Centrifuge 5425	Eppendorf
	…Rotor: F24	
	BiofugePico	Heraeus Instruments
	Rotor: 3324	
	Z32 HK	Hermle

	Rotor: 221.17 V20	
Thermoblock	Thermomixer compact Thermostat plus	Eppendorf Eppendorf
Thermocycler	T gradient T-personal T1 Thermocycler Peqstar 2	Biometra Biometra Biometra Peqlab
Ultra-centrifuge	Sorvall WX Ultra Series Centrifuge Rotor: T-865 Sorvall Discovery M150SE Rotor: S140-AT	ThermoScientific ThermoScientific
Ultra-low temperature freezer	U725	New Brunswick
Ultra-pure water system	MiliQ® Integral Water Purification System	Merk Milipore
UV-Vis-Spectrometer	8453 UV-Visible System	Agilent
Vacuum pump	Chemistry Hybrid pump RC6 (freeze and dry machine) Laboport (sterile filtration)	Vacuubrand KNF lab
Vortexer	VX100 Zx3	Axon Velp Scientifica

2.1.2 Kits, Enzymes and consumables

Table 2.2 Kits, Enzymes and consumables used in this study

Product	Name	Company
Kits		
Plasmid isolation kit	E.Z.N.A® Plasmid DNA Mini Kit	Omega Bio-Tek
	NucleoSpin® Plasmid Easy Pure	Macherey-Nagel
PCR clean-up kit	Nucleospin® Gel and PCR cleanup	Macherey-Nagel
Genomic DNA isolation kit	NucleoSpin® Microbial DNA	Macherey-Nagel
Protein quantification kit	Pierce™ BCA protein assay kit	Thermo Scientific
Enzymes		
DNAse	DNAseI	AppliChem
Exonuclease	T5 exonuclease (10U/µl)	New England Biolabs
Ligase	*Taq* DNA ligase (10 U/µl)	New England Biolabs
Lysozym	Lysozyme	Roth
Polymerase	Phusion Phusion (2U/µl) *Pfu*	Self-made RPTU New England Biolabs Selfmade RPTU
Buffers for polymerases	5x Phusion HF buffer 5x Phusion GC buffer 10x PCR buffer without $MgCl_2$ 10x *Taq* reaction buffer	New England Biolabs New England Biolabs Sigma Aldrich New England Biolabs
Protease	Trypsin Lys-C	Sigma Aldrich Sigma Aldrich
Restriction enzymes	*Nco*I-HF *Xho*I	New England Biolabs New England Biolabs

	*Sac*I-HF	New England Biolabs
	*Nhe*I-HF	New England Biolabs
	*Dpn*I	New England Biolabs
Buffers for restriction enzymes	CutSmart	New England Biolabs
	rCutSmart (for HF-enzymes)	New England Biolabs
Consumables		
Centricons	Amicon Ultra-4 Ultracel 10k	Merck
Column material	Strep-Tactin®XT 4Flow® beads	IBA Lifesciences
	Strep-Tacin sepharose	IBA Lifesciences
Consumables for HPLC		
Syringe	1 ml syringe	Braun
	1 ml syringe Tbc without needle	Dispomed
Cannula	Sterican 0.60 x 25 mm BL/LB	Braun
Filter	PHENEX PTFE membrane 0.2 µm 4 mm syringe filters	Phenomenex
Glass bottles	ROTILABO screw neck ND8 vials	Roth
Insert for glass bottles	ROTILABO ND8 micro-inserts ND8 0.1 ml borosilicate glass, clear	Roth
Lid for glass bottles	Screw caps with bore holes	Roth
Consumables for microscopy		
Cover slip	Cover slips 24 x 60 mm #1,5	Menzel-Gläser
	Cover slips 24 x 60 mm #2	Epredia
Objective glass plate	76 x 26 mm cutted	Diagonal
Immersion oil	Immersol 518 F	Zeiss
Coomassie stain	Coomassie Brilliant Blue G250	Serva
Cuvettes	Single-use Standard halbmikro 1.6 ml	Hartenstein
Dialysis tube	Servapore dialysis tubing, MWCO 12 000-14 000, diameter 16 mm	Serva
Detergent DDM	Dodecyl-β-d-maltoside	Roth
dNTPs	10 mM dNTP mix	Axon
Electroporation cuvettes	Gene Pulser / MicroPulser 0.2 cm gap, sterile	BioRad
Filter units	Cell culture bottle top filtration unit, full assembly, 0.22 µm, 500 ml, sterile	Starlab
	Nalgene Rapid-Flow 75 mm filter unit, 500 ml	Thermo Scientific
Loading Dye for agarose gels	Purple Loading Dye (6x)	New England Biolabs
Marker proteins for SEC	Blue Dextran	Sigma
	Apoferritin from equine spleen	Sigma
	Alcohol dehydrogenase from *Saccharomyces cerevisiae*	Sigma
	Albumin from chicken egg white	Sigma
	Carbonic anhydrase	Sigma
Markers for agarose gels	GeneRuler 1kb plus	Thermo Scientific
Microtiter plate	96-well-flat bottom	Sarstedt
	96-well flat cellstar	Greiner
	96-well Nunc MicroWell Nunclon flat	ThermoScientific
Petri dishes	Petri dish 92 x 16 mm PS transparent	Sarstedt
Petri dishes square	120 x120 x17 mm PS	Greiner
Polyethylen glycol	PEG 8000	New England Biolabs
Polymer DIBMA	Diisobutylene/maleic acid copolymer	Glycon Biochemicals
Protease inhibitors	cOmplete™ protease inhibitor cocktail, EDTA-free	Roche

Protein markers for SDS-PAGE	Unstained protein Standard, Broad Range (10 - 200 kDa)	New England Biolabs
	Colour Prestained Protein Standard, Broad Range (10 - 250 kDa)	New England Biolabs
	Blue Prestained Protein Standard, Broad Range (11 – 250 kDa)	New England Biolabs
	Prestained Protein Marker	Proteintech
Syringe filters	0.45 µm pore size PVDF (sterile)	Starlab
	0.22 µm pore size PVDF (sterile)	Starlab
Western blot membrane	ROTI transfer membrane PVDF 0.45 x 30 cm	Roth
Whatman paper	0.95 mm	Roth

2.1.3 Strains

The following bacterial strains were used in this study.

Table 2.3 Bacterial strains used in this study

Name	Relevant properties	Reference
E. coli		
BL21 (DE3)	F$^-$ *ompT gal dcm lon hsdS$_B$*($r_B^- m_B^-$) λ(DE3 [*lacI lacUV5-T7p07 ind1 sam7 nin5*]) [*malB*$^+$]$_{K-12}$(λ^S)	Studier *et al.*, 1986
BTH101	F', *cya*-99, *araD*139, *galE*15, *galK*16, *rpsL*1 (Str^R), *hsdR*2, *mcrA*1, *mcrB*1, *relA*1	Battesti *et al.*, 2012; Karimova *et al.*, 2001
DH5α	F$^-$ *endA1*, *glnV44*, *thi-1*, r*ecA1*, *relA1*, *gyrA96*, *deoR*, *nupG*, *purB20* φ80d*lacZ*ΔM15 Δ(*lacZYA- argF*)U169, hsdR17(r_K^- m_K^+), λ$^-$	Hanahan, 1985
S17-1	Tp^r Sm^r *recA*, *thi*, *pro*, *hsdR*$^-$M$^+$ RP4-2-Tc: Mu: Km Tn*7*, λ*pir*	de Lorenzo *et al.*, 1994
P. aeruginosa		
PAO1	Wildtype (WT)	Dunn *et al.*, 1971
Δ*nbdA*	Markerless deletion of *nbdA* (PA3311) in PAO1	Rüger, 2019
Δ*pilA*	Markerless deletion of *pilA* (PA4525) in PAO1, constructed with pASC11	This work
Δ*nbdA* Δ*pilA*	Markerless double mutant of *nbdA* and *pilA*	This work
PAO1::*nbdA*-Flag	3xFlag-tag C-terminally fused to *nbdA* in original *nbdA* gene locus, constructed with pASC06	This work
PAO1::*nbdA*-Strep	Genomic integration of a C-terminal *nbdA*-Strep fusion into the original *nbdA* gene locus	Zehner unpublished (RPTU)
PAO1::*nbdA-mNeonGreen*	Genomic integration of *nbdA-mNeonGreen*-6xHis fusion into the original *nbdA* gene locus	Gerbracht, 2021
PAO1::*nbdA-Venus*	Genomic integration of *nbdA-Venus*-6xHis fusion into the original *nbdA* gene locus	Gerbracht, 2021
PAO1::*pilO*-mCherry	C-terminal mCherry-tag fused to *pilO* (PA5042) in the original gene locus, constructed with pASC27	This work

PAO1::mRuby3-*pilT*	N-terminal mRuby3-tag fused to *pilT* (PA0395) in the original gene locus, constructed with pASC28	This work
PAO1::*nbdA*-Venus::*pilO*-mCherry	C-terminal mCherry-tag fused to *pilO* (PA5042) in the original gene locus, constructed with pASC27, in PAO1::*nbdA*-Venus background	This work
Protein overproduction in *P. aeruginosa*		
Δ*nbdA* pHERD26T	Δ*nbdA* containing pHERD26T, Tet^R	Rüger 2019
Δ*nbdA* pMRP12	Δ*nbdA* containing pMRP12, Tet^R, production of NbdA-Strep (NbdA $_{MHYT\text{-}AGDEF\text{-}EAL}$)	Gerbracht, 2021
Δ*nbdA* pMRP13	Δ*nbdA* containing pMRP13, Tet^R, production of untagged NbdA (NbdA*$_{MHYT\text{-}AGDEF\text{-}EAL}$)	Rüger, 2019
Δ*nbdA* pMRP14	Δ*nbdA* containing pMRP14, Tet^R, production of NbdA $_{MHYT\text{-}AGDEF\text{-}AAL}$	Rüger, 2019
Δ*nbdA* pASC04	Δ*nbdA* containing pASC04, Tet^R, production of NbdA $_{AGDEF\text{-}EAL}$	Gerbracht, 2021
Δ*nbdA* pMKE02	Δ*nbdA* containing pMKE02, Tet^R, production of NbdA $_{AGDEF\text{-}AAL}$	Gerbracht, 2021
Δ*nbdA* pJRE02	Δ*nbdA* containing pJRE02, Tet^R, production of NbdA $_{MHYT\text{-}AGDEF}$	Rehner, 2020 (RPTU)
Δ*nbdA* pJRE01	Δ*nbdA* containing pJRE01, Tet^R, production of NbdA $_{MHYT}$	Rehner, 2020 (RPTU)
Δ*nbdA* pASC19	Δ*nbdA* containing pASC19, Tet^R, production of NbdA $_{AGAAF\text{-}EAL}$	This work
PAO1 pHERD26T	WT containing pHERD26T, Tet^R	Rüger, 2019
PAO1 pMRP12	WT containing pMRP12, Tet^R, production of NbdA $_{MHYT\text{-}AGDEF\text{-}EAL}$	Rüger, 2019
PAO1 pMRP13	WT containing pMRP13, Tet^R, production of untagged NbdA (NbdA*$_{MHYT\text{-}AGDEF\text{-}EAL}$)	Rüger, 2019
PAO1 pASC09	WT containing pASC09, Tet^R, production of MucR-Strep (PA1727)	This work
PAO1 pASC10	WT containing pASC10, Tet^R, production of BifA-Strep (PA4367)	This work
PAO1 pHERD26T-*coxH*-Strep	WT containing pHERD26T-*coxH*-Strep, Tet^R, production of CoxH-Strep	This work
PAO1 pASC20	WT containing pASC20, Tet^R, production of PilB (PA4525)	This work
PAO1 pASC21	WT containing pASC20, Tet^R, production of PilB-Strep (PA4526)	This work
PAO1 pASC23	WT containing pASC23, Tet^R, production of mNeonGreen-6xHis	This work
PAO1 pASC24	WT containing pASC24, Tet^R, production of Venus-6xHis	This work
PAO1 pASC25	WT containing pASC25, Tet^R, production of NbdA-mNeonGreen-6xHis	This work

PAO1 pASC26	WT containing pASC26, Tet^R, production of NbdA-Venus-6xHis	This work
PAO1 pME6032	WT containing pME6032, Tet^R	Karcher, 2021 (RPTU)
PAO1 pASC07	WT containing pASC07, Tet^R, production of NbdA-3xFlag	This work
PAO1::*pilO*-mCherry pASC25	PAO1::*pilO*-mCherry containing pASC25, production of NbdA-mNeonGreen-6xHis	This work
PAO1::*pilO*-mCherry pASC26	PAO1::*pilO*-mCherry containing pASC25, production of NbdA-Venus-6x-His	This work
PAO1::mRuby3-*pilT* pASC25	PAO1::mRuby3-*pilT* containing pASC25, production of NbdA-mNeonGreen-6xHis	This work
PAO1::mRuby3-*pilT* pASC26	PAO1:: mRuby3-*pilT* containing pASC25, production of NbdA-Venus-6xHis	This work
PAO1::*pilO*-mCherry pKGE20	PAO1::*pilO*-mCherry containing pKGE20, production of NbdA-mNeonGreen-6xHis (pME6032 vector)	This work
PAO1::*pilO*-mCherry pKGE21	PAO1::*pilO*-mCherry containing pKGE21, production of NbdA-Venus-6x-His (pME6032 vector)	This work

2.1.4 Plasmids

Plasmids are circular genetic elements, that can be used in biotechnology for various applications. Long-time storage of plasmids was carried out in nuclease-free water at -20 °C. Plasmid names and relevant properties can be obtained from Table 2.4.

Table 2.4 Plasmids used in this study

ID	Name	Properties	Reference
Construction of genomic mutants			
	pEXG2	Allelic exchange vector with pBR origin, *sacB*, Gm^R	Rietsch *et al.*, 2005
pASC11	pEXG2-pilA_del	pEXG2-derivate, truncated version of *pilA* (PA4525) flanked by 358 bp upstream and 388 bp downstream region of original gene locus to generate a markerless *pilA* deletion mutant in *P. aeruginosa*, Gm^R	This work
pASC06	pEXG2-NbdA-Flag-3312	pEXG2-derivate, C-terminal part of *nbdA* (PA3311) coding region with a 3x Flag-tag for integration in *P. aeruginosa*, Gm^R	This work
pASC27	pEXG22-pilO-mCherry	pEXG2-derivate, C-terminal part of *pilO* (PA5042) coding region with a mCherry-tag for integration in *P. aeruginosa*, Gm^R	Koch *et al.*, 2021
pASC28	pEXG2-mRuby3-pilT	pEXG2-derivate, N-terminal part of *pilT* (PA0395) coding region with a mRuby3-tag for integration in *P. aeruginosa*, Gm^R	Koch *et al.*, 2021
pME6032 derivates			
	pME6032	P_{tac}-promoter, low copy number plasmid, Tet^R	Heeb *et al.*, 2002
pASC07	pME6032-NbdA-Flag	pME6032-derivate, coding sequence of *nbdA* with a C-terminal 3xFlag-tag, Tet^R	This work

pKGE20	pME6032-NbdA-mNeonGreen	pME6032-derivate, coding sequence of *nbdA* with a C-terminal mNeonGreen-tag from *Branchiostoma lanceolatum* followed by a C-terminal 6xHis-tag, Tet^R	Gerbracht, 2021
pKGE21	pME6032-NbdA-Venus	pME6032-derivate, coding sequence of NbdA with a C-terminal Venus-tag from *Aequorea victoria* followed by a 6xHis-tag, Tet^R	Gerbracht, 2021
pHERD26T-derivates			
	pHERD26T	Shuttlevector for *E. coli* and *P. aeruginosa*, Tet^R, P_{BAD} promoter	Qiu *et al.*, 2008
	pHERD26T-Strep	pHERD26T-derivate, integrated Strep-tagII between *Nco*I and *Sac*I restriction site, Tet^R	Rehner, 2020 (RPTU)
pASC09	pHERD26T-MucR-Strep	pHERD26T-derivative, coding sequence of *mucR* (PA1727) from PAO1 (genomic DNA) with a C-terminal Strep-tagII, Tet^R	This work
pASC10	pHERD26T-BifA-Strep	pHERD26T-derivative, coding sequence of *bifA* (PA4367) from PAO1 (genomic DNA) with a C-terminal Strep-tagII, Tet^R	This work
	pHERD26T-CoxH-Strep	pHERD26T-derivative, coding sequence of *coxH* from *Oligotropha carboxydovorans*, Tet^R	Haak, unpublished (RPTU)
pMRP12	pHERD26T-NbdA-Strep	pHERD26T-derivative, coding sequence of *nbdA* (PA3311) with C-terminal Strep-tagII, Tet^R	Rüger, 2019
pMRP13	pHERD26T-NbdA	pHERD26T-derivative, coding sequence of *nbdA*, Tet^R	Rüger, 2019
pJRE01	pHERD26T-MHYT-Strep	pHERD26T-derivative, coding sequence of the MHYT-domain of *nbdA* with a C-terminal Strep-tagII, Tet^R	Rehner, 2020 (RPTU)
pJRE02	pHERD26T-MHYT-AGDEF-Strep	pHERD26T-derivative, coding sequence of the MHYT- and AGDEF-domain of *nbdA* with a C-terminal Strep-tagII, Tet^R	Rehner, 2020 (RPTU)
pMRP14	pHERD26T-NbdA-MHYT-AGDEF-AAL-Strep	pHERD26T-derivative, coding sequence of *nbdA*, amino acid exchange E494A*, C-terminal Strep-tagII, Tet^R	Rüger, 2019
pASC04	pHERD26T-AGDEF-EAL-Strep	pHERD26T-derivative, coding sequence of *nbdA* AGDEF and EAL domain starting at E266* with a C-terminal Strep-tagII, Tet^R	Scherhag, 2019 (RPTU)
pMKE02	pHERD26T-AGDEF-AAL-Strep	pHERD26T-derivative, coding sequence of *nbdA* AGDEF and EAL domain starting at E266*, amino acid exchange E494A*, C-terminal Strep-tagII, Tet^R	Karcher, unpublished (RPTU)
pASC19	pHERD26T-AGAAF-EAL-Strep	pHERD26T-NbdA-AGDEF-AAL-derivate, amino acid exchange D369A* and E370A*, Tet^R	This work
pASC20	pHERD26T-PilB	pHERD26T-derivate, coding sequence of *pilB* (PA4526) from PAO1 (genomic DNA), Tet^R	This work

pASC21	pHERD26T-PilB-Strep	pHERD26T-derivate, coding sequence of *pilB* (PA4526) from PAO1 (genomic DNA) with a C-terminal Strep-tagII, Tet^R	This work
pASC22	pHERD26T-BifA	pHERD26T-derivate, coding sequence of *bifA* (PA4367) from PAO1 (genomic DNA), Tet^R	This work
pASC23	pHERD26T-mNeonGreen	pHERD26T-derivate, coding sequence of mNeonGreen-tag with a C-terminal 6xHis-tag, Tet^R	This work
pASC24	pHERD26T-Venus	pHERD26T-derivate, coding sequence of Venus-tag with a C-terminal 6xHis-tag, Tet^R	This work
pASC25	pHERD26T-NbdA-mNeonGreen	pHERD26T-derivate, coding sequence of *nbdA* with a C-terminal mNeonGreen-tag and a 6xHis-tag, Tet^R	This work
pASC26	pHERD26T-NbdA-Venus	pHERD26T-derivate, coding sequence of *nbdA* with a C-terminal Venus-tag and a 6xHis-tag, Tet^R	This work
Plasmids for B2H analysis			
	pUT18	B2H-vector, coding sequence of the T18-fragment of *cyaA* catalytic domain, *lac*-promoter, Amp^R	Karimova *et al.*, 2001
	pUT18C-zip	N-terminal T18, leucine zipper of GCN4, Amp^R, positive control for B2H	Karimova *et al.*, 2001
	pUT18C-AGDEF-EAL	N-terminal T18, coding sequence of *nbdA* AGDEF-EAL domain, Amp^R	Beganovic, 2018 (RPTU)
pASC13	pUT18C-pilA	N-terminal T18, coding sequence of *pilA* (PA4525), Amp^R	Unbehend, 2022 (RPTU)
pASC14	pUT18-pilB	C-terminal T18, coding sequence of *pilB* (PA4526), Amp^R	Unbehend, 2022 (RPTU)
pASC30	pUT18-fleQ	C-terminal T18, coding sequence of *fleQ* (PA1097), Amp^R	Scherhag *et al.*, 2023
pASC31	pUT18-czcR	C-terminal T18, coding sequence of *czcR* (PA2523), Amp^R	Scherhag *et al.*, 2023
pASC32	pUT18-PA4200	C-terminal T18, coding sequence of PA4200, Amp^R	Scherhag *et al.*, 2023
	pUT18-sadC	C-terminal T18, coding sequence of *sadC* (PA4332), Amp^R	Beganovic, 2018 (RPTU)
	p25N	B2H-vector, coding sequence of the T25-fragment of *cyaA* catalytic domain, *lac*-promoter, Kan^R	Claessen *et al.*, 2008
	pKT25-zip	N-terminal T25, leucine zipper of GCN4, Kan^R, positive control for B2H	Karimova *et al.*, 2001
	p25N-nbdA	C-terminal T25, coding sequence of *nbdA* (PA3311), Kan^R	Beganovic, 2018 (RPTU)
pASC17	p25N-MHYT	C-terminal T25, coding sequence of *nbdA* MHYT domain, Kan^R	Unbehend, 2022 (RPTU)
	p25N-AGDEF-EAL	C-terminal T25, coding sequence of *nbdA* AGDEF-EAL domain, Kan^R	Beganovic, 2018 (RPTU)

*amino acid (aa) position from the new annotation by RPTU, resulting in a 726 aa protein.

2.1.5 Primers

Primers are short oligonucleotides that can be used for amplifying DNA e. g. for cloning or examination of strains. They were ordered at Eurofins genomics (Ebersberg, Germany), in salt-free lyophilised form and stored at -20 °C in nuclease-free water. Primers for Gibson assembly were designed with the NEBuilder Assembly Tool (version 2.8.1, New England Biolabs). Primer sequences can be obtained from Table 2.5.

Table 2.5 Primers used in this study

Primer name	Sequence 5'→3'
Construction of *pilA* deletion mutant	
UpF_pilA_short_fwd	agctcgagcccggggatcctGGTGCGTCACCAGCGACA
UpR_5711_laventie	CACAACCTTTCGGAGTGAACATGATCAAGGTAAAGCCTTTTTGAGC
DownF_5712_laventie	GCTCAAAAAGGCTTTACCTTGATCATGTTCACTCCGAAAGGTTGTG
DownR_pilA_short_rev	caagcttctgcaggtcgactCTCAGCCTGGACGACATGC
Classic cloning	
nbdA_for (KpnI)	ATCCGGGGTACCCGGTCAACTGCTGCGCCA
C3FLAG_rev (XhoI)	ATCACTCGAGTCAGTCACTCATTTATCGTCGTCATCTTTGT
Gibson assembly	
Nbda-Flag_fwd	tgccatggtacccgggagcttCATTTATCGTCGTCATCTTTGTAG
Nbda-Flag_rev (Fragment_2_rev)	caggaaacagaattcgagctATGGATTGGCAAGGCCTG
mucR_for	aagaaggagatatacataccATGCTTATCAGCAGCTACAACCAGGTTCTTG
mucR_rev	tttcgaactgcgggtggctcCATGCGGCGACGCTGGCGAG
bifA_for	aagaaggagatatacataccATGAAACTGGACTCCCGACACAG
bifA_rev	tttcgaactgcgggtggctcCATGCGGGCCGTTCGCTG
pH_pilB_for	aagaaggagatatacataccATGAACGACAGCATCCAAC
pH-pilB-rev	tttcgaactgcgggtggctcTTAATCCTTGGTCACGCG
pHS-PilB_rev	tttcgaactgcgggtggctcCATGCATCCTTGGTCACGCG
Neon/Venus_for	aagaaggagatatacataccATGGTGAGCAAGGGCGAG
Nbda_ÜE_MR_for #2630	tttaagaaggagatatacataccATGGATTGGCAAGGCCTG
pHERD_His_rev	tttcgaactgcgggtggctcCTAGTGATGATGGTGATGGTGC
Site directed mutagenesis	
QC_AGDEF_to_ AGAAF_for	GCGCTTCGCCGGCGCCGCGTTCTGCGTGCTAGCCGACCTCACCC
QC_AGDEF_to_ AGAAF_rev	GGGTGAGGTCGGCTAGCACGCAGAACGCGGCGCCGGCGAAGCGC
Sequencing primers	
seq_pilA_del	CTTTTCGCTGATGGCGTCCCGCGG
#503	GCGGATCCGAAAGCGGCAGCCTGGCGATC
NbdA_EcoRI_for	GATCGAATTCAATCTCGGCCGGGCCAGC
pEXG2_seq_rev	GTTCGCTCGCGTATCGGTGATTCATTCTG
pEXG2_seq_for	CGACCTCATTCTATTAGACTCTCGTTTGGATTGC
pME6032_seq_F	CAGTTGCAAACCCTCACTGA
#2605 ptac_seq	GAGCGGATAACAATTTCACACAG

seq_pBAD3	TTAGCGGATCCTACCTGACGC
#130_pBAD_fwd	ATGCCATAGCATTTTTATCC
M13_for	GTAAAACGACGGCCAGT
seq_pHERD_for	CTCTTCGCTATTACGCCAGC
pilO_seq_for	GCTCAGCTCGAACAGCAGG
pilO_seq_rev	TCTCCGTCAGGAACGATTTCG
pilT_seq_for	CGATGAAGTGCCAGTTCAAGG
pilT_seq_rev	CGTGGACGAATTCGATCGG

2.2 Molecular methods

2.2.1 Determination of DNA concentration

The concentration of extracted DNA was determined spectroscopically as nuclidic acids absorb light at 260 nm. The concentration of DNA was measured at the NanoDrop Lite Spectrophotometer (ThermoScientific). The purity of the DNA was determined by the ratio A260/A280, which should be above 1.8. Alternatively, the DNA concentration was estimated in an agarose gel (2.2.5) by comparison to the intensity of different marker signals.

2.2.2 Isolation of genomic DNA

Genomic DNA was isolated with a genomic DNA isolation kit (NucleoSpin® Microbial DNA by Macherey-Nagel) according to manufacturer's recommendations (Table 2.2). Cell lysis was carried out on a test tube vortexer (Zx3 by Velp Scientifica) for 15-20 min. The DNA was eluted in sterile ultra-pure water. Genomic DNA was stored at -20 °C.

2.2.3 Preparation of plasmid-DNA

Plasmids were isolated from *E. coli* DH5α or S17-1 containing the desired plasmid with a plasmid extraction kit according to the manufacturer's recommendations (Table 2.2). Plasmids were eluted in 30-50 µl ultra-pure water and stored at -20 °C.

2.2.4 Polymerase chain reaction

The polymerase chain reaction (PCR) can be used to amplify DNA fragments. A PCR consits of three phases that are repeated several times. After each cycle, the amount of the DNA fragment is doubled. The first step is the denaturation. Thereby, the DNA is denatured at 95 °C where the hydrogen bonds between the bases dissolve and the double helix separates in two individual strands. This is followed by the annealing step, the binding of specific primers to the DNA at temperatures of between 50 °C and 70 °C, dependent on the primers melting temperature. Subsequently, the elongation step is carried out. Thereby, a heat-stable polymerase generates a complementary strand to the DNA segment flanked by primers. This procedure was repeated 35-times to ensure a high yield of DNA fragments.

Manufacturers of components can be obtained from Table 2.2, 2.4 and 2.5. The respective PCR programme is shown in Table 2.6.

Standard PCR mixture with *Pfu*-polymerase:	final concentration
1 µl template DNA (10-100 ng)	0.2-2 ng/µl
5 µl 10x PCR Buffer without $MgCl_2$	1x
5 µl $MgSO_4$ (100 mM)	10 mM
1 µl dNTPs (10 mM)	200 µM
2,5 µl DMSO (100%)	5 %
1 µl Primer for (20 µM)	0.4 µM
1 µl Primer rev (20 µM)	0.4 µM
1 µl *Pfu*-polymerase (selfmade)	
ad 50 µl with H_2O	

Standard PCR mixture with *Phusion*-polymerase:	final concentration
1 µl template DNA (10-100 ng)	0.2-2 ng/µl
10 µl 5x Phusion HF-buffer (NEB)	1x
1 µl dNTPs (10 mM)	200 µM
2,5 µl DMSO (100 %)	5 %
1 µl Primer for (20 µM)	0.4 µM
1 µl Primer rev (20 µM)	0.4 µM
1 µl *Phusion*-polymerase (selfmade)	
ad 50 µl with H_2O	

Table 2.6 Standard PCR program. (*) annealing temperature was adjusted dependent on the primer melting temperature.

Step	Duration	Temperature	
Primary denaturation	2 min	95 °C	
Denaturation	30 s	95 °C	35 cycles
Annealing	30 s	58 °C-72 °C*	
Elongation	30 s/kb	72 °C	
Final elongation	7 min	72 °C	
Storage	-	4 °C	

Alternatively to purified DNA, plasmid DNA from a bacterial colony could be used as a template for PCR. In a so-called colony-PCR, a single colony was picked from an agar plate with a toothpick and resuspended in 10 µl sterile distilled water. 1 µl of the suspension was used as template. The primary denaturation was extended to 10 min to lyse the cells. This method was mainly used for the rapid screening of potential clones e. g. after gibson cloning.

2.2.5 Agarose gel electrophoresis

Gel electrophoresis was performed to separate DNA according to fragment size. Since DNA has a negative overall charge due to the phosphate residues, it migrates towards the anode when voltage is applied. Small DNA fragments can move faster through the meshes of an agarose gel than large fragments. For a gel, 0.8 % (w/v) agarose was dissolved in 1x TAE buffer by heating. The DNA samples were mixed with 6x Loading Dye (Table 2.2) and then inserted in the gel pockets. A marker was used as a reference (Table 2.2). The gels were run at 120 V for 45-60 min. Subsequently, the DNA in the gel was stained in an ethidium bromide bath for about 15 min. Ethidium bromide is a dye that can incorporate into DNA leading to fluorescence when exposed to UV light. Gels were examined in the GelDoc station (Table 2.1).

50x TAE buffer pH 8
40 mM Tris / acetate
1 mM EDTA

2.2.6 Restriction digest

Restriction enzymes recognise a specific DNA sequence and cut the DNA in a defined region. To digest a DNA fragment, 100-200 ng DNA was mixed with 1 µl restriction enzyme and corresponding buffer (Table 2.2) in a total volume of 10-50 µl. The samples were incubated for 20 min at 37 °C. The reaction was stopped at 80 °C for 10 min. Restriction digest was checked by agarose gel electrophoresis for expected fragement sizes.

2.2.7 Clean-up of DNA fragments

After a PCR or a restriction digest, DNA was cleaned-up to remove residual primers, enzymes or ions that could otherwise interfere with downstream processes. The clean-up was carried out with a kit (Table 2.2) according to the manufactureres recommendations. DNA was eluted in distilled water and stored at -20 °C.

2.2.8 Gibson cloning

In a Gibson assembly, several DNA fragments can be ligated in a single reaction by matching overhangs (Gibson *et al.*, 2009). The overlapping regions of individual DNA fragments were 20-40 bp long. In the Gibson assembly reaction, a T5 exonuclease removes the 5'-ends of the DNA. The thereby created phosphorylated overhangs attach to each other by basepair matching. The included DNA ligase joins the fragments at the phosphate backbone and a DNA polymerase fills in the gaps. These overlapping regions were introduced to the respective fragment by designed primers in a PCR. Vectors were linearised with appropriate restriction enzymes (2.2.6). Then 50-70 ng of the vector, and a 3-fold molar excess of fragments were pipetted into a final volume of 5 µl. The ratio was calculated with the NEBioCalculator tool (version 1.15.4, New England Biolabs). Subsequently, 15 µl of Gibson assembly mix was added, mixed by pipetting and the sample was incubated at 50 °C

for one hour. Then, the plasmids were transformed into competent *E. coli* DH5α cells (2.3.2) and checked for correctness by colony-PCR (2.2.4) or toothpick minipreparation (2.2.9). From positive candidates plasmids were isolated (2.2.3) and verified by sequencing (2.2.10).

5x isothermal reaction buffer:
25 % (w/v) PEG 8000
500 mM Tris HCl
50 mM $MgCl_2$
50 mM DTT
50 mM NAD
1 mM each dNTP (dATP, dGTP, dCTP, dTTP)

Gibson assembly mix:
320 µl 5 x isothermal reaction buffer
0,64 µl T5 exonuclease (10 U/µl)
20 µl Phusion DNA polymerase (2 U/µl)
160 µl *Taq* DNA ligase (40 U/µl)
99,36 µl H_2O

2.2.9 Analysis of plasmid DNA with toothpick minipreparation

With the toothpick minipreparation method, plasmid DNA was isolated from cultures for the screening for a desired plasmid size e. g. after Gibson assembly (2.2.7). A colony was picked from an agar plate with a toothpick and resuspended in 50 µl EDTA solution (10 mM). 50 µl fresh NSS solution was added, and the samples were mixed by vortexing. The tubes were incubated for 5 min at 70 °C. Afterwards, 1.5 µl KCl solution (4 M) was added followed by 5 min incubation on ice. Samples were centrifuged for 3 min at 13 000 rpm and the supernatant was transferred in a fresh test tube. 12 µl of the supernatant were mixed with 3 µl Loading dye and loaded on an agarose gel (section 2.2.5). The empty vector was used as a control.

NSS solution
0.2 M NaOH
0.5 % (w/v) SDS
20 % (w/v) saccharose

2.2.10 Sequencing

The correctness of vectors or DNA fragments was verified by sequencing. For this purpose, a sample containing 400-500 ng template DNA and an associated primer (final concentration 2.5 µM) was prepared in a total volume of 10 µl. The sequencing was carried out by the company Eurofins Genomics (Ebersberg, Germany) using the Sanger method.

2.2.11 QuikChange mutagenesis

With a QuikChange mutagenesis, single amino acids in plasmids can be exchanged. Primers were created with the intention of exchanging the necessary amino acid with the least amount of base modifications. If suitable, integration of a silent site was chosen with ApE plasmid editor software (version 3.1.3, ©2003-2022 by M. Wayne Davis). The primers were designed to have a length between 25 and 45 bp with a melting temperature of about 78 °C and the exchange roughly in the middle of the sequence. Base sequence of primers can be obatined from Table 2.5. To exchange singel

amino acids, the desired plasmid is first isolated from *E. coli* (2.2.3). A standard PCR is pipetted as described in 2.2.4, using the the *Phusion* polymerase. The desired plasmid was deployed as template, while the specific QuikChange primers introduce the mutation during amplification. The settings for the PCR program for a QuikChange PCR can be obtained in Table 2.7. After the PCR, the template plasmid is degraded in a restriction digest with *Dpn*I, an enzyme that specifically cuts methylated DNA derived from *dam*$^+$ cells (Mierzejewska *et al.*, 2014; Shenoy *et al.*, 2003). Therefore, 1 µl of the enzyme *Dpn*I was added to the reaction mixture and was further incubated for 1 h at 37 °C. The digestion was stopped by heating at 80 °C for 20 min. 10 µl of the cooled mixture was transformed into competent *E. coli* DH5α cells (2.3.2, 2.3.3) and tested for correctness by restriction digest (2.2.6) and sequencing (2.2.10).

Table 2.7 PCR program for QuikChange mutagenesis

Step	Duration	Temperature	
Primary denaturation	30 s	95 °C	
Denaturation	30 s	95 °C	18 cycles
Annealing	1 min	60 °C	
Elongation	1 min/kb	68 °C	
Final elongation	5 min	68 °C	
Storage	--	4 °C	

2.2.12 Splicing by overlap extention PCR

The method from Hmelo *et al.*, 2015 was deployed to generate an integration vector for markerless deletion or insertion mutants in *P. aeruginosa*. The mutant alleles were thereby generated *in vitro* by overlap extention PCR and are subsequently cloned in the target vecotor. To facilitate crossover the mutant allel is flanked by regions of homology to the chromosome upstream and downstream. In the first step, the upstream and downstream regions are amplified seperately by PCR with specific primers, that indroduce desired overhangs for integration in the target vector or for the generation of the mutant allel. The primers for the overlap extention PCR were designed according to Hmelo *et al.*, 2015 and sequences can be obtained from Table 2.5. The upstream fragment was generated with the Up-F and Up-R primer, whereas the downstream fragment was generated with the Down-F and Down-R primer pair. Fragments were checked for purity and expected length by agarose gel electrophoresis (2.2.5). A clean-up was carried out to remove residual primers or contaminants (2.2.7). In a second PCR, the two fragments for upstream and downstream regions are combined with the help of specific overhangs that were introduced through the primers resulting in a truncated ORF of the target gene. In this step, the primers Up-F and Down-R were utilised. The generated mutant allel was further cloned in the target vector by Gibson assembly (2.2.8).

2.3 Microbiological methods

2.3.1 Cultivation of *E. coli* and *P. aeruginosa* cells

Granulated media were dissolved in ultra-pure water according to the manufacturers instructions. Media were sterilised by autoclaving at 121 °C for 15-20 min. Composition of utilised media can be found in Table 2.8. If not stated otherwise, cells were cultured in sterile LB medium. Pseudomonas isolation agar was used to isolate *P. aeruginosa* after conjugation (2.3.5). MacConkey Agar was used for B2H analysis (2.3.7). If applicable, antibiotics or sugars were added to the media. Heat-sensitive solutions were sterile filtered with membrane filters (pore diameter 0.2 µm) and added to the media after autoclaving. Concentrations of the antibiotics or additives can be taken from Table 2.9.

Table 2.8 Media for cultivation of microorganisms

Media	Composition		Company
LB medium (Lurina/Miller)	10 g/l	tryptone	Roth
	10 g/l	NaCl	
	5 g/l	yeast extract	
		pH 7.0 ± 0.2	
LB agar (Lurina/Miller)	10 g/l	tryptone	Roth
	10 g/l	NaCl	
	5 g/l	yeast extract	
	15 g/l	agar	
		pH 7.0 ± 0.2	
Difco™ Pseudomonas isolation agar (PIA)	20 g/l	peptones (bacto)	Becton Dickinson
	1.4 g/l	magnesium chroride	
	10 g/l	potassium sulfate	
	0.025 g/l	Irgasan	
	13.5 g/l	agar	
	20 ml/l	glycerin	
		pH 7.0 ± 0.2	
MacConkey agar	17 g/l	peptones (gelatin)	AppliChem
	10 g/l	lactose	
	5 g/l	NaCl	
	3 g/l	peptones (meat and casein):	
	1.5 g/l	bile salts	
	0.03 g/l	Neutral red	
	0.001 g/l	crystal violett	
	13.5 g/l	agar	
		pH: 7.1 ± 0.2	

Cultivation of cells was carried out either on solid media or in liquid culture. For solid media, plates were casted in sterile petri dishes. Cells were either applied with a sterile inoculation loop or a drigalsky spatula. Plates were incubated for 16 h at 37 °C. Glasware for inoculation of cultures were sterilized by dry heat (180 °C for 3 h). For a liquid preculture, LB medium was filled in a sterile test tube or erlenmeyer flask and supplemented with antibiotic if nessessary. Single colonies were picked with a sterile toothpick from an agar plate and added to the medium. The preculture was incubated

for 16 hours at 37 °C and 160 rpm shaking. Long term storage of bacteria was carried out at -80 °C. For *E. coli*, 600 µl of a liquid culture was mixed with 400 µl sterile glycerol, whereas 925 µl liquid culture of *P. aeruginosa* was supplemented with 75 µl sterile DMSO before freezing.

Table 2.9 Antibiotics and media supplements

Antibiotic	**Stock solution (mg/ml)**	**Diluent**	**Final concentration (µg/ml)**	
			E. coli	*P. aeruginosa*
Ampcilin (Amp)	100	water	100	-
Gentamycin (Gm)	100	water	10	300
Kanamycin (Kan)	50	water	50	-
Tetracycline (Tet)	50	70 % ethanol	5	150
Supplement	**Stock solution**		**Final concentration**	
IPTG	400 mM	water	100 µM	
L(+) arabinose	20 % (w/v)	water	0.1 % (w/v)	
Maltose	20 % (w/v)	water	1 % (w/v)	
Sucrose	50 % (w/v)	water	15 % (w/v)	

To determine the cell density of a liquid cultures, the optical density (OD) was measured at a wavelength of $\lambda = 600$ nm in a photometer. This method is based on the assumption that a higher bacterial density leads to more scattering of light. An $OD_{600} = 0.1$ corresponds to a cell density of about $2*10^7$ cells per ml. Samples with a high density e. g. cultures with an $OD_{600} > 1$ were diluted in fresh media and the OD_{600} of the original culture was calculated by multiplication with the dilution factor. A cuvette with LB medium served as a reference.

2.3.2 Chemical competent *E. coli* cells

Competence is the ability of cells to take up DNA from their environment. Competent *E. coli* cells were prepared using the following chemical procedure: First, 500 µl of a preculture was added to 50 ml fresh LB medium. The culture was incubated at 37 °C shaking until it reached an OD_{600} between 0.5 and 0.6. Then, cells were centrifuged at 3094 x g for 10 min and 4 °C. The cell pellet was resuspended in 50 ml sterile $CaCl_2$ solution (50 mM) and incubated on ice for 1 h. After a second centrifugation step, the pellet was resuspended in 2.5 ml sterile $CaCl_2$ solution (50 mM) supplemented with 15 % (v/v) glycerol. Finally, 200 µl of resuspended cell solution were aliquoted into test tubes, shock frozen in liquid nitrogen and stored at -80 °C.

2.3.3 Transformation of chemical competent *E.coli* cells

The process of competent cells taking up DNA from the environment is called transformation. To facilitate the uptake of plasmid DNA in *E. coli* cells, the cells were heat shocked. Either 15 µl Gibson assembly mix or 80-100 ng purified plasmid was added to 200 µl of thawed, competent *E. coli* cells and incubated on ice for 20 min. This was followed by a heat shock at 42 °C for 2 min, during which

the cells took up the plasmid. Then 700 µl LB medium was added and cultures were incubated for 1 h at 37 °C and 160 rpm. The cells were centrifuged for 5 min at 5000 rpm (Centrifuge 5415D from Eppendorf), the pellet was dissolved in 100 µl medium and the entire volume was plated out onto selective agar plates. Incubation took place over night (~16 h) at 37 °C. In case that two plasmids were transformed at the same time, the antibiotic concentration of selective agar plates was halfed.

2.3.4 Electroporation of *P. aeruginosa* cells

To introduce plasmids in *P. aeruginosa* cells, an electroporation of electrocompetent cells was carried out. First, 3 ml *P. aeruginosa* preculture was spun down with 8000 x g for 2 min at 4 °C. The cell pellet was washed twice in 1 ml ice-cold sucrose solution (0.3 M) and resuspended in 200 µl sucrose solution. 500 ng plasmid DNA was added to electrocompetent *P. aeruginosa* cells. Mixtures were transferred into precooled electroporation cuvettes (BioRad, Table 2.2) and cells were electroporated at 2.5 kV with 200 Ω and 25 µF (Program "Ec2" in the electroporation device MicroPulser by BioRad, 2.1.1). Preheated LB medium was added immediately, and cells were transferred to a test tube and regenerated for 2 h at 37 °C and 160 rpm shaking. Afterwards, cells were plated on selective LB agar plates and incubated for 24 h at 37 °C. Single colonies were restreaked at selective agar plates and protein production was tested by westerblot analysis (2.4.11).

2.3.5 Diparental mating of *P. aeruginosa* cells

Plasmids can be transferred in *P aeruginosa* via diparental mating with a donor strain carrying the desired plasmid. In this work, *E. coli* S17-1 was used as donor strain (Table 2.3). A preculture of the donor strain carrying the desired plasmid, and the recipient strain was prepared. The two strains were mixed 9:1 (donor:recipient) in a volume of 2 ml and incubated for 30 min at room temperature. Cells were spinned down at 4000 rpm for 1 min at RT (Centrifuge 5415D by Eppendorf), and the pellet was resuspended in 100 µl LB medium. The bacteria suspension was dropped on a LB plate and incubated for 24 h at 37 °C. Bacteria were subsequently scratched from the plate and resuspended in 1 ml sterile 0.9 % (w/v) NaCl-solution. A dilution series up to 10^{-7} was pipetted and 100 µl of each dilution was plated on selective PIA plates containing the appropiate antibiotic (2.3.1). The plates were incubated over night at 37 °C. Single colonies were restreaked on selective PIA plates twice to ensure elimination of the donor strain.

2.3.6 Generating markerless mutants in *P. aeruginosa*

Markerless mutants were generated with two-step allelic exchange according to Hmelo *et al.*, 2015. The mutant allel was created with splicing by overlapp extention PCR (2.2.12) and cloned in the integration vector by Gibson assembly (2.2.8). The integration vector carries a ColE1 origin of replication and therefore cannot be replicated in *P. aeruginosa*. The vector further carries an antibiotic marker, and a suicide gene for counter-selection (Hmelo *et al.*, 2015). The integration vector was introduced in *P. aeruginosa* by diparental mating (2.3.5) and cells were plated on selective agar plates.

As the vector cannot replicate in *P. aeruginosa*, a site-specific chromosomal integration event or single cross-over must occur to obtain resistance to the antibiotic. Thereby a merodiploid cell is generated. In a secound homologous recombination event, the vector backbone can be excised from the chromosome, generating the mutant allel. These double-crossover mutants are counter-selected by selection for the loss of a conditional suicide gene. In this work, the letal gene was *sacB* from *B. subtilis* that encodes a levansucrase. Addition of sucrose to the growth medium induces formation of toxic polysaccarides (Pelicic *et al.*, 1996). For the counter-selection, 10 potential clones were picked from PIA plates containing antibiotic and inoculated on LB agar plates at 37 °C. The 10 clones were subsequenly restreaked on LB agar plates wirh 15 % sucrose. Plates were incubated for 24 h at 37 °C and again restreaked on LB agar with sucrose. On these plates, either the double-crossover mutants, or the cells that reverted to wildtype are able to grow. Alternatively, loss of function mutation in the *sacB* gene could lead to sucrose resistant meroploid mutnts. These mutants however would still be carry the antibiotic marker. To select for antibiotic sensitive mutants, 10 potential clones were streaked out on LB agar plates, LB agar plates with sucrose and LB agar plates containing antibiotic. After incubation at 37 °C for 24 h, antibiotic sensitive clones were screened by colony-PCR (2.2.4). The wildtype served as a control. Positive fragments were controlled by sequenzing (2.2.10).

2.3.7 Bacterial adenylate cyclase two hybrid (B2H) assay

The interaction of two target proteins was tested using a bacterial adenylate cyclase two hybrid (B2H) assay. Thereby the adenylate cyclase from *B. pertussis* is used as a reporter. The protein can be split in two subunits: T18 and T25. Each subunit is genetically fused to a gene encoding a target protein. If the two target proteins interact with each other, the adenylate cyclase activity is restored, resulting in cAMP production. The production of cAMP can be monitored by reporter gene expression. In this work, the decrease in pH when activating the *lac*-operon through the CAP/cAMP complex was monitored on MacConkey agar plates, that contain the pH indicator neutral red. The B2H protein-protein interaction assays were carried out as previously described (Claessen *et al.*, 2008; Karimova *et al.*, 1998; Ouellette *et al.*, 2017). Competent *E. coli* BTH101 cells were produced as described in 2.3.2 and each batch was checked for susceptibility towards ampicillin and kanamycin, and for formation of colourless/yellow colonies on MacConkey agar. The competent BTH101 cells were co-transformed with one plasmid carrying the T25 subunit fused to a target gene and a second plasmid carrying the T18 subunit fused to a target gene (Table 2.4). For each interaction test, empty vector controls were also included. 4-5 single colonies were resuspended in 50 µl LB medium and 5 µl were dropped on MacConkey agar plates supplemented with 0.5 mM IPTG, 50 µg/ml kanamycin and 100 µg/ml ampicillin and incubated for 24 hours at 30 °C followed by 24 hours at room temperature. A positive interaction results in red colonies. Pictures were taken in a light cabinet.

2.4 Proteinbiochemical Methods

2.4.1 Production of proteins in *P. aeruginosa*

Protein production in *P. aeruginosa* PAO1 was carried out in liquid LB medium in baffled erlenmeyer flasks. For the cultivation of the wildtype, the OD_{600} was initially set to 0.01 from a preculture (2.3.1) in LB medium. The culture was incubated at 37 °C and 100 rpm for 7 hours to stationary phase. Cells were harvested by centrifugation at 17 500 x g for 15 min. Cell pellets were stored at -20 °C.

2.4.2 Homologous overproduction of proteins in *P. aeruginosa*

For the homologous overexpression of genes in *P. aeruginosa*, a strain carrying an expression vector for production of the target protein (Table 2.3) was grown in LB medium supplemented with appropriate antibiotic (2.3.1). The OD_{600} was initially set to 0.05 from a preculture in LB medium containing antibiotic. Cultures were grown at 37 °C and 100 rpm shaking. When cells reached OD_{600} = 0.5, gene expression was induced with arabinose or IPTG for pHERD26T- or pME6032-derivates, respectively. The cells were further grown for 5 hours at 37 °C (stationary phase). In the case of a subsequent affinity purification, the cells were alternatively incubated at 17 °C for 16 h. Cells were harvested at 17 500 x g for 15 min, and pellets were stored at -20 °C.

2.4.3 Isolation of bacterial membranes

Cell pellets were thawed at 4 °C and lysis buffer with protease inhibitor mix (Roche, 2.1.2) was added in a ratio 1:2 gram per cell wet weight. Subsequently, cells were treated with lysozyme and DNAseI for 20 min on ice. Cell disruption was performed by sonication for 3 min total, with 20 s pulse intervals followed by 30 s cooling. The crude extract was centrifuged for 15 min at 7000 x g at 4 °C. The supernatant was further used. Membranes were isolated by ultracentrifugation at 100 000 x g for 1 hour at 4 °C. Membrane pellets were resuspended in solubilization buffer to 200 mg/ml membrane wet weight.

Lysis buffer pH 8
50 mM Tris / HCl
300 mM NaCl

2.4.4 Preparation of polymer stocks

Polymer stocks were prepared by dialyzing 10 % (w/v) diisobutylene/maleic acid polymer (DIBMA) in solubilization buffer in 300-fold volume twice for 36 h (membrane: MWCO 3.5 kDa). Polymer solutions were filtered (0.45 µm pore size), and concentration was measured using an Abbemat 500 refractometer (Anton Paar, Graz, Austria) as previously described (Grethen *et al.*, 2017).

2.4.5 Solubilisation efficiency test

With the solubilization efficiency test, the required concentration of detergent or polymer for the solubilisation of *P. aeruginosa* membrane proteins was determined (**Fig. 2.1**). Therefore, *P. aeruginosa* PAO1 cells were cultivated as described in 2.4.1, and membranes were isolated (2.4.3). DIBMA polymer stocks were prepared as described (2.4.4). The solubilisation test was carried out using 40 mg/ml membrane wet weight and different DIBMA or DDM concentrations between 0.2 % and 4.64 % (w/v). This corresponds to a ratio of polymer/detergent to membrane ($R_{polymer/membrane,}$ $R_{detergent/membrane}$) of 0.05 to 1.16. A sample without polymer or detergent served as a control. Table 2.10 shows the polymer or detergent concentrations that were tested. For solubilisation, samples were incubated over night with gentle shaking on a rotation wheel. For the solubilisation efficiency of the polymer DIBMA, three different buffers and conditions were tested. For the detergent DDM, one solubilisation test was carried out. Parameters for the solubilisation tests can be obtained from Table 2.10. Non-solubilized material was removed by ultracentrifugation (200 000 x g for 10 min at 4 °C). The protein content of the supernatant and the pellet were determined with a BCA assay (2.4.7) and solubilisation efficiency was calculated as described in 2.7.2.

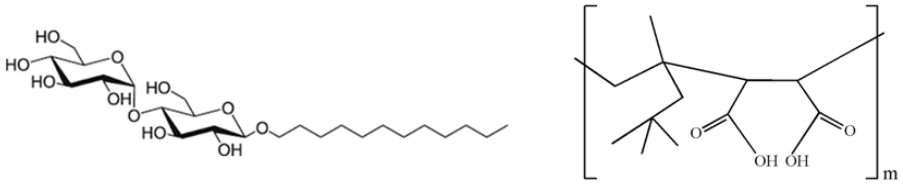

Fig. 2.1 Structure of the DDM and DIBMA. The detergent dodecyl-β-D-maltoside (DDM) is depicted left, the polymer poly-diisobutylene/maleic acid (DIBMA) on the right. The structure was drawn in ChemDraw (Std. 7.0).

Table 2.10 Parameters for the solubilisation efficiency tests. RT = room temperature. Protease inhibitor mix by Roche was used (2.1.2). Ratio refers to the ratio of polymer to membrane ($R_{pol./mem.}$) or detergent to membrane ($R_{det./mem.}$), e. g. using 40 mg/ml membrane wet weight and 4 % polymer, results in a ratio of 1.

Parameter	**Polymer DIBMA**			**Detergent DDM**
	test A	**test B**	**test C**	
Buffer	Solubilisation test buffer A	Solubilisation test buffer B	Solubilisation buffer	Solubilisation test buffer buffer A
Temperature	4 °C	RT	RT	4 °C
Protease inhibitor mix	no	yes	yes	no
Ratio range tested	0.125 - 0.75	0.25 - 1.16	0.25 - 1.16	0.05 – 0.5
Concentration range tested	0.5 % - 3.0 %	1.0 % - 4.64 %	1.0 % - 4.64 %	0.2 % - 2 %
Tested polymer/detergent concentrations (%)	0, 0.5, 1, 1.5, 1.75, 2, 2.5, 3	0, 1, 2, 2.5, 3, 3.5, 4, 4.64	0, 1, 2, 2.5, 3, 3.5, 4, 4.64	0, 0.2, 0.5, 1, 1.5, 2

Solubilisation test buffer A pH 7.5
25 mM Tris / HCl
125 mM NaCl
10 mM $MgCl_2$

Solubilisation test buffer B pH 6.8
50 mM Tris / HCl
125 mM NaCl
10 mM $MgCl_2$

Solubilisation buffer pH 6.8
50 mM Tris / HCl
300 mM NaCl
10 mM $MgCl_2$

2.4.6 Solubilisation of membrane proteins with DIBMA polymer

For solubilisation of membrane proteins from *P. aeruginosa*, membranes were isolated as described (2.4.3) and resuspended in solubilisation buffer (2.4.5) supplemented with cOmplete® Protease inhibitor mix (Roche) to a final concentration of 200 mg/ml membrane wet weight. The polymer stock was prepared as described in 2.4.4. Solubilization of membrane proteins was carried out using final concentration of 40 mg/ml membrane fraction wet weight and 3.5 % (w/v) DIBMA ($R_{polymer/membrane}$ = 0.875). Samples were incubated at room temperature over night with gentle shaking. Non-solubilized material was removed by ultracentrifugation (200 000 x g for 10 min at 4 °C), and the supernatant was filtered (0.45 µm PVDF).

2.4.7 Solubilization of membrane proteins with detergent

To solubilize membrane proteins with the detergent DDM, a stock solution of 2 % DDM in solubilisation buffer (2.4.5) was prepared. The membrane proteins were isolated as described in 2.4.3. For solubilisation, final concentrations of 40 mg/ml membrane wet weight and 1 % DDM were mixed in solubilisation buffer. Solubilisation was carried out over night at 4 °C under gentle shaking on a rotation wheel. Non-solubilized material was removed by ultracentrifugation (200 000 x g for 10 min at 4 °C).

2.4.8 Determination of protein concentration

To determine the protein content of a protein mixture, a protein quantification kit (Pierce™ BCA protein assay kit by Thermo Scientific) was used according to the manufacturer's recommendations. The test was carried out in a 96-well plate. A BSA calibration curve was measured for every plate. Plate assays were read at 562 nm in a plate reader (FLUOstar Omega by BMG Labtech).

For purified proteins, the protein content was measured at 280 nm. Extinction coefficients were estimated with the method of Hill and van Hippel (Protein Calculator v3.4). Thereby, protein content was calculated with the lambert-beer law:

$$ABS_\lambda = \varepsilon_\lambda * c * d$$

ABS_λ	Absorption at a wavelength λ (AU)
ε_λ	Extinction coefficient at a wavelength λ (M^{-1} cm^{-1})
c	Concentration (M, mol*l^{-1})
d	Thickness of the cuvette (cm)

2.4.9 SDS-PAGE

Sodium-dodecyl-sulfate polyacrylamide gel electrophoresis (SDS-PAGE) is a method to separate proteins according to their charge to mass ratio. SDS contains a hydrophobic tail and a hydrophilic head with a negative charge, and acts as a detergent. The protein sample is treated with SDS where the molecule binds to hydrophobic parts of denatured proteins and applies a negative charge. When a voltage is applied, the smaller proteins move faster through the gel matrix than larger proteins. To separate proteins, a polyacrylamide gel was self-casted. Therefore, glass plates (BioRad) were cleaned and assembled in the appliance. A gel consists of 3 different layers on top of each other: at the bottom there is the stop gel that prevents leakage during the casting process and also prevents proteins from migrating out of the gel. Above is the separation gel, where the proteins are separated. On top there is the stacking gel that contains pockets for sample insertion. Also, the matrix pores are wide to allow proteins to enter the separation gel simultaneously.

When casting the polyacrylamide gel, all components except for APS and TEMED are mixed (Table 2.11). APS and TEMED initiate the polymerization and were added shortly before casting. First, the stop gel is casted, followed by the separation gel by adding APS and TEMED, mixing, and filling the mixture in the gel chambers. While polymerizing, the separation gel was topped with isopropanol. After polymerization, the isopropanol was removed, and the stacking gel was casted on top. A comb inserted the pockets. Gels were stored in moist paper towels at 4 °C. To run a gel, the gel was inserted in the gel chamber that was filled with 1x Running buffer. To prepare samples for SDS-PAGE, the samples were mixed with 4x SDS sample buffer, heated at 95 °C for 10 min and centrifuged for 5 min at 5000 rpm. 2-15 µl sample were loaded on the gel. Gels were run at 190-200 V for 50-60 mins at room temperature.

Table 2.101 Composition of polyacrylamide gels. Rotiphorese Gel 30 (30 %, acylamide:bisacrylamide 37.5:1 by Roth) was stored at 4 °C. Components excluding APS and TEMED were premixed and kept on ice until polymerisation.

Component	Stacking gel	Separation gel (10 %)	Separation gel (12.5 %)	Stop gel
Rotiphorese Gel 30	1.4 ml	5.3 ml	6.7 ml	420 µl
Stacking gel buffer	2 ml	-	-	-
Seperation gel buffer	-	4 ml	4 ml	250 µl
Water	4.6 ml	6.7 ml	5.3 ml	333 µl
10 % APS	30 µl	80 µl	80 µl	13 µl
TEMED	20 µl	8 µl	8 µl	2 µl

10 x Running buffer pH 8.8
0.25 M Tris / HCl
1.92 M glycin
1 % (w/v) SDS

4x SDS sample buffer pH 6.8
240 mM Tris / HCl
8 % (w/v) SDS
40 % (v/v) Glycerol
20 % (v/v) β-mercaptoethanol
0,04 % (w/v) bromphenol blue

Stacking gel buffer pH 6.8	Separation gel buffer pH 8.8
0.5 M Tris / HCl	1.5 M Tris / HCl
4 % (w/v) SDS	0.4 % (w/v) SDS

2.4.10 Coomassie staining of SDS-PAGE separated proteins

To visualise proteins in an SDS-PAGE, gels were stained in Coomassie stain for 15 min at room temperature (22 °C) under gentle shaking. Subsequently, gels were destained in Coomassie destainer solution or distilled water, until gels had the desired colouration intensity. In a stained SDS-PAGE, purity and size of purified proteins or a mixture of proteins can be visualised.

Coomassie stain	Coomassie destainer
10 % (v/v) acetic acid	10 % (v/v) acetic acid
30 % (v/v) ethanol	30 % (v/v) ethanol
10 g/l Coomassie Brilliant Blue G250	

2.4.11 Western blot

In a western blot, specific proteins are visualised by immunodetection. Beforehand, protein samples were separated by SDS-PAGE. Then, the proteins were transferred to a membrane where specific antibodies bind to their targets. Binding of antibodies was visualised in a detection reaction. First, the PVDF membrane was activated in methanol for 2 min and washed in ultra-pure water. The membrane and the polyacrylamide gel were equilibrated in Towbin buffer for 15 min. Proteins were transferred to the membrane with the semi dry blotting technique. The blotting sandwich was assembled by placing the membrane and the gel between two Whatman papers, and proteins were transferred for 17 min at 18 V. Protein-free areas on the membrane were blocked in blocking solution (3 % BSA in TBS-T) for 1 hour at room temperature or for 16 hours at 4 °C. The blocking solution was washed off 3 times with TBS-T. Then, the membrane was incubated in antibiotic solution for 1 h. Utilised antibody solutions are listed in Table 2.12. After the antibody bind to the antigen, the membrane was washed several times in TBS-T. If applicable, the membrane was subsequently incubated for 1 h in a secondary antibody solution. To detect the protein bound antibodies, a colour reaction with the conjugated enzyme alkaline phosphatase was carried out. Therefore, the membrane was equilibrated in AP buffer, and 33 µl NBT and 66 µl BCIP were added. The reaction was stopped by washing the membrane with distilled water.

Table 2.12 Antibodies.

Antibody	Antigen	Dilution	Manufacturer
6x-His Tag monoclonal (HIS.H8)	His-tag	1:2 000 in TBS-T	invitrogen
Anti-mouse IgG-alkaline phosphatase	Mouse IgG	1:10 000 in TBS-T	Sigma-Aldrich
Strep-Tactin AP conjugate*	Strep-tagII	1:4 000 in TBS-T	IBA
Anti-Flag monoclonal M2	Flag-tag	1:2 000 in TBS-T	Sigma

(*) Strep-Tacin is chemically not an antibody, but a streptavidin variant optimised for Strep-tagII fusion protein binding. However, handling and application was the same as for antibodies.

Towbin buffer pH 8.3-8.5 (not adjusted)
25 mM Tris / HCl
192 mM glycin

AP-Puffer pH 9.5
100 mM Tris / HCl
100 mM NaCl
5 mM $MgCl_2$

TBS-T pH 7.4
20 mM Tris / HCl
500 mM NaCl
0.005 % (w/v) Tween-20

NBT stock solution
50 mg/ml in DMF

BCIP stock solution
100 mg/ml in 70 % DMF

2.4.12 Size exclusion chromatography

In a size exclusion chromatography, particles are separated according to their hydrodynamic radius. Polymer nanodiscs were separated by size exclusion chromatography on an ÄKTA Purifier 10 system with a Superose 6 Increase GL 10/300 column (GE Healthcare, Chicago, USA) in solubilization buffer (2.4.5). Membrane proteins were isolated and solubilised as described in 2.4.3 and 2.4.5. The solubilised membrane sample was filtered (pore size 0.45 µm) and protein content was determined (2.4.8). 200 µl sample, equivalent to 300–400 mg protein was run with a flow rate of 0.2 ml/min at 4 °C. Elution of proteins was monitored at 280 nm. 250 µl fractions were collected. Fractions from 8.22 ml to 10.22 ml were pooled to 1 ml fraction size. Between 10.22 ml – 11.22 ml and 17.22 ml - 23.22 ml fractions were pooled to a fraction size of 500 µl. Fractions between 8.22 ml and 23.22 ml elution volume were subjected to mass spectrometry analysis. An overview with elution volumes and fraction sizes in the three replicates can be found in the appendix (Table A1). The void volume of 7.07 ml was determined with blue dextran. The marker proteins apoferritin (443 kDa), alcohol dehydrogenase (150 kDa), albumin (66 kDa), and carbonic anhydrase (29 kDa) were used for apparent size determination (Table 2.2). Thereby, for each marker protein, the elution volume was divided by the void volume (V_e/V_0) and plotted against the logarithmic molecular weight of the protein (log MW). A linear regression curve was created in Excel and the formula was used to calculate the apparent molecular weight of proteins based on their elution volume.

2.4.13 Protein precipitation with acetone

For protein precipitation proteins fractions were transferred to fresh test tubes and six times the volume of the sample ice-cold acetone (100 %) was added. Samples were vortexed for 30 s and incubated at -80 °C over night. Subsequently, samples were centrifuged at 20 000 x g for 25 min at 4 °C. The supernatant was discarded, and the pellet was washed in four times sample volume ice-cold 80 % (v/v) acetone. Samples were centrifuged again at 20 000 x g at 4 °C for 25 min and the protein pellets were dried in the safety cabinet.

2.4.14 Sample preparation for MS: In solution digest and desalting

Precipitated proteins were dissolved in urea buffer, and a final concentration of 12.5 mM 1,4-dithiothreitol (DTT) was added to the samples and incubated for 30 min at room temperature. Afterwards, a final concentration of 25 mM chloracetamide was added and samples were stored for 25 min in the dark. The solutions were diluted in 25 mM ABC to a final concentration of 4 M urea. Subsequently,1 mM $CaCl_2$ and Lys-C (1:50 w/w LysC/protein) were added and incubated for 2 h at 37 °C. Then, samples were diluted in ABC/ACN buffer to a final concentration of 1 M urea and trypsin was added in a ratio 1:50 (w/w) trypsin/protein. In solution digest was carried out for 16 h at 37 °C. To ensure complete digestion, trypsin was added (1:100 w/w trypsine/protein) and incubated for 20 min. Samples were acidified by supplementing trifluoroacetic acid to 1 % final concentration. Tryptic peptides were desalted on C18-StageTips (Rappsilber *et al.*, 2007). The C18-StageTips were activated in methanol and equilibrated in buffer B and buffer A (100 µl each). Each time, flow through was accelerated by centrifugation at 500 x g for 3 min. The complete volume of the tryptic samples was loaded, and the tips were centrifuged, until the samples passed through the tip entirely (5 min at 500 x g). Then, the tips were washed in 100 µl buffer A, and proteins were eluted in 75 µl buffer B (last centrifugation: 8 min at 500 x g). Finally, eluted tryptic peptides were dried completely in a rotational vacuum concentrator for ~30 min.

Urea buffer	ABC/ACN buffer
8 M urea	5 % (v/v) acetonitrile
25 mM ammonium bicarbonate (ABC)	25 mM ABC
Buffer A	Buffer B
0.1 % (v/v) formic acid	0.1 % (v/v) formic acid
	80 % (v/v) acetonitrile

2.4.15 Mass spectrometry

In solution digest and clean-up of samples was carried out as previously described (2.4.14). The following MS analysis was carried out by M. Räschle (Storchovà group, Molecular Genetics, RPTU): Tryptic peptides were analysed on a Q Exactive HF™ Mass Spectrometer coupled in-line to EASY-nLC 1200 ultra-high pressure chromatography system (both Thermo Fisher Scientific, Waltham, USA). For MS analysis, desalted peptides were separated on a 50 cm reverse phase column with an

inner diameter of 75 µm (New Objective, Woburn, Massachusetts, USA) packed in-house with 1.8 µm ReproSil-Pur 120 C18-AQ particles (Dr. Maisch GmbH, Ammerbruch-Entrigen, Germany) using a 90 min non-linear gradient of 2–95 % buffer B (0.1 % (v/v) formic acid, 80 % (v/v) acetonitrile) at a flow rate of 250 nl/min. All MS data was recorded with a data dependent acquisition strategy. Survey scans were acquired with a resolution of 60'000 at m/z = 200. The top 15 most abundant precursor with charge > 2 were selected for fragmentation. MS/MS scans were acquired with a resolution of 15'000 at m/z = 200. All other parameters can be obtained from raw files available at the ProteomExchange repository (PXD039702 and PXD039700). MS data was processed with the MaxQuant software (version 2.0.1.0). Peak lists were searched against protein sequences derived from the Pseudomonas Genome DB (version 20.2, (Winsor *et al.*, 2016)) applying a false-discovery rate (FDR) of 0.01 for peptides and proteins, a minimal peptide length of 7 amino acids and at least two peptides for quantification. "Match between run" was disabled.

2.4.16 Pulldown of tagged NbdA

For pulldown analysis, *P. aeruginosa* PAO1 strains carrying a pHERD26T-plasmid for the expression of NbdA-Strep or untagged NbdA as a control (Table 2.3) were used. Cultures were grown (2.4.2), membrane proteins were isolated (2.4.3) and solubilized into a nanodisc library as described (2.4.6). The nanodisc library was incubated for 4 hours under gentle shaking at 4 °C with Strep-Tactin®XT 4Flow® beads**.** Unbound proteins were removed by gravity flow, and beads were washed twice with twenty column volumes wash buffer. Proteins bound to the beads were eluted by adding three column volumes StrepXT elution buffer. Samples were digested and analysed by MS as described (2.4.14, 2.4.15). StrepXT-column material was regenerated by washing with 10 mM NaOH and stored at 4 °C.

StrepXT wash buffer pH 8	StrepXT elution buffer pH 8
100 mM Tris / HCl	100 mM Tris / HCl
150 mM NaCl	150 mM NaCl
1 mM EDTA	1 mM EDTA
	50 mM biotin

2.4.17 Heterologous overproduction of proteins in *E. coli*

For the overexpression of genes in *E. coli*, the desired expression vector for production of the target protein (Table 2.3) was transformed in competent BL21 (DE3) cells (2.3.2, 2.3.3). Cells were cultured in LB medium supplemented with appropriate antibiotic (2.3.1). The OD_{600} of the culture was initially set to 0.05 from a preculture in LB medium containing antibiotic. Cultures were grown at 37 °C and 100 rpm shaking. When the culture reached an OD_{600} of 0.5, target gene expression was induced. The cells were further incubated at 17 °C for 16 h. Cells were harvested at 17 500 x g for 15 min, and pellets were stored at -20 °C.

2.4.18 Affinity chromatography

Cytoplasmic fusion proteins were purified by affinity chromatography. Beforehand, proteins were produced either in *E. coli* (section 2.4.17) or *P. aeruginosa* (section 2.4.2). Cell pellets were thawed at 4 °C and lysis buffer (section 2.4.3) was added in a ratio 1:2 gram per cell wet weight. Subsequently, cells were treated with lysozyme and DNAseI for 20 min on ice. Cell disruption was performed by sonication for 3 min total, with 30 s pulse intervals followed by 30 s cooling. The crude extract was centrifuged at 43 000 x g for 1 h at 4 °C. The resulting supernatant was utilised as lysate for protein purification. The affinity chromatography column was equilibrated with at least 10 column volumes of the corresponding wash buffer (Table 2.13). Afterwards, the lysate was added to the column and the flow through was collected. Subsequently, the column was washed with 10 column volumes wash buffer to remove unbound proteins. Proteins were eluted by addition of 3 column volumes elution buffer. Afterwards, the column was regenerated and stored in storage buffer at 4 °C. Proteins were stored short-term on ice at 4 °C. Long term storage of proteins was conducted at -80 °C.

Table 2.13: Buffers used for affinity chromatography.

Buffer	Strep-Tactin resin	Strep-TactinXT 4 Flow resin
Wash buffer	Lysis buffer (section2.4.3)	StrepXT wash buffer (section 2.4.16)
Elution buffer	Strep elution buffer pH 8 50 mM Tris / HCl 150 mM NaCl 2.5 mM desthiobiotin	StrepXT elution buffer (section 2.4.16)
Regeneration buffer	Buffer R pH 8 50 mM Tris / HCl 150 mM NaCl 1 mM EDTA 1 mM HABA (hydroxy-azophenyl-benzoic acid)	StrepXT wash buffer containing10 mM NaOH
Strorage buffer	Buffer R	StrepXT wash buffer (section 2.4.16)

2.4.19 Phosphodiesterase activity assay by high pressure liquid chromatography (HPLC)

The PDE activity of purified proteins was tested by an activity test that was subsequently analysed in by HPLC. The desired protein was produced (2.4.17) and purified by affinity chromatography (2.4.18). Eluted protein solutions were rebuffered by filling them in a dialysis tube and transferring it in dialysis buffer (ET buffer) for 16 h at 4 °C under gentle stirring. Protein concentration of purified proteins was determined as described (2.4.8). In the activity test, a final concentration of 25 µM purified protein was mixed with 50 µM GTP in ET buffer. If applicable, 100 µM $MnCl_2$ was also added. The reaction was started by addition of 50 µM c-di-GMP. Reactions were stopped by heat (95 °C, 15 min) immediately after the indicated incubation time. Afterwards, the samples were

centrifuged (15 630 x g, 15 min) to remove denatured proteins. The supernatant was filtered (0.2 µm PTFE) and nucleotides were analysed in a HPLC device. Standard substances for GTP, GMP, c-di-GMP and pGpG were also analysed. Before the measurement, the column was equilibrated with filtered and degassed running buffer (HPLC running buffer A) for at least 1 h. Degassing was carried out in an ultrasonic bath for 15 minutes at 4 °C. Finally, 30-50 µl of each sample was injected to the column and analysed with a flow rate of 1 ml/min. During the measurement, a methanol gradient was used (Table 2.14). After analysis, the column was purged and stored in 20 % (v/v) methanol.

Tabelle 2.14 Running buffer composition during HPLC measurements.

Time[min]	HPLC running buffer A proportion [%]	HPLC running buffer B proportion [%]
0	100	-
4.0	100	-
7.5	90	10
8.5	90	10
11.5	70	30
12.0	100	-
20.0	100	-

HPLC running buffer A
0,1 % (v/v) acetic acid
10 mM ammonium acetate

HPLC running buffer B
100% methanol

ET/dialysis buffer pH 8
50 mM Tris / HCl
100 mM NaCl
5 mM $MgCl_2$

2.5 Phenotypic assays

2.5.1 Drop dilution assay

To monitor the growth of *P. aeruginosa* mutants on agar plates, an overnight culture of the desired strain was diluted to an OD_{600} = 0.1 in 1 ml LB medium supplemented with antibiotic if necessary. A dilution series in LB medium with antibiotic was pipetted until a dilution of 10^{-5}. The volume of 1 µl for the dilutions 10^{-1}-10^{-5} was dropped on LB agar plates containing antibiotic and if applicable 0.1 % arabinose. Drop dilution assay plates were incubated at 37 °C for 16 h. Pictures were taken in a light cabinet.

2.5.2 Extraction of nucleotides from *P. aeruginosa* cultures

For the extraction of nucleotides from *P. aeruginosa* cultures, a preculture was diluted 1:20 in 40 ml LB supplemented with tetracycline (2.3.1) and incubated at 37 °C and 160 rpm shaking. When cells reached OD_{600} = 0.5, gene expression was induced by adding 0.1 % arabinose. The cells were cultured for 5 h at RT (22 °C) with 160 rpm shaking. Each extraction was carried out in technical triplicates. Therefore, the OD_{600} was adjusted to 1.5 in 5 ml volume and cells were centrifuged (3150 x g, 20 min, 4 °C). Cell pellets were resuspended in 500 µl LB medium, transferred to fresh test tubes and washed

twice in 500 µl fresh medium (centrifugation for 20 min at 4 °C and 2500 x g). Cells were centrifuged again; pellets were resuspended in 300 µl extraction solvent and incubated on ice for 15 min. Afterwards, the mixtures were heated at 95 °C for 10 min and centrifuged at 20 800 x g for 10 min at 4 °C. The resulting supernatant was transferred to a fresh test tube. The pellet was extracted another two times with 200 µl extraction solvent, followed by incubation on ice for 15 min and centrifugation (20 800 x g, 10 min, 4 °C). Each time, the supernatant was transferred to the fresh test tube (in total 700 µl extract). After the third extraction step, the remaining pellets were stored at -20 °C and further used for protein quantification (see below). The extracts were incubated at -20 °C over night to precipitate remaining proteins. Subsequently, extracts were centrifuged again at 20 800 x g for 20 min at 4 °C. The resulting supernatants were transferred to fresh tubes, rapidly frozen and stored at -80 °C over night. Then, extracts were lyophilised for 24 h at 0.004 mbar and -80 °C. For each tested strain, at least three biological replicates with three technical replicates each were prepared.

For total protein quantification, cell pellets were resuspended in 800 µl NaOH solution (0.1 M), vortexed and heated for 15 min at 95 °C, until the pellets were completely dissolved. Samples were centrifuged at 20 800 x g for 10 min at 4 °C and 10 µl of the supernatant was used for protein quantification with the BCA assay kit (section 2.4.6). Protein quantification was carried out in technical triplicates for each sample.

Extraction solvent (2:2:1)
40 % (v/v) acetonitrile
40 % (v/v) methanol
20 % (v/v) water

2.5.3 Measurement of nucleotide content of *P. aeruginosa* extracts

Nucleotides were extracted from *P. aeruginosa* cultures as described (section 2.5.2). Quantification of lyophilised nucleotide messengers was carried out by Hanna Becker (AG Richling, Department of chemistry, RPTU) according to a modified protocol from Bähre *et al.*, 2017: [redacted]

[redacted]. The limit of detection (LOD) and limit of quantification (LOQ) for the described method are 10 nM and 20 nM for GMP and 0.01 nM and 0.1 nM for c-di-GMP and pGpG, respectively.

Table 2.15 Compound specific parameters. Q = quatropole, DP = declustering potential, CE = collision energy, CXP = collision cell exit potential.

Compound	Q1 mass	Q3 mass	DP [V]	CE [V]	CXP [V]
GMP	363.9	151.9	36	21	14
	363.9	134.9	36	67	18
c-di-GMP	690.9	152.1	51	41	12
	690.9	539.9	51	31	28
pGpG	709.1	152.0	56	37	16
	709.1	558.1	56	29	30
$^{15}N_5{}^{13}C_{10}$-GMP	378.9	162.0	51	21	14
	378.9	144.0	51	65	14
$^{15}N_{10}{}^{13}C_{20}$-c-di-GMP	720.9	162.0	46	45	14
	720.9	560.1	46	31	24

For the quantification of the nucleotides GMP, c-di-GMP and pGpG the stabile isotope dilution analysis (SIDA) was used. [redacted] The quantitative contents of GMP, c-di-GMP and pGpG in the bacteria extracts were calculated for the three biological replicates referred to the protein content.

2.5.4 Phage sensibility assay

Phages are viruses infecting bacteria, that rely on the host to reproduce. The phage DMS3*vir* is a lytic derivate of the phage DMS3 that was isolated by Budzik *et al.*, 2004 from a clinical *P. aeruginosa* isolate. The original phage DMS3 contains double stranded DNA (50-65 kb) and consist of a tail approximately 110 nm in length and an icosahedral head with a diameter of approximately 50 nm (Budzik *et al.*, 2004). The phage infects *P. aeruginosa* strains PAO1, PA14 and several clinical isolates, thereby the type IV pili (T4P) are receptors for the phage (Budzik *et al.*, 2004). Since the utilized phage DMS3*vir* (GenBank reference NC_008717) performs the lytic cycle only as it lacks the virulence gene required for phage genome integration into the host genome, phage infection efficiency can be used as a measure for surface piliation of the cells (Laventie *et al.*, 2019). A phage stock was prepared by filtering a lysed PAO1 culture (0.22 µm pore size). The phage titer was determined by a plaque assay. Therefore, a serial dilution of the phage stock was pipetted in sterile LB media, and 100 µl of relevant dilutions were mixed with 100 µl of a PAO1 preculture in 3 ml molten soft agar (LB with 0.8 % agar, ~42 °C). Subsequently, soft agar mixtures were mixed and poured on standard LB plates. When the soft agar solidified, plates were incubated at 37 °C for 16 h. The plaque forming units (PFU) were counted (**Fig. 2.2**), and the phage titer was calculated with at least 3 dilutions. For long term storage of a phage reference stock, a preculture of PAO1 was diluted 1:5 in fresh LB media and incubated for 15 min at 37 °C shaking to initiate growth. Approximately 10^8 PFU/ml were added to the culture (multiplicity of infection (MOI) ~1) and vortexed shortly. Samples were incubated for 15 min at room temperature, then sterile glycerine solution was added to a final concentration of 25 % (v/v). Samples were mixed, frozen in liquid nitrogen, and stored at -80 °C.

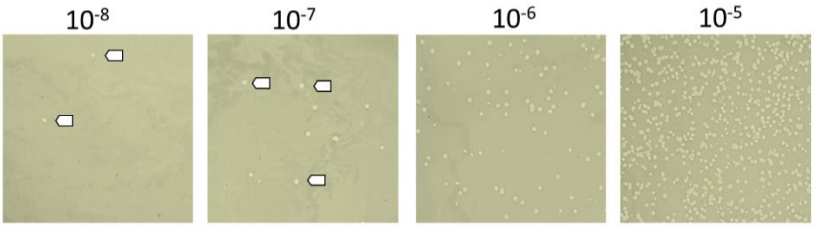

Fig. 2.2 Plaque formation on soft agar plates. Phage titer was determined by plaque assay, where a serial dilution of the phage stock for DMS3*vir* was poured into soft agar with PAO1 cells. Several plaques indicated by white arrows.

To test the PAO1 WT and deletion mutants, cells were grown in LB media in 96-well plates. Overnight cultures were diluted in LB media to an OD_{600} of 0.05 and 200 µl cell suspension was filled in each well. 10^3 PFU of the phage DMS3*vir* were added for the infection test, to a growth control only medium was added. Plates were incubated at 37 °C with orbital-shaking. OD_{595} was measured every 30 min for 24 h total.

For the overproduction strains with pHERD26T-derivate plasmids, cells were grown in LB-Tet$_{150}$. Precultures were diluted in LB-Tet$_{150}$ to an OD_{600} of 0.05 and 200 µl cell suspension was filled in each well. Plates were incubated at 37 °C shaking for 3.5 hours, then gene expression was induced with 0.1 % arabinose. 1 hour after induction phages (10^5 PFU) were added to the infection test, whereas media was added to the growth control. Plates were further incubated at 37 °C shaking, while measuring the OD_{595} every 30 min to monitor growth or lysis.

For the overproduction strains with pME6032-derivate plasmids, cells were grown in LB-Tet$_{150}$. Precultures were diluted in LB-Tet$_{150}$ to an OD_{600} of 0.05 and 200 µl cell suspension was filled in each well. IPTG and phages (10^5 PFU) were added immediately, and plates were incubated at 37 °C shaking. A growth control without phages was also prepared. Plates were further agitated for 24 h at 37 °C, while the OD_{595} was recorded every 30 min.

2.6 Microscopy

2.6.1 Preparation of agarose pads

To prepare agarose pads for microscopy, 1.2 % agarose was dissolved in PBS buffer by heating. Hot agarose solution was poured into SDS gel chambers with 1 mm spacers. When the agarose cooled down, it was cut into square pads and placed on a clean objective slide.

PBS buffer pH 7.4
10 mM Na_2HPO_4
1.8 mM KH_2PO_4
2.7 mM KCl
137 mM NaCl

2.6.2 Cell morphology of *P. aeruginosa* mutants

To determine the cell morphology of different *P. aeruginosa* mutants, a preculture of the desired strain was diluted 1:20 in fresh LB media containing antibiotic where required. Cells were grown at 37 °C at 160 rpm until OD_{600} = 0.5. Cultures were cooled to RT (22 °C) and protein production was induced with 0.1 % arabinose. Cells were further incubated for 5 h at 22 °C with 160 rpm shaking. Cultures were diluted 1:4 in fresh medium and 3 µl were dropped on an agarose pad (section 2.6.1). When the drop was dried, the agarose pad was covered with a cover slip and cells were analysed in an CLSM microscope (LSM 800, AxioObserver by Zeiss) with a Plan-Apochromat 63x/1.4 oil DIC M27 objective in TLC mode.

2.6.3 Detection of fluorophores in confocal microscopy

For detection of the fluorescent proteins by CLSM the following laser lines were utilised. Excitation and emission spectra of the proteins are depicted in Fig. A7.

Table 2.16: Settings for detection of fluorophores and coupled fusion proteins. Ex λ = Excitation wavelength, Em λ = Emission wavelength.

Fluorophore	Laser	Ex λ	Detection Em λ
mNeonGreen	argon	488 nm	491-544 nm
Venus	argon	514 nm	519-588 nm
mCherry	HeNe	594 nm	599-696 nm
mRuby3	HeNe	543 nm	550-658 nm

2.6.4 Localisation of overproduced NbdA in *P. aeruginosa* cells

To determine the cellular localisation of overproduced NbdA in *P. aeruginosa*, a preculture of the desired strain was diluted 1:20 in fresh LB media containing antibiotic. Cells were grown at 37 °C at 160 rpm until an OD_{600} = 0.5. Cultures were cooled to RT (22 °C) and target gene expression was induced with 0.1 % arabinose. Cells were further incubated for 5 h or over night at 22 °C at 160 rpm. Cultures were diluted 1:4 in fresh medium containing antibiotic and arabinose. 3 µl of the cell dilution was dropped on an agarose pad. When the drop was dried, the agarose pad was covered with a cover slip and cells were analysed in an CLSM microscope (LSM 800, AxioObserver by Zeiss) with a Plan-Apochromat 63x/1.4 oil DIC M27 objective and the ZEN software (version 3.2 black 14.0 by Zeiss). Images were taken with four times averaging. The laser and detection settings can be obtained from Table 2.16. Images were further analysed with the Zen lite software (version 3.5, blue edition). Only cells that were completely visible and in focus were included in the counting. Total cell counts are given as sample size *n* in the respective figure legends.

2.6.5 Co-localisation of NbdA with pili components

To determine the cellular co-localisation of NbdA and the pili subcomponents PilO or PilT in *P. aeruginosa*, cells containing chromosomally integrated fusions of PilO and PilT to the fluorophores mCherry or mRuby3, respectively, were used. For the detection of NbdA, cells contained chromosomally integrated, or plasmid encoded fusions of NbdA to the fluorophores mNeonGreen or Venus. For cultures of strains with a chromosomally integrated NbdA fusion, a preculture of the desired strain was diluted 1:20 in fresh LB media. Cells were grown at 37 °C at 160 rpm for 7 h or 16 h. To determine the cellular co-localisation of plasmid encoded, overproduced NbdA with pili subcomponents a preculture of the desired strain was diluted 1:20 in fresh LB media containing antibiotic. Cells were grown at 37 °C at 160 rpm until OD_{600} = 0.5. Cultures were cooled to RT (22 °C) and protein production was induced with 0.1 % arabinose. Cells were further incubated for 5 h at 22 °C with 160 rpm shaking.

Cultures were diluted 1:4 in fresh medium containing antibiotic and arabinose if applicable. 3 µl of the cell dilution was dropped on an agarose pad. When the drop was dried, the agarose pad was covered with a cover slip and cells were analysed in an CLSM microscope (LSM 800, AxioObserver by Zeiss) with a Plan-Apochromat 63x/1.4 oil DIC M27 objective and the ZEN software (version 3.2 black 14.0 by Zeiss). The laser settings can be obtained from Table 2.16. Images for the different fluorophores were taken in separate frames with four times averaging. Images were further edited

with the Zen lite software (version 3.5, blue edition) and cropped with the software Corel Draw. Only cells that were completely visible and in focus were counted for the co-localisation. Total cell counts are noted as sample size *n* in the respective figure legends.

2.6.6 Atomic force microscopy of *P. aeruginosa* cells

Atomic force microscopy was carried out by J. Seehase (AG Ziegler, Department of physics and biophysics of complex interfaces, RPTU). A preculture was prepared for *P. aeruginosa* WT and Δ*pilA* as described in 2.3.1. The NbdA overproduction strain PAO1 pMRP12 was cultivated as described in 2.4.2 at 17 °C. Precultures were diluted in sterile 0.9 % (w/v) NaCl solution to an OD_{600} of 0.03. Cells were immobilised on poly-D-lysine coated cover slips (Biocoat™ poly-d-lysin 12 Mm by Corning) that were glued to objective slides (Menzel glass 76 x 26 mm by ThermoScientific). Therefore 250 µl of bacterial solution was dropped on the cover slip and incubated for 30 min at RT. Non-adhered cells were removed by washing the objective slide with 5 ml sterile ultra-pure water. Afterwards, the slide was dried in the sterile bench for 30 min at RT. Atomic force microscopy was carried out in a JPK Nanowizard 3 AFM (Bruker) microscope using a MSNL-10 cantilever C with 0.01 $N*m^{-1}$ spring constant (Bruker). Surface profiles were captured in contact mode with a size of 2 µm x 2 µm, a resolution of 512 x 512 pixels, IGain 30 Hz, PGain 0.001, setpoint 0.15 nN and a linear scan rate of 0.25 Hz.

2.7 Data analysis

If not stated otherwise, data analysis was carried out in Excel (version 2112, Microsoft, Redmond, USA). Plots were created with Origin Lab (version 2022 SR, OriginLab, Northampton, USA). Microscopy images were created in CorelDraw GraphicsSuite (version 2017, Corel Corporation, Ottawa, Canada). Miscellaneous pictures were created with PowerPoint (version 2112, Microsoft, Redmond, USA).

2.7.1 Statistical analysis

Experimental data was tested for significant changes. Only biological replicates were considered for statistic evaluation. Technical replicates were averaged. If not stated otherwise, average and standard deviation of biological replicates were calculated with the respective formula in Excel (version 2112, Microsoft, Redmond, USA). To determine which statistical test is appropriate, data was tested for normal distribution in Origin according to Shapiro-Wilk or Kolmogorov-Smirnov. When data was normally distributed, a Student's *t*-test was performed in Excel. The tail was dependent on the tested hypothesis and if the datasets were compared for changes (two-tailed test) or for higher/lower values (one tailed test). The type of *t*-test was determined with *F*-test as a test for equal variances, which was also performed in Excel. If the result of the *F*-test was > 0.05, data was homoscedastic (type 2), if the

F-test < 0.05, the data was heteroscedastic (type 3). For paired datasets, type 1 was used. If the data was not normal distributed, a *U*-test according to Mann and Whitney was performed for unpaired data in Excel. Thereby ranks were calculated with the following formula:

$$=\text{RANK}(i;[\text{Matrix1:Matrix2}];1)+(\text{COUNT}([\text{Matrix1:Matrix2}])+1-\text{RANK}(i;[\text{Matrix1:Matrix2}];1)-\text{RANK}(i;[\text{Matrix1:Matrix2}],0))/2.$$

The significance level was 0.05, with $0.01 < p < 0.05$ (*), $0.001 < p < 0.01$ (**) and $p < 0.001$ (***). For multiple comparisons, a *p*-value correction according to Bonferroni or Benjamini-Hochberg was carried out.

Formula for Bonferroni correction:

$$\text{new } p-\text{value} = \frac{\text{calculated } p-\text{value}}{\text{number of comparisons}}$$

Formula for Benjamini-Hochberg corrections:

$$\text{new } p-\text{value} = \text{calculated } p-\text{value} * \left(\frac{\text{number of comparisons}}{\text{rank}_{\text{calculated } p-\text{value}}}\right)$$

2.7.2 Calculation of solubilisation efficiency

Solubilisation efficiency was calculated according to Glueck *et al.*, 2022. The solubilisation efficiency test was carried out as described (2.4.5) For each detergent concentration (*i*) the protein content of the solubilised (S3) and the non-solubilised (P3) fractions was determined with a BCA assay (2.4.6). The protein content of the supernatant ($S3_0$) and pellet ($P3_0$) of a sample without detergent or polymer was also determined and served as a control. Efficiency was calculated as follows:

$$Eff_i = \frac{S3_i - S3_0}{(S3_i - S3_0) + P3_i}$$

i	Detergent or polymer concentration
Eff_i	Efficiency for a detergent or polymer concentration *i*
S3	Protein content in supernatant after third centrifugation (µg/ml), contains solubilised membrane proteins
P3	Protein content in pellet after third centrifugation (µg/ml), contains unsolubilised membrane proteins and particles
$S3_0$	Protein content of supernatant without detergent or polymer (µg/ml)
$P3_0$	Protein content of pellet without detergent or polymer (µg/ml)

The ratio of polymer or detergent to membrane content (*x*-values) was plotted against the calculated efficiency (*y*-values). Membrane concentrations were kept constant, so the ratio is proportional to the detergent or polymer concentration. Maximal theoretical efficiency was calculated with a non-linear fit function by using the Excel solver plugin.

$$Fit_i = \frac{x * R_{\text{polymer/membrane}}}{y_{0.5} + R_{\text{polymer/membrane}}} \qquad Fit_i = \frac{x * R_{\text{detergent/membrane}}}{y_{0.5} + R_{\text{detergent/membrane}}}$$

i	Detergent or polymer concentration
Fit_i	Fitted efficiency for a detergent or polymer concentration i
x	Maximal theoretical efficiency
$y_{0.5}$	Value at half maximal efficiency
R	Ratio polymer or detergent to membrane content

To solve the equation and get a maximal efficiency, the following constraints were calculated:

$$SR_i = [(\mathrm{S3}_i - \mathrm{S3}_0) - Fit_i]^2$$

$$SRR = \sum SR_i$$

SRR is thereby a measure for the distance of the fit function to the experimentally obtained values. With the solver function in Excel (GRG-non-linear), the values for x and $y_{0.5}$ were changed until *SSR* was as close to zero as possible while $x \geq 0$ and $y_{0.5} \geq 0$. Three restarts were performed. Maximal theoretical efficiency was directly determined as x.

2.7.3 Analysis of mass spectrometry data

MS data analysis for nanodisc library: Raw data are available via ProteomeXchange with identifier PXD039702. Mass spectrometry data was analysed with Perseus (version 1.6.15.0) (Tyanova *et al.*, 2016). Data was filtered to exclude contaminants, proteins only identified by site and matching to reverse database. For the nanodisc library data, intensity based absolute quantification (IBAQ) values were scaled to an interval spanning from 0 to 1. The scaling was carried out for each replicate individually. To generate a heatmap of all identified proteins, the proteins were sorted by their maximal relative abundance based on IBAQ. Sorting was also performed independently for each replicate. Data were mapped to the Pseudomonas Genome database (Winsor *et al.*, 2016). Protein name, subcellular localisation, predicted molecular weight, pI, and sorting in the COG category was obtained from this database. For subcellular localisation, only the highest confidence class was considered (class 1 > class 2 > class 3). The fraction with the highest measured intensity and thereby IBAQ value was considered the peak elution fraction (relative abundance based on IBAQ = 1). The respective elution volume was used to calculate the apparent molecular weight of each protein in each replicate using the formula shown in 2.4.12.

MS data analysis for pulldown: Raw data are available via ProteomeXchange with identifier PXD039700. Mass spectrometry data was analysed with Perseus (version 1.6.15.0) (Tyanova *et al.*, 2016). For pulldown data analysis, LFQ intensities were $\log_2$ transformed and filtered to have 4 valid values in all four replicates of the NbdA pull-down samples. Missing values in the control pull-downs were replaced with values drawn from a normal distribution centred around the detection limit of the MS instrument with a width of 0.3 and a downshift of 1.8 with respect to the standard deviation and mean of all protein intensities of each sample (Tyanova *et al.*, 2016). Two sample *t*-tests with permutation-based false discovery rate (FDR) control were carried out in Perseus. Two significance cut-offs were applied to call Class A (S0=4, FDR<0.01) and Class B (S0=4, FDR between 0.05 and 0.01) interactors.

2.7.4 Correlation analysis

Global correlation analysis was carried out in Excel with the data analysis plugin. Global correlation analysis was carried out for each replicate separately. An Excel sheet with the identified proteins, their locus tag and the relative abundance in each fraction was prepared. Based on this dataset, a correlation matrix was created with variation over rows. First column contained the caption (in this case the locus tag). A correlation matrix is created with the following formula:

$$=\text{CORREL}(\text{OFFSET}(\text{firstvariable\_range},,\text{ROWS}(\$1:1)-1),\ \text{OFFSET}(\text{firstvariable\_range},,\text{COLUMNS}(\$A:A)-1))$$

Coefficients range from -1 for negative correlation, 0 for no correlation and 1 for positive correlation. In a histogram, the number of each correlation coefficient was counted. Thereby, all correlation coefficients were sorted in groups. The groups had a size of 0.1. Correlation of a protein with itself results in a maximal correlation coefficient of 1. These comparisons were excluded for the count of the correlation coefficient, as they only represent number of proteins. As the number of identified proteins was not the same for the three datasets, the relative number of proteins in each group in dependence to the total number of identified proteins was calculated. The relative amount was used to compare the three replicates, by calculating the average and standard deviation.

2.7.5 Cluster analysis

Hierarchical cluster analysis is a statistical method used to analyse large data sets. The objective of a cluster analysis is to arrange elements in a way that elements belonging to the same group (cluster) are more similar to each other than to the elements in another group. The hierarchical cluster analysis was carried out in Perseus (version 1.6.15.0). The relative abundance based on IBAQ was used for clustering for the three replicates. Thereby, a rows tree was created with Pearson distance and none constrain. Reprocessing with k-means was enabled. Either an average, single or complete linkage was set. Initial number of clusters was 300, with maximal 10 iterations and 5 restarts. No columns tree was created. Results were displayed in a heatmap with a dendrogram. Distance threshold maximum

(one cluster) was 0.95 for average linkage, 1.71 for complete linkage and 0.80 for single linkage. The proportion of proteins from a complex in the same cluster was calculated for each replicate individually: only the cluster that contained the most proteins from one complex was considered regarding the cluster size and the proportion of proteins from a complex. These values were calculated first for each complex individually and then averaged between the three replicates.

2.7.6 Prediction of protein structures (AlphaFold, PyMOL)

AlphaFold2 is a DeepMind approach to predict a proteins 3D structure from its aa sequence. Thereby, the program uses artificial intelligence (AI), machine learning and neural networks for the prediction (Jumper *et al.*, 2021). In this work, the protein structures for NbdA, as well as the interaction with the proteins PilA, PilB, SadC, PA4200 and CzcR were predicted in AlphaFold 2 provided by ColabFold (www.colab.research.google.com/github/sokrypton/ColabFold/blob/main/beta/AlphaFold2_advanced.ipynb). Input sequences for proteins in *P. aeruginosa* were obtained from the Pseudomonas Genome DB (Winsor *et al.*, 2016). For the full length NbdA the new annotation was used, resulting in a 726 aa protein (Gerbracht, 2021). Sequences were searched with the MMseq2 tool. Alpha fold was run with the pTMscore ranking for protein complex prediction. Turbo use was enabled. Protein structures were predicted with 5 models with max. 3 recycles. The model type was alphafold2_multimer3. If not stated otherwise, the model with the highest rank (rank_1) was shown. The predicted structure was further analysed in PyMOL (version 2.5.4, Schrödinger) and final pictures were directly exported.

2.7.7 Measurement of cell length with ImageJ

Cell length of *P. aeruginosa* cells in images derived from microscopy (2.6.2) were measured in ImageJ. The scale of the original image was given in the Zen 3.5 blue edition (Zeiss). The scale of the image was imported in ImageJ using the “set scale” function. Cell length was measured with the “measure” function in ImageJ by drawing a line from one cell pole to the opposite pole. Only cells that were visible completely and in focus were measured. Measurements were exported into an Excel sheet, and average and standard deviation were calculated.

3 Results

3.1 Complexom: Characterization of a soluble protein library

In the first part of this thesis the amphiphilic polymer DIBMA was used for protein solubilisation to investigate membrane protein complexes. It was tested whether protein complexes are preserved in nanodiscs, and if new complexes could be predicted by complexome profiling. For this purpose, a soluble library of membrane proteins from *P. aeruginosa* PAO1 was generated using the polymer DIBMA for nanodiscs formation. Subsequently, protein-nanodiscs were separated by size and relevant fractions were subjected to mass spectrometry. The obtained data was analysed for properties of identified proteins, elution profiles of described complexes as well as global approaches to classify the data. In addition, proteins of the c-di-GMP signalling network were analysed for co-occurrence (Scherhag *et al.*, 2023).

3.1.1 Solubilisation efficiency with the polymer DIBMA

To generate a soluble library of *Pseudomonas aeruginosa* membrane proteins with the polymer DIBMA, first the solubilisation efficiency was tested (2.4.5). Thereby different conditions, buffers and polymer concentrations were tested to get the highest soluble protein yield while keeping the polymer concentration as low as possible to avoid downstream interference. A solubilisation efficiency test with the detergent DDM was carried out as a control. Final DDM concentrations of 0.2 %, 0.5 %, 1 %, 1.5 %, and 2 % were tested. The solubilisation test buffer A was used, and solubilisation was carried out at 4 °C. Under these conditions the solubilisation efficiency of DDM for *Pseudomonas* membranes was about 80 % with a calculated maximal efficiency of 85 % (**Fig. 3.1 A**). The optimal detergent concentration was 1 %, as there is little further increase in solubilisation when increasing the DDM concentration.

For the solubilisation with the polymer DIBMA, in the first solubilisation test, final polymer concentrations of 0.5 %, 1 %, 1.5 %, 1.75 %, 2 %, 2.5 % and 3 % were used. With the solubilisation test buffer A and a solubilisation temperature of 4 °C, less than 5 % solubilisation efficiency was observed (**Fig. 3.1 B**, green dots). To increase the solubilisation efficiency, the pH of the buffer was lowered to 6.8 (solubilisation test buffer B), protease inhibitor was added, and solubilisation was carried out at room temperature. Further, the polymer concentration range was extended, and the final polymer concentrations 1 %, 2 %, 2.5 %, 3 %, 3.5 %, 4 % and 4.64 % were tested. With the changed conditions, a solubilisation efficiency of 21 % with a calculated maximal efficiency of 25 % was achieved (**Fig. 3.1 B**, blue line and dots). To further increase the solubilisation efficiency and protein yield, the salt concentration in the buffer was increased to 300 mM NaCl (solubilisation buffer). The tested polymer concentrations were the same as for the previous test, ranging from 1 % to 4.64 %. Also in this solubilisation test, protease inhibitor mix was added, and the solubilisation was carried out at room temperature. Under these conditions the efficiency was 40% with a theoretical maximal efficiency of 46 % (**Fig. 3.1 B**, red line and dots).

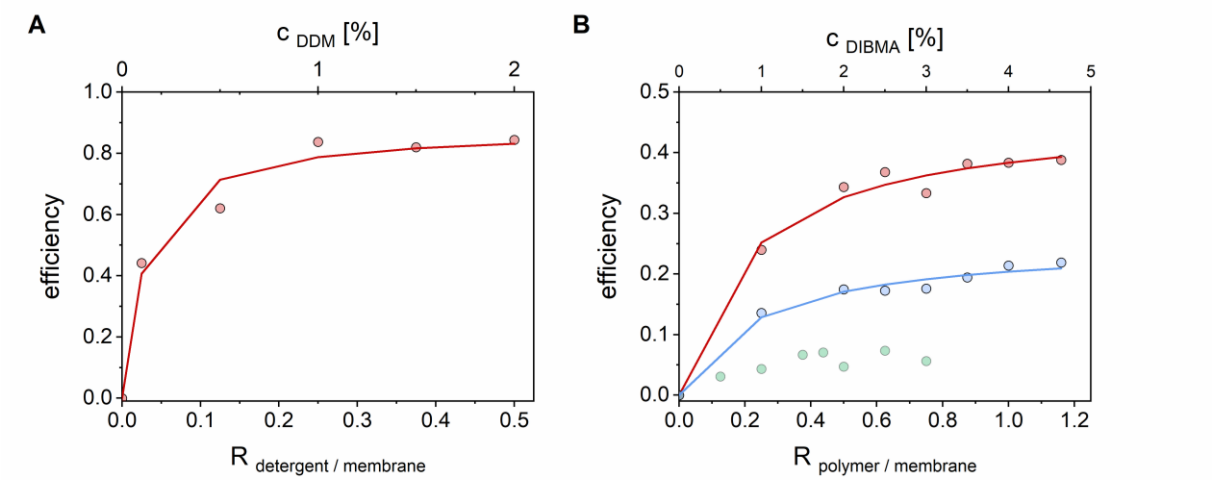

Figure 3.1 Solubilisation efficiency test with DDM and DIBMA. **A**: Solubilisation efficiency was plotted against the DDM concentration. As the membrane concentration was kept constant, the ratio of detergent to membrane was also plotted. Red dots show experimentally determined efficiency, the red line shows the fitted efficiency (see method section 2.4.5 and 2.7.2). Calculated maximal efficiency for DDM was 85 %. **B**: Solubilisation efficiency was plotted against the DIBMA concentration. As the membrane concentration was kept constant, the ratio of polymer to membrane was also plotted. Dots show experimentally determined efficiency, the lines show the fitted efficiency (see section 2.7.2). Green: first solubilisation test with solubilisation test buffer A containing 25 mM Tris HCl pH 7.5, 125 mM NaCl, 10 mM $MgCl_2$ at 4 °C. Blue: second solubilisation efficiency test with solubilisation test buffer B containing 25 mM Tris HCl pH 6.8, 125 mM NaCl, 10 mM $MgCl_2$ and protease inhibitor mix at room temperature. Red: third solubilisation efficiency test with solubilisation buffer containing 25 mM Tris HCl pH 6.8, 300 mM NaCl, 10 mM $MgCl_2$ and protease inhibitor mix at room temperature. Calculated maximal efficiency for DIBMA was 46 %.

Due to the adjusted conditions during solubilisation, the protein content of the solubilised membrane fraction was sufficient for further experiments. With DIBMA concentrations above 3.5 % the solubilisation efficiency was approximately 40 % and nearly no further increase in solubilisation efficiency when increasing the DIBMA concentration to 4 % or 4.64 % was observed. To keep the polymer concentration as low as possible in the sample to avoid downstream interference, a concentration of 3.5 % DIBMA corresponding to a ratio of 0.875 polymer to membrane was used for follow-up experiments.

3.1.2 Preparation of a soluble protein library for PAO1 membrane proteins

For the investigation of membrane protein complexes in *P. aeruginosa* PAO1, a global approach was carried out. Three biological replicates of a PAO1 culture were grown at 37 °C until stationary phase. The membranes were isolated, and membrane proteins were solubilised into nanodiscs with the optimised conditions tested in 3.1.1. Subsequently, the protein nanodiscs were subjected to size exclusion chromatography (**Fig. 3.2**). Here, the nanodiscs were separated according to size and fractions of 250 µl volume were collected. Absorption at 280 nm was measured to monitor elution of proteins, and absorption at 220 nm to monitor the free polymer. In addition, protein content of the fractions was determined with a BCA assay. The chromatograms for the three replicates all show a large protein peak at 12 ml elution volume, and a smaller peak at 21 ml. Replicates 1 and 3 show an additional peak at approximately 7 ml elution volume, that is only scarcely observable in replicate 2.

This elution volume corresponds to the limit of separation of the column and indicates insoluble or aggregated particles. The elution of the polymer also influences the profile. Free polymer, as indicated by absorption at 220 nm, elutes mainly at 16-20 ml elution volume.

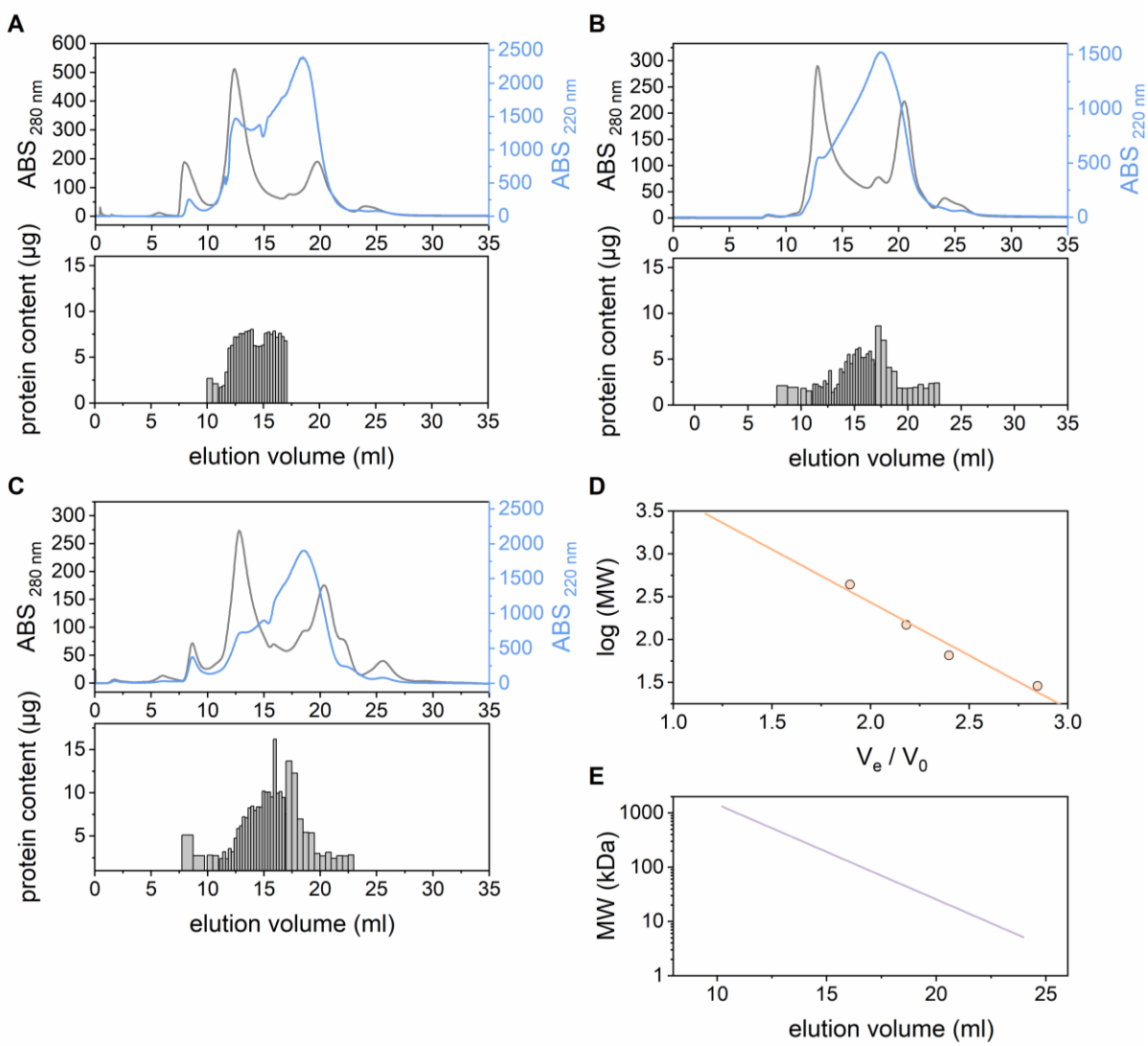

Figure 3.2 Size-exclusion chromatography of PAO1 membrane proteins. Three biological replicates were analysed. Membrane proteins were solubilised with DIBMA polymer and 300-400 µg protein were injected on a Äkta Purifier 10 system with a Superose 6 Increase GL 10/300 column. **A**, **B**, **C**: Upper panel depicting a chromatogram with absorption at 280 nm for protein content (grey line) and 220 nm for DIBMA absorption (blue line). Lower panels showing the estimated protein content of the different fractions by BCA assay (2.4.8). Replicate 1 (A), 2 (B) and 3 (C). **D**: Calibration curve for Superose 6 Increase GL 10/300 column. The marker proteins Apoferritin (443 kDa), alcohol dehydrogenase (150 kDa), albumin (66 kDa) and carbonic anhydrase (29 kDa) were used for apparent molecular weight determination. The log of the molecular weight of marker proteins was plotted against the quotient of the elution volume (V_e) and the void volume (V_0) (orange dots). Formula of the calibration curve (orange line) was calculated in Excel with linear fit function. **E**: Estimated apparent molecular weight in dependency of the elution volume.

The protein content of the samples was higher in fractions at 12-19 ml elution volume, and lower in early and later fractions (8-11 ml and 19-23 ml). In replicate 1, in total 26 fractions between 10.22-17.22 ml elution volume were subjected to mass spectrometry. For replicate 2 and 3, 40 fractions covering a larger range between 8.22-23.22 ml were analysed in MS. Fractions at the beginning (8.22-

11.22 ml) and at the end (17.22-23.22 ml) of the analysed range were pooled. A detailed overview of fraction sizes and elution volume for the three replicates can be obtained from Table A1. To determine approximal apparent protein sizes as a function of the elution volume, a calibration curve with marker proteins of known sizes was drawn (**Fig. 3.2 D**). The linear fit has a function of $y = -1.2386x+4.9118$ with $y = \log (MW)$ and $x = V_e/V_0$. Thereby, the analysed fractions cover the apparent protein sizes from 5 kDa to 2963 kDa (**Fig. 3.2 E**). Off note, the apparent protein size was determined with soluble proteins without polymers. Therefore, the calculated apparent molecular weight does not necessarily match with the sizes of proteins eluting from the column.

3.1.3 Properties of identified proteins

In the three replicates combined, a total amount of 3358 proteins were identified (**Fig. 3.3 A**). This corresponds to 60 % of the annotated proteins in *P. aeruginosa* PAO1 (5570 protein in total). Out of all identified proteins, around 70 % were detected in all three replicates, and around 86 % of proteins were identified in two out of three replicates. This shows that the protein composition in the three replicates was very similar. To further determine the composition of the library, the annotated subcellular localisation of proteins on the Pseudomonas Genome DB (Winsor *et al.*, 2016) was assigned to the identified proteins. Only the highest confidence class for the localisation was considered. Approximately half of the identified proteins were classified as cytosolic proteins (**Fig. 3.3 B**). The second largest group are proteins from the cytoplasmic membrane. Here, 580 cytoplasmic membrane proteins were identified, which corresponds to 48 % of all annotated membrane proteins in PAO1 (1194 proteins). Furthermore, 50 proteins from the outer membrane and 307 proteins predicted to reside in outer membrane vesicles were identified. About 575 proteins were detected whose subcellular localisation is unknown.

To test whether proteins from different subcellular localisations show a different elution behaviour, the proteins were sorted by their subcellular localisation and the peak elution fractions were analysed (**Fig. 3.3 C**). Remarkably, proteins of different subcellular localisations show distinct elution patterns. Cytosolic proteins, periplasmic proteins, and extracellular proteins were identified mostly in later fractions (> 18, corresponding to elution volumes > 15 ml), whereas proteins from the cytoplasmic membrane, the outer membrane, and outer membrane vesicles were identified in early fractions (< 18, concordant to elution volumes < 15 ml). Elution in the early fractions corresponds to a larger hydrodynamic radius and thereby particle size. As the membrane proteins are embedded in a shell of lipids into the nanodisc particles, it is expected that they exhibit a larger apparent molecular weight.

To check whether this observation is not due to a general larger size of membrane proteins in comparison to soluble proteins, and to obtain the factor of size increase for membrane proteins, the apparent molecular weight of each protein was calculated according to the calibration curve in 3.1.2. This value was divided by the predicted molecular weight for each protein obtained from the Pseudomonas Genome DB. In average, the apparent size of membrane proteins (cytoplasmic membrane and outer membrane) increased 11 times compared to the predicted molecular weight,

whereas for cytosolic proteins it is 5 times increased (**Fig. 3.3 D**). The higher increase for membrane proteins is probably due to the embedded lipids in the nanodisc, that soluble proteins do not have. Soluble proteins eluting in this volume range are likely to be present in large complexes or interact with nanodiscs.

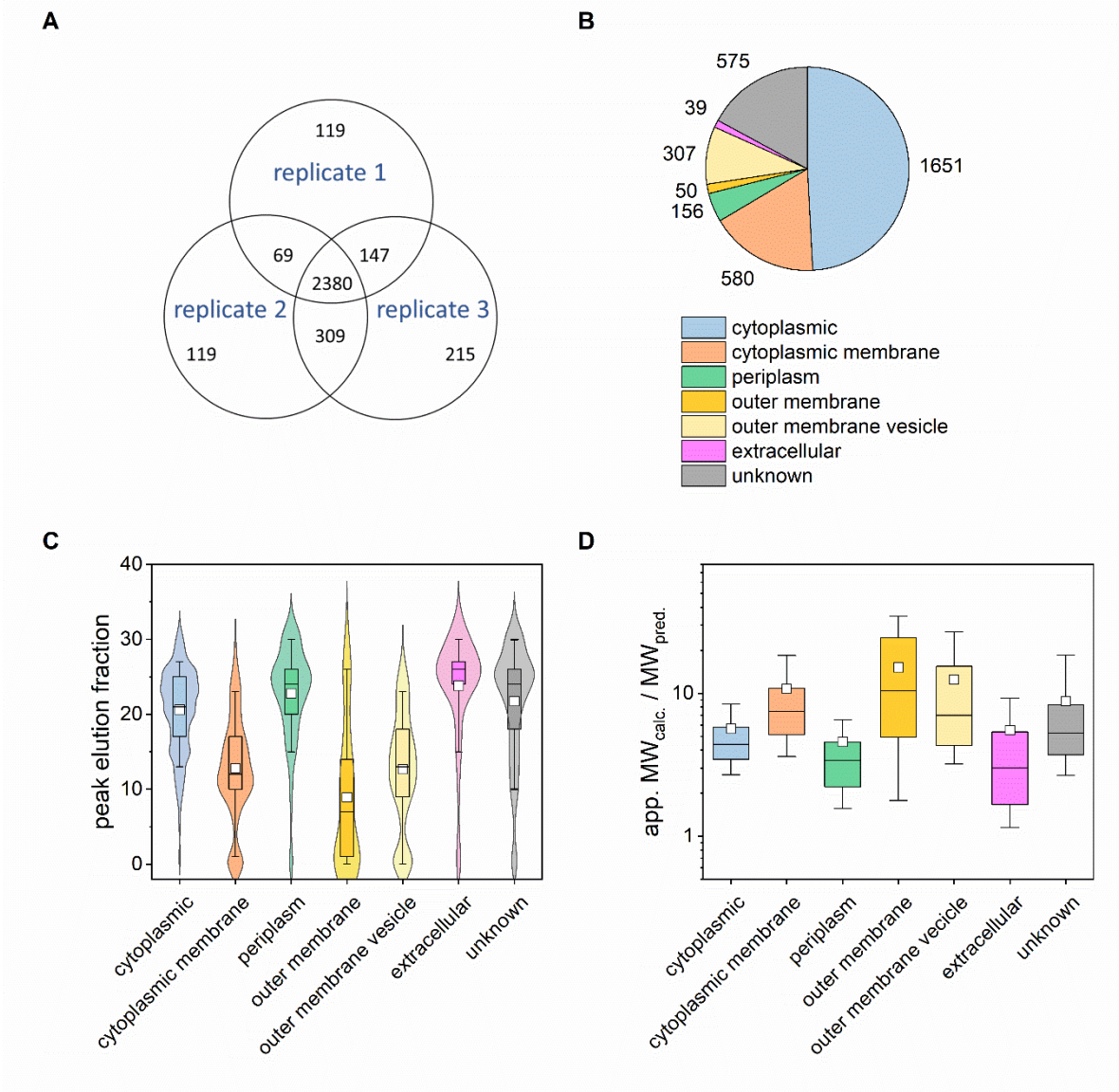

Fig. 3.3 Analysis of the composition of the proteome library from PAO1. A: Venn Diagram of the library depicting the numbers of all identified proteins in the three replicates. **B**: Pie chart showing the distribution of the identified proteins among the different subcellular compartments as predicted for each protein by the Pseudomonas Genome DB (Winsor *et al.*, 2016). Only the highest confidence for the localisation was considered. **C**: Violin plot showing the distribution of peak elution fractions (fraction with the highest measured intensity) for each protein grouped by their predicted subcellular localisation. Averages from three replicates were used. Boxes indicate the range of 25 %–75 % of the data, whiskers the range of 10 %–90 %. Median (black line) and average (white square) of the peak elution fraction for the different subcellular localized proteins are shown. Violines show the smoothing via the Kernel equation with equal areas. **D**: Box plot depicting the quotient of the calculated apparent molecular weight (app. MW_{calc}) and the predicted molecular weight ($MW_{pred.}$) from the Pseudomonas Genome DB sorted by predicted subcellular localisation. Boxes indicate the range of 25 %–75 % of the data, whiskers the range of 10 %–90 %. Median (black line) and average (white square) are also shown.

Further, properties of identified proteins and not identified proteins were compared. Protein properties, such as predicted size, charge, or functional groups, were obtained from the Pseudomonas Genome DB (Winsor *et al.*, 2016). In this comparison it was checked whether the mentioned properties had an influence on the detection in this dataset. However, no sustaincial changes were found in the group of identified proteins compared to the non-identified proteins (Fig. A2).

In addition, elution profiles of identified proteins were analysed. The relative abundance of each protein was calculated based on the intensity based absolute quantification (IBAQ) value, that is proportional to the protein amount (Krey *et al.*, 2014; Schwanhäusser *et al.*, 2011). When looking at the heatmap of the three replicates, it is visible that there is a uniform distribution of proteins in all the fractions. Elution of individual proteins is rather broad (**Fig. 3.4**). In average, one protein was identified in 17 out of 40 fractions with the upper 90 % of its IBAQ value. The proteins do not elute in single well-defined peaks but over the whole length of analysed fractions. In replicate 2, the relative abundance in the first fractions was low, which was also indicated in chromatogram of the SEC, where only a very small protein aggregation peak was observed (3.1.2). Similarly, in fractions with an elution volume > 21 ml also a lower relative amount of protein was detected in replicate 2 and 3. This area corresponds to very small apparent protein size (< 15 kDa).

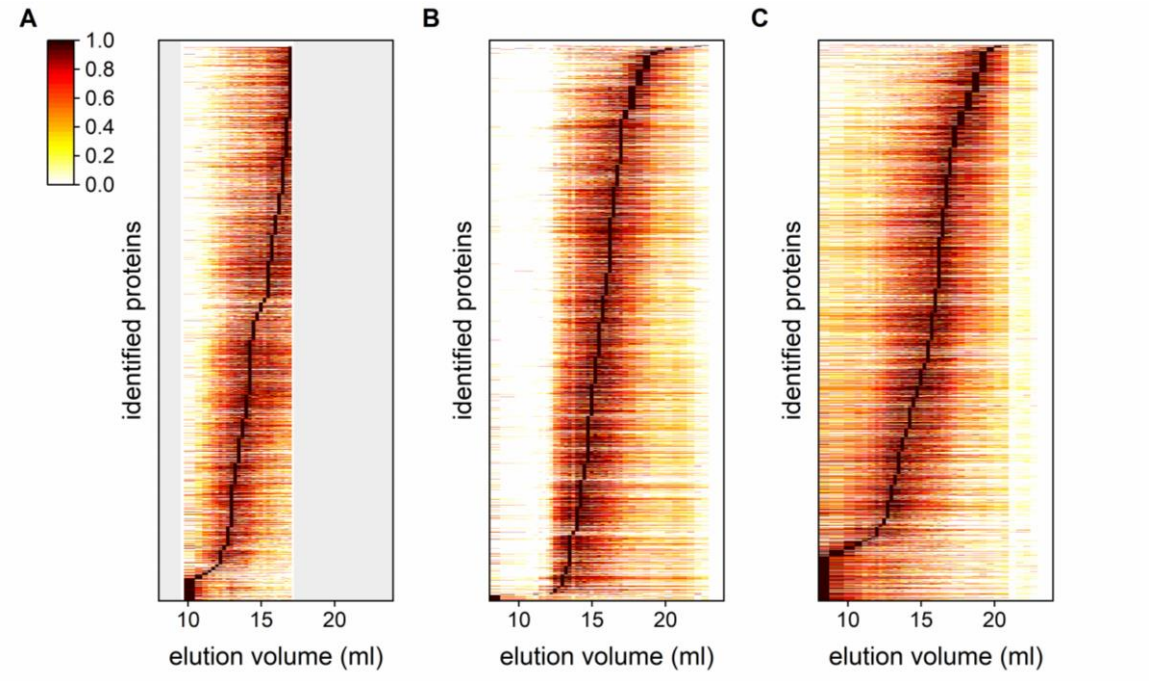

Fig. 3.4 Heatmap of all proteins identified in mass spectrometry. For all identified proteins (*y*-axis) the individual elution profile from size exclusion chromatography (*x*-axis) is shown. The relative abundance of each protein is colour coded: high relative abundance is shown in dark red, low relative abundance is depicted in pale yellow to white (see colour scale). The relative abundance of proteins was determined based on the IBAQ value. Proteins were sorted by the fraction with the maximal relative abundance. **A**, **B**, **C**: Depicted are replicate 1 (A), replicate 2 (B) and replicate 3 (C). Grey areas in replicate 1 show fractions that were not subjected to mass spectrometry analysis.

The figure shows further the elution of proteins along the molecular separation range of the column lacking a clear size separation of individual complexes. This is probably due to the size heterogeneity inherent to flexible polymer-encapsulated lipid-bilayer nanodiscs (Glueck *et al.*, 2022; Oluwole *et al.*, 2017).

3.1.4 Elution profiles of described complexes

To test whether native membrane-protein complexes are preserved in the nanodisc library, the elution profiles of protein components of several well-described protein complexes were compared. To this end, more than 20 described membrane-protein complexes (Table A2) were selected, and the elution profiles of the individual components were analysed. The focus was on stable complexes that were identified experimentally, e. g. by pulldown analysis, co-IP, or Native PAGE. The intensitiy of the proteins indicated stable detection (Fig. A2). We found that the protein components from each tested complex co-occurred in several fractions for all the tested complexes. One example of a *bona fide* membrane complex is the cytochrome oxidase cbb3-1 (Comolli *et al.*, 2004; Kawakami *et al.*, 2010). This complex is part of the respiratory chain and consists of four membrane-integrated protein subunits, CcoNOPQ (Comolli *et al.*, 2004; Jo *et al.*, 2017). In our dataset, all proteins from this complex were identified, and the proteins showed largely overlapping elution profiles (**Fig. 3.5 A**). All proteins eluted with the highest abundance at an elution volume of 13-16 ml.

Complexes that consist of a membrane part as well as cytosolic or periplasmic-associated proteins were also tested. One example is the SEC-SRP complex, consisting of a membrane channel SecYEG and membrane-associated helper proteins: SecB is the chaperone that binds the unfolded protein and SecA is an ATPase that drives the export through the SecYEG channel. YidC, SecDF, and YajC facilitate protein export. The proteins FtsY and Ffh help with the insertion of proteins into the membrane (Ma *et al.*, 2003; Müller *et al.*, 2001). Again, most proteins showed largely overlapping elution profiles, with maximum abundances at elution volumes of 13.5–16 ml (**Fig. 3.5 B**). The chaperone SecB eluted in later fractions, independently of the SecYEG complex, corresponding to a smaller hydrodynamic size.

Another protein complex tested for coelution is the type IV pili (T4P) membrane alignment subcomplex PilMNOP (Ayers *et al.*, 2009). This complex connects the membrane motor in the cytoplasmic membrane to the outer membrane subcomplexes (e.g., secretin pore subcomplex PilQ and PilF) and also interacts with the major pilin subunit PilA (Burrows, 2012; Tammam *et al.*, 2013). All proteins of the complex were detected in the library and showed a similar elution profile, with high relative abundances at elution volumes of 12–18 ml (**Fig. 3.5 C**).

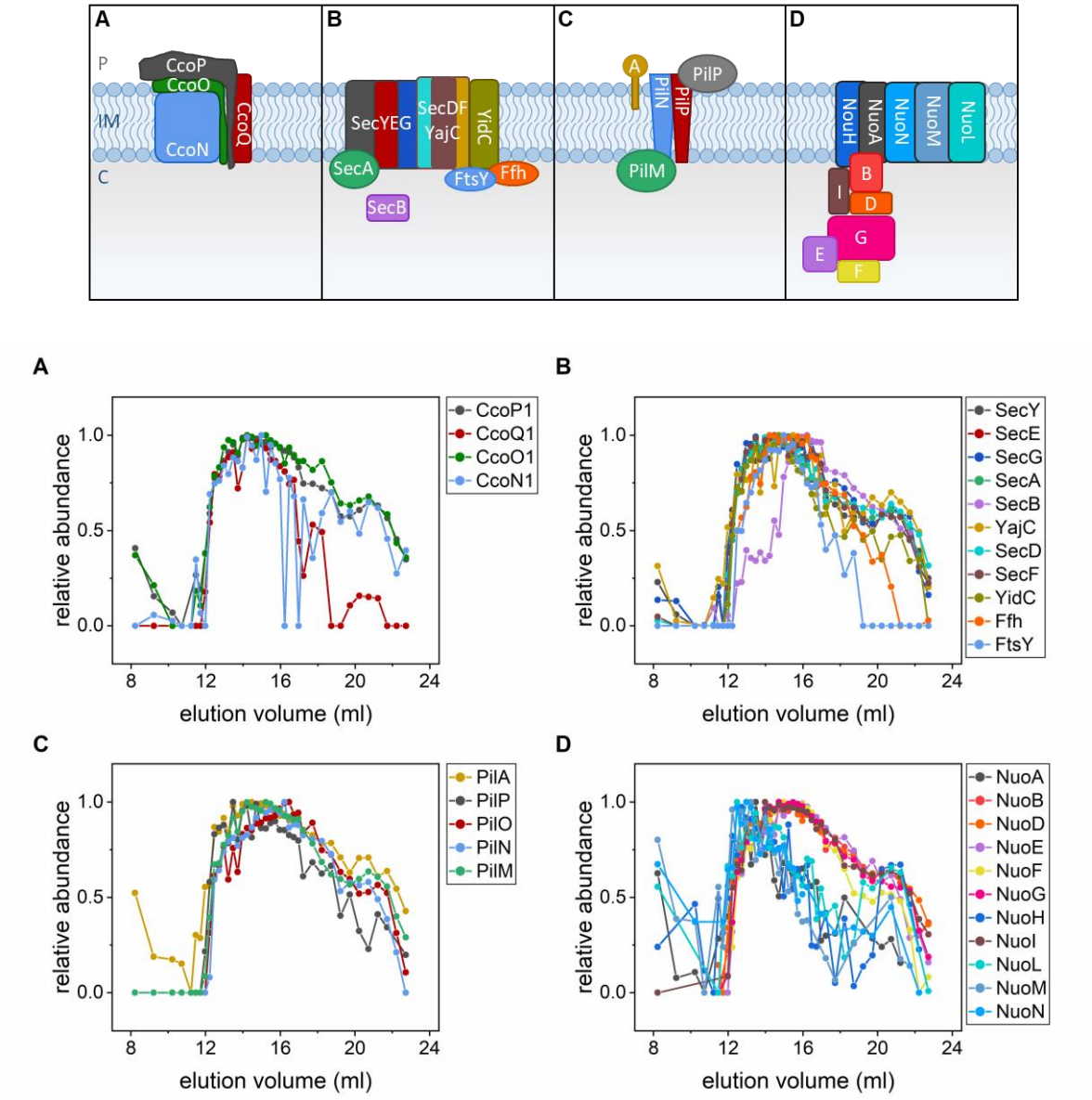

Fig. 3.5 Elution profiles of described membrane protein complexes. The relative abundance of each protein was plotted against the elution volume from size exclusion chromatography. Data from replicate 1 is shown. **A**: Cytochrome oxidase cbb3-1 complex. **B**: Secretion machinery (SEC-SRP). **C**: Pilus assembly subcomplex PilMNOP with the major pilin PilA. **D**: NADH dehydrogenase complex.

Large complexes, such as the NADH-dehydrogenase (NuoABDEFGHIJKLMN) involved in the respiratory chain were also analysed: The NADH-dehydrogenase complex consists of three subunits, namely, the dehydrogenase domain, the connecting domain, and the membrane domain (Berrisford *et al.*, 2016). All identified proteins of the complex showed high relative abundances in 12–14 ml elution volume, indicating the existence of a large protein complex (**Fig. 3.5 D**). However, with increasing elution volume, the relative abundance of the membrane part (blue colours) decreased, whereas the hydrophilic dehydrogenase subunit and the connecting subunit remained at high relative abundances until 16.5 ml elution volume (red colours). This indicates that the library contains both a large NADH dehydrogenase complex as well as several subcomplexes. The same pattern was

observed for other large complexes consisting of a membrane part and a cytosolic part, e. g. the ATPase complex.

When proteins from a complex were identified, they always co-occurred in the same fractions as their interacting partners. This holds true for both pure membrane-protein complexes and mixed complexes that contain both integral membrane proteins as well as associated proteins. These results indicate that non-covalent protein–protein interactions are preserved in the native nanodisc library. Elution profiles show overlapping elution profiles, suggesting a preservation of complexes.

3.1.5 Global correlation analysis

As described in the previous chapter, the tested described membrane complexes showed overall a good coelution indicating the occurrence of certain complexes. Sequentially, it was tested how the coelution of described complexes operates within the context of the whole dataset. The assumption was that complex formation would result in resembling elution profiles. A global correlation analysis was carried out, where every identified protein was tested for linear regression with every other identified protein. This is a pairwise approach to identify proteins with profiles as similar as possible. The closer the correlation coefficient approaches 1, the higher the similarity of the profiles. The global correlation analysis resulted in high correlation coefficients in the protein comparisons (**Fig. 3.6 A**). Especially in replicate 2, correlation coefficients were high throughout the dataset. When counting how often which correlation coefficient was calculated in the three replicates, it was observed that they were not normally distributed, but there was a shift towards higher correlation coefficients (**Fig. 3.6 B**). This confirms that a high proportion of proteins show a similar elution profile. In the next step it was tested if the described complexes also show a correlation, and if this correlation can be separated from the background. Indeed, most of the complexes showed a positive correlation: 16 out of 23 (70 %) tested complexes showed an average correlation coefficient above 0.6, while five complexes (22 %) show an average correlation above 0.8, indicating a strong correlation (**Fig. 3.6 C**). The complexes with the highest average correlation were the transporters DppBCDF and TriABC, the lipid synthesis complex LptBGFC, the flagella motor complex MotAB, and the T4P motor. All these complexes consisted of less than five proteins. Larger complexes that consist of more than six proteins often showed a broader distribution of correlation coefficients, for example complex I from the respiratory chain, the SEC-SRP complex or the T6SS. This observation suggests that larger complexes may also elute as smaller subcomplexes, or that they lack stability.

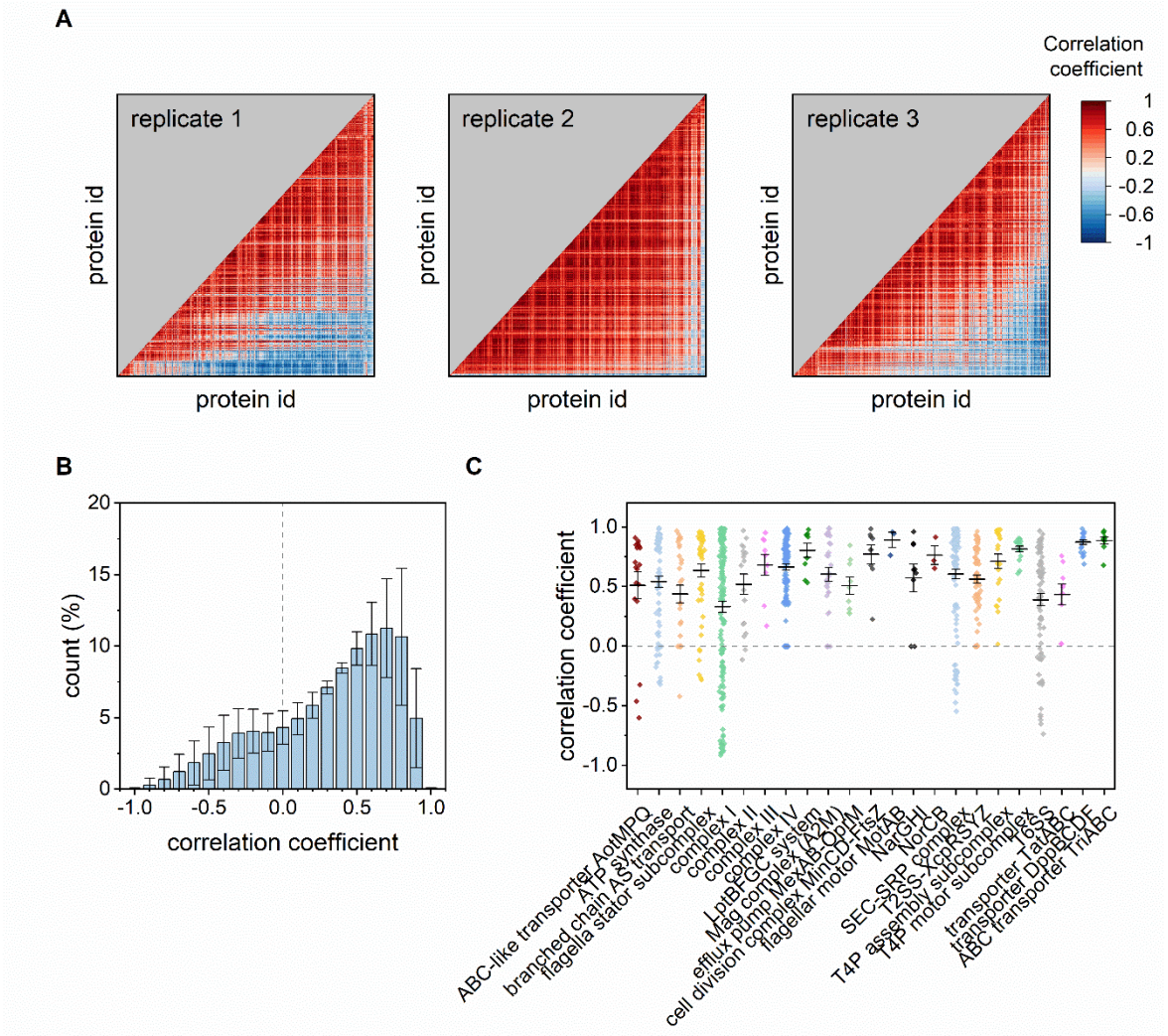

Fig. 3.6 Correlation analysis of all identified proteins. A: A global correlation analysis was performed in Excel with the data analysis plugin. All proteins were tested for linear regression for each replicate individually. Colour gradient from red (positive correlation) to blue (negative correlation). **B**: Histogram of all calculated correlation coefficients in the three replicates. Bars depicting relative amount of each correlation coefficient (referred to identified proteins in each replicate), error bars indicate standard deviation between the three replicates. Class size: 0.1. **C**: Correlation coefficients of described complexes. Line depicts the average correlation coefficient for each complex with error bars showing the standard error. Dots show the individual correlation coefficients in the three replicates.

However, even high correlation coefficients need to be interpreted in the context of the whole dataset. When analysing the correlation of known protein complexes, it was found that the distribution mirrors the total distribution of the entire dataset. Although certain protein complexes display high correlation in all three datasets, there was a noteworthy number of other proteins that exhibited similar or even greater correlation, albeit they are not associated. For example, for the T4P motor complex, the average correlation was above 0.8 in all three datasets. Still only 30 % of proteins occur in the first 500 top hits of the proteins, meaning that 70 % of the proteins from the T4P motor complex are below the top 500 top hits for correlation. Therefore, the global correlation analysis of protein elution profiles was not suitable for complex detection.

3.1.6 Cluster analysis

Cluster analysis is a statistical method used to analyse large data sets. The objective of a cluster analysis is to arrange elements in a way that elements belonging to the same group (cluster) are more similar to each other than to the elements in another group. Thereby, the clusters are not predefined but are formed during the sorting process. A cluster analysis is a global approach, compared to the correlation coefficient that is a pairwise comparison. A hierarchical cluster analysis for all elution profiles of the three replicates was carried out. The different linkage algorithms average, complete and single were applied (**Fig. 3.7 A**, **B** and **C** respectively). In all three analyses, elution profiles of clustered proteins show a similar pattern for the three replicates, suggesting that the separation of proteins and resulting elution profiles were reproducible for the majority of proteins. Proteins with a similar elution profile were sorted in the same clusters with a low distance threshold. As expected, fluctuating elution profiles often resulted in clusters with a higher distance threshold.

Known membrane protein complexes (Table A2) were assayed for detection in the same clusters in dependency to cluster size (**Fig. 3.7 D** and **E**). With increasing cluster size, also the proportion of proteins from one complex found in the same cluster increases. For the single linkage, higher proportions of proteins were sorted in the same cluster, however, the cluster size was also high indicating low specificity. For example, for 100 defined clusters, with the single linkage on average 90 % of proteins from a complex were found in the same cluster. However, this cluster had an average size of 2213 proteins and comprised 75 % of all identified proteins. With the complete linkage algorithm, cluster size was smaller in average (e. g. for 100 defined clusters: 348 proteins per cluster) but also the proportion of proteins from one complex in the same cluster was low (~25 %). The average linkage algorithm appears to perform best for the tested dataset and described complexes. Here with 100 defined clusters, about 58 % of proteins from one complex were sorted in the same cluster, that had an average size of 724 proteins. With all three linkage methods, it was also observed that proteins from different complexes were often sorted in the same cluster. Considering cluster size and proportion of proteins found in one cluster, no substantial grouping of the known complexes could be determined.

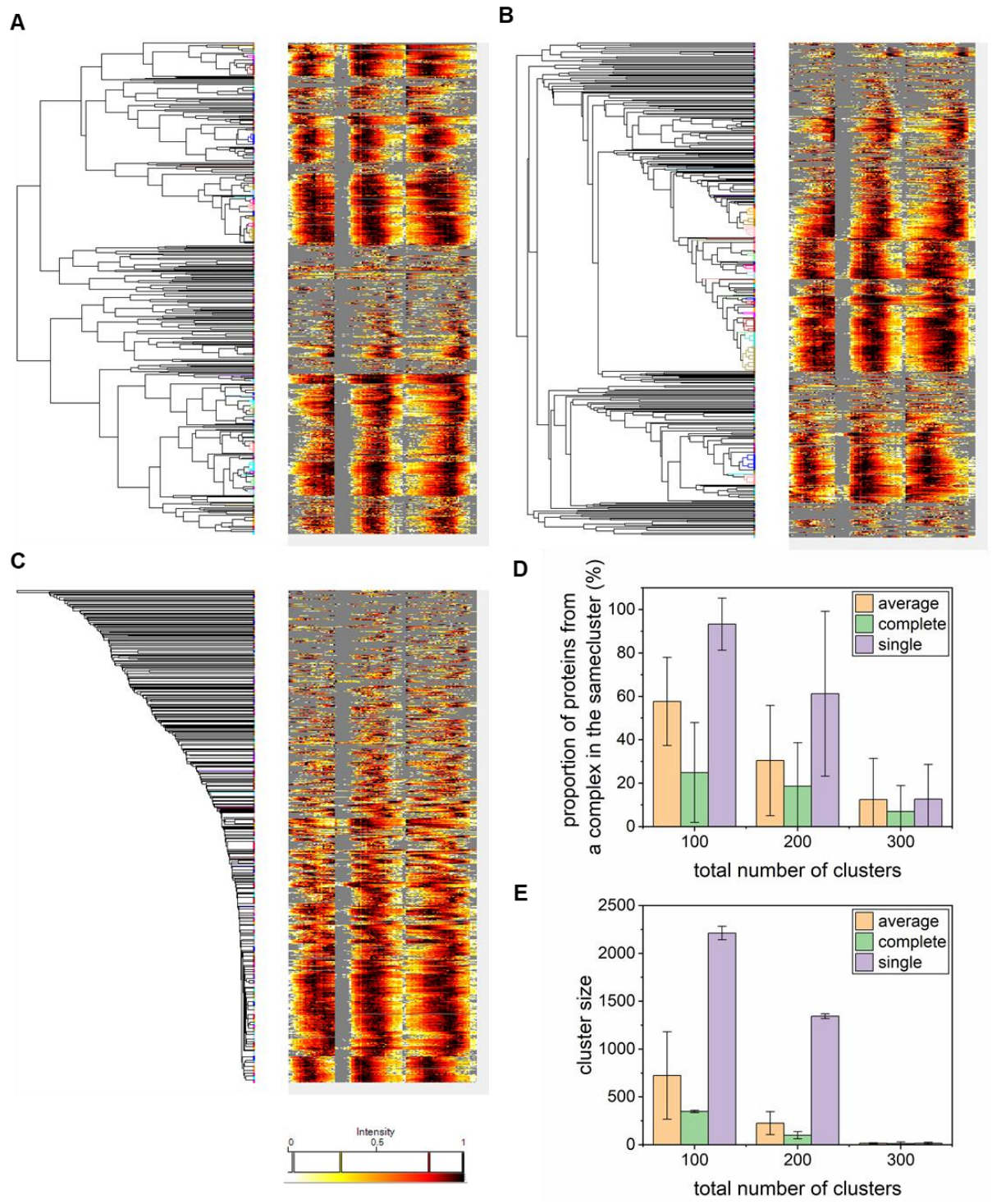

Fig. 3.7 Hierarchical cluster analysis of the three replicates. Cluster analysis was carried out in Perseus based on Pearson distance with either average linkage (**A**), complete linkage (**B**), or single linkage (**C**). Described complexes were analysed for occurrence in the same cluster (**D**). The proportion of proteins from one complex that was found in the same cluster was calculated for each complex. Average of all tested complexes is displayed with the standard deviation. **E**: respective size of the cluster containing the highest proportion of proteins from one complex. Average for all tested complexes is depicted, error bars indicate the standard deviation.

Therefore, the dataset was not suitable to detect interacting proteins on basis of similar elution profiles. As described in section 3.1.5, many proteins show a similar elution profile, making genuinely interacting proteins and the background indistinguishable.

3.1.7 Analysis of proteins from the c-di-GMP network

Proteins involved in c-di-GMP signalling were investigated in further detail. *P. aeruginosa* PAO1 encodes 43 proteins containing GGDEF/EAL/HD-GYP domains, that are potentially involved in making and breaking the messenger molecule. Out of these, 33 proteins are predicted to reside in the membrane. Throughout the three datasets obtained in this work, 29 of deducted c-di-GMP modulating proteins (67 %) were identified, of which 17 proteins were detected in all three replicates (**Fig. 3.8**, Table A3). Out of the 33 predicted membrane proteins, 24 proteins (73 %) were identified in the three datasets. The elution profiles of GGDEF/EAL/HD-GYP domain proteins were similar for most proteins in the three replicates. This indicates that elution profiles of proteins were reproducible (cf. 3.1.16). The identified proteins exhibited different profiles: some appear to separate over a broad range with a maximum in fraction 10-15 (elution volume 12.97-14.47 ml), while other proteins display a distinctive separation profile with fluctuating relative abundances. There was no noticeable difference in the elution profiles of membrane proteins and cytosolic proteins.

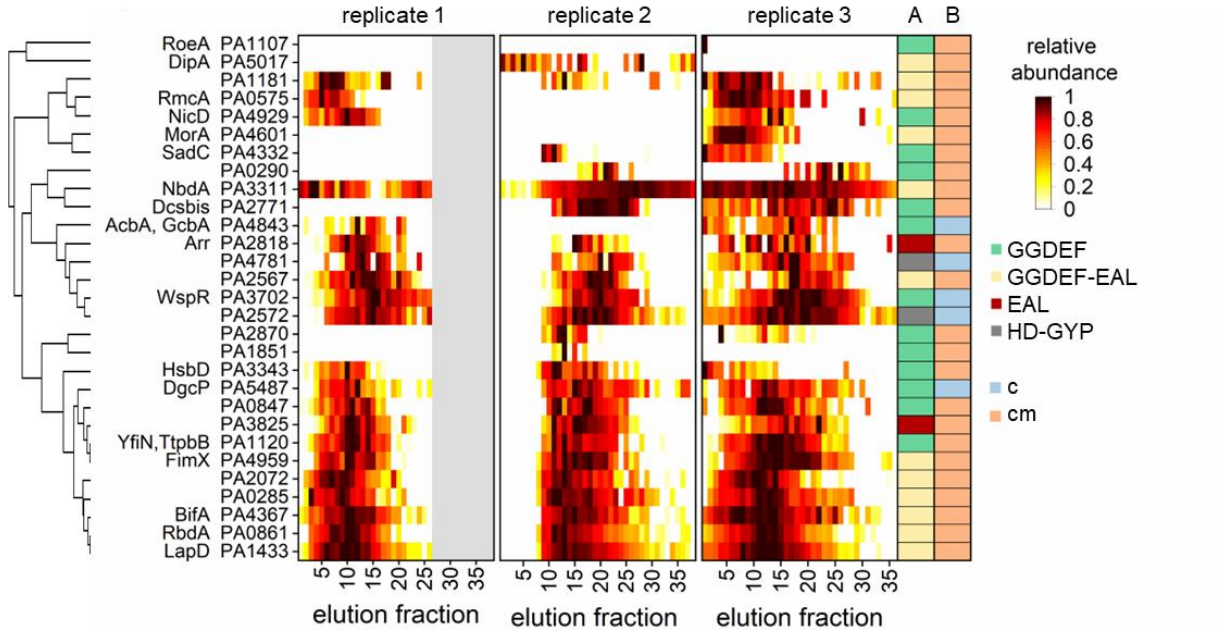

Fig. 3.8 Elution profiles of identified GGDEF/EAL/HD-GYP proteins. All proteins containing either a GGDEF, EAL or HD-GYP domain were depicted in a heatmap. Colour gradient showing the relative abundance based in IBAQ value. High abundance is coloured red, low abundance yellow to white. Replicate 1 (left panel), replicate 2 (second panel), and replicate 3 (third panel). Colour coding shows domain structure of the proteins (panel A) and predicted subcellular localisation (panel B). c: cytoplasmic, cm: cytoplasmic membrane. Proteins were sorted by hierarchical clustering with Pearson distance and complete linkage.

It has been suggested and in certain instances confirmed that c-di-GMP-producing and degrading proteins localize close to their cellular targets for a specific local regulation (Sarenko *et al.*, 2017). Therefore, the library was tested for co-occurrence and co-elution of described protein-protein interactions involving GGDEF/EAL/HD-GYP domain containing proteins. For instance, the Wsp chemosensory-like signal transduction complex was selected (Güvener *et al.*, 2007). This system

consists of a core complex (WspABDE), the methyltransferase WspC, the methyl esterase WspF, and the diguanylate cyclase WspR, which produces c-di-GMP in response to surface contact (Güvener *et al.*, 2007; Hickman *et al.*, 2005; O'Neal *et al.*, 2022). In the nanodisc library, proteins of the core complex WspABDE and, furthermore, WspF and WspR were reproducibly identified. The methyltransferase WspC was not detected in this study. The elution profiles of the individual proteins were overall similar but revealed increasing differences in later fractions, again indicating the presence of subcomplexes lacking one or several protein components (**Fig. 3.9 A**). The methyl esterase WspF eluted in a clearly different profile from the rest of the complex. This protein is required to turn off the sensory system by demethylation of WspA (Hickman *et al.*, 2005). Therefore, WspF might not be recruited to the complex in these experimental conditions.

Another membrane-associated complex including a c-di-GMP modulating protein is the tripartite periplasmic signalling system YfiNBR. In this dynamic system, the periplasmic protein YfiR can bind and thereby inactivate the cytoplasmic membrane diguanylate cyclase YfiN. In the presence of an unknown signal, the outer membrane component YfiB competes for binding of the periplasmic protein YfiR and, thereby, releases and activates the diguanylate cyclase YfiN (Giardina *et al.*, 2013; Malone *et al.*, 2012). All components of the system were detected in two out of three replicates, but individual proteins showed very different elution profiles (**Fig. 3.9 B**). The diguanylate cyclase YfiN had a broad elution profile and with highest abundance at 13.2 ml elution volume, comparable to most proteins from the cytoplasmic membrane. YfiB was detected in the first fraction, and at elution volumes of 13–17 ml. The early elution of the outer membrane protein YfiB in the first fraction might indicate aggregate formation, while the later elution fractions likely contain the soluble protein. The periplasmic protein YfiR was detected in later fractions (>13 ml elution volume) with an irregular profile. All three components of the YfiNBR system eluted independently, indicating that this system experiences only weak interactions or that the nanodiscs did not preserve the complex in the library.

A stable interaction was as well reported for the diguanylate cyclase DgcP and the landmark protein FimV in *P. aeruginosa* PA14. The correct localisation for DgcP to the cell pole depends on FimV (Nicastro *et al.*, 2020). Both proteins (alias DgcH and FimV in PAO1) showed an overlapping elution peak in fractions with 11.7–13.5 ml elution volume, but more pronounced deviations in the later fractions (**Fig. 3.9 C**).

Another tested protein-protein interaction pair is an example for a direct interaction of a c-di-GMP effector with its cellular target: the c-di-GMP binding protein FimX was reported to interact with the T4P ATPase PilB that fuels pilus function (Jain *et al.*, 2017). In the library, both proteins FimX and PilB were detected and showed overlapping elution in the first 15 fractions (elution volume of 10–14 ml), while PilB showed a broader elution profile, probably due to additional interactions with components of the pilus machinery (**Fig. 3.9 D**).

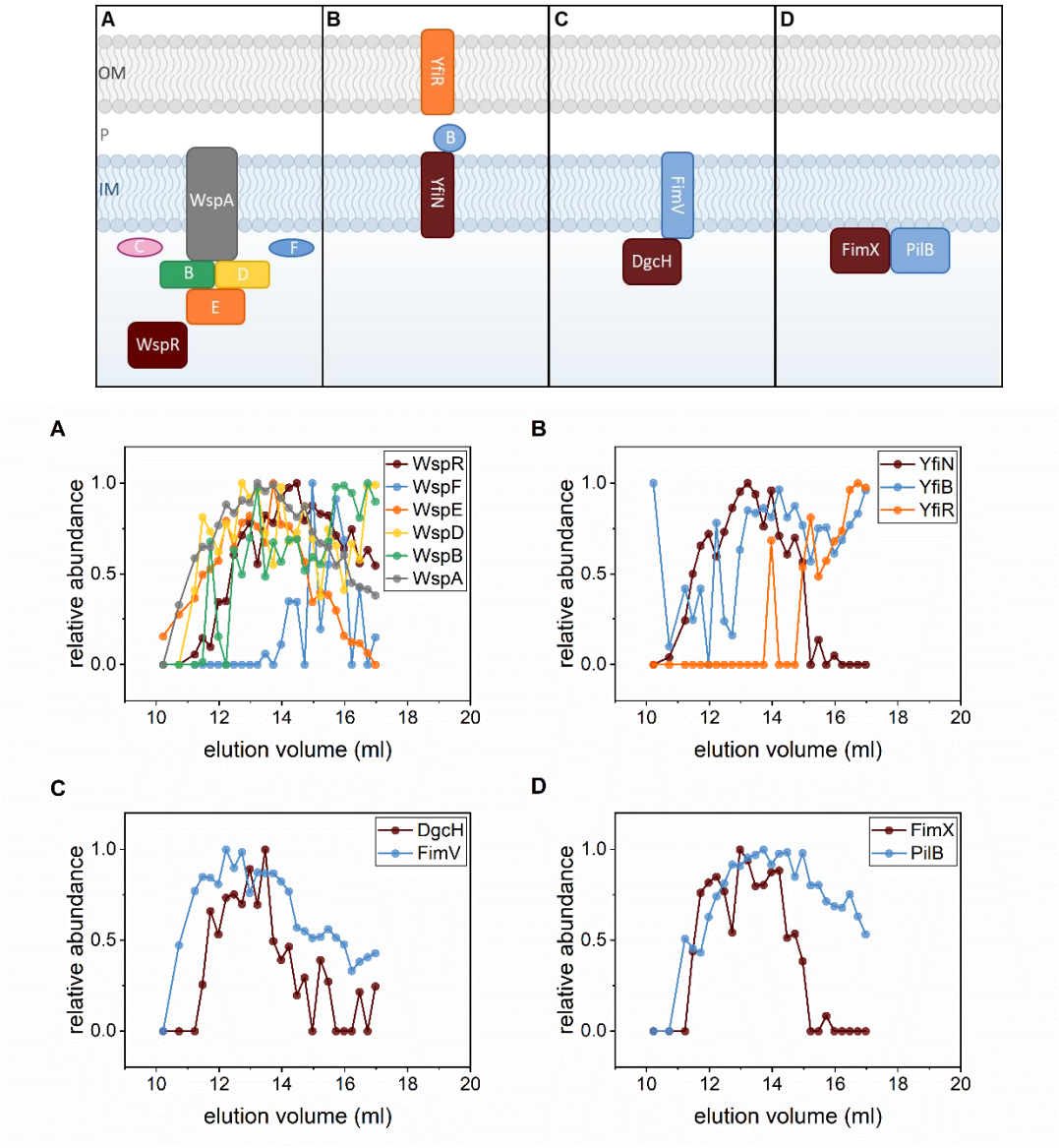

Fig. 3.9 Elution profiles of complexes involved in c-di-GMP signalling. The relative abundance of each protein was plotted against the elution volume from size exclusion chromatography. Data from replicate 3 is shown. **A**: Elution profiles for the surface sensing Wsp system associated with the diguanylate cyclase WspR. **B**: The redox or membrane perturbation recognizing system YfiNBR. **C**: The interaction partners DgcH (DgcP in PA14) and the landmark protein FimV. **D**: The c-di-GMP specific sensor protein FimX and the ATPase PilB involved in T4P extension.

The results indicate that known interactions of c-di-GMP signalling proteins could be tracked in our dataset, suggesting a preservation of these interactions. However, also the elution profiles of c-di-GMP regulating proteins and their interaction partners were not limited to specific fractions but broadly distributed over the whole elution volume, thereby making a prediction of complexes not possible (cf. section 3.1.5 and 3.1.6).

3.1.8 Detection of NbdA

The phosphodiesterase NbdA was detected in the mass spectrometry data in all three replicates with high abundance and a sequence coverage of 45.8 % (Fig. A1). Most peptides that were identified derived from the GGDEF or EAL domain. Only one peptide originating from the MHYT domain was

identified. Expression data indicate enhanced *nbdA* transcript levels in the stationary phase or after heat shock (Gerbracht, 2021). For the analysis of protein interations of NbdA, we tried to detect the protein as Flag-tagged variant under the control of its native promoter. Therefore, a *nbdA*-Flag fusion was integrated into the original gene locus by homolous recombination (2.3.6). Cells were cultured for three, five or 16 hours at 37°C, and proteins from whole-cell samples were seperated by SDS-PAGE (**Fig. 3.10**). In the western blot, the NbdA-Flag variant was not detected in cultures grown three, five or 16 hours. When *nbdA*-Flag was encoded on a plasmid under the control of an inducible *tac* promoter, the protein could be detected three hours after induction: NbdA-Flag has a calculated size of 83 kDa, and in the western blot there is a signal at about 70 kDa. The smaller size in the gel has previously been observed (Gerbracht, 2021; Rüger, 2019) and is probably due to the hydrophobic parts of the protein. Detection of NbdA under the control of the native promoter was aditionally assayed using a strain containig a chromosomally integrated *nbdA*-mNeonGreen-His fusion, as well as a strain containing a *nbdA*-Strep fusion. In both cases, membrane proteins were isolated (2.4.3) and separated on a SDS-PAGE. Immuno-detection of His-tagged or Strep-tagged protein variants was conducted with specific antibodies against the respective tag (Tabe 2.12, Fig. A1). However, NbdA was not detected in either western blot.

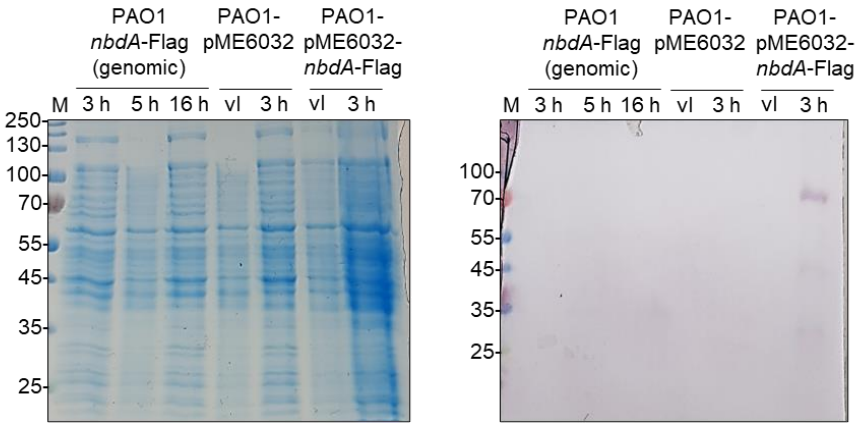

Fig. 3.10 Detection of NbdA under control of the native promoter. SDS-PAGE (left) and western blot (right) of a test expression for Flag-tagged NbdA. Cells containing a genomically integrated *nbdA*-Flag fusion in the original gene locus of *nbdA* were grown at 37 °C and after 3 h, 5 h and 16 h a whole-cell sample was collected. As a control, a culture with Flag-tagged NbdA on the low copy vector pME6032 was used. When the culture reached a OD_{600} of 0.5, protein production was induced with 100 µM IPTG. Samples were collected 3 h after induction. vI shows the sample before induction. Whole-cell samples were resuspended in 4x SDS sample buffer, incubated for 10 min at 95 °C, centrifuged and loaded on the gel. Flag-tagged proteins were detected with the M2-Flag-antibody (primary) and anti-mouse IgG-AP conjugate (secondary), with a colorimetric reaction.

The detection of NbdA under the control of its native promoter was not achieved by western blot analysis. However, there is evidence that the protein is produced in stationary phase by transcription data, CLSM data and proteomic data (Gerbracht, 2021).

3.2 Interaction partners of NbdA

In the second part of the thesis, the PDE NbdA was analysed in more detail. The protein was stably identified in the proteomic data in stationary phase, however in western blot the protein could not be detected. To investigate possible interaction partners of this protein, an overexpression strain was used to ensure stable protein production. The nanodisc-forming polymer DIBMA was tested for its suitability for a targeted pulldown approach of membrane proteins (Scherhag *et al.*, 2023).

3.2.1 Identification of novel protein interaction partners of NbdA by pulldown assay

To investigate interaction partners of the membrane protein NbdA, a targeted pulldown approach was carried out (2.4.16). It is described that *nbdA* is naturally expressed in the stationary phase (Gerbracht, 2021), and the native protein was stably detected in the proteome under stationary culture conditions (cf. 3.1.7). Tagged fusion proteins under the control of the native promoter were not detected in western blot (section 3.1.8). To ensure stable detection, *nbdA* was genetically fused to a C-termial Strep-tagII and ectopically expressed on a pHERD26T vector backbone (pMRP12, Rüger, 2019). The culture overproducing Strep-tagged NbdA was grown until stationary phase to allow presence of native interaction partners. Cells were harvested, lysed by sonication and membranes were isolated by several centrifugation steps. From the isolated membranes, a nanodisc library was created using the polymer DIBMA. Nanodiscs containing tagged NbdA were enriched via affinitiy chromatography. A culture overproducing untagged NbdA in the same vector background (pMRP13, Rüger, 2019) was used as a negative control. This control comprised the background and proteins that bind unspecificly to the affinity beads. Moreover, false hits derived from altered protein levels associated with *nbdA* overexpression could be excluded with this control. In an additional control, the affinity beads were blocked by treatment with 50 mM biotin, to prevent Strep-tagged proteins from binding to the column.

The individual steps of the pulldown experiment were analysed in a SDS-PAGE (**Fig. 3.11 A**). In the elution fraction of the pulldown, several proteins with different sizes were observed. The fusion protein NbdA-Strep was detected in a western blot, at a size of about 70 kDa (**Fig. 3.11 B**). This observed molecular weight is lower than the predicted molecular weight of the Strep-tagged NbdA variant of 81.6 kDa. The size difference of Strep-tagged NbdA variants has already been desribed in previous studies (Rüger, 2019; Gerbracht, 2021). The additional proteins detected in the elution sample are candidate interaction partners of NbdA, proteins co-occuring in the same nanodiscs or proteins binding unspecifically to either the column material or the nanodiscs. Some signals are also visible in the control sample with untagged NbdA. Presence of proteins in this control is a hint for unspecific binding to the column material. In the control sample with the blocked beads, no protein signal is visible. This control was therefore not further subjected to mass spectrometry analysis.

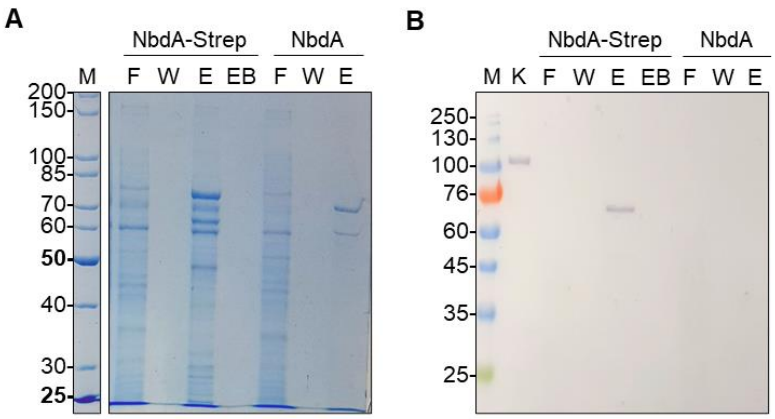

Fig. 3.11 Detection of NbdA after StrepXT-pulldown. Membrane proteins were solubilised with DIBMA. Pulldown was perfomed on a Strep-TactinXT column with *P. aeruginosa* membrane protein fraction isolated from cells overproducing NbdA with a C-terminal Strep-tagII (PAO1 pMRP12). Cells overproducing NbdA without a tag were used as control (PAO1 pMRP13). F: flow through, W: wash fraction, E: elution, EB: elution after blocking beads with 50 mM biotin, K: positive control for western blot (RdmS, 115 kDa). **A**: SDS-PAGE of pulldown samples. M: Unstained protein Standard, Broad Range (10 - 200 kDa). **B**: Western blot of pulldown samples. M: Prestained Protein Marker. NbdA-Strep was detected with anti-Strep-Tactin AP conjugate and a colorimetric reaction with NBT and BCIP.

For each pulldown sample with tagged NbdA as well as for the control, four replicates were prepared and proteins were analysed in mass spectrometry. The protein with the highest intensity was found to be a biotin binding protein (LiuD), followed by the target protein NbdA, the pili protein PilA, the biotin containing protein OadA, the 50S ribosomal protein RplB and the chaperone GroEL. Enrichment of biotin binding proteins is a known characteristic of Strep-columns (Schmidt *et al.*, 2021; Skerra *et al.*, 2000) yet these proteins were equally enriched in the control sample. The high abundance of the ribosomal protein and the chaperone might be due to protein overexpression. It was also observed that polymers interact non-specifically with charged proteins and lipids (Glueck *et al.*, 2022; Pollock *et al.*, 2022). The LFQ intensities were log transformed and missing values were imputed (section 2.7.3). For the four replicates, the fold change between the NbdA pulldown sample and the control as well as the significance (*p*-value) were calculated and plotted in a volcano plot (**Fig. 3.12**). In the NbdA pulldown sample, 163 proteins were highly significant enriched (FDR < 0.01) (Table A4, red). Among the most enriched proteins with high significance is the target protein NbdA. 45 % of the highly enriched proteins were predicted cytoplasmic proteins, 31 % are predicted to be located in the cytoplasmic membrane, and 10 % have unknown localisation. Proteins of different COG cathegories were identified, the largest groups were amino acid transport and metabolism (14), signal transduction mechanisms (13) and cell wall/membrane/envelope biogenesis (12). Interestingly, several transcriptional regulators (e.g. CzcR, LasR, and RhlR) involved in regulation, antibiotic resistance and quorum sensing were detected among the top hits (Dieppois *et al.*, 2012; Gambello *et al.*, 1993; Gilbert *et al.*, 2009). In addition to NbdA, two other members of c-di-GMP signalling were identified and enriched with high significance: The PDE RmcA and the effector protein FleQ.

In total in the NbdA pulldown sample there were 417 proteins significantly enriched (FDR < 0.05) (Table A4, orange). 40 % of the enriched proteins were predicted cytoplasmic proteins, 34 % are predicted to be located in the cytoplasmic membrane, and 10 % have unknown localisation. Proteins of different COG cathegories were identified, the largest groups were signal transduction mechanisms (46), amino acid transport and metabolism (45), and cell wall/membrane/envelope biogenesis (28). In addition to NbdA, six other members of c-di-GMP signalling network were identified and significantly enriched: The PDE RmcA, the PDE RbdA, the DGC SadC, the putative PDE PipA, and the membrane effector LapD. All members are predicted cytoplasmic membrane proteins and were also identified in the proteome in stationary phase PAO1 cells. Additionally, the c-di-GMP specific effector protein FleQ was also identifed.

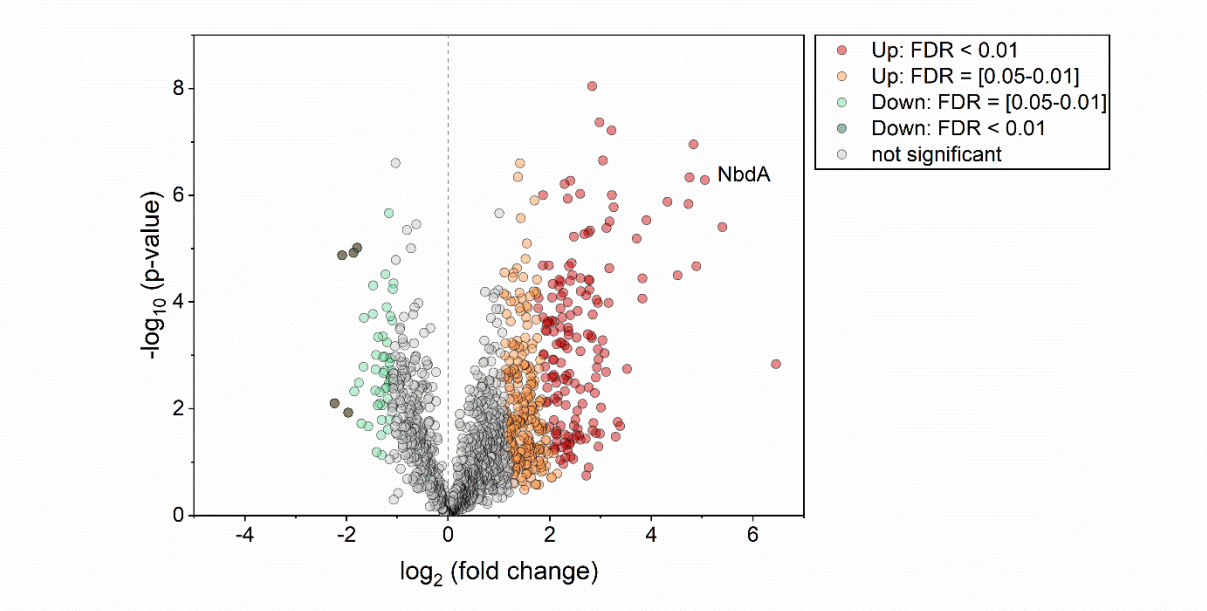

Fig. 3.12 Volcano plot of NbdA-Strep pulldown. NbdA-Strep and interacting proteins were enriched from the library on Strep-Tactin XT resin and compared to controls from strains expressing untagged NbdA. In each case, four technical replicates were analysed. The plot shows the $\log_2$ of the fold change of the NbdA pulldown sample compared to the control sample plotted against the negative $\log_{10}$ of the *p*-value. The volcano plot shows the results of a modified Student's *t*-test with permutation-based FDR control calculated from four replicates in each group (Tusher *et al.*, 2001). Two significance thresholds were applied to call significantly changed proteins. Class A: S0 = 4, FDR <0.01, dark green and red; Class B: S0 = 4, FDR = [0.05–0.01], light green and orange. Proteins that showed no significant change are depicted in grey.

Eight members of the c-di-GMP network were identified, but were not enriched in the pulldown (BifA, PA4396, PA2567, PA0847, MorA, PA2027, PA3825 and DgcH). All of them except PA4396 were also identified in the PAO1 proteome (section 3.1.7). On the other hand, there were 53 proteins significantly reduced in the pulldown compared to the control sample, five of them were even highly significant (Table A5, green). The majority of reduced proteins were predicted cytosolic proteins (62 %), proteins in outer membrane vesicles (15 %) and proteins with unknown localisation (11 %).

3.2.2 Verification of protein-protein interactions by B2H assay

More than 400 proteins were significantly enriched in the pulldown and thus candidates for interaction partners of NbdA (**Fig. 3.13 A**). However, these may include many false positives. To confirm the protein interaction of highly enriched or interesting candidates, bacterial adenylate cyclase two hybrid (B**2**H) assays were performed. Therefore, NbdA and the candidate protein were genetically fused to two independent subunits of the adenylate cyclase of *Bordetella pertussis* and co-transformed into the *E. coli* test strain (Karimova *et al.*, 1998). Robust interaction of two fusion proteins was indicated by an elevated cAMP content in *E. coli*, resulting in red colonies on McConkey agar. In the empty vector control, yellow-coloured colonies were observed (**Fig. 3.13 B**). For each tested interaction, negative controls containing one fusion protein and one empty vector were included. From the list of highly enriched proteins, CzcR, a transcription factor involved in swarming motility, and the hypothetical protein PA4200 were selected for B2H analyses. A strong positive interaction with NbdA was observed for both proteins (**Fig. 3.13**).

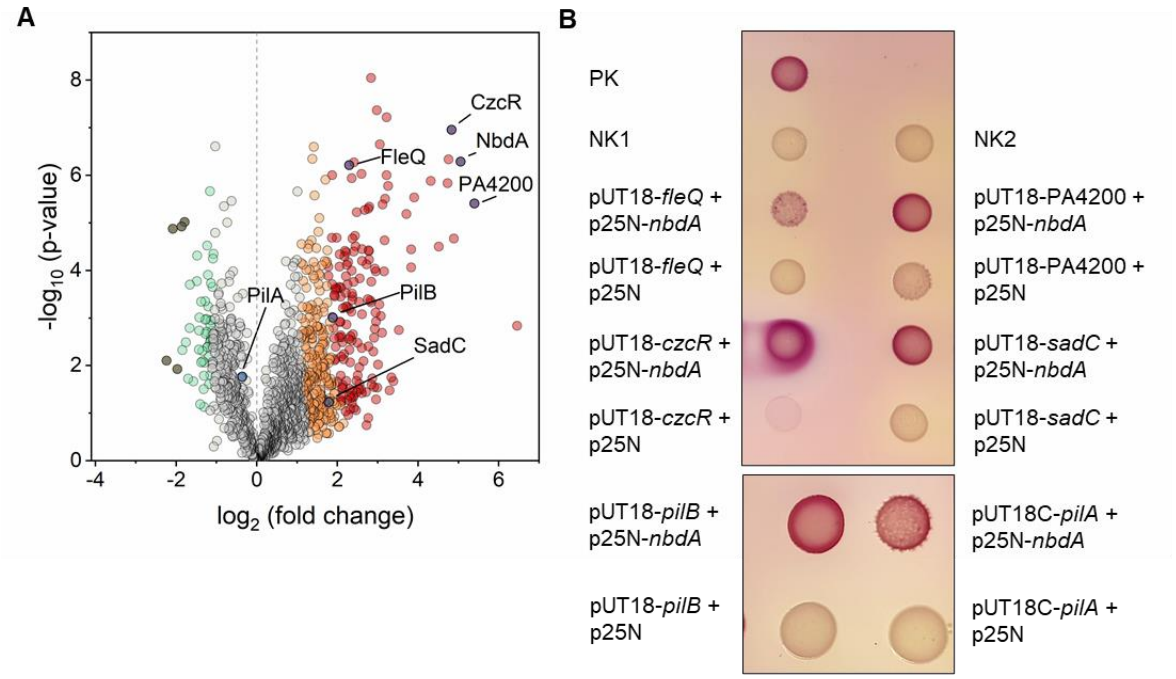

Fig. 3.13 B2H test for protein-protein interaction with candidate proteins. A: Volcano plot of the NbdA pulldown. The plot shows the $\log_2$ of the fold change of the NbdA pulldown sample compared to the control sample plotted against the negative $\log_{10}$ of the p- value. Two significance thresholds were applied to call significantly changed proteins. Class A: S0 = 4, FDR <0.01, dark green and red; Class B: S0 = 4, FDR = [0.05–0.01], light green and orange. Proteins that showed no significant change are depicted in grey. Proteins tested for direct interaction with NbdA are shown in blue. **B**: Bacterial adenylate cyclase two hybrid (B2H) assay for the interaction of NbdA with the target proteins FleQ, PA4200, CzcR, SadC, PilB and PilA. PK: positive control, interaction test of pUT18-*nbdA*$_{cyt}$ with p25N-*nbdA*. NK1: negative control #1, interaction test of pUT18 and p25N-*nbdA*. NK2: negative control #2: interaction test of put18 and p25N empty vectors. Plates were incubated at 30 °C for 48 h.

Significantly enriched in the pulldown assay, although not among the top hits, was the c-di-GMP-responsive transcription factor FleQ (Hickman *et al.,* 2008). For this candidate the colony only showed a pale red colour, the interaction with NbdA could not be confirmed in the B2H system. Among the moderately enriched proteins in the pulldown assay, also the diguanylate cyclase SadC was detected. An interaction of SadC with NbdA has been shown previously (Beganovic, 2018). The B2H analysis validated the positive interaction of SadC with NbdA.

Among the potential NbdA interactors also several T4P components were found. One of them was PilB, the T4P ATPase known to promote polymerization of the pilus subunits during attachment and twitching motility of *P. aeruginosa* (Mattick, 2002; Turner *et al.*, 1993; Whitchurch *et al.*, 1991). Although not being one of the top enriched proteins, PilB was robustly detected with 20 peptides and its levels were more than 3.5-fold enriched over those in the untagged control strain. The B2H test could confirm PilB as an interactor of NbdA (**Fig. 3.13**). As the intensity of the pilin subunit PilA was high throughout all pulldown samples, it was hypothesised that the overexpression of NbdA might influence PilA levels. A direct interaction of the proteins was already shown (Unbehend, 2022). The B2H analysis verified the positive interaction of PilA and NbdA.

To gain further insight into which part of NbdA is responsible for the interaction, also the subdomains were tested. The MHYT subdomain contains the N-terminal membrane domain, while the $NbdA_{cyt}$ subdomain represents the cytosolic part of the protein consisting of the GGDEF and the EAL domain. Negative controls with the empty vectors show yellow-coloured colonies (**Fig. 3.14**). The highly enriched transcription factor CzcR, and the hypothetical protein PA4200 showed a strong positive interaction with $NbdA_{cyt}$ but no interaction with the MHYT domain (**Fig. 3.14 A**). For the c-di-GMP-responsive transcription factor FleQ red coloured colonies were observed for the interaction of both subdomains. An interaction of the cytosolic part of NbdA with the diguanylate cyclase SadC was already shown (Beganovic, 2018) and could be verified. No interaction of SadC with the MHYT domain of NbdA was observed. For the T4P ATPase PilB, the B2H test showed a positive interaction with both subdomains of NbdA, the MHYT domain as well as the cytosolic domains (**Fig. 3.14 B**). The pilin subunit PilA showed no interaction with the MHYT domain or $NbdA_{cyt}$ in the B2H test. However, consistent with Unbehend (2022), after further incubation of the plates for another 48 h, a slightly red colour for the interaction of PilA and the MHYT domain of NbdA was observed (data not shown). In summary, these results show that a soluble library of membrane proteins in nanodiscs can be used to co-purify interaction partners of membrane proteins and thereby reveal novel protein-interaction networks.

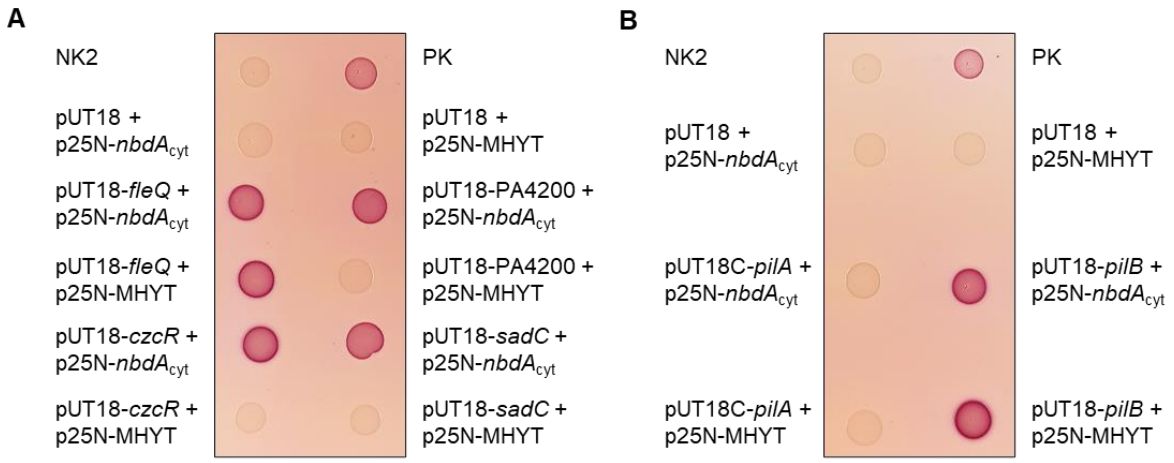

Fig. 3.14 B2H test for protein-protein interaction between candidate proteins and NbdA subdomains. Target proteins FleQ, PA4200, CzcR, SadC, PilB and PilA were tested for interaction with NbdA subdomains. MHYT: N-terminal MHYT domain of NbdA. NbdA$_{cyt}$: cytosolic part of NbdA, consisting of the GGDEF and EAL domain. PK: positive control, interaction test of pUT18-*nbdA*$_{cyt}$ with p25N-*nbdA*. NK2: negative control #2: interaction test of put18 and p25N empty vectors. **A** and **B**: Plates after 24 h at 30 °C.

3.3 Phenotypic effects of altered NbdA contents in *P. aeruginosa*

The protein NbdA has been subject of various previous studies (Gerbracht, 2021; Liu *et al.*, 2022a; Rüger, 2019; Xin *et al.*, 2019). Although some phenotypes were associated with the PDE activity of NbdA, most of the phenotypes are still not fully understood. To gain more insight into the function of NbdA, cell morphology, growth on solid media, nucleotide levels, activity, and localisation of NbdA was assayed. In addition, a possible role of NbdA in pilus regulation was tested by phage infection assays and co-localisation studies with pili subdomains.

3.3.1 Growth on plates and cell morphology

P. aeruginosa cells overproducing NbdA were shown to have a defect in growth on solid surfaces (Gerbracht, 2021). The overexpression of the MHYT domain alone was sufficient to trigger the reduced growth on agar plates (Gerbracht, 2021). Thus, it was tested whether this effect is specific to the MHYT domain of NbdA, or wether other MHYT domain proteins have a similar effect when overexpressed. The protein MucR from PAO1 with a similar domain structure like NbdA, and the MHYT domain protein CoxH from *O. carboxyvorans* were used. Further, to exclude that the growth defect derived generally from the overexpression of a membrane protein, the PDE BifA from PAO1 containing one transmembrane domain was also tested (**Fig. 3.15 A**). All proteins were cloned in a pHERD26T vector and fused with a C-terminal Strep-tagII. Protein production was confirmed by western blot (**Fig. 3.15 B** and **C**). Overproduction of NbdA was confirmed 3 h and 5 h after induction. Overproduced MucR was detected at a size of approximately 75 kDa (calculated molecular weight of 75.5 kDa). The membrane protein BifA had a calculated molecular weight of 78.6 kDa and could be detected at approximately this size in the western blot.

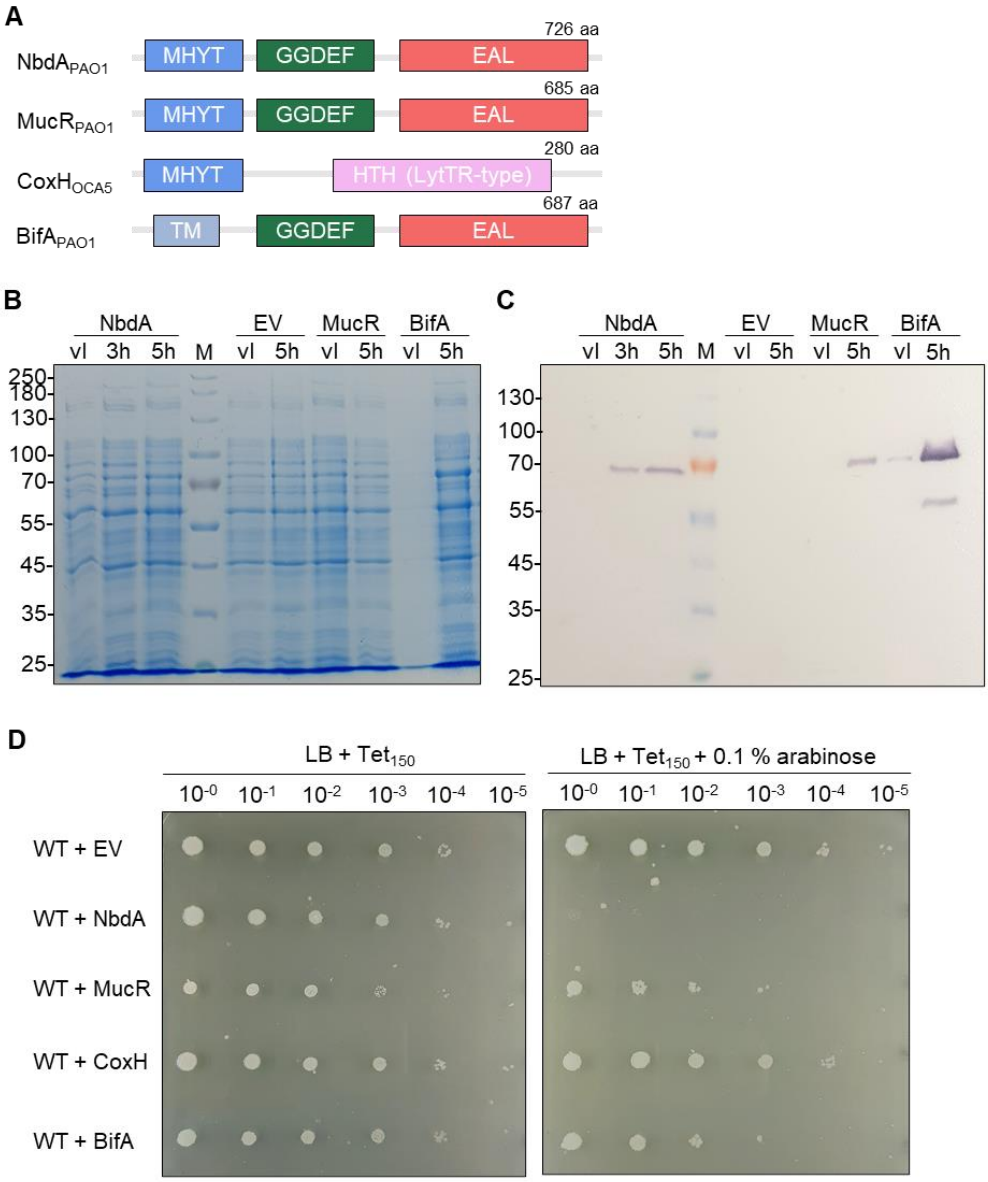

Fig. 3.15 Overproduction of membrane proteins in *P. aeruginosa*. A: Domain structure of the proteins NbdA from *P. aeruginosa*, MucR from *P. aeruginosa*, CoxH from *O. carboxidovorans*, and BifA from *P. aeruginosa*. Domain names for MHYT, GGDEF and EAL domain represent a characteristic amino acid motif. TM: transmembrane domain. HTH: helix-turn-helix motif. **B** and **C**: SDS-PAGE and western blot of a test expression for the production of Strep-tagged NbdA (PAO1 pMRP12), MucR (PAO1 pASC09) and BifA (PAO1 pASC10) in PAO1. EV: PAO1 cells carrying empty vector pHERD26T. Cultures were grown at 37°C until they reached OD_{600} of 0.5 and gene expression was induced with arabinose. After induction cultures were incubated at room temperature (22 °C). Whole-cell samples were analysed. M: Colour Prestained Protein Standard, Broad Range (10 - 250 kDa). vI: sample before induction, 3h: sample 3 h after induction with 0.1 % arabinose, 5h: sample 5 h after induction with 0.1 % arabinose. Strep-tagged proteins were detected with anti-Strep-Tactin AP conjugate and a colorimetric reaction with NBT and BCIP. **D**: Growth on plates of *P. aeruginosa* PAO1 cells overproducing different membrane proteins. WT + EV: PAO1 pHERD26T, WT + NbdA: PAO1 pMRP12, WT + MucR: PAO1 pASC09, WT + CoxH: PAO1 pHERD26T-*coxH*-Strep, WT + BifA: PAO1 pASC10. The assay was performed in biological triplicates. Precultures were set to an OD_{600} of 0.1 and a serial dilution from 10^{-1} to 10^{-5} was prepared. 1 µl of each dilution was dropped on LB agar containing tetracycline (Tet) and if applicable 0.1 % arabinose. Plates were incubated for 16 h at 37 °C.

The strains overproducing the target proteins were dropped in a serial dilution on agar plates that contained the inductor of protein production arabinose, and on control plates (**Fig.3.15 D**). On the control plates, all strains showed normal growth until a dilution of 10^{-4}. Colonies of the MucR strain were a bit smaller, and the preculture showed enhanced clumping, probably due to DGC activity of MucR. On plates containing the inductor arabinose, the empty vector control, and the CoxH overproduction strain showed normal growth until a dilution of 10^{-4}. The MucR and BifA overproduction strains showed growth until a dilution of 10^{-3}. The NbdA overproduction strain, however, showed a severe growth defect, with only weak growth in the 10^{0} dilution.Hence, the growth defect observed is specific for the overproduction of the MHYT domain of NbdA as other MHYT domain proteins or membrane proteins did not result in such a severe growth reduction on solid media. Notably, overeproduction of NbdA encoded on the low-copy vector pME6032 did not result in a defect in growth on plates (Fig. A5).

It was also revealed by Gerbracht, 2021 that cells overproducing NbdA show an elongated cell morphology, which is dependent on the presence of the MHYT domain. Thus, cell morphology of strains overproducing different MHYT domain proteins (MucR and CoxH) or a membrane protein (BifA) was investigated (**Fig. 3.16 A**). Furthermore, the cells' lengths were determined by *in silico* measurement (**Fig. 3.16 B**). All cells in the non-induced samples show rod like cell morphology with a cell length of approimately 2 µm. Similar to Gerbracht, 2021, overexpression of *nbdA* resulted in an elongated cell morphology, with cells up to of 7.8 µm in length. Remarkably, cells with a regular size of 2 µm were also present in the culture alongside to elongated cells of various sizes. Overproduction of the MHYT domain containing proteins MucR and CoxH, as well as the membrane protein BifA, did not result in changed cell morphology or cell length. After induction, all cells were rod shaped and about 2 µm long.

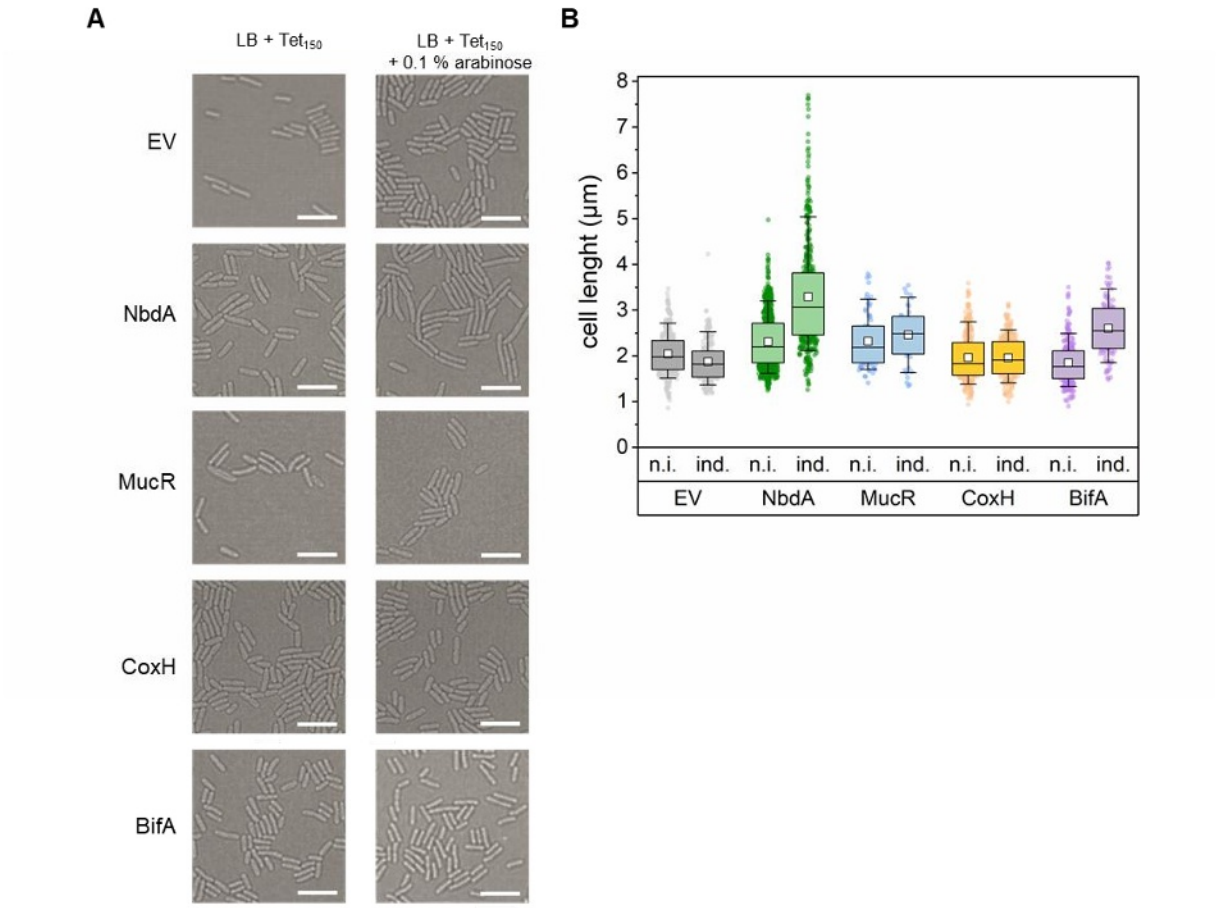

Fig. 3.16 Cell morphology and measurement of cell length of *P. aeruginosa* mutants overproducing different membrane proteins. **A**: Microscopy of PAO1 cells containing different pHERD26T derivates for the overproduction of NbdA, MucR, CoxH and BifA. All proteins carried a C-terminal a Strep-tagII. EV: empty vector control, PAO1 carrying pHERD26T. Cultures were grown to an OD_{600} of 0.5 at 37 °C. After induction with 0.1 % arabinose, cultures were incubated for 5 h at room temperature (right panel). An uninduced culture under the same conditions served as a control (left panel). For microscopy, cells were immobilised on agarose pads. Images were taken in a Zeiss LSM 880 by transmitted light microscopy. Scale bar: 5 µm. **B**: Evaluation of cell length from microscopy images. Cell length was measured with the Zeiss Blue software and ImageJ. Boxes depict the range of 25 %–75 % of the data, whiskers the range of 10 %–90 %. Median (black line) and average (white square) are also shown. Dots show individual cell sizes. EV: empty vector control PAO1 pHERD26T with n = 339 for not induced (n.i.) and n = 202 for induced culture (grey). NbdA: PAO1 pMRP12 (green), with n = 635 for not induced, and n = 583 for induced culture, MucR: PAO1 pASC09 (blue), with n = 74 for not induced, and n = 132 for induced culture, CoxH: PAO1 pHERD26T-*coxH*-Strep (yellow), with n = 288 for not induced, and n = 240 for induced culture, BifA: PAO1 pASC10 (violet), with n = 240 for not induced, and n = 379 for induced culture.

3.3.2 Nucleotide levels of a *nbdA* deletion mutant

Metabolites were measured from culture extracts for the wildtype PAO1 and a markerless *nbdA* deletion mutant. Identification and quantification of metabolites by MS was performed in collaboration with [redacted]. From the 4 biological replicates, 24 buckets could be identified (Table A6). Of the identified buckets, one compound was significantly enriched in the WT compared to the *nbdA* deletion strain. The identified metabolite β-nicotinamide adenine dinucleotide was about 3-fold enriched in the WT. However, other components were found to be different in WT and *nbdA* deletion but were not identified (Fig. A4). Masses and retention time of these components are listed in Table A6.

Identification of these compounds could provide valuable insight into possible function of NbdA in the cell. Although no phenotype was observed for Δ*nbdA* so far, there seem to be differences in metabolite levels. As the mass range was high, low abundant metabolites were not detected. For example, the nucleotide c-di-GMP was not detected with this method.

Nucleotide levels of *P. aeruginosa* cultures were determined. Thus, nucleotides were extracted from whole-cell samples and quantified by mass spectrometry in collaboration with H. Becker and S. Stegmüller (AG Richling, Department of chemistry, RPTU). Since a reduction in nucleotide levels of culture extracts was observed after only a few days of incubation (data not shown), a consistent timing of sample preparation, lyophilisation and measurement was carefully attended to obtain reproducible results. The PAO1 cultures had a c-di-GMP content of about 15 pmol/mg protein (**Fig. 3.17 A**). For a *nbdA* deletion strain, no change in c-di-GMP levels compared to WT was observed, which is consistent with previous studies (Rüger, 2019; Xin *et al.*, 2019; Zemke *et al.*, 2020). Notably, also a c-di-GMP isomer was detected in the cell extracts of PAO1 and the *nbdA* deletion strain (**Fig. 3.17 B**). The isomer had the same mass as c-di-GMP but showed a different fractionation pattern. The amount of this isomer was the same in both cultures, around 8 pmol/mg protein. The c-di-GMP degradation product pGpG could not be quantified, as contents were below the limit of quantification (LOQ). The WT and the Δ*nbdA* strain both showed a GMP level of about 1.3-1.5 nmol/mg protein. (**Fig. 3.17 C**). The GMP content of the cultures was therefore about 100x higher that the amount of c-di-GMP or the isomer, since the GMP contents in a cell are also influenced by other factors than c-di-GMP metabolism, like DNA replication, growth rate or protein biosynthesis.

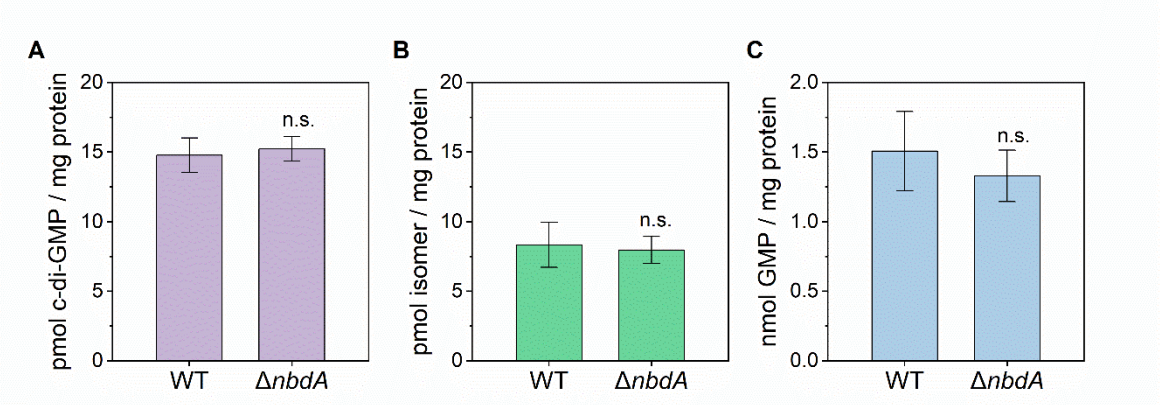

Fig. 3.17 Nucleotide levels of *P. aeruginosa* PAO1 (WT) and *nbdA* deletion mutant (Δ*nbdA*). Cells were grown in LB media at 37 °C until the culture reached an OD_{600} of 0.5. Then cultures were incubated at room temperature (22 °C) for 5 h. For each strain, three biological replicates with three technical triplicates for the nucleotide extraction were analysed with a QTrap 5500 tandem mass spectrometer (collaboration with AG Richling, Department of chemistry, RPTU). For the quantification of the nucleotides GMP, c-di-GMP and pGpG the stabile isotope dilution analysis (SIDA) was used. Bars showing the nucleotide content referred to the protein content. Error bars indicate the standard deviation. A two-tailed Student's *t*-test was performed to test for significant differences of Δ*nbdA* compared to the WT. Significance level $p < 0.05$ (*), n.s.: not significant. **A**: c-di-GMP level of PAO1 (WT) and Δ*nbdA*. **B**: Levels of an unidentified c-di-GMP isomer. The quantification was based on the standard curve for bis-(3'5')-c-di-GMP. **C**: GMP levels of PAO1 (WT) and Δ*nbdA*.

In summary, no significant differences in c-di-GMP or GMP levels could be observed for the Δ*nbdA* strain. Levels of pGpG were too low for quantification. A c-di-GMP isomer with similar amount in both tested strains was also detected.

3.3.3 Measurement of global c-di-GMP levels in *P.aeruginosa* cultures

In a *nbdA* deletion strain, no significant changes in nucleotide levels could be observed. To find out whether the protein possesses PDE activity *in vivo*, the nucleotide levels in a strain overproducing NbdA was measured. Further, the nucleotide levels in seven strains overproducing different NbdA protein variants were measured (Tab. 3.1). Therefore, several plasmids for the overproduction of the full-length NbdA protein, enzymatic inactive variants and its subdomains were used (Tab.2.4). A strain carrying the empty vector pHERD26T was used as a control.

Tab. 3.1 Overproduction of NbdA variants in *P. aeruginosa*. All NbdA variants were encoded on a pHERD26T vector. The overexpression plasmids were introduced into PAO1 Δ*nbdA* background. All NbdA variants carried a C-terminal Strep-tagII, except the marked (*) strain overproducing full-length NbdA. Utilised strains and plasmids can be obtained from Table 2.3 and 2.4, respectively.

Name of variant	Properites	Strain name
NbdA or NbdA $_{\text{MHYT-AGDEF-EAL}}$	Full-length NbdA	Δ*nbdA* pMRP12
NbdA* $_{\text{MHYT-AGDEF-EAL}}$	Full-length NbdA, untagged	Δ*nbdA* pMRP13
NbdA $_{\text{MHYT-AGDEF-AAL}}$	Full-length NbdA, conserved EAL motif exchanged to AAL	Δ*nbdA* pMRP14
NbdA $_{\text{AGDEF-EAL}}$	NbdA lacking the MHYT domain	Δ*nbdA* pASC04
NbdA $_{\text{AGDEF-AAL}}$	NbdA lacking the MHYT domain, conserved EAL motif exchanged to AAL	Δ*nbdA* pMKE02
NbdA $_{\text{AGAAF-EAL}}$	NbdA lacking the MHYT domain, AGDEF motif exchanged to AGAAF	Δ*nbdA* pASC19
NbdA $_{\text{MHYT-AGDEF}}$	NbdA lacking the EAL domain	Δ*nbdA* pJRE02
NbdA $_{\text{MHYT}}$	NbdA lacking the GGDEF and EAL domain	Δ*nbdA* pJRE01

Protein production of NbdA variants in *P. aeruginosa* was confirmed by western blot (**Fig. 3.18**). The full length NbdA (NbdA $_{\text{MHYT-AGDEF-EAL}}$) as well as the inactive NbdA variant (NbdA $_{\text{MHYT-AGDEF-AAL}}$) were detected at a size of about 70 kDa and appear thereby smaller than the predicted size of 82 kDa (cf. section 3.3.1). The cytosolic protein variants NbdA $_{\text{AGDEF-EAL}}$, NbdA $_{\text{AGDEF-AAL}}$ and NbdA $_{\text{AGAAF-EAL}}$ all had a predicted size of about 53 kDa and could be detected at approximately this size in the western blot. The NbdA $_{\text{MHYT-AGDEF}}$ protein variant was detected at a size of approximately 50 kDa and had a predicted size of 52 kDa. The MHYT domain of NbdA (NbdA $_{\text{MHYT}}$) has a size of 32 kDa yet appears smaller in gel at a size of about 25 kDa. Also, the intensity of the signals in the western blot varied between overproduction of different protein variants, as already observed (Gerbracht, 2021).

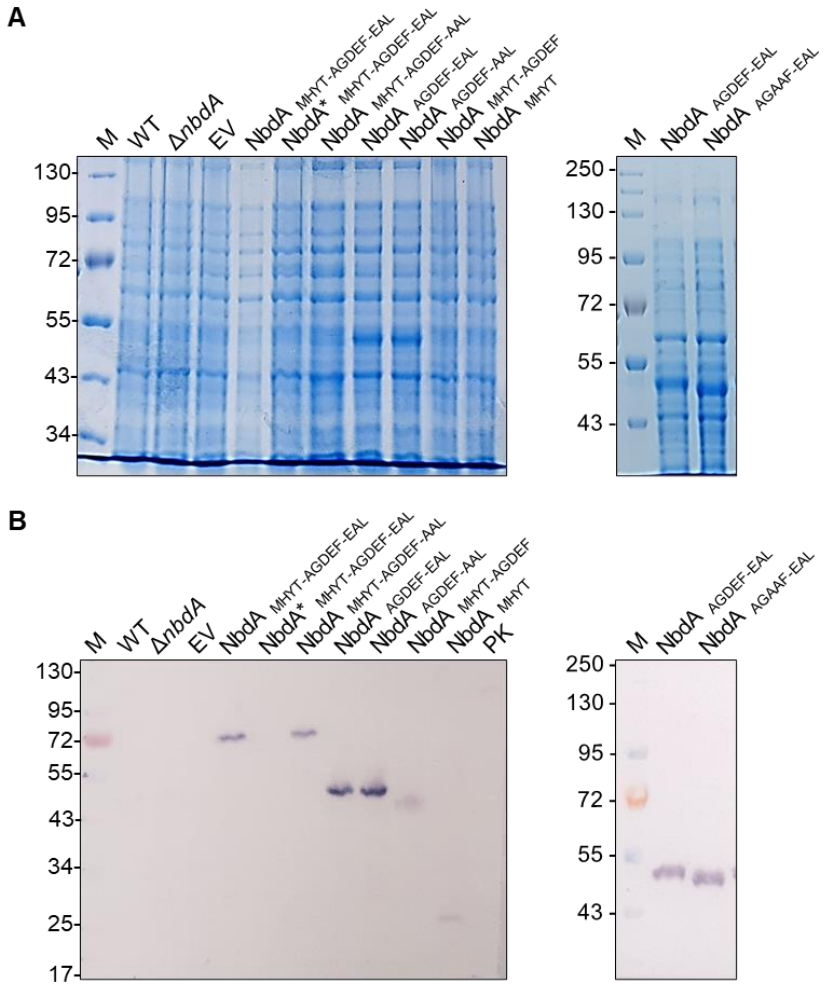

Fig. 3.18 Overproduction of NbdA variants in *P. aeruginosa*. All overexpression plasmids were introduced into PAO1 Δ*nbdA* background. All NbdA variants carried a C-terminal Strep-tagII, except the marked (*) strain overproducing full-length NbdA. Whole-cell samples were analysed. EV: Δ*nbdA* cells carrying empty vector pHERD26T.**A**: SDS-PAGE and **B**: Western blot of a test expression for Strep-tagged NbdA variants in Δ*nbdA* background. M: Colour Prestained Protein Standard, Broad Range (10 - 250 kDa). Cultures were grown at 37 °C until cells reached an OD_{600} of 0.5. Protein production was induced by addition of 0.1 % arabinose and cultures were grown for 5 h at room temperature (22 °C). Strep-tagged proteins were detected with anti-Strep-Tactin AP conjugate and a colorimetric reaction with NBT and BCIP. PK: positive control, RdmS (115 kDa).

With protein production confirmed, global nucleotide levels of the strains were determined. For the control strain harbouring the empty vector pHERD26T (EV) a c-di-GMP level of about 12 pmol/mg protein was determined, similar to the WT and Δ*nbdA* mutant (3.3.2). The c-di-GMP levels of the strain overproducing full-length Strep-tagged NbdA was significantly reduced to approximately 6 pmol/mg protein (**Fig. 3.19 A**). In the strain overproducing the untagged NbdA, c-di-GMP levels were lower but not significantly reduced. Interestingly, overproduction of inactive NbdA ($NbdA_{MHYT\text{-}AGDEF\text{-}AAL}$) resulted in significantly higher global c-di-GMP levels of ~23 pmol/mg protein. As expected, no significant change in global c-di-GMP levels were observed for strains overproducing variants lacking the EAL domain ($NbdA_{MHYT}$ and $NbdA_{MHYT\text{-}AGDEF}$). Surprisingly, overproduction of NbdA variants lacking the MHYT domain resulted in highly (~35x) increased global c-di-GMP levels. This increase was independent of the phosphodiesterase activity

of NbdA, as overproduction of an inactive variant (NbdA $_{AGDEF-AAL}$) also showed enhanced c-di-GMP levels. To test if the c-di-GMP might be produced by the GGDEF domain of NbdA, the conserved motif was mutated to AGAAF to abolish possible DGC activity. Still, global c-di-GMP levels were highly increased upon overproduction of this variant (NbdA $_{AGAAF-EAL}$). In conclusion, overproduction of the cytosolic domains of NbdA seem to trigger the increase of cellular c-di-GMP levels independently of the deducted enzymatic activity.

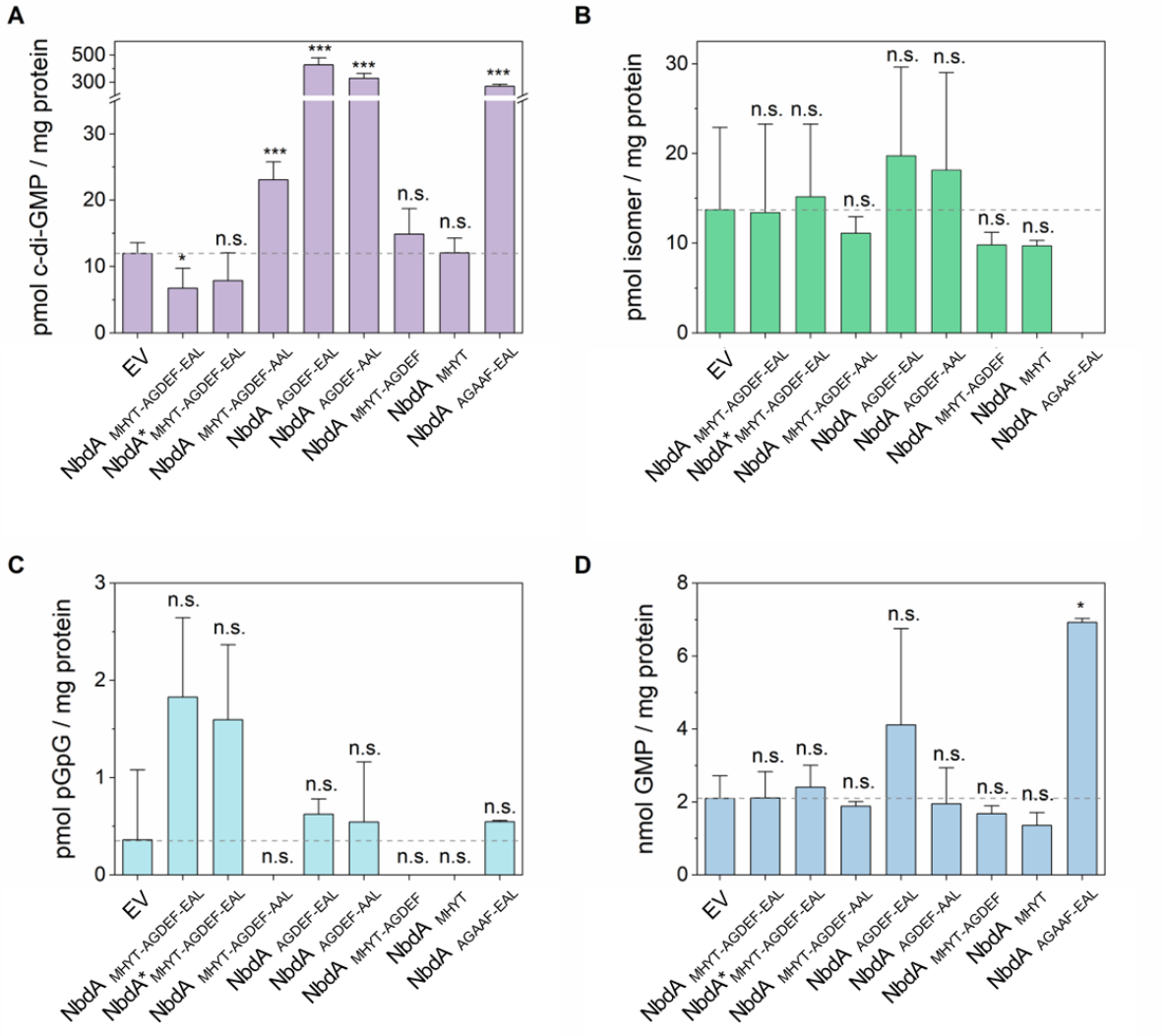

Fig. 3.19 Concentrations of nucleotides in *P. aeruginosa* PAO1 Δ*nbdA* strains overproducing NbdA variants. Cells were grown in LB media at 37 °C until an OD_{600} of 0.5. Then, target gene expression was induced with 0.1 % arabinose and cultures were incubated at room temperature (22 °C) for 5 h. PAO1 Δ*nbdA* cells containing different pHERD26T derivates for the overproduction of NbdA variants were tested. All variants were fused to a C-terminal Strep-tagII, except for the strain labelled "NbdA*$_{MHYT-AGDEF-EAL}$". Cells containing the empty vector were used as control (EV). For each strain, three biological replicates with three technical triplicates for the nucleotide extraction were analysed with a QTrap 5500 tandem mass spectrometer (collaboration with AG Richling, Department of chemistry, RPTU). For the quantification of the nucleotides GMP, c-di-GMP and pGpG the stabile isotope dilution analysis (SIDA) was used. Bars showing the nucleotide content per protein. Error bars indicate the standard deviation. A two-tailed Student's *t*-test was performed to test for significant differences of overexpression strains compared to the EV. Level of significance $p < 0.05$ (*), $0.01 < p < 0.05$ (**), $p < 0{,}01$ (***), n.s.: not significant. For multiple comparisons, *p*-values were adjusted according to Benjamini-Hochberg. **A**: c-di-GMP levels of cultures overproducing different NbdA variants. **B**: Levels of an unidentified c-di-GMP isomer. Quantification based on 3'5'-c-di-GMP standard curve. For NbdA $_{AGAAF-EAL}$, the isomer could not be quantified. **C**: pGpG levels of cultures overproducing different NbdA variants. **D**: GMP levels of cultures overproducing different NbdA variants.

The unidentified c-di-GMP isomer (section 3.3.2) was also identified in the overexpression strains. The levels of the isomer were with about 13 pmol/mg protein slightly elevated compared to the WT and *nbdA* deletion mutant (**Fig. 3.19 B**). For most strains, the isomer concentration showed a high variation between replicates. No significant differences in isomer levels were detected for the eight tested strains. Thus, the global cellular concentration of the unknown c-di-GMP isomer was independent on NbdA variant overproduction.

Global intracellular levels of pGpG were determined in the tested overexpression strains. In general pGpG concentrations showed high variation within the biological replicates (**Fig. 3.19 C**). It was observed that pGpG was very unstable over time, even when extracted and lyophilised. The time period from extraction to MS measurement was therefore crucial for the detection of pGpG. Measured pGpG levels ranged from ~0,25 pmol/mg protein for the empty vector control to ~1,9 pmol/mg protein for the overexpression of *nbdA*. For the overproduction of inactive NbdA (NbdA $_{\text{MHYT-AGDEF-AAL}}$), and variants lacking the EAL domain (NbdA $_{\text{MHYT-AGDEF}}$ and NbdA $_{\text{MHYT}}$), no pGpG could be quantified. Overall, differences of pGpG levels were not significant.

Global GMP levels of the tested overexpression strains were also determined. In the empty vector control strain, GMP levels of about 2 nmol/mg protein were measured, which was similar to the concentration in the wildtype or Δ*nbdA* mutant. No significant differences in GMP levels were detected for almost all strains. The overexpression of the cytosolic NbdA variant with an inactive GGDEF domain (NbdA $_{\text{AGAAF-EAL}}$) showed higher GMP levels than the vector control.

The c-di-GMP isomer was tested for being the frequently occuring (2’5’)-(3’5’)-c-di-GMP isomer, short 2’3’c-di-GMP (**Fig. 3.20**). *In vivo*, the nucleotide 2’3’-c-di-GMP has so far only been detected in Drosophila C virus-infected *Drosophila melanogaster*, where it activates the STING pathway as an innate immune response (Cai *et al.*, 2023). Therefore, standards were ordered and also analysed by MS.

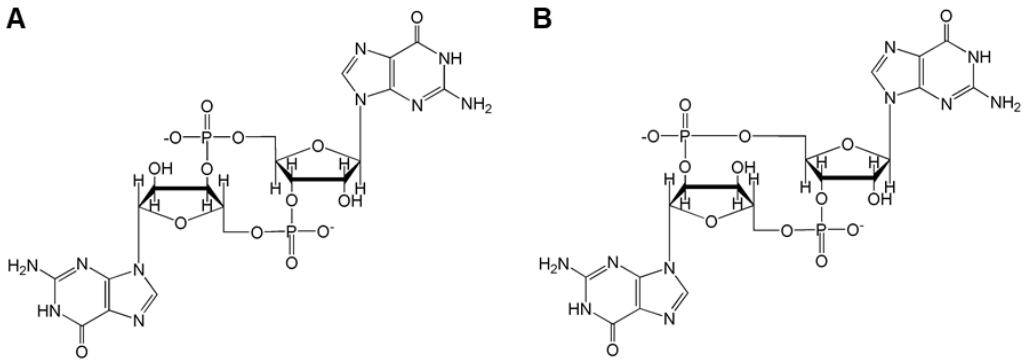

Fig. 3.20 Structure of bis-(3’5’)-c-di-GMP and (2’5’)-(3’5’)-c-di-GMP. Chemical structure of c-di-GMP isomers. Structures were created with ChemDraw (Std. 7.0). **A**: Structure of bis-(3’5’)-c-di-GMP. Both phosphate groups form a 3’5’ connection, linking two ribose sugar rings. **B**: In (2’5’)-(3’5’)-c-di-GMP, one phosphate group is connected via the 3’carbon of ribose, whereas the other phosphate group is conntected to the 2’carbon of ribose.

Nucleotide determination and identification by MS was performed by H. Becker and S. Stegmüller (AG Richling, Department of chemistry, RPTU). The MS analyses revealed that the c-di-GMP isomer that was detected in all culture samples was not 2'3'-c-di-GMP. As the concentration was apparently not influenced by presence or absence of NbdA or its variants, no further attempt to identify this compound was made.

3.3.4 *In vitro* activity assay of NbdA using HPLC

An enzymatic assay using unlabelled c-di-GMP as substrate was performed to test the PDE activity of affinity purified NbdA $_{AGDEF-EAL}$. As Li *et al.*, 2013 described a GTP-dependent activity of NbdA $_{AGDEF-EAL}$, GTP was also added to the samples. The assay was conducted in presence of manganese ions (**Fig. 3.21 A**) or magnesium ions (**Fig. 3.21 B**). In HPLC analysis of the enzyme assays, peaks for GTP and c-di-GMP are detectable at 4.3 min and 11.6 min, respectively the start of the reaction (t_0). After 2 h incubation, no substrate c-di-GMP could be detected in the enzyme assay sample with manganese ions, indicating turnover of c-di-GMP. Simultaneously, a new peak with a retention time of 10.9 min was detected, which coelutes with the pGpG standard. In mass spectrometry analysis, formation of pGpG was confirmed (**Fig. 3.21 C**). After 16 h incubation, the peak with a retention time of 10.9 min decreases, while a new peak at a retention time of 12.1 ml is detected (marked with *). This peak does not coincide to any of the tested standards. In mass spectrometry analysis of the sample, the peak could not be identified, however, mass transitions might fit to 2'3'-pGpG or 2'3'-c-di-GMP (Fig.A3, ZFA Metabolomics, MHH Hannover). For the enzyme test with magnesium ions, after 2 h incubation most of the substrate c-di-GMP is still present, while only a portion was degraded to pGpG, as indicated by the formation of a new peak at 10.9 min retention time. After 16 h incubation, the c-di-GMP peak (11.8 min) is further decreased while the peak at a retention time of 10.9 min (pGpG) increased. In addition, the unknown peak with a retention time of 12.1 min (*) was also detected. Mass spectrometry analysis of the 16 h sample revealed presence of c-di-GMP and pGpG (**Fig. 3.21 D**). Quantification of c-di-GMP and pGpG in this sample is not valid, as the amount was above the upper limit of quantification (ULOQ).

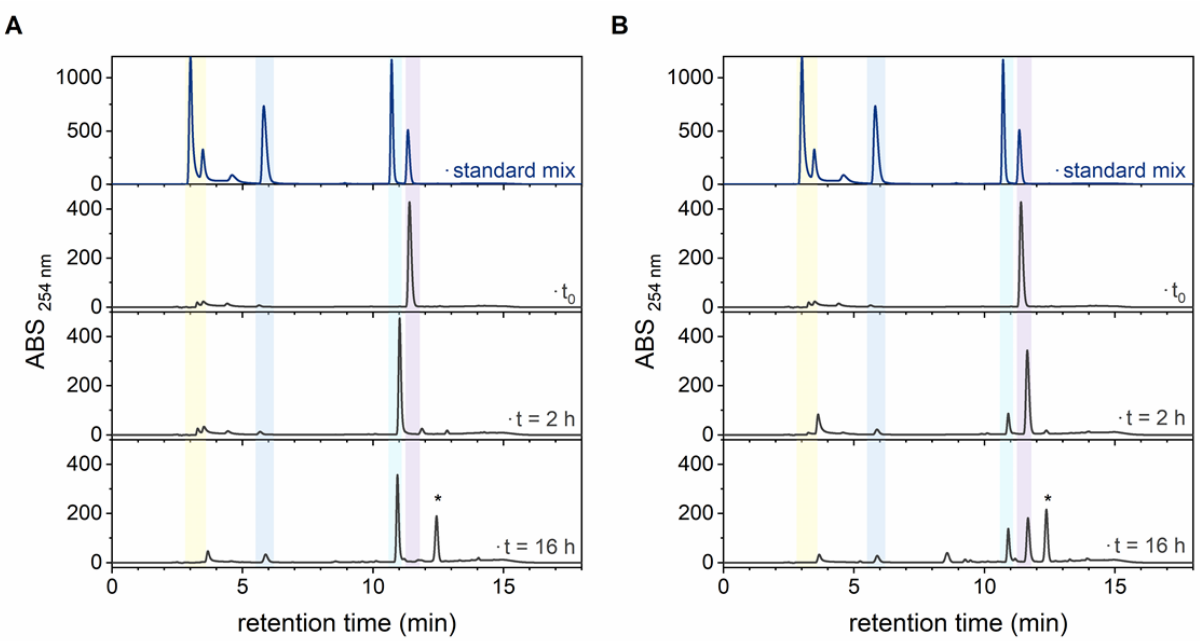

C

sample	c-di-GMP (nM)	pGpG (nM)
t_0	-	-
t = 2 h	1280	4300
t = 16 h	4,77	3400

D

sample	c-di-GMP (nM)	pGpG (nM)
t_0	-	-
t = 2 h	-	-
t = 16 h	5570	6040

Fig. 3.21 Phosphodiesterase activity assay of NbdA $_{AGDEF-EAL}$. A NbdA $_{AGDEF-EAL}$ variant carrying a C-terminal Strep-tagII was produced in *E. coli* BL21 (DE3) and purified by affinity chromatography. For the enzymatic assay, 25 µM protein final concentration was used. The protein was supplemented with 10 mM manganese ions (**A**) or magnesium ions (**B**). 50 µM GTP and 50 µM c-di-GMP were added to start the reaction. 50 µl sample volume was injected into the HPLC and run according to method section. Retention time of the standard substances GTP (yellow), GMP (blue), pGpG (turquoise) and c-di-GMP (violet) were marked. **C** and **D**: Quantification of nucleotides by MS in the H. Bähre group (ZFA Metabolomics, MHH Hannover). For c-di-GMP and pGpG the LLOQ was 1.47 nM and ULOQ was 4990 nM. Chromatograms of the samples can be obtained in the appendix, Fig. A3. (-) sample not tested.

The unknown peak (*) was further analysed by mass spectrometry in collaboration with the AG Richling (Department of chemistry, RPTU) to identify the new formed substance. With stable isotope standards and MS analysis it could be excluded that the substance is either GTP, GMP, pGpG, c-di-GMP or the 2'3'-c-di-GMP isomer. Further, the compound was not identical to the unidentified c-di-GMP isomer that was detected in culture extracts (section 3.3.3).

3.3.5 Phage infection assay of a *nbdA* deletion mutant

The interaction of NbdA with the type IV pili ATPase PilB as well as the major pilin PilA was demonstrated by B2H assay (section 3.2.2). Thus, it was investigated whether the deletion of *nbdA* affects type IV pili formation. For this purpose, a phage infection assay was performed with the phage DMS3*vir*. The phage only infects cells that form type IV pili on the cell surface (Laventie *et al.*, 2019). The test was carried out in 96-well plates and the OD_{595} was measured to monitor growth or lysis of the cultures. The PAO1 wildtype (WT), markerless deletion mutants for *nbdA* and *pilA*, and

a double mutant (Δ*pilA* Δ*nbdA*) were utilised. For all tested strains, the growth control without phages showed normal growth with typical growth phases (**Fig. 3.22,** grey lines). The phage infection test for the wildtype shows normal growth in the first 4 h of incubation. After ~5 h incubation the OD_{595} decreases, which indicates a lysis of cells by the phage DMS3*vir* (**Fig. 3.22 A**). A control strain without functional pili, Δ*pilA*, shows normal growth in an infection test, similar to the sample without phages (**Fig. 3.22 B**). An infection test of the Δ*nbdA* mutant showed lysis after ~5 h incubation similar to the infection curve of the wildtype strain (**Fig. 3.22 C**). Therefore, the deletion of *nbdA* did not affect phage susceptibility. This indicated that the piliation of Δ*nbdA* is similar to the piliation of the WT. A double mutant Δ*pilA* Δ*nbdA* was also resistant to phage infection (**Fig. 3.22 D**). After the infection test, the phage titer was estimated for each strain in triplicates. For the WT and Δ*nbdA*, a phage titer of $3.2*10^{11}$ PFU and $3.3*10^{11}$ PFU was evaluated. Thus, no discernible impact of *nbdA* deletion on the phage titer after infection assay was detected. For the resistant Δ*pilA* strain, a considerably lower value of $1.7*10^{3}$ PFU was counted, which corresponds approximately to the previously added amount of phages.

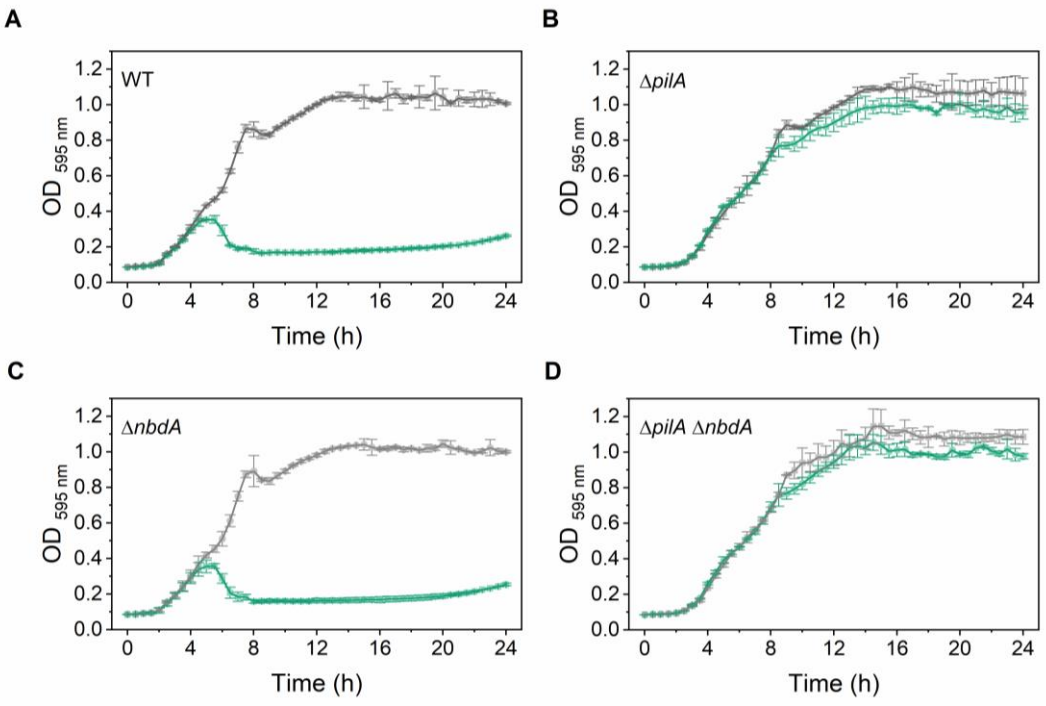

Fig. 3.22 Phage infection assay of *P. aeruginosa* deletion mutants. Cells were cultured in a 96-well plate in LB media at 37 °C. Starting OD_{600} was set to 0.05. The OD_{595} was measured every 30 min in a Tecan Plate reader. Infection assays were performed in biological triplicates with three technical replicates each. 10^{3} PFU of DMS3*vir* were added to test for phage infection. Dots show the average of the biological triplicates, error bars indicate the standard deviation. **A**: Growth control (grey) and phage infection (green) for the wildtype (WT) which was PAO1. **B**: Growth control (grey) and phage infection (green) for markerless deletion mutant for *pilA.* **C**: Growth control (grey) and phage infection (green) for a markerless Δ*nbdA* mutant. **D:** Growth control (grey) and phage infection (green) for a double mutant Δ*pilA* Δ*nbdA*.

3.3.6 Phage infection assay of NbdA overproducing strains

The *nbdA* deletion mutant did not show indications to a changed piliation of the cells. As pili proteins were found in the pulldown assay of cells overproducing NbdA, it was assayed whether the overproduction of NbdA might influence cell piliation. This was carried out indirectly with a DMS3*vir* phage infection test, where lysis of cells relates to piliation (Laventie *et al.*, 2019). A set of seven strains were tested for phage susceptibility (section 3.3.3, Table 3.1). The strains are overexpressing genes that encode different NbdA variants on a pHERD26T vector. The empty vector was used as reference.

In a uninduced control, all strains show a similar growth like the empty vector control (**Fig. 3.23**, grey lines). When phages were added to the uninduced cultures, almost all show a decrease in OD_{595} after approximately 12 h incubation (**Fig. 3.23**, blue lines). The strain carrying the full-length NbdA (NbdA $_{MHYT\text{-}AGDEF\text{-}EAL}$), however, showed a slightly delayed drop in OD_{595} after ~14 h. For the strains with induced gene expression, almost all strains show a normal growth without phages (**Fig. 3.23**, red lines). The strains overproducing NbdA $_{MHYT\text{-}AGDEF\text{-}EAL}$, and the inactive variant NbdA $_{MHYT\text{-}AGDEF\text{-}AAL}$ only grew to a lower OD_{595} of about 0.85 instead of 1.1 for the empty vector control. When DMS3*vir* phages were added, the empty vector control shows a lysis of cells as measured by a decrease in $OD_{595\ nm}$ (**Fig. 3.23**, green lines), similar to the uninduced sample. For the strain overproducing NbdA $_{MHYT\text{-}AGDEF\text{-}EAL}$, there was no difference in $OD_{595\ nm}$ between the sample without phages and the sample containing phages. This was also observed for the strain overproducing the inactive variant NbdA $_{MHYT\text{-}AGDEF\text{-}AAL}$ and therefore independent of PDE activity. Notably, the two strains showed impaired growth when induced. In an infection test, all strains that overproduced a NbdA variant carrying the MHYT domain did not exhibit a noticeable cell lysis or decrease in OD_{595}. Conversely, the overproduction of cytosolic NbdA variants (NbdA $_{AGDEF\text{-}EAL}$, NbdA $_{AGDEF\text{-}AAL}$, and NbdA $_{AGAAF\text{-}EAL}$) resulted in lysis after approximately 15 h. Mutations in the GGDEF or EAL domain abolishing the DGC or PDE activity respectively did not affect lysis behaviour compared to NbdA $_{AGDEF\text{-}EAL}$. Still, compared to the empty vector control strains overproducing cytosolic NbdA variants showed a delayed lysis.

In summary, the overproduction of NbdA $_{MHYT\text{-}AGDEF\text{-}EAL}$ and NbdA $_{MHYT\text{-}AGDEF\text{-}AAL}$ leads to reduced growth. Strains overproducing protein variants that contain the MHYT domain displayed no apparent lysis, while strains overproducing cytosolic NbdA variants showed a delayed lysis compared to the empty vector control.

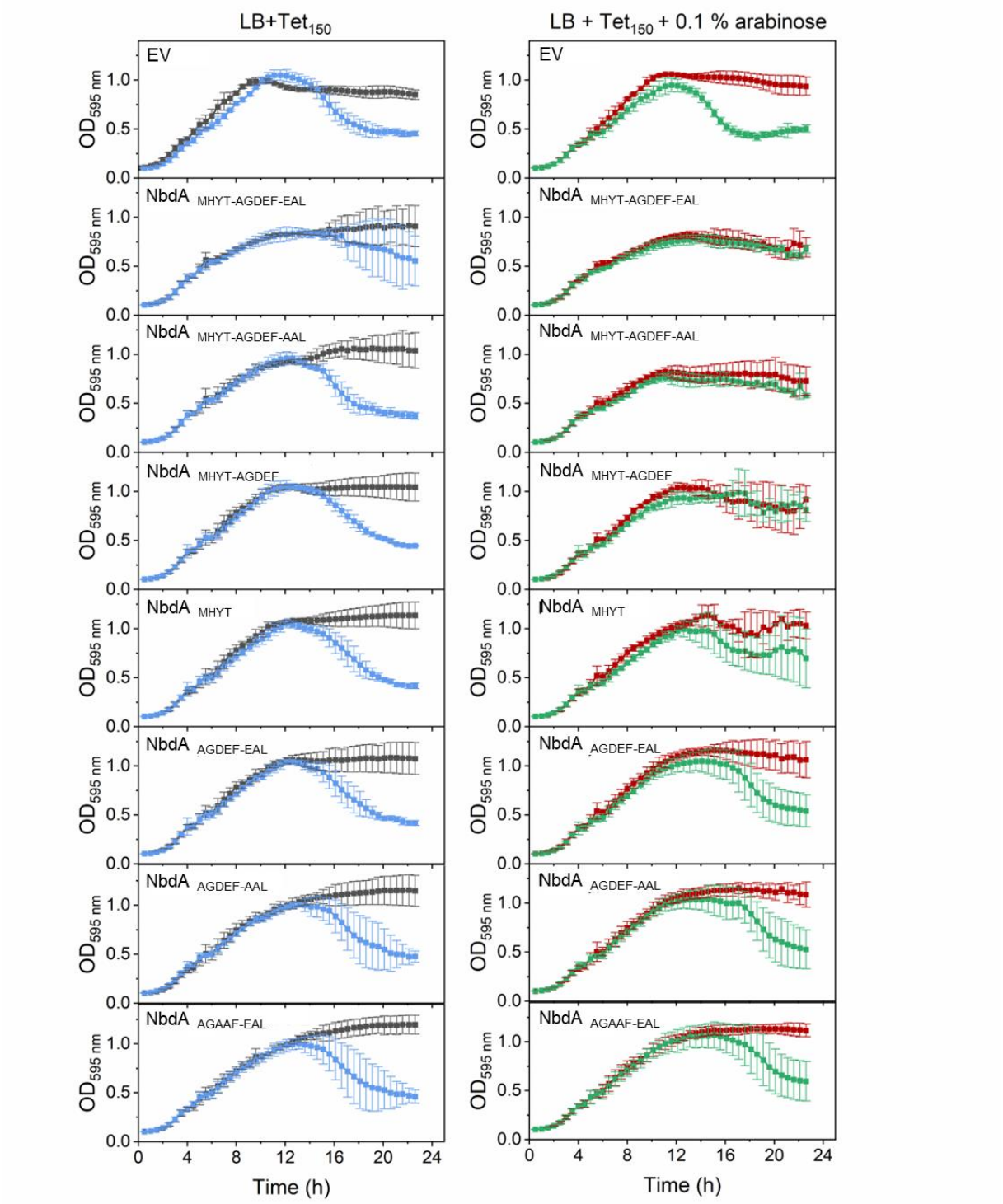

Fig. 3.23 Phage infection assay of PAO1 Δ*nbdA* strains overproducing different NbdA variants (pHERD26T-encoded). PAO1 Δ*nbdA* cells containing different pHERD26T derivates for the overproduction of NbdA variants were tested. All variants were fused to a C-terminal Strep-tagII. EV: empty vector control (Δ*nbdA* pHERD26T). Cells were cultured in a 96-well plate in LB media at 37 °C. Starting OD_{600} was set to 0.05. The OD_{595} was measured every 30 min in a Tecan Plate reader. Infection assays were performed in biological triplicates with three technical replicates each. After 3 h, protein production was induced by adding 0.1 % arabinose. Phages (10^5 PFU) were added one hour after induction. Dots show the average of the biological triplicates, error bars indicate the standard deviation. Uninduced sample (left) with a growth control (grey) and a lysis control (blue). Induced samples (right) with a control without phages (red) and phage infection test (green).

To check whether the absence of a lysis in the strains overproducing full-length NbdA is due to their reduced growth or the protein overproduction, also a moderate overproduction strain was tested, whereby NbdA was encoded on the vector pME6032. The vector pME6032 is a low-copy number plasmid with a titratable *tac* promoter. Overproduction of NbdA encoded on a pME6032 vector does not result in strong elongated cells (Gerbracht, 2021). Also, the cells show no change in growth on agar plates when gene expression was induced (Fig. A5 and A6). Protein production was verified in a western blot (section 3.1.8). A phage infection test of a strain overproducing NbdA encoded on a pME6032 vector was performed, and cells carrying the empty vector were used as a control. Uninduced cultures of a NbdA overproduction strain showed a similar growth curve like the empty vector control (**Fig. 3.24,** grey dots and lines). With the addition of phages, both strains show a lysis after approximately 11 h (**Fig. 3.24,** blue dots and lines). When gene expression was induced, the overexpression strain displayed no difference in growth compared to the empty vector control (**Fig. 3.24,** red dots and lines). However, in the phage assay, the empty vector control shows a lysis after 11 h incubation similar to the uninduced sample, whereas the strain overproducing NbdA showed no visible lysis of cells. The $OD_{595\ nm}$ begins to decrease slightly after 20 h (**Fig. 3.24,** green dots and lines).

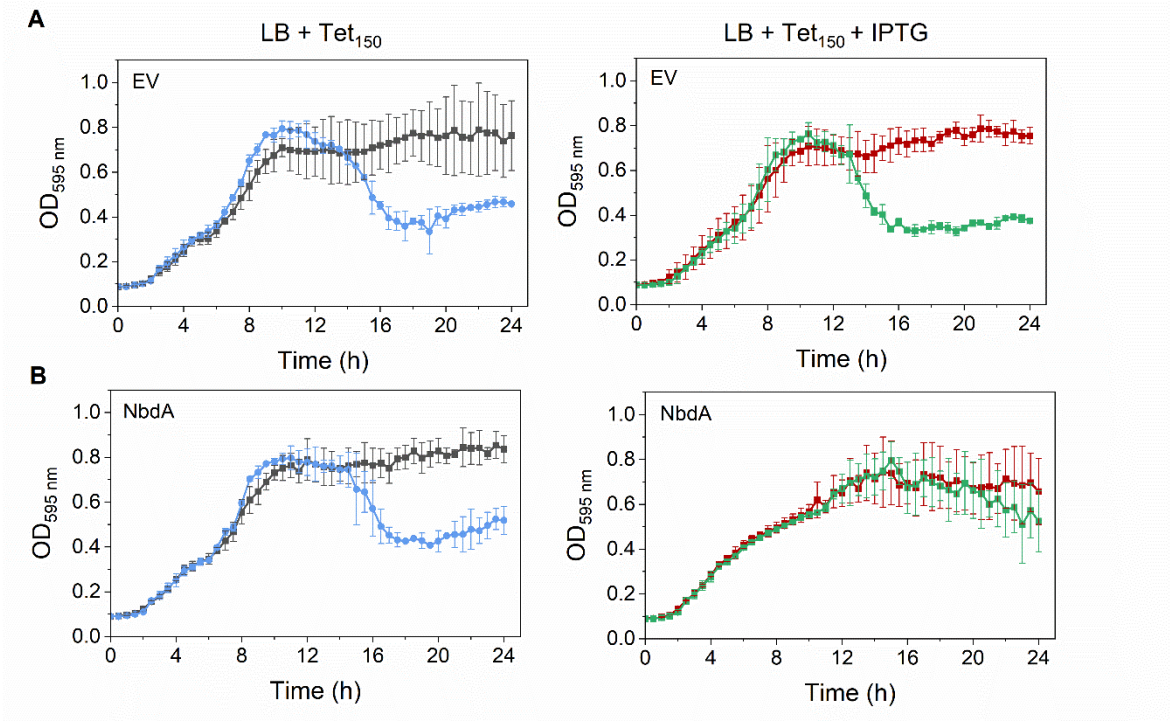

Fig. 3.24 Phage infection assay of PAO1 pME6032 (EV) and PAO1 pASC07 (NbdA). Cells were cultured in a 96-well plate in LB media at 37 °C. Starting OD_{600} was set to 0.05. The OD_{595} was measured every 30 min in a Tecan plate reader. Infection assays were performed in biological triplicates with three technical replicates each. Protein production was induced by adding 100 µM IPTG. Where applicable, phages (10^5 PFU) were added. Dots show the average of the biological triplicates, error bars indicate the standard deviation. Uninduced sample (left) with a growth control (grey) and a lysis control (blue). Induced samples (right) with a control without phages (red) and lysis test (green).

The phage titer of all cultures was estimated in triplicates after the lysis. The strains carrying the empty vector control had a titer of $2*10^{12}$ PFU ± 2 % and $2.7*10^{12}$ PFU ± 2.1 % for the sample without and with IPTG, respectively. The strain overproducing NbdA showed a reduced phage titer of $6*10^{10}$ PFU ± 1.2 %, while the uninduced sample was with $1.7*10^{12}$ PFU ±1.4 % comparable to the empty vector control. Hence, moderate overproduction of NbdA does not result in altered growth but still reduces cell lysis by the phage DMS3*vir*. This indicates that NbdA overproduction might influence type IV piliation.

3.3.7 Investigation of cells overproducing NbdA by AFM

The results from the phage assays indicated to a changed piliation of the cells overproducing NbdA. In collaboration with the AG Ziegler (Department of physics and biophysics of complex interfaces, RPTU), atomic force microscopy (AFM) was carried out to visualise cellular appendages. To this end, the wildtype PAO1, a Δ*pilA* mutant, and a strain overproducing Strep-tagged NbdA (PAO1 pMRP12) were examined. The polar flagellum of the wildtype, the Δ*pilA* mutant as well as the NbdA overproduction strain were clearly visible (**Fig. 3.25**, blue arrow heads). In addition, thinner filamentous structures, potentially resembling pili with a thickness of approximately 5 nm, were observed near the cell poles. These structures were detected in both the wildtype and the NbdA overproduction strain (**Fig. 3.25**, white arrow heads). No structures were identified in the Δ*pilA* mutant. It was observed that the NbdA overproduction strain exhibits a greater number of potential pili than the WT. However, as only 2-4 cells per strain from one biological replicate were analysed, no conclusive statement can be made.

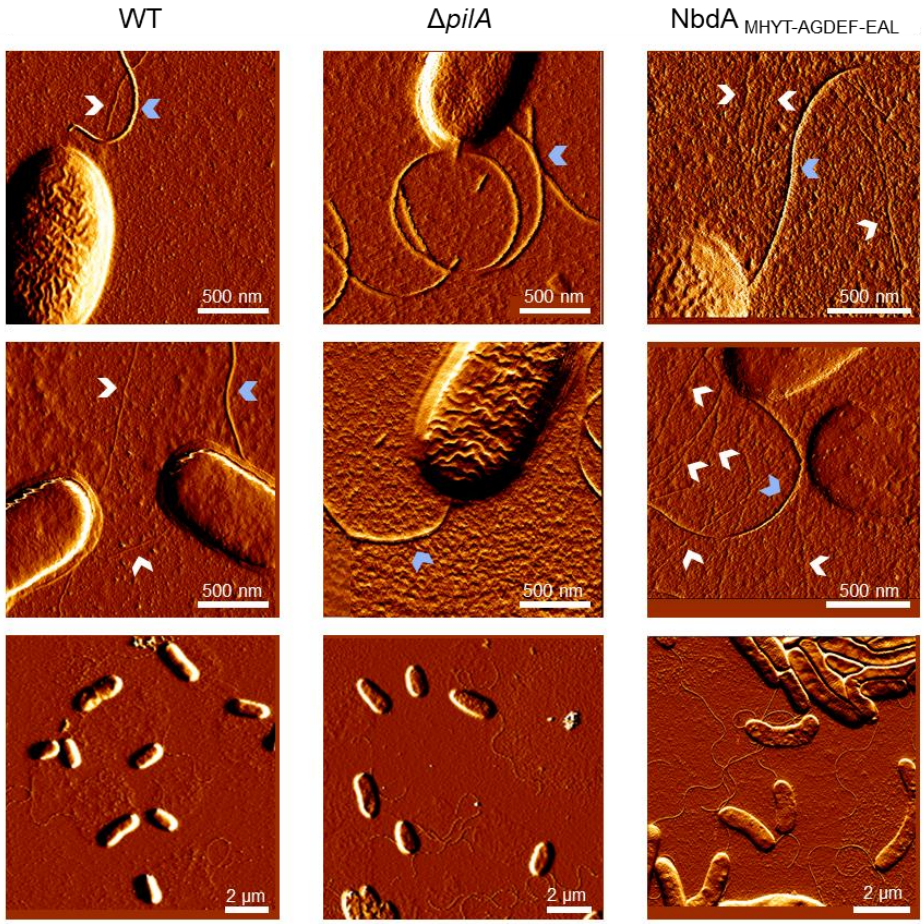

Fig. 3.25 Atomic force microscopy of PAO1 (WT), Δ*pilA* and PAO1 pMRP12 (NbdA MHYT-AGDEF-EAL). Cells were grown in LB media at 37 °C, gene expression was induced by addition of arabinose. Cells were further incubated for 16 h at 22 °C. For microscopy, cells were diluted in fresh medium. Cells were immobilised on poly-D-lysine coated plates for 30 min. Slides were washed to remove non-attached cells. The images were recorded by J. Seehase (AG Ziegler, Department of physics and biophysics of complex interfaces, RPTU). Potential flagella were marked by blue arrow heads, filamentous thinner structures, potential type IV pili, were indicated by white arrow heads.

3.3.8 Localisation of overproduced NbdA

Localisation of overproduced NbdA in *P. aeruginosa* PAO1 was examined by confocal laser scanning microscopy. In previous studies, the localisation of fluorescently labelled NbdA was determined with *nbdA* under the control of the original promoter or encoded on a pME6032 plasmid (Gerbracht, 2021; Karcher, 2021). However, most phenotypic studies were conducted with NbdA variants encoded on a pHERD26T vector (Gerbracht, 2021; Rehner, 2020; Rüger, 2019). Therefore, PAO1 strains carrying pHERD26T expression vectors, that contain *nbdA* fused to the sequence of the fluorescent proteins mNeonGreen or Venus, were used in this study. As a control, strains overproducing only the fluoresphores were utilised. For the strains overproducing only the fluorophores mNeonGreen or Venus, a uniform distribution of fluorescence over the whole cell body was observed (**Fig. 3.26 A**). The overproduction of fluorescent NbdA variants resulted either in a diffuse fluorescence signal, in a fluorescent signal located in the membrane region, or in foci at one or both cell poles (**Fig. 3.26 B** and **C**).

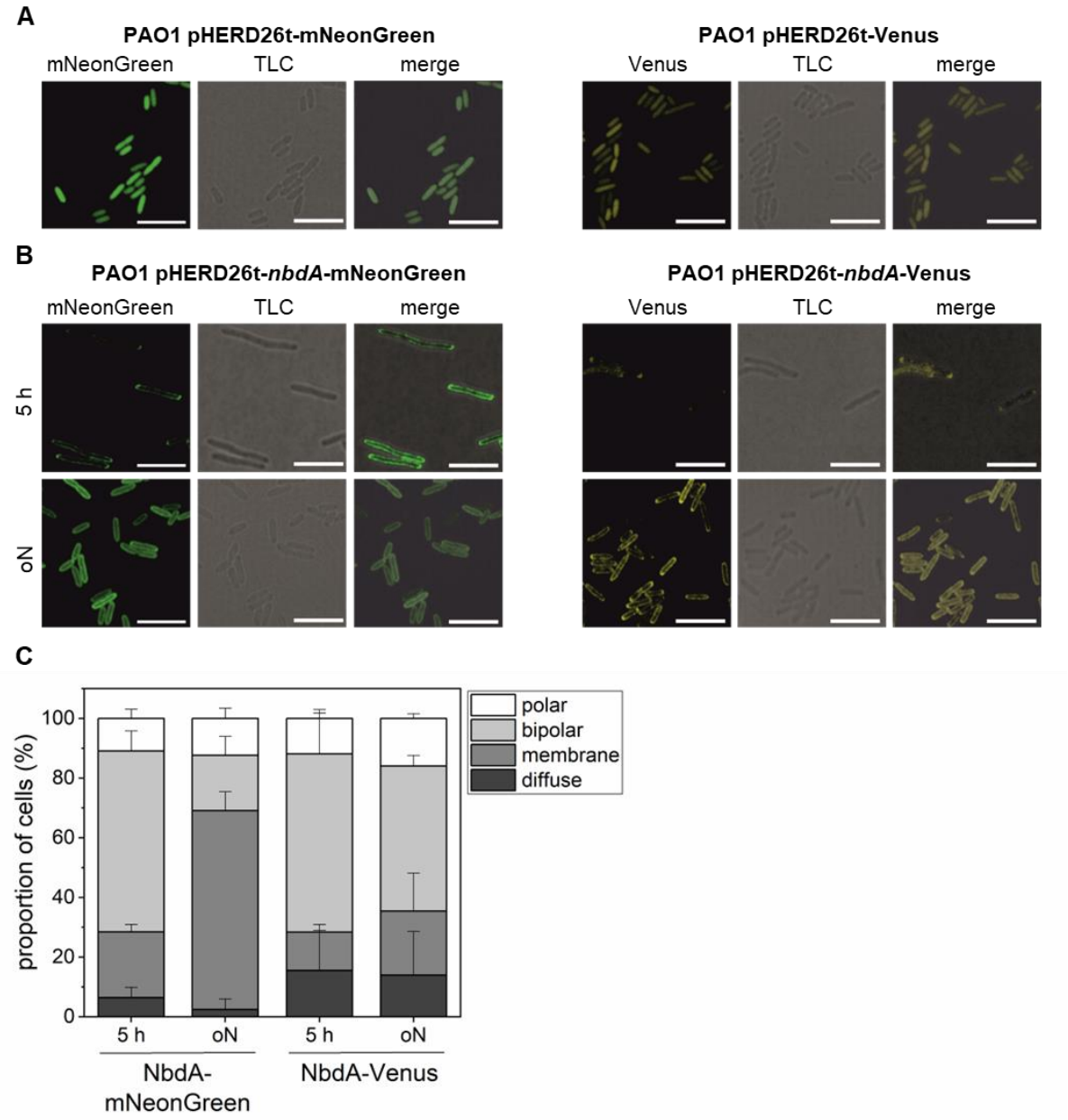

Fig. 3.26 Localisation of overproduced NbdA. Cultures overproducing different fluorescent protein variants were grown at 37°C until the culture reached an OD_{600} of 0.5. Gene expression was induced by arabinose. After induction, cell were grown at 22 °C for 5 h or 16 h (oN) **A**: Control strains carring the vector pHERD26T with the fluorophores mNeonGreen and Venus. For microscopy, cells were immobilised on agarose pads. Images were taken in a Zeiss LSM 880. The fluorophore mNeonGreen was exited with the 488 nm laser line, Venus was exited using the 514 nm laser line. TLC: transmitted light channel. Scale bar: 5 µm. **B**: Localisation of overproduced NbdA after 5 h and 16 (oN) after induction. Cells were immobilised on agarose pads. Images were taken in a Zeiss LSM 880. NbdA-mNeonGreen was excited at 488 nm, NbdA-Venus was exited at 514 nm. TLC: transmitted light channel. Scale bar: 5 µm. **C**: Evaluationof NbdA localisation in cells overproducing the fluorescently tagged protein. Fluorescent signals were either polar, biopolar, evenly distributed in the membrane or diffuse. Total cell counts: NbdA-mNeonGreen 5 h: n = 902, oN: n = 485, NbdA-Venus 5 h: n = 146, oN: n = 287. Bars showing relative proportion of cells with the respective fluorescence signal. Error bars indicate the standard deviation.

Five hours after induction, the majority of cells (60.6 % for NbdA-mNeonGreen and 59.8 % for NbdA-Venus) exhibited a bipolar signal. A small amount of cells showed a polar (10 %, 12 %) or diffuse signal (6 %, 15 %). About 22 % of cells overproducing NbdA-mNeonGreen and 13 % of cells

overproducing NbdA-Venus showed a signal that was located in the membrane of the cell. When protein production was induced over night, NbdA-mNeonGreen exhibited a membrane localised signal in the majority of cells (67 %), while only 21 % of cells showed this localisation for the strain overproducing NbdA-Venus. The majority of NbdA-Venus overproducing cells had a bipolar fluoescence signal (49 %), which was the second largest group for NbdA-mNeonGreen overproducing cells (19 %). Polar signals were observed in 12 % and 16 % of cells for NbdA-mNeonGreen and NbdA-Venus, respectively, while a diffuse signal was observed in 2.5 % (NbdA-mNeonGreen) and 14 % (NbdA-Venus) of cells. Thus, in the majority of cells overproducing fluorescently labelled NbdA resulted in either a bipolar fluorescence or a signal predominantly located in the membrane.

3.3.9 Co-localisation of NbdA with the pili protein PilO

In previous studies, the co-localisation of NbdA and the piliated pole was suggested (Gerbracht, 2021). In this work, additional indications that NbdA might be associated to the T4P machinery emerged (section 3.2.2, 3.3.6 and 3.3.7). To test for co-localisation of overproduced NbdA with the piliated pole, the genes *pilO* and *pilT* encoding pili components were genetically fused to the fluorescence tags mCherry and mRuby3, respectively, and integrated in the original gene locus, according to Koch *et al.*, 2021. The resulting strains produce fluorescently labelled protein variants of PilO and PilT. For both constructs, a polar localisation of the fusion protein at the piliated pole without disturbing the type IV pili function was described (Koch *et al.*, 2021). For the strain expressing mRuby3-*pilT*, 95 % of cells showed no signal, 3.3 % showed a polar signal, and 1.2 % showed a bipolar signal. In total, 243 cells were counted. However, due to the small proportion of cells showing a clear signal, further testing for the co-localisation with NbdA was not pursued. The strain expressing *pilO*-mCherry showed a polar localised signal in approximately half of the cells (47 %) (**Fig. 3.27**). About 9 % of cells showed a bipolar fluorescence signal. A little less than half of the cells did not show a signal (44 %). In total, 1129 cells were counted. The cells expressing *pilO*-mCherry show a usual rod shape and cell size of about 2 µm.

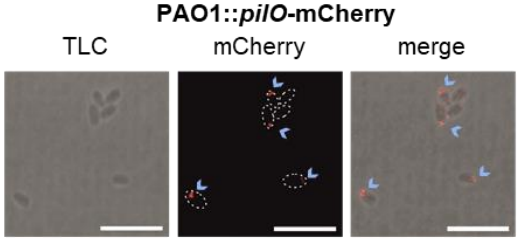

Fig. 3.27 Localisation of PilO-mCherry. A PAO1::*pilO*-mCherry strain was created according to Koch *et al.*, 2021. Cells were grown at 37 °C until they reached an OD_{600} of 0.5. Cells were further grown for 5 h at room temperature (22 °C). For microscopy, cells were immobilised on agarose pads. Images were taken in a Zeiss LSM 880. The fluorophore mCherry was exited with the 594 nm laser line. TLC: transmitted light channel. Scale bar: 5 µm.

The co-localisation of PilO and overproduced NbdA was examined by CLSM. Therefore, the strain PAO1::*pilO*-mCherry carrying a pHERD26T-derivate for either NbdA-mNeonGreen or NbdA-Venus overproduction was used. As described before, cells that strongly overproduce NbdA fusion proteins showed elongated cell morphology. Similar to the sample without NbdA overproduction, approximately half of the cells did not show a clear PilO-mCherry signal, which was 44 % of cells for the NbdA-mNeonGreen overproduction and 59 % of cells for the NbdA-Venus overproduction strain (**Fig. 3.28**). When the fluorescent PilO-mCherry signal was located bipolar, NbdA displayed also bipolar localisation. This was the case in 8 % and 7 % of cells for NbdA-mNeonGreen and NbdA-Venus overproduction, respectively. When the signal of PilO-mCherry was polar localised, fluorescent-labelled NbdA showed predominantly a bipolar localisation (25 % for NbdA-mNeonGreen and 24 % for NbdA-Venus). Alternatively, NbdA showed either a polar signal at the same or opposite pole, or a diffuse signal.

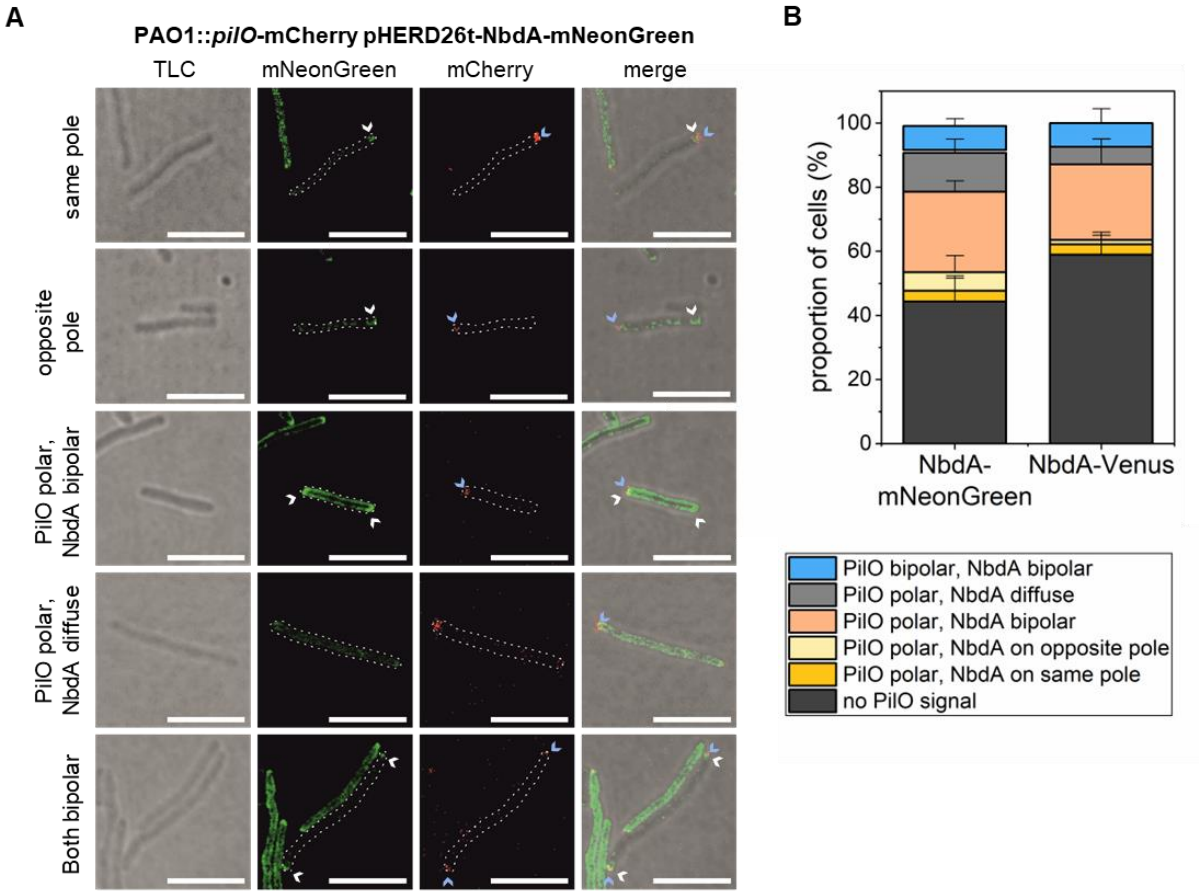

Fig. 3.28 Co-localisation of overproduced NbdA with PilO. PAO1::*pilO*-mCherry pHERD26T-NbdA-mNeonGreen and PAO1::*pilO*-mCherry pHERD26T-NbdA-Venus cells were grown at 37 °C until they reached an OD_{600} of 0.5. NbdA overproduction was induced by addition of 0.1 % arabinose. Cultures were further incubated for 5 h at room temperature (22 °C). For microscopy, cells were immobilised on agarose pads. Images were taken in a Zeiss LSM 880. The fluorophore mCherry was exited with the 594 nm laser line, mNeonGreen was exited with the 488 nm laser, Venus was exited with the 514 nm laser line. **A**: Examples of the localisation of PilO and overproduced NbdA. Fluorescence signals for PilO and NbdA were either on the same pole, on opposite poles, both bipolar, or PilO was polar and NbdA was bipolar or diffuse. TLC: transmitted light channel. Scale bar: 5 µm. **B**: Evaluation of the co-localisation of PilO and overproduced NbdA. Depicted are the proportions of cells for each signal combination that was observed. Error bars indicate the standard deviation for biological triplicates. Total cell counts: NbdA-mNeonGreen: n = 96, NbdA-Venus: n = 125.

Fluorescently labelled protein variants for PilO and NbdA (pHERD26T-derivate encoded) exhibited the same localisation (either both bipolar or both polar on the same pole) in 10 % and 12 % of the cells overproducing the mNeonGreen- and Venus-tagged NbdA variant, respectively.

Similar to section 3.3.8, fluorescent NbdA variants were frequently bipolar localised when strongly overproduced. In contrast, when under the control of its native promoter as well as in a moderate overproduction, the localisation of NbdA was demonstrated to be predominantly polar (Gerbracht, 2021). Therefore, fluorescent tagged NbdA variants under the control of the native promoter were also tested for co-localisation with the fluorescent PilO variant. The strain PAO1::*nbdA*-Venus::*pilO*-mCherry was cultured for 16 h at 37°C, prepared as described in section 2.6.5, and analysed by CLSM. However, the fluorescently labelled NbdA variant did not result in a clear signal for evaluation (data not shown).

Also, a moderate overproduction of fluorescently labelled NbdA variants were tested for the co-localisation with the fluorescent PilO variant. Thereby, NbdA variants were encoded on the low-copy vector pME6032. Similar to previous results (Gerbracht, 2021), less than half of the cells demonstrated a diffuse signal of NbdA, which was 42 % for the cells containing the NbdA-mNeonGreen fusion protein and 33 % of cells containing NbdA-Venus (**Fig. 3.29**). In cells where the PilO-mCherry signal was polar localized, the signal for NbdA was either polar and on the same pole, or on the opposite pole, bipolar localized, or showed a diffuse signal. Co-localisation of PilO and NbdA on the same pole was observed for 22 % of cells for mNeonGreen-tagged NbdA or 28 % for Venus-tagged NbdA. The number of cells demonstrating bipolar localisation of both NbdA and PilO was 8 % (mNeonGreen tagged NbdA) and 12 % (Venus tagged NbdA). This adds up to 30 % (NbdA-mNeonGreen) and 40 % (NbdA-Venus) of cells showing the same localisation for NbdA and PilO. A localisation on opposite poles was observed for 13 % (NbdA-mNeonGreen) and 16 % (NbdA-Venus) of cells correspondingly.

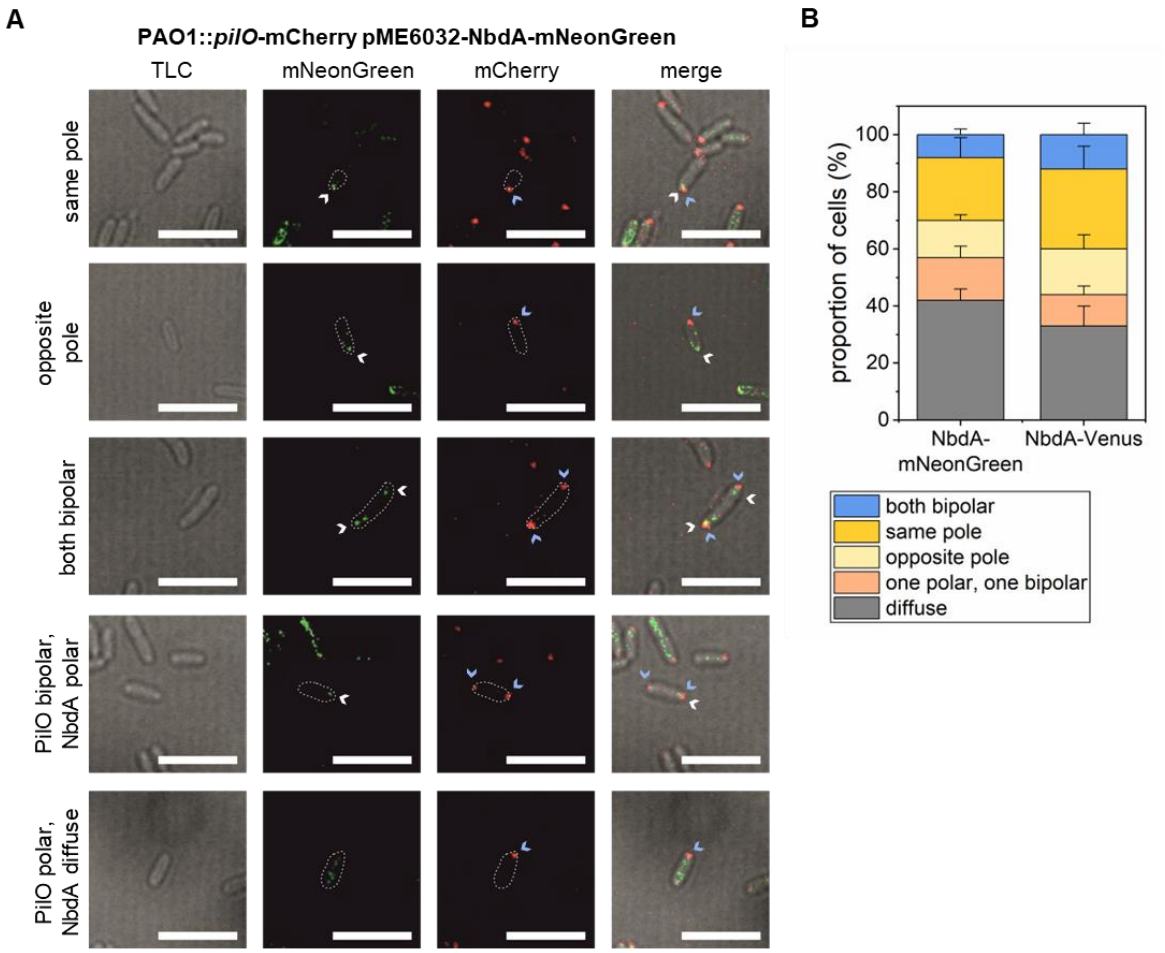

Fig. 3.29 Co-localisation of overproduced NbdA with PilO. PAO1::*pilO*-mCherry pME6032-NbdA-mNeonGreen and PAO1::*pilO*-mCherry pME6032-NbdA-Venus cells were grown at 37 °C until they reached an OD_{600} of 0.5. NbdA overproduction was induced by addition of 100 µM IPTG. Cultures were further incubated for 5 h at room temperature (22 °C). For microscopy, cells were immobilised on agarose pads. Images were taken in a Zeiss LSM 880. The fluorophore mCherry was exited at 594 nm, mNeonGreen was exited with the 488 nm laser, Venus was exited with the 514 nm laser. **A**: Examples of the localisation of PilO and overproduced NbdA. Fluorescence signals for PilO and NbdA were either on the same pole, on opposite poles, both bipolar, or PilO was polar and NbdA was bipolar or diffuse. TLC: transmitted light channel. Scale bar: 5 µm. **B**: Evaluation of the co-localisation of PilO and overproduced NbdA. Depicted are the proportions of cells for each signal combination that was observed. Error bars indicate the standard deviation for biological duplicates. Total cell counts: NbdA-mNeonGreen: n = 166, NbdA-Venus: n = 293.

4 Discussion

4.1 A soluble library of membrane proteins in polymer nanodiscs

Membrane proteins and their complexes have been investigated successfully with the use of detergents and liposomes, e. g. the bacterial β-barrel assembly machinery (BAM) complex, and ATP transporters (Hollenstein *et al.*, 2007; Hu, 2021; Iadanza *et al.*, 2016; Xu *et al.*, 2013). In the past two decades, nanodiscs have evolved as powerful tools to stabilize membrane proteins in solution, preserving their lipid-bilayer environment. Thereby, amphiphilic polymers extract membrane proteins directly from cellular membranes without the need of detergents (Knowles *et al.*, 2009; Oluwole *et al.*, 2017). In this work, the polymer DIBMA was used to extract membrane proteins directly from the membrane fraction of *P. aeruginosa* to generate a stable and soluble nanodisc library. The library was then subjected to size exclusion chromatography with subsequent characterization by mass spectrometry. The aim of this approach was to extract membrane proteins along with all peripheral and associated proteins within a lipid-bilayer environment as a basis for the study of complexes and protein–protein interactions under native-like conditions. The recovery of more than twenty described membrane protein complexes of various sizes suggests that this method is suitable to preserve membrane protein complexes. However, elution profiles of the proteins were not specific enough to predict new protein-protein interactions. By combining the nanodiscs solubilisation method with a targeted pulldown approach, new interaction partners of the bait protein NbdA were identified.

4.1.1 Reproducibility and coverage of protein identification

Adjacent to conventional solubilisation methods, nanodiscs forming polymers have been used to investigate membrane proteins in solution (Knowles *et al.*, 2009; Oluwole *et al.*, 2017). Previous work has shown increased stability of nanodisc-embedded membrane proteins (Barniol-Xicota *et al.*, 2018; Dilworth *et al.*, 2021; Oluwole *et al.*, 2017; Pollock *et al.*, 2018; Swainsbury *et al.*, 2014). This allowed the elucidation of functions, structures, and interactions of a growing number of membrane proteins and complexes (Dilworth *et al.*, 2021; Dörr *et al.*, 2014; Janson *et al.*, 2022; Thoma *et al.*, 2020). Moreover, stable proteome libraries from prokaryotic and eukaryotic cell membranes have recently been generated in polymer nanodiscs (Carlson *et al.*, 2019; Glueck *et al.*, 2022). In this work, a soluble membrane protein library was generated using the polymer DIBMA to extract proteins directly from the membrane fraction of *P. aeruginosa*. The conditions for solubilisation were optimized in a solubilisation efficiency test, with buffer composition matching to the qualitative range for DIBMA (Sawczyc *et al.*, 2023). In order to extract membrane proteins along with all peripheral and associated proteins in a lipid-bilayer environment, rigorous washing and separation of membrane fractions were omitted. Consequently, this approach enriches membrane proteins but also results in a high abundance of soluble proteins. The library was then subjected to size exclusion chromatography

with subsequent characterization by mass spectrometry. The protein content of the library was highly reproducible, as a very good match of data from three biological replicates was found regarding the identified proteins and co-fractionation pattern.

The proteome of the cell envelope of *P. aeruginosa* PAO1 has been thoroughly studied by conventional methods (Blonder *et al.*, 2004; Choi *et al.*, 2011; Nouwens *et al.*, 2000; Peng *et al.*, 2005, Düvel *et al.*, 2012; Kumari *et al.*, 2014; Magnowska *et al.*, 2014; Motta *et al.*, 2020). Comparing the native nanodisc library with results from previous works, the proteome coverage is similar to data obtained by conventional methods. Notably, not all available proteome data represent the same growth conditions of the cells, though some variation is expected when compared against the previous data. Casabona *et al.*, 2013, identified 991 proteins from inner membrane fractions prepared by sucrose centrifugation and subsequent mass spectrometry, of which 964 proteins were also found in our library. In very similar growth conditions, Kumari and coworkers identified 2965 proteins from membrane fractions after extraction with harsh detergents and organic solvents (Kumari *et al.*, 2014). In our native nanodisc library, about 86 % of these proteins (2556 proteins) were detected and stably extracted. In an in-depth proteomic analysis of *P. aeruginosa* PAO1, about 2539 membrane-associated proteins were detected from cells in the exponential growth phase (Motta *et al.*, 2020). We were able to identify about 69 % of those proteins (1769 out of 2539) in our library and, additionally, 1568 proteins that had not been detected in the previous work. The protein composition regarding the predicted subcellular localisation of identified proteins was comparable to previous studies, although cytoplasmic proteins were slightly overrepresented in this study (48 %). In other proteomic approaches, the proportion of cytoplasmic proteins was 15-30 % (Blonder *et al.*, 2004; Kumari *et al.*, 2014). This could either be due to non-stringent washing of the membrane pellet, or interactions between cytoplasmic proteins and the membrane. Additionally, the high charge density of DIBMA has been shown to result in non-specific interactions with charged proteins and lipids (Glueck *et al.*, 2022; Pollock *et al.*, 2022). Furthermore, a high relative proportion of OMV-proteins was observed: While for most of the subcellular localisations about half of the annotated proteins were identified, the proportion for outer membrane proteins was higher with ~80 %. Usually, OMVs are constantly produced and released from *P. aeruginosa* (Choi *et al.*, 2011; Lee *et al.*, 2008). OMV-proteins were probably detected while passaging through the inner membrane before vesicles are formed. A similarly high proportion of OMV-proteins was described in Casabona *et al.*, 2013. In summary, the results show the good extraction capacity of DIBMA for membrane proteins of *P. aeruginosa* PAO1, enabling a high coverage of the entire membrane proteome within native nanodiscs. The major advantage of the nanodisc library over previous proteome work is that the soluble library preserves a nanoscale lipid-bilayer environment around the extracted proteins but nevertheless is suitable for downstream experimental analyses.

The subcellular localisation of the identified proteins was partly reflected in the elution profile from the size exclusion chromatography. In general, it became apparent that all proteins in the library eluted

with rather broad size distributions. Furthermore, proteins from the outer membrane eluted very early in SEC, indicating incomplete extraction. In elution volumes close to void volume of the column, particles with a high hydrodynamic radius are eluting (>5 000 000 Da). However, whether the eluting proteins are part of very large protein complexes or aggregates cannot be clearly distinguished in this experimental set up and would for instance require analysis of light scattering (Barth *et al.*, 1994). In this work the elution fractions close to the void volume were excluded from the analysis. Overall, predicted membrane proteins eluted in earlier fractions than soluble proteins. Also, membrane proteins showed 11-15 times increase in apparent size to predicted size, while soluble proteins showed approximately 5 times increase. The increased hydrodynamic radius for membrane proteins is probably directly related to their integration into nanodiscs, which is the most obvious reason for the different elution behaviour of proteins in the presented dataset. Still, the apparent size increase for soluble proteins could be a hint to protein interactions with membrane compounds, complex formation, multimerization or interaction with free polymer. Conversely, this means that the apparent molecular weight for soluble and nanodisc-embedded proteins does not correlate directly to the theoretical molecular weight of the proteins. Therefore, it is not reliable to conclude from the apparent molecular weight if the fractions correspond to individual proteins or complexes. Moreover, shape, possible multimerization, interactions to other proteins, unspecific interactions with the column material and interaction with bound or free polymer could influence the elution behaviour of proteins (Barth *et al.*, 1994; Bloustine *et al.*, 2003; Kunji *et al.*, 2008). The broad size distributions and incomplete extraction into DIBMA nanodiscs have previously been observed and are considered the major bottleneck for the use of this polymer in SEC studies (Glueck *et al.*, 2022). More recent, partially glycosylated polymers such as Glyco-DIBMA (Danielczak *et al.*, 2022), electroneutral polymers such as Sulfo-DIBMA (Glueck *et al.*, 2022; Janson *et al.*, 2022), and certain small-molecule amphiphiles (Mahler *et al.*, 2021) form nanodiscs having narrower size distributions and, thus, might overcome this limitation in future studies. Alternatively, other membrane mimetics like peptidiscs can be used for generating global membrane protein interactomes (Carlson *et al.*, 2018). Conventional solubilisation methods, in particular detergent solubilisation, have frequently been used in combination with gel-based separation techniques for the investigation of complexomics in bacteria, archeae, and eukarya (Berger *et al.*, 2021; Senkler *et al.*, 2017; Spaniol *et al.*, 2022; Versantvoort *et al.*, 2019; Wessels *et al.*, 2009).

4.1.2 Preservation of complexes in the library

The elution profiles of individual components from several known membrane-protein complexes were tested for similarities. For tested protein complexes different elution profile types were observed. Stable complexes showed a clear coelution of complex components e. g. the secretion apparatus (SEC-SRP), and the type IV pilus assembly subcomplex (see section 3.1.4) were strongly correlated in the present study. For two partite complexes two main profiles that overlap were observed: For instance, the NADH dehydrogenase complex shows one profile corresponding to the

membrane part (NuoA and NuoLMN) and a second profile for the cytosolic part of the complex (NuoBDEFG, and I). This observation was reproducible throughout the replicates and independent on the protein's intensity (Fig. A2). Individual proteins that either interact transiently, or do not interact at all show no clear coelution, as could be observed for SecB and the SEC-SRP complex.

Since most described complexes showed a good co-elution of individual proteins, it was subsequently tested if the elution profiles could give hints for novel protein-protein interactions. It was assumed that an interaction would result in similar profiles. To test for similar elution profiles, either a global correlation analysis or a cluster analysis was carried out. The reliability of the results was tested using the previous selected set of described membrane complexes. Correlation is defined as a description of a (linear) relationship between quantitative variables, thereby measuring the strength or extent of an association between the variables (Gogtay *et al.*, 2017). Usually, correlation analysis is used in statistics to search for similarities between two data sets. Although the described proteins showed overall a good correlation, the global correlation analysis revealed an overall shift of the correlation coefficients to high values. Thus, well-correlated protein pairs cannot be distinguished from non-interacting proteins in the dataset, and the elution profiles from this library could not be used for complexome profiling or *de novo* interactome prediction.

Similarly, a hierarchical cluster analysis was carried out to sort the elution profiles according to similarities. The categorisation into clusters is carried out freely without pre-formed categories, but exclusively on the basis of the data (Bridges, 1966). The feasibility to detect described membrane protein complexes from this sorting process was tested with the described protein complexes. It was observed that proteins from one complex were often not exclusively found in the same cluster, or that clusters that contained full complexes were very large. Therefore, the explanatory power of the clusters was not sufficient to make assumptions about interacting proteins. It is possible that different clustering parameters - like distance threshold, linkage method or number of clusters - lead to different results.

Nonetheless, the dimensions of nanodiscs in size exclusion chromatography indicates that the proteome library contains very large nanodisc particles likely to contain membrane-protein complexes, that enabled the targeted search for membrane-protein interactions (see section 4.1.4). However, no new interactions could be predicted due to the similarity and overlap of the profiles, likely caused by the size distribution of the nanodiscs (see section 4.1.4).

4.1.3 The c-di-GMP regulation network

The second messenger c-di-GMP regulates biofilm formation, motility, virulence, and cell cycle progression in many different bacteria (Hengge, 2009). Most bacteria have multiple enzymes that can produce or degrade c-di-GMP, and these enzymes are often present at the same time in the cell (Hou *et al.*, 2023; Motta *et al.*, 2020, Sommerfeldt *et al.*, 2009). It has previously been observed in *E. coli* that several c-di-GMP modulating proteins are controlled by the formation of regulatory supermodules (Hengge, 2021; Sarenko *et al.*, 2017). These supermodules are mainly formed by the

c-di-GMP-producing or degrading enzymes, specific effectors, and cellular target structures, e. g. the flagellar system (Dahlstrom *et al.*, 2018; Richter *et al.*, 2020; Sarenko *et al.*, 2017). We identified about 29 proteins potentially involved in c-di-GMP synthesis or degradation in the nanodisc library of *P. aeruginosa* and a further nine c-di-GMP binding effector proteins. Most of the identified proteins are membrane-integrated or likely to be membrane-associated. To our knowledge, the dataset presented in this work is thus far the largest set of proteins detected from the c-di-GMP network of *P. aeruginosa* (Bense *et al.*, 2022; Blonder *et al.*, 2004; Casabona *et al.*, 2013; Düvel *et al.*, 2012; Kumari *et al.*, 2014). In our nanodiscs library, GGDEF/EAL proteins were detected together with their described interaction partner(s) in the overlapping fractions, indicating preservation of these interactions. However, elution profiles were broad, and correlation was upshifted for the whole dataset, which limits the feasibility for *de novo* predictions of protein-protein interactions (4.1.2).

4.1.4 Polymer nanodiscs for targeted protein-protein interaction investigation

Although the global data analysis from the membrane protein library did not reveal new protein complexes, the elution profiles indicated presence of membrane complexes. To provide experimental evidence for the preservation of protein complexes in the native nanodisc library, a pulldown approach coupled with mass spectrometry was carried out. As a bait, the membrane protein and active PDE NbdA was used, from a strain overproducing the target protein to ensure detection and sufficient amounts. In contrast, overexpression of a membrane protein can alter its folding or localisation, as well as affecting translocation machineries, biogenesis of proteins or membrane integrity (Luirink *et al.*, 2005; Wagner *et al.*, 2007). In the analysis of protein–protein interactions, the stability of the complex is the most critical factor. When dealing with membrane proteins, the proper extraction process, and the lipid environment of the membrane proteins after extraction affect the stability of membrane-protein complexes the most (Overduin *et al.*, 2019). By combining solubilisation of membrane proteins with nanodisc forming polymers with affinity chromatography and MS, 417 novel candidates for the interaction with the phosphodiesterase NbdA were enriched. It should be noted, that with this strategy some of the hits are false positives, e. g. proteins that interact with the membrane material or the polymer itself. The interaction of NbdA with the enriched proteins CzcR, PA4200, SadC, and PilB, that could be further verified by the B2H assay. The physiological role of the interaction of these proteins with NbdA is discussed in chapter 4.2.2. Overall, the results in this work demonstrate the usefulness of native nanodisc libraries combining DIBMA extraction and affinity-based pulldown coupled to mass spectrometry for identifying novel protein–protein interactions. With this work, a large number of candidate interactors for the membrane phosphodiesterase NbdA were detected, especially in the c-di-GMP network and four candidates were verified by B2H analyses.

4.2 The PDE NbdA

Although the role of the membrane integrated PDE NbdA has been investigated in *P. aeruginosa* for a decade, its exact function remains undefined. Previous investigations on NbdA revealed that the protein induces unforeseen phenotypes when overexpressed. This research builds upon the previous work of Rüger, 2019 and Gerbracht, 2021 and includes testing the peculiarity of certain phenotypes, gaining additional insight into its regulation of c-di-GMP, and further assessing the possibility of interaction or regulation of type IV pili. The findings were implemented to specify the role of NbdA within the intricate c-di-GMP system of *P. aeruginosa*.

4.2.1 Specificity of phenotypes caused by the MHYT domain of NbdA

In the work of Rüger, 2019, Rehner, 2020 and Gerbracht, 2021, the phenotypic consequences of overproduction of NbdA and variants were investigated. It was observed that overexpression of *nbdA* strongly reduced growth on plates after induction of gene expression. Moreover, cells in liquid culture that overproduce NbdA were elongated. In Gerbracht, 2021 it was shown that these phenotypes are dependent on the presence of the MHYT domain. It was previously shown in *E. coli* that the overexpression of inner membrane proteins can result in impaired growth and cell elongation, presumably by altering cell division or an inhibition of cells entering the stationary phase (Gubellini *et al.*, 2011; Wagner *et al.*, 2007). It was proposed that the overproduction of the MHYT domain has a similar effect. However, the cells overproducing inner membrane proteins in *E. coli* showed no indication of envelope stress nor folding stress. The occurrence and extent of changes in growth were rather dependent on the biochemical and biophysical properties of the individual proteins (Gubellini *et al.*, 2011). The results presented in this work indicate that the phenotypes are specific to NbdA, as neither the MHYT domain containing proteins MucR and CoxH nor the membrane anchored PDE BifA do result in the previously mentioned phenotypes. Therefore, the MHYT domain of NbdA seems to have specific properties, that lead to the altered growth phenotypes. When comparing the amino acid sequence to other MHYT domain containing proteins, NbdA seem to have some differences in sequence compared to other predicted MHYT domain proteins (**Fig. 4.1**). Although similar in size (~200 aa), the MHYT domain of NbdA and MucR share a sequence similarity of 44.8 %. The MHYT domain of CoxH with ~80 aa is smaller and has 32 % sequence similarity to the MHYT domain of NbdA. Thus, the growth defect and cell elongation of cells overproducing NbdA variants containing the MHYT domain could be related to structure and possibly the associated function. However, it is not defined which properties are responsible for the observed effects, or what the function of NbdA or its MHYT domain is.

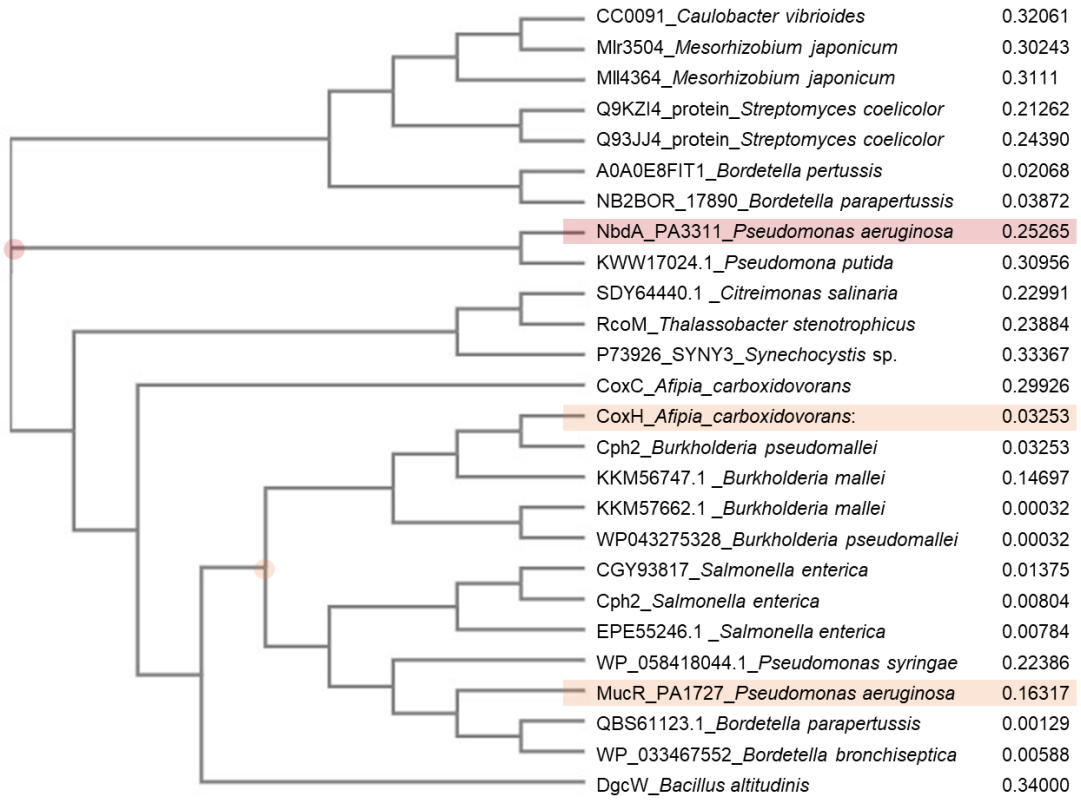

Fig. 4.1 Multiple sequence alignment of MHYT domain protein sequences. A multiple sequence alignment with the MHYT domains of different proteins from various species was carried out in Clustal omega. Amino acid range belonging to the MHYT domains of individual proteins were obtained from Uniprot database. NbdA is highlighted red, MucR and CoxH are highlighted in orange.

Notably, the growth defect on agar plates of cells overproducing NbdA seems to be coupled to specific growth conditions. Normal growth was described for the same strain, when cells grew at room temperature or on centrimide agar for three days (Rüger, 2019). Multiple other phenotypes of proteins related to c-di-GMP were dependent on certain environmental conditions, like carbon sources or oxygen availability (Mattingly *et al.*, 2018; Hwang *et al.*, 2023; Schmidt *et al.*, 2016). Presence of cofactors, signals, substrates, or interaction partners have been shown to modulate activity or extent of generated output (Giacalone *et al.*, 2018; Mattingly *et al.*, 2018; Schmidt *et al.*, 2016). For instance, the DGC YfiN induces growth arrest only on gluconeogenetic carbon sources since the GTP pools are already depleted from the energy costly pathway (Hwang *et al.*, 2023). The MHYT domain was postulated to bind copper, however, copper deprivation on PAO1 does not result in a growth phenotype if the copper-independent terminal oxidase CIO is present (Frangipani *et al.*, 2008). The signal of NbdA is still unclear, but in (Agbadaola, 2023) it was shown that binding of heme and iron could stimulate NbdAs PDE activity *in vitro*. Depletion of iron results in slower growth in PAO1 (Lin *et al.*, 2015). Additionally, the growth defect on solid media seems to be more severe than in liquid medium. Similarly, strain with a deletion of the gene encoding the protein Fur (ferric uptake regulator) showed no growth on solid media, but cells grow in liquid. The protein regulates iron uptake, storage

and detoxification. What causes the growth defect is not known, it was shown that it is not due to iron toxicity (Pasqua *et al.*, 2017).

Alternatively, the MHYT domain might interact with other proteins and thereby trigger the growth and cell morphology phenotypes. In the B2H assay it was shown that the MHYT domain can be involved in the interaction of two proteins, e. g. in the interaction with the pilus motor PilB. The type IV pilus machinery has also been shown to regulate cell division, for instance in *C. crescentus*. Here the minor pilin PilA acts as a signal for kinase PleC, that regulates cell cycle initiation (Del Medico *et al.*, 2020). In *P. aeruginosa*, type IV pili components are recruited to sites of future cell division, to preinstall the assembly complex (IM) and PilQ (OM) in the cell envelope (Carter *et al.*, 2017). The interaction with the MHYT domain might block correct pili complex formation, which might result in the growth defect, but so far, no involvement of PilA or PilB in cell division has been found in *P. aeruginosa*. In the pulldown, however, there were also proteins enriched that have a function in DNA positioning, replication organisation, and transcription which is important for cell division (Egan *et al.*, 2013). It was also shown in PA14, that proteins (e. g. PA2285, PA2287) that interact with proteins involved in transcription (RpoC) or cell division (FtsZ) can arrest growth, resulting in persister formation (Long *et al.*, 2019). Nonetheless, said interaction partner candidates from the pulldown assay have to be confirmed with additional methods, and the physiological role has to be investigated further. Possible interaction partners are further discussed in 4.2.2.

Interestingly, the growth phenotypes upon overproduction of NbdA, namely no growth on plates and cell elongation, were dependent on the presence of the MHYT domain and could not be observed in a moderate overexpression strain. In the moderate overexpression, *nbdA* was encoded on the low-copy vector pME6032 instead of the high copy vector pHERD26T. Here, also after induction of gene expression, the cells grew on solid agar plates and showed no elongation (Fig. A5 and A6). Similarly, the GGDEF domain protein CdgI from *E. coli* was described to be toxic when overexpressed from a high copy vector, but not from a low-copy vector (Sarenko *et al.*, 2017). Under standard laboratory condition the protein CdgI was not expressed, and the physiological role is unknown. An involvement of c-di-GMP regulating proteins in cell division has been demonstrated, e. g. in *C. crescentus*, positioning and activity of PleD is involved in regulating cell division (G1-S transition) via the c-di-GMP binding protein CckA (Lori *et al.*, 2015). Moreover, it was shown that an imbalance in nucleotide levels could also result in reduced cell proliferation (Diehl *et al.*, 2022). A recent publication has described the involvement of the c-di-GMP regulating protein YfiN in cellular growth in *E. coli*. The active DGC regulates growth arrest on gluconeogenetic carbon sources by depleting cellular GTP. Thus, the protein contributes to increasing antibiotic tolerance (Hwang *et al.*, 2023). Although a similar regulation for NbdA is unlikely, as the growth defect and elongation were demonstrated to be independent on the PDE activity but were rather dependent on the presence of the MHYT domain of NbdA, it shows that c-di-GMP regulating proteins are interlinked with cell cycle regulation. The slowdown of cell division was also described to be a strategy for survival and

infection, where a subpopulation of cells enters a dormant-like state with reduced metabolic activity and higher antibiotic resistance (Lewis, 2007). The so-called persister cells prevalently occur in stationary phase and later stages of biofilms, but the underlying signalling events leading to their formation are not described in detail (Keren *et al.*, 2004; Mulcahy *et al.*, 2010). The formation was shown to occur stochastically, while certain environmental stimuli promote persister formation, e. g. nutrient-limitation, DNA damage, or diverse stress responses (heat, oxidative stress, antibiotic, acid, osmotic) (reviewed in Wilmaerts *et al.*, 2019). Whether the growth impairment noticed in the NbdA overproduction strain is implicated in persister production requires further investigation.

In summary, the growth defect observed for the MHYT domain overexpression was specific to the MHYT domain of NbdA, dose-dependent and coupled to specific environmental conditions. The cause of the observations or the physiological role of the described phenotypes is not known so far.

4.2.2 Interaction partners of NbdA

Previous studies have shown that in *E. coli*, the regulation of many c-di-GMP modulating proteins is achieved through formation of regulatory supermodules (Hengge, 2021; Sarenko *et al.*, 2017). These supermodules consist of c-di-GMP-producing or degrading enzymes, specific effectors, and cellular target structures, e. g. T4P machineries or the flagellar system (Dahlstrom *et al.*, 2018; Richter *et al.*, 2020; Sarenko *et al.*, 2017). When discussing the role of the new identified interaction partners, it should be considered that they were identified in a strain overproducing NbdA. This might lead to altered gene expression and protein composition, which differentiate from the native conditions when NbdA is present. This could lead to identifying interacting proteins that are not present together with NbdA under native conditions (false positives). On the other hand, physiological relevant interaction partners might not be present under the chosen conditions (false negatives). NbdA was shown be expressed in the stationary phase, after 7 h growth at 37 °C (Gerbracht, 2021) which was consistent with the proteomic data provided in this study. Therefore, similar conditions were chosen for the pulldown assay to ensure presence of interacting proteins. As a control a strain overexpressing untagged NbdA was selected to minimize false positive hits due to different expression in the NbdA overproducing strain. Indeed, all confirmed interaction partners except CzcR were also identified in stationary growing PAO1 wildtype cells alongside NbdA in at least two out of three replicates.

<u>The hypothetical protein PA4200</u>

The interaction partner PA4200 was one of the top enriched proteins in the pulldown assay with high significance. B2H analysis could confirm PA4200 as an interactor of NbdA. Additional testing of NbdA's subdomains showed an interaction of PA4200 with the cytosolic part of NbdA. The protein is a predicted cytosolic protein and uncharacterized so far. However, PA4200 is a homologue of the YtnP lipase from *B. subtilis* (Kukavica-Ibrulj *et al.*, 2008). The protein YtnP from *Bacillus paralicheniformis* was shown to inherit lactonase activity, thereby hydrolysing acylated homoserine lactones (AHL) that are involved in quorum sensing (QS) in Gram-negative bacteria (Djokic 2022). It was further demonstrated that YtnP from *B. subtilis* was able to exert quorum

quenching activity (Schneider *et al.*, 2012). Thereby, *ytnP* expression was dependent on streptomycin production from *Streptomyces griseus* (Schneider *et al.*, 2012). It was proposed to be a general defence response to presence of antimicrobioals and other stressors that can damage the cells (Schneider *et al.*, 2012). In general, lipases were shown to catalyze the formation and cleavage of long chain acylglycerols, important for pathogenicity and biofilm formation (Jaeger *et al.*, 1999; Stehr *et al.*, 2003). Likewise, in *P. aeruginosa* the lipase LipC was shown to regulate EPS composition, biofilm formation and motility (Rosenau *et al.*, 2010; Tielen *et al.*, 2010) or diverse other lipases are characterized virulence factors damaging host tissue (König *et al.*, 1996; Wang *et al.*, 2021). The expression of PA4200 in *P. aeruginosa* is regulated by the transcription factor PycR, that also controls expression of two pyruvate carboxylase genes (directly upstream), and genes for lipid metabolism, lipolytic activity, anaerobic respiration, and biofilm formation (Kukavica-Ibrulj *et al.*, 2008). Although, activity or role of PA4200 in *P. aeruginosa* has not been investigated, it was demonstrated that *P. aeruginosa* synthesises quorum quenching enzymes (e. g. PA2385) to modulate its own QS-dependent pathogenic potential (Sio *et al.*, 2006). These enzymes were proposed to act as virulence repressors during iron starvation; or to allow the use of AHL signalling molecules as an energy source (Lin *et al.*, 2003; Sio *et al.*, 2006). It was also shown in previous studies, that QS and c-di-GMP are interlinked in *P. aeruginosa* and other bacteria (Srivastava *et al.*, 2012; Ueda *et al.*, 2009) In PA14, TpbA senses AHLs and dephosphorylates the DGC TpbB (YfiN) which reduces its c-di-GMP production (Ueda *et al.*, 2009). In turn, low c-di-GMP levels increase expression of QS-regulated genes presumably through PqsR, thereby stimulating virulence and rhamnolipid formation (Lin Chua *et al.*, 2017).

It is possible that either through lipase activity or connection with the QS-system in *P. aeruginosa*, PA4200 might be involved in survival or virulence (**Fig. 4.2**). A role of NbdA for virulence was demonstrated in PA14 in a mouse model (Kulasakara *et al.*, 2006). The role of the interaction of NbdA and PA4200 is yet to be determined.

The response regulator CzcR

The novel interaction partner CzcR was also top enriched in the pulldown with high significance. The B2H assay showed an interaction of CzcR with the full-length NbdA, as well as with the cytosolic part. No interaction was detected with the MHYT domain. The protein CzcR is part of the CzcS/CzcR two-component system regulating heavy metal efflux and virulence (Dieppois *et al.*, 2012). CzcS is a membrane anchored histidine kinase that senses Zn^{2+} stress and modulates phosphorylation of the response regulator CzcR (Wang *et al.*, 2017). CzcR regulates the expression of different genes by direct interaction with the promoter region in response to Zn^{2+} stress, as it was shown for the genes encoding MexAB-OprM and MexGHI-OpmD efflux pumps. CzcR represses their expression which increases susceptibility to aminoglycoside and fluorquinolon antibiotics (**Fig. 4.2**) (Chen *et al.*, 2023). Additionally, the expression of *oprD* encoding a porin, that is the entrance for carbapenem antibiotics is downregulated by CzcR (Dieppois *et al.*, 2012). CzcR also regulates swimming and swarming

under Zn^{2+} stress by activating expression of flagella genes (*flgBCDE, flgFGHOJK* and PA1442/*fliMNOPQR*/*fhlB*) (Liu *et al.*, 2022b). It was further demonstrated to induce expression of genes encoding the heavy metal efflux pump CzcCBA in response to zinc, cadmium and cobalt, thereby inducing resistance to these metals (Perron *et al.*, 2004). The response regulator also activates its own expression, creating a positive feedback loop (Dieppois *et al.*, 2012). In the presence of zinc, CzcR also positively regulates expression of *lasI*, thereby regulating QS and QS-mediated phenotypes (Dieppois *et al.*, 2012). Moreover, CzcR represses pyocyanin biosynthesis via repression of *phzA1* by direct promoter interaction and indirect repression of *phzA2*, especially under Zn^{2+} stress (Dieppois *et al.*, 2012). Expression of CzcR is regulated by AlgZ, which regulates infection and iron acquisition (Little *et al.*, 2018). The physiological role of the interaction of CzcR with NbdA has to be further studied.

The DGC SadC

Interactions between DGCs and PDEs controlling the same c-di-GMP pool have been frequently observed in previous studies (Dahlstrom *et al.*, 2018; Lindenberg *et al.*, 2013; Sarenko *et al.*, 2017; Xu *et al.*, 2022). In the pulldown assay, a single DGC was found to be significantly enriched: the DGC SadC, whose interaction with NbdA was confirmed by B2H assay. Further testing of NbdA subdomains showed that the interaction is attributed to the cytosolic part of NbdA. This finding is consistent with previous studies where the interaction of NbdA and SadC was shown in B2H assays in PAO1 or the respective homologs of *P. fluorescence* Pf0 (Beganovic, 2018; Dahlstrom *et al.*, 2018). SadC is an active DGC, that is involved in surface-dependent increase of c-di-GMP, swarming motility and early biofilm formation in PA14 (Merritt *et al.*, 2007). It was demonstrated that the flagellar stator MotC directly interacts with SadC stimulating its DGC activity and promoting biofilm formation (**Fig. 4.2**). This interaction is indirectly regulated by c-di-GMP that is bound to the effector FlgZ. The FlgZ-c-di-GMP complex interacts with MotCD and in turn disengages it from the flagellar motor, enabling interaction with SadC and creating a positive feedback loop (Baker *et al.*, 2019). The system was shown to be fine-tuned by SadC's interaction with the T4P alignment complex component PilO, that inhibits DGC activity of SadC in a planktonic state promoting motility (Webster *et al.*, 2021). It was further proposed that the T4P tip protein PilY1 regulates c-di-GMP levels in response to surface tension via interaction with PilO (Webster *et al.*, 2022). Since the T4P tip protein and force sensor PilY1 also interacts with PilO, it was proposed that SadC is responsible for the increase in c-di-GMP levels after surface encounter in PA14 (Webster *et al.*, 2022). Interestingly, the proteins PilO and MotC, both described to interact with SadC, were also significantly enriched in the pulldown assay. Additionally, ethanol-dependent motility repression in PA14 was dependent on SadC and MotCD delocalisation. Thereby it was proposed that the signal ethanol alters the membrane structure, which is either recognised by PilY1, PilMNOP or PilVWX (Lewis *et al.*, 2019). Notably, the force sensitive region in PilY1 in PA14 is not present in PAO1.

In PAO1, SadC was shown to be more active under anaerobic conditions, thereby stimulating alginate synthesis in anoxic conditions (Schmidt *et al.*, 2016). Alginate synthesis regulation was proposed to function via the Alg44 effector, that senses c-di-GMP produced by the DGC SadC. Oxygen-dependent regulation of SadC's DGC activity was mediated by the regulators OadA and OadI. OdaI is a predicted dioxygenase reductase with a [Fe-S] cluster and a FAD/NAD(P) binding site, and thereby proposed to be the oxygen-responsive element of the pathway (Schmidt *et al.*, 2016).

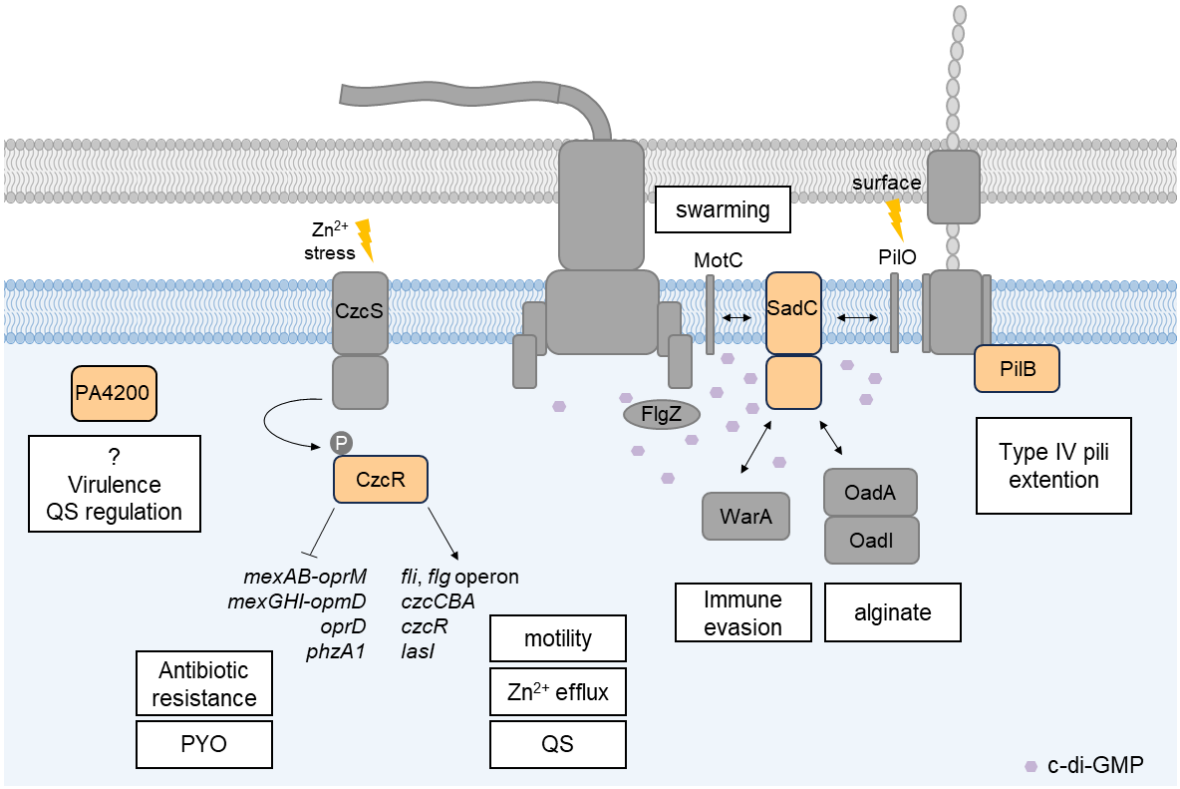

Fig. 4.2 Functions of PA4200, CzcR, SadC and PilB, potential interaction partners of NbdA. Possible interaction partners depicted in orange. The hypothetical protein PA4200 is a potential lipase involved in virulence or quorum sensing regulation. The protein CzcR is a response regulator altering expression of efflux pumps involved in antibiotic resistance and Zn efflux. Further CzcR was demonstrated to regulate expression of flagella genes and genes involved in QS and pyocyanin (PYO) production. The DGC SadC has multiple functions, it is involved in swarming motility, surface sensing and biofilm formation. Moreover, through the interaction with WarA SadC is involved in O-antigen modification and immune evasion. In anaerobic conditions, DGC activity of SadC is regulated by OadA and OadI to control alginate production. The protein PilB is an ATPase involved in T4P polymerization, thereby stimulating pilus extention.

In PAK SadC was shown to be regulated RsmA, that is controlled by the Gac/Rsm pathway (Moscoso *et al.*, 2014). RsmA was further shown to regulate more than 500 targets involved in T6S, assembly of T4P, virulence or biofilm formation (Brencic *et al.*, 2009; Moscoso *et al.*, 2014). Additionally, a role of SadC in regulation of LPS O-antigen synthesis was shown in PAK. Thereby SadC interacts with the c-di-GMP binding methyltransferase WarA recruiting it to the inner membrane. WarA activation results in altered LPS O-antigens and immune cell evasion (McCarthy *et al.*, 2017).

Since both proteins, NbdA and SadC exhibit polar localisation within the cell (Gerbracht, 2021; Schmidt *et al.*, 2016) and a direct interaction was demonstrated, it implies that both proteins might regulate the same c-di-GMP pool through performing opposite roles. Proximity and interaction of

DGCs and PDEs responsible for governing the same local c-di-GMP pool are prevalent (Kunz *et al.*, 2020; Richter *et al.*, 2020; Sarenko *et al.*, 2017). However, it is probable that additional DGCs or PDEs are involved in the regulation of the c-di-GMP pool. The integration of the SadC-NbdA interaction in the c-di-GMP network is further discussed in chapter 4.2.5. It is also possible for the proteins to modulate each other's activity through interaction or heterodimerization which could elucidate the c-di-GMP levels observed for overproduced NbdA variants, discussed in section 4.2.4. Heterodimerization has been suggested to occur between GGDEF/EAL domain proteins (Dahlstrom *et al.*, 2018; Valentini *et al.*, 2016a).

The pilus motor protein PilB

Although not being one of the top enriched proteins, PilB was robustly detected, and its levels were more than 3.5-fold enriched with high significance. In a B2H assay, the interaction of NbdA and PilB was confirmed, and it was shown that both the membrane anchored MHYT domain as well as the cytosolic part of NbdA contribute to the interaction with PilB. The protein PilB is one of the four core proteins necessary for T4P assembly. T4P are cellular appendages that are involved in adhesion, movement over a surface with twitching motility, mechanosensing, DNA uptake and protein secretion (Pelicic, 2023). PilB was shown to form hexameric ring-shaped structures that bind to the pilus assembly platform. Through ATPase activity, the protein stimulates pilin polymerization and thereby pilus extension (**Fig. 4.2**). Thereby, it was shown that the ATPases for pili polymerization (PilB) and retraction (PilT and PilU) compete for binding to the T4P machinery (Jakovljevic *et al.*, 2008). Notably, PilB is not the only pilus component to be significantly enriched in the pulldown, also enrichment of the pilus assembly subcomplex protein PilO, the prepilin peptidase PilD, the minor pilin PilY2, and the potential pilus retraction ATPase PilU was highly significant. In previous studies, it has been shown that T4P are regulated by c-di-GMP in *P. aeruginosa*. The T4P formation is dependent on the c-di-GMP binding protein FimX, promoting twitching motility and microcolony formation (Huang *et al.*, 2003; Jain *et al.*, 2017). At high intracellular c-di-GMP levels, T4P formation was independent of FimX, suggesting different ways of T4P assembly under different environmental conditions (Jain *et al.*, 2012). Moreover, the c-di-GMP effector protein FimW was shown to regulate pili dependent attachment after surface contact (Laventie *et al.*, 2019). In turn, the T4P components were demonstrated to influence intracellular c-di-GMP levels, as it was shown for the minor pilins PilY1, PilW and PilX, as well as for the assembly protein PilO, probably regulating DGC activity of SadC (Kuchma *et al.*, 2010; Kuchma *et al.*, 2012; Webster *et al.*, 2021) (see also function of SadC above).

Further candidate proteins

In addition to the confirmed interaction partners of NbdA, there were still many proteins identified as candidates for protein-protein interaction. Among them were further proteins involved in the c-di-GMP regulating network. Those include the other GGDEF/EAL/HD-GYP domain containing proteins RmcA, RbdA, PipA and LapD. A possible interaction or proximity of these proteins might

indicate that they control the same c-di-GMP pool. For RbdA, it was shown to control the MapZ-mediated flagella motor switching in PAO1 together with NbdA and DipA (Xin *et al.*, 2019). DipA was not identified in the presented dataset. The potential interaction of NbdA with other c-di-GMP related proteins may alter global c-di-GMP levels, discussed in 4.2.4. Proteins that have been described to coincide frequently with c-di-GMP-modulating proteins, e. g. QS, virulence, or transcription factors were enriched in this study (Hall *et al.*, 2018; Lin Chua *et al.*, 2017). Furthermore, proteins involved in DNA replication and cell division were identified, where the interaction of NbdA might explain the growth phenotypes observed (cf. 4.2.1). Also, a large number of proteins involved in amino acid transport were identified. However, interaction of NbdA with the identified candidates remains to be verified and the physiological relevance of the interactions are yet to be determined. In general, many DGCs and PDEs have been described to form direct protein-protein interactions to other c-di-GMP modulating enzymes, effectors, cellular targets, or regulating proteins (Dahlstrom *et al.*, 2018; Feirer *et al.*, 2015; Richter *et al.*, 2020; Sarenko *et al.*, 2017; Webster *et al.*, 2021).

4.2.3 Involvement in pili regulation

There are several indications that NbdA might be involved in the regulation of T4P. An interaction of NbdA with the T4P has already been proposed by Gerbracht, 2021 since the localisation pattern of NbdA and the T4P were shown to be similar in PAO1. In this work, co-localisation with the pili component PilO was tested, to determine whether NbdA is localised to the piliated pole. Additionally, the pulldown analysis identified the ATPase PilB as a candidate interaction partner of NbdA. By B2H assay the interaction of NbdA and PilB was confirmed. It was also noticeable that the NbdA overproduction strain exhibited a high abundance of the major pilin PilA. In a B2H assay, an interaction of NbdA with PilA was shown, consistently with previous studies (Unbehend, 2022).

PilO is an essential protein for the T4P assembly, that was demonstrated to localise at foci of intact T4P machines (Koch *et al.*, 2021). In mid-log phase cells, the protein was shown to localise either polar or bipolar (Koch *et al.*, 2021). The observed pattern of PilO localisation in this study was similar to previous studies, although a higher fraction of cells exhibited polar PilO localisation instead of bipolar localisation. The variations could be due to different experimental conditions: Koch and coworkers used mid-log growing cells that grew in cysteine-free EZ rich medium (Koch *et al.*, 2021), while in this work, cells in stationary growth phase cultured in LB medium were used. CLSM studies with overproduced NbdA in the PilO-labelled strain indicated an occasional localisation of NbdA at the cell poles carrying T4P machineries. For a strain with fluorescently labelled PilT, only a small proportion of cells actually showed a signal. The pilus retraction protein PilT was demonstrated to specifically bind to poles with active pilus machines, and previous results indicated that about two third of intact T4P machineries actively make pili (Koch *et al.*, 2021). The low proportion of cells showing a clear PilT signal might either have technical reasons, or cells produced fewer pili under

the conditions used. Further, an interaction of NbdA with the pilin ATPase PilB was demonstrated in the pulldown and B2H assay. PilB was shown to localise at the leading pole for twitching direction in *P. aeruginosa* (Kühn *et al.*, 2021). Thus, cells on agar plates exhibited a bipolar PilB localisation with asymmetric distribution (Chiang *et al.*, 2005). Polarity of twitching direction and thus PilB localisation was shown to be regulated by the chemotaxis-like Chp-system controlling two antagonistic response regulators PilG (promoting cell polarity) and PilH (promoting polarity switch) (Kühn *et al.*, 2023). Surface sensing by the T4P activated the Chp-system, that results in phosphorylation of PilG and cell polarity. Increased T4P formation stimulates mechanosensing at the same pole, thereby feeding a positive feedback loop. Inactivation of the system and polarity switching is mediated by phosphorylated PilH, that was shown to reduce PilG phosphorylation (Kühn *et al.*, 2023). Interaction of NbdA with PilB indicates that NbdA is occasionally located at the leading pole facing twitching direction. Notably, co-localisation of two proteins in CLSM is not imperative for an interaction (St Croix *et al.*, 2005). Direct interaction of NbdA and pilus components could be tested for instance by FRET or BIFC, which would give both information about localisation in the cell and interaction. Moreover, co-localisation of NbdA and the piliated pole could be tested in CLSM with labelled T4P. Previous studies demonstrated, that introducing the amino acid exchange A86C in PilA through a point mutation in the gene sequence enables pili labelling with thiol-reactive maleimide dyes without disturbing T4P dynamics (Ellison *et al.*, 2017; Koch *et al.*, 2021).

The protein-protein interaction might be an indication for either NbdA regulating T4P formation, or *vice versa* the T4P machinery modulating functions of NbdA. In *C. crescentus* concentration of the minor pilin PilA in the inner membrane acts as an input signal for the kinase PleC, that regulates c-di-GMP signalling via phosphorylation of the DGC PleD to initiate cell-cycle progression. Thereby the pili act as surface sensors (Del Medico *et al.*, 2020). A similar function of T4P was also shown in *P. aeruginosa* where the PilA concentration in the inner membrane changes dependent on surface stiffness, which mediates cell division and virulence (Koch *et al.*, 2022).

Possible alteration of T4P in the strains overproducing NbdA variants were examined in a phage assay. The T4P specific phage DMS3*vir* is a modified lytic version of DMS3 (Budzik *et al.*, 2004), that lost the ability for lysogenic infection (communication with M. Shasha Bruderer, U. Jenal group, University Basel). Overexpression of *nbdA* either from a high or low copy vector resulted in reduced susceptibility towards the phage DMS3*vir*. This observation led to the assumption, that overexpression of *nbdA* might result in decreased piliation of cells, since mutants without T4P (e. g. Δ*pilA* or Δ*pilD*) were shown to be resistant towards phage infection (Budzik *et al.*, 2004). However, in the AFM images, the strain overexpressing *nbdA* produced more pili than the wildtype. In general, it was shown in PAO1 that planktonic cells typically display between 0-2 pili, while surface attached cells can have eight or more pili (Laventie *et al.*, 2019). Since the AFM images were taken in surface attached cells and only 2-4 cells for each strain were analysed, it is not clear whether this observation is a coincidence or a substantial change. Therefore, the piliation of cells overexpressing *nbdA* should

be reassured with larger sample size and alternative methods like TEM or T4P labelling. Assuming that the overexpression of *nbdA* results is increased pili extension e. g. due to PilB activation by NbdA, how does that fit to the observations in the phage assay? The exact mechanism by which the phage DMS3*vir* infects its host is not described so far. However, electron microscopy investigations of other pilus-specific phages for *P. aeruginosa* propose that the phages attach themselves to the pilus by their lateral tail fibers. Subsequently, pilus retraction draws the phage towards the cell surface, where the phage injects its DNA (Bradley *et al.*, 1974). It was proposed that phages might also use the outer membrane pore of T4P for DNA injection (Bradley *et al.*, 1974; Narulita *et al.*, 2016). It can be postulated the interaction of NbdA and PilB leads to a shift to favour pilus extension over retraction. It was shown that the two ATPases for pili polymerization and retraction compete for the T4P machinery (Jakovljevic *et al.*, 2008). PilB activation by NbdA might also occur indirectly, e. g. by NbdA enhancing the PilB interaction to the machinery. Either way, the result would be increased pilus polymerization and less pilus retraction. This could hinder infection, as the phages attached to pili are constantly pushed away from the cell and unable to inject their DNA. Formation of more pili could also prompt the phages to attach to different pili at the same cell. In the B2H assay, both the MHYT domain as well as the cytosolic part of NbdA contributed to the interaction, which could explain why overproduction of all the tested variants resulted in slower lysis of cells by the phage DMS3*vir*.

Besides potentially extenuating phage entry, NbdA might also counteract the infection. The phage DMS3 encodes the protein Aqs1 (anti-quorum-sensing protein 1), which facilitates phage infection by inhibiting the hosts QS systems through direct binding to LasR (Shah *et al.*, 2021). LasR activates expression of the Rhl and PQS systems. Especially the PQS system was described to be involved in phage defence (Moreau *et al.*, 2017). Interestingly, the regulators LasR, as well as RhlR were found among the top enriched proteins in the NbdA pulldown experiment with a fold change of 4.8 and 3.2 respectively. However, the interference of NbdA with QS was not reported so far. The phage protein Aqs1 was also shown to directly interact with PilB, thereby preventing pilus assembly and superinfection (Shah *et al.*, 2021). It is possible that the overexpression of NbdA counteracts the effect of Aqs1 during infection thereby reducing infection efficiency. Alternatively, due to interaction with NbdA, the target PilB (and potentially LasR) could become less accessible to Aqs1.

On the other hand, it is possible that an excess of NbdA and its variants could alter the protein composition of the cells, which results in the decreased infection efficiency of the phage. Reduced expression of a phage receptor is a common mechanism by which bacteria acquire phage resistance (Wang *et al.*, 2023). It is also possible that the overproduction of a membrane proteins has secondary effects on surface receptors for the phage since the MHYT domain containing variants show a stronger effect of partial resistance against phage infection. It was demonstrated that enhanced production of a membrane protein reduces the abundance of native membrane components (Wagner *et al.*, 2007).

Further, the formation and mechanics of T4P are influenced by the c-di-GMP level in *P. aeruginosa* (Jain *et al.*, 2012). Indirect effects from c-di-GMP dependent functions, like EPS secretion have been described to decrease susceptibility to phage infection (Wang *et al.*, 2023). However, overproduction of all NbdA variants resulted in slower lysis, independent of their cellular c-di-GMP levels. In the moderate overproduction of NbdA, the cells do not show an elongated cell morphology or reduced growth after induction of gene expression, either on plates or in liquid medium. Still, cells overproducing NbdA were demonstrated to have a delayed lysis in the phage infection assay, indicating that this phenotype is not due to impaired cell division or growth defect observed in the strong overproduction strain.

So far, no influence of the deletion of *nbdA* on twitching motility, adhesion (Gerbracht, 2021) or T4P specific phage susceptibility has been observed. Possibly, the influence of NbdA on T4P requires certain conditions e. g. media, temperatures, cell density, or surface-attachment. The reason why there was no influence of deletion of *nbdA* in the phage assay might be that NbdA is transcribed in the stationary phase, whereas the phages infect exponential growing bacteria. To ensure NbdA production in the cells, further knowledge about the transcriptional and translational regulation of NbdA would be helpful, as well a good understanding of pili dynamics under the conditions. T4P of individual cells could be visualised with TEM, this method is often used to investigate piliation of cells (Bruzaud *et al.*, 2015; Laventie *et al.*, 2019; Schmidt *et al.*, 2022). A larger sample size would allow to test for significance of observations. Also, the low-copy vector overexpression strain should be used preferably since no growth phenotype has been observed. A quantitative western blot with a specific PilA antibody could provide evidence whether more PilA is produced in the NbdA overproduction strain. In combination with shearing of surface pili, it could be defined if the strain also has more pili on the cell outside. Continuative studies by AFM could provide information on the mechanical properties of the T4P in different strains (Lu *et al.*, 2015).

4.2.4 Influence of NbdA on c-di-GMP levels

In this study, the influence of the deletion as well as the overexpression of *nbdA* and several truncated variants on the whole-cell c-di-GMP level was tested. Absolute quantification of nucleotides was thereby carried out according to Bähre *et al.*, 2017 in collaboration with the AG Richling (Department of chemistry, RPTU). Global c-di-GMP levels measured in this work were consistent with previous studies (Lin Chua *et al.*, 2017). Deletion of *nbdA* resulted in WT like global c-di-GMP levels, as it was already described (Eilers *et al.*, 2022; Rüger, 2019; Xin *et al.*, 2019). Only the minority of genes encoding GGDEF/EAL-HD-GYP domain containing proteins are capable of changing the global c-di-GMP level when deleted in PAO1 (Eilers *et al.*, 2022).

Overproduction of full-length NbdA in PAO1 lead to reduced global c-di-GMP levels indicating a PDE activity of NbdA *in vivo* under the chosen conditions. PDE activity of a cytosolic NbdA variant was also shown by *in vitro* activity assays with purified protein that was heterologous produced in

E. coli (Li *et al.*, 2013). Similarly, in Rüger, 2019 an *E. coli* complementation assay suggested PDE activity of NbdA. It was also demonstrated that the overexpression of *nbdA* in PAO1 results in reduced global c-di-GMP levels while overexpression of an inactive AAL variant did not (Rüger, 2019). Interestingly, in this work the overproduction of the inactive full-length protein (NbdA $_{\text{MHYT-AGDEF-AAL}}$) resulted in significantly increased global c-di-GMP levels. On the one hand, these results demonstrate that an intact EAL motif is mandatory for the PDE activity, as it was shown for other PDEs (Ahmad *et al.*, 2011; Tchigvintsev *et al.*, 2010; Viruega-Góngora *et al.*, 2022). On the other hand, it indicated that NbdA may affect c-di-GMP levels also through other mechanisms than its PDE activity.

Surprisingly, the overproduction of cytosolic NbdA variants resulted in ~35x increased global c-di-GMP levels. Since purified NbdA $_{\text{AGDEF-EAL}}$ exhibited PDE activity *in vitro*, one would anticipate a decrease in c-di-GMP levels. For some GGDEF-EAL domain proteins, a dual function as DGC and PDE have been demonstrated (Feirer *et al.*, 2015; Ferreira *et al.*, 2008; Viruega-Góngora *et al.*, 2022). For instance, the GGDEF-EAL protein DcpA from *Agrobacterium tumefaciens* was shown to have PDE activity in the natural host, while in a heterologous host (*E. coli*) the protein exhibits DGC activity. The PDE activity of DcpA was dependent on the presence of regulatory factors (PruA, PruR), that are not present in *E. coli* (Feirer *et al.*, 2015). Even though NbdA is a dual domain protein it is unlikely that the increased amount of c-di-GMP is produced by NbdA directly: No DGC activity of NbdA was observed in Li *et al.*, 2013, unless the AGDEF motif is mutated to a GGDEF motif. Further mutating the AGDEF motif to an AGAAF motif eliminates important amino acids for substrate binding which abolishes a potential DGC activity (Chan *et al.*, 2004; Schirmer, 2016). Still, the increase of global c-di-GMP level was observed for the strain overproducing this variant (NbdA $_{\text{AGAAF-EAL}}$). Additionally, abolishing PDE activity by exchanging the EAL motif to AAL did not influence this phenotype. Thus, the increase in c-di-GMP likely comes from other c-di-GMP regulating proteins, e. g. through the activation of one or several DGCs, or by inhibiting PDEs. Direct protein-protein interaction between DGCs and PDEs has been shown multiple times: In a global B2H screen in *E. coli*, many GGDEF domain proteins showed strong heterodimer formation (Sarenko *et al.*, 2017). Also, in a global B2H screen in *P. fluorescens*, especially GGDEF or dual domain proteins showed a high capacity for protein-protein interaction to multiple interactors from the GGDEF/EAL domain proteins (Dahlstrom *et al.*, 2018). In several cases, the activity of one protein is regulated by the other. Examples for a direct interaction of a DGC and a PDE are LchP (PDE) and LchD (DGC) from *L. enzymogenes*, or YciR and YdaM in *E. coli* (Lindenberg *et al.*, 2013; Xu *et al.*, 2022). Regulation can also include multiple modules and effector proteins. For instance, the trigger PDE YciR (also called PdeR) from *E. coli* was shown to inherit PDE activity. The protein is also directly interacting with the DGC YdaM (also DgcM) via the GGDEF-GGDEF domains. It was speculated that the heterodimerization of the two proteins leads to the inhibition of the DGC YdaM, that is only active as a homodimer. However, through the interaction with YdaM, YciR also inhibits the effector

protein MlrA by direct protein-protein interaction. The regulation of YciR is mediated through the proteins PDE activity that is necessary to regulate the inhibition of YdaM and MlrA. Thereby, the c-di-GMP is produced by another module, consisting of the DGC YegE (DgcE) and the PDE YhjH (PdeH). YciR without PDE activity (EAL motif exchanged to AAL) is still inhibiting YdaM and MlrA but is no longer regulated by the first module (YegE and YhjH). Thereby, the protein YciR is a PDE and a c-di-GMP effector at the same time (Lindenberg *et al.*, 2013; Weber *et al.*, 2006).

The interaction is probably mediated by the cytosolic domains of NbdA since overproduction of the cytosolic NbdA variants all showed a strong increase in c-di-GMP levels. The inactive full-length variant (NbdA $_{\text{MHYT-AGDEF-AAL}}$) exhibited moderate enhanced c-di-GMP levels, whereas the strain overproducing the MHYT domain alone exhibited no alteration in the messenger levels compared to the empty vector control. Activation of one or more DGCs could explain the enhanced c-di-GMP levels in the NbdA $_{\text{AGDEF-EAL}}$, NbdA $_{\text{AGDEF-AAL}}$, and NbdA $_{\text{AGAAF-EAL}}$ overproduction strains. As a possibly interacting DGC, SadC is a promising candidate. It is the only DGC that was significantly enriched in the pulldown assay, and a protein-protein interaction between the two proteins or the respective homologs was demonstrated (Beganovic, 2018; Dahlstrom *et al.*, 2018). Thereby, it was observed that the presence of the cytosolic part of NbdA is mandatory for the interaction with SadC, as the MHYT domain alone did not interact with SadC. The DGC activity of SadC was further demonstrated to be regulated by other proteins: interaction with PilO inhibits DGC activity of SadC in PA14 (Webster *et al.*, 2021) or OadI inhibits SadC under aerobic conditions in PAO1 (Schmidt *et al.*, 2016). Interaction with NbdA could also impede inhibition of SadC, resulting in increased c-di-GMP levels.

Conversely, the increase in c-di-GMP could be due to inhibition of other PDEs in *P. aeruginosa*. Several PDEs were enriched in the NbdA pulldown assay, however these interactions have to be verified by a second method, e. g. B2H, FRET, BICF or Co-IP. The enriched proteins were PipA (PA0285), BifA (PA4367) and RbdA (PA0861). All PDEs were already shown to increase the global c-di-GMP level when deleted in PAO1 (PipA: ~3x increased, BifA: ~1.5x increased, RbdA: ~1.2x increased) (Eilers *et al.*, 2022). In *E. coli*, it was already described that the deletion of the master PDE *pdeH* results in a 11x increased global c-di-GMP level (Sarenko *et al.*, 2017). In *P. aeruginosa*, there is no master PDE described, however, through the interaction with multiple PDEs a similar effect may be achieved.

The increase in c-di-GMP in the mutants overproducing cytosolic NbdA variants may not be due to direct protein-protein interaction between NbdA and c-di-GMP producing or degrading proteins, but rather indirectly through other factors, e. g. interaction with regulatory proteins, altered metabolite levels or stress. The activity of several DGCs and PDEs has been demonstrated to be dependent on metabolites, ions or small molecules (Okegbe *et al.*, 2017; Randall *et al.*, 2022; Rossi *et al.*, 2017). Alternatively, it is possible that overproduced NbdA binds c-di-GMP without degrading it, depriving the cell of soluble messenger. During extraction procedure and the associated denaturation of the

proteins, the bound signalling molecule is released, which leads to the increased measured values of the global c-di-GMP content. EAL domains have been shown to bind c-di-GMP, in some cases even when the EAL motif was exchanged to AAL (Lindenberg *et al.*, 2013; Newell *et al.*, 2009; Rao *et al.*, 2008). Other than that, in this work only the global c-di-GMP levels were measured, which does not display cell heterogeneity, that was already shown for *P. aeruginosa* (Christen *et al.*, 2010).

Novel nucleotides and products in *P. aeruginosa*

Interestingly, the PDE NbdA not only yields pGpG as a product, but also generates a still unknown product (section 3.3.4, "unknown peak", "*"). It is suggested to be a nucleotide, since the compound is probably formed from pGpG, absorbs light with a wavelength of 254 nm and has a similar retention time as pGpG or c-di-GMP. The PDE YciR from *E. coli* was shown to have a canonical PDE activity, resulting in the production of pGpG and GMP (Weber *et al.*, 2006). Additionally, the protein showed a so called 5'-PDE activity (Lindenberg *et al.*, 2013) in a radiolabelled activity assay: With radiolabelled c-di-[^{32}P]GMP as substrate the produced GMP was further degraded to radiolabelled phosphate. A fast-running product could also directly be formed from GTP and was proposed to be a triphosphate, as in an assay with radiolabelled [α^{32}P]GTP as substrate, also a fast running radiolabelled product was generated (Lindenberg *et al.*, 2013). However, no further structure or physiological role of this product was analysed. The PDE YciR has been shown to be important for virulence in uropathogenic *E. coli* (UPEC) by lowering c-di-GMP levels and thereby reducing the proinflammatory response in the host (Zhang *et al.*, 2022).

In the cultures extracts from *P. aeruginosa*, in addition to canonical bis-(3'5')-c-di-GMP a c-di-GMP isomer could be detected in the MS measurements (called "isomer"). This isomer had the same precursor ion and mass as canonical c-di-GMP but showed a different fractionation pattern (see 3.3.2 and 3.3.3). A similar observation was also made in previous studies in culture extracts from *E. coli* (Spangler *et al.*, 2010), *P. aeruginosa* (Bähre *et al.*, 2017), or *B. subtilis* (Gao *et al.*, 2013). Analysis of collision-induced dissociation (CID) spectra predicted the molecule to be a dinucleotide with a 2'3'-cyclic phosphate, termed 2'3'-c-pGpG (Gao *et al.*, 2013) (**Fig. 4.3**). However, the configuration of this molecule remains unproven, and its biological function is still unknown. As stated above, different production levels of NbdA and variants did not significantly influence the amount of the isomer, therefore no further studies were conducted. Notably, the unknown peak (*) detected in the enzymatic assay of NbdA $_{AGDEF\text{-}EAL}$ in HPLC showed a different pattern in the MS measurements than the isomer and was therefore presumed to be a different product (see above).

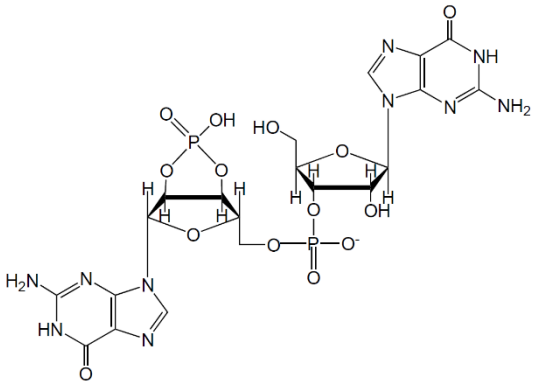

Fig. 4.3 Structure of a c-di-GMP isomer with a 2'3' circular connected phosphate in the same ribose sugar ring, as well as a canonical 3'5' connected phosphate connecting two ribose sugar rings. The molecule was termed 2'3'-c-pGpG (Gao *et al.*, 2013). Structure drawn in ChemDraw (Std. 7.0).

However, this work indicates that there are uncharacterised nucleotides produced in *P. aeruginosa*, that were either detected in culture extracts or in an *in vitro* enzyme assay with NbdA $_{\text{AGDEF-EAL}}$. Finding out more about the structure and biological function of the novel nucleotides is intriguing.

4.2.5 Local function of c-di-GMP regulating proteins and cell heterogeneity

NbdA has been reported to be involved in biofilm dispersal, swimming motility, and rhamnolipid production of *P. aeruginosa* (Li *et al.*, 2013; Liu *et al.*, 2022a; Xin *et al.*, 2019). These functions are directly related to the nucleotide second messenger c-di-GMP and the enzymatic activity of NbdA (**Fig. 4.4**). The current model for c-di-GMP signalling suggests the organisation of local signalling supermodules alongside global factors for specific functions in the cell (Hengge, 2021; Junkermeier *et al.*, 2023). It was previously suggested that NbdA rather has a local function than acting on global scale. Deletion of *nbdA* did not result in phenotypic effects for c-di-GMP related outcomes like biofilm formation or motility, and the global c-di-GMP levels in the cells remained unchanged (Gerbracht, 2021; Rehner, 2020; Rüger, 2019).

The results of Gerbracht, 2021 and Rüger, 2019 indicate that NbdA possesses other functions besides PDE activity, since several phenotypes were independent from the PDE activity of the protein. Also so-called trigger PDEs were identified in *E. coli* and *P. aeruginosa*, where they modulate cellular functions via direct protein-protein interactions besides their PDE activity (Hengge, 2016). For instance, the protein RpfR was shown to be an active PDE that could modulate the activity of the thioesterase RpfF through direct protein-protein interaction (Mhatre *et al.*, 2020; Waldron *et al.*, 2019). NbdA might also regulate other cellular functions via direct protein-protein interaction, e. g. through the interaction with the confirmed interacting proteins SadC, PilB, CzcR and PA4200 or so far unknown interaction partners (**Fig. 4.4**). NbdA as a multidomain protein might integrate multiple signals and thereby fine-tune multiple outcomes. Similarly, the PDE RmcA from *P. aeruginosa* has been demonstrated to integrate multiple stimuli, sensed by four PAS domains each binding a different

cofactor (Okegbe *et al.*, 2017). As the perceived signal for MHYT domains, O_2, CO, or NO have been postulated by Galperin *et al.*, 2001. Alternatively, the signal might be heme or iron, as it was shown to activate PDE activity of NbdA *in vitro* (Agbadaola, 2023).

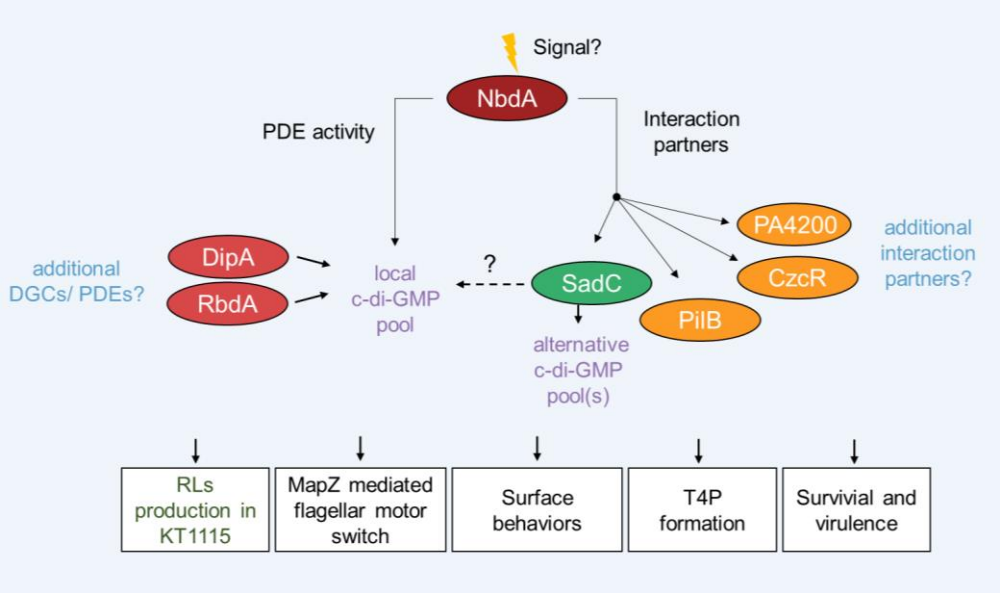

Fig. 4.4 The PDE NbdA has multiple functions in *P. aeruginosa*. Besides the PDE activity of NbdA that was shown to regulate RLs production in KT1115 (Liu *et al.*, 2022a) and the flagellar motor switch in PAO1(Xin *et al.*, 2019), NbdA may also fine-tune cellular processes by direct protein-protein interactions.

Considering the described phenotypes, localisation, and the interaction partners, NbdA may be involved in adapting surface behaviours and motility. As described in Xin *et al.*, 2019, the PDE activity of NbdA is probably involved in regulating a local c-di-GMP pool, together with DipA and RbdA, and controlling the flagella motor switch. Thereby it was proposed that the proteins localise to the chemoreceptor array to fine-tune chemotactic responses (Xin *et al.*, 2019). The PDE activity of NbdA is potentially modulated in response to environmental signals, which directs the cells to more favourable conditions. In addition, NbdA might also control T4P formation through interaction with PilB. In a recent publication, it was shown that PilB preferably localises to the leading pole, thereby facilitating directed twitching motility in response to a signal (Kühn *et al.*, 2023). The process is called mechanotaxis, and the regulatory system is similar to the chemotaxis system controlling directed swimming motility. It was shown in PAO1, that the polarity for T4P can switch between the two poles and is regulated by two antagonistic response regulators PilH and PilJ (Kühn *et al.*, 2023). Similar to its function in the flagellar motor switch through c-di-GMP, NbdA might modulate also mechanotaxis in response to a signal, e. g. by promoting PilB activity and pilus polymerisation on one pole facing the desired direction. The positioning of PilB was also demonstrated to be influenced by PilA in a positive feedback loop dependent on the mechanical load applied to the pili (Kühn *et al.*, 2023). In PAO1 as well as in PA14, it was shown that NbdA is transcribed in the stationary phase, and present in 2-3 days old biofilms (Gerbracht, 2021; Gür *et al.*, 2023), so probably nutrients become limited. Modulation of the flagella motor switch, or the formation of T4P supports the migration of

cells to more favourable conditions. At the same time, mechanisms to cope with potential harming conditions could be upregulated, e. g. through CzcR the efflux of antibiotics or heavy metals while further promoting swimming motility. Through the interaction with SadC, NbdA might also be involved in evasion of immune response (McCarthy *et al.*, 2017), and inducing surface attachment and production of EPS that might protect the cells (Pang *et al.*, 2019; Rasamiravaka *et al.*, 2015). Furthermore, NbdA potentially reduces growth which could be a mechanism to cope with harmful environments, like it was for example shown in persister formation (Keren *et al.*, 2004; Mulcahy *et al.*, 2010). Thus, the potential regulation might improve survival or virulence of the cells. In PA14, a *nbdA* transposon mutant exhibited reduced virulence in a mouse model (Kulasakara *et al.*, 2006).

It is also possible, that NbdA is involved in attachment of cells after a surface contact. It was shown that in *P. aeruginosa*, the cells are surface primed after encounter to a surface, which is probably mediated by SadC (Armbruster *et al.*, 2019). In this process, NbdA could potentially modulate DGC activity of SadC, which could result in faster c-di-GMP increase and surface attachment. Moreover, surface attached cells were shown to be more virulent and to contain less NADH (Perinbam *et al.*, 2020). An altered NADH level was observed for the deletion mutant of *nbdA* in comparison with the wildtype.

NbdA being present or active in only a subpopulation of cells is also possible (**Fig. 4.5**). Thereby, it might be that NbdA is only affecting a subpopulation of cells, and therefore the impact of NbdA on a global population cannot be observed. Most of the results in the context of NbdA were only made for global cell cultures, and not for individual cells. Cell heterogeneity in *P. aeruginosa* for c-di-GMP levels has been described after cell division and upon surface contact (Christen *et al.*, 2010; Laventie *et al.*, 2019). It was shown in PAO1 biofilms, that through bimodal expression of *hecE* two subpopulations of cells with different c-di-GMP levels are established: Cells where HecE is present exhibit higher c-di-GMP levels by inhibition of the PDE BifA and activation of the DGC WspR, resulting in robust biofilm formation. In contrast, cells without HecE revert to a motile lifestyle for new surface colonisation (Manner *et al.*, 2023). This division of labour strategy enhances the survival and virulence of *P. aeruginosa* populations (Gomez *et al.*, 2023). One possible function might be that NbdA regulates detachment of a subpopulation in surface attached cells. Through PDE activity of NbdA, cells might become motile, e. g. by regulation of flagella or T4P for colonisation and virulence. Generally, low c-di-GMP levels are associated with motility, detachment, and QS-mediated virulence (Hengge, 2016, Lin Chua *et al.*, 2017). PDE activity of NbdA was shown to enhance RL synthesis after prolonged fermentation (Liu *et al.*, 2022a), and RL were described to aid detachment of cells from a biofilm (de Kievit, 2009). It is however likely, that in this processes, additional factors like DGCs, PDEs, effectors, two-component systems, or receptors are involved.

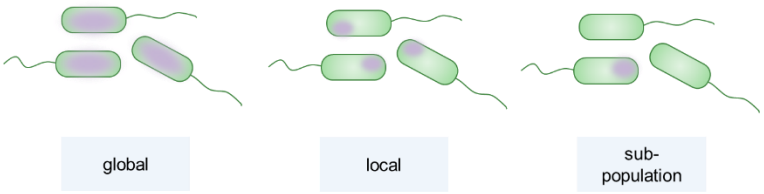

Fig. 4.5 Levels of regulation for DGCs and PDEs. Enzymes modulating c-di-GMP act either on a global scale or regulate a local c-di-GMP pool for specific outcomes. Heterogeneity in c-di-GMP levels in a population was observed in *P. aeruginosa*, e. g. after cell division on a surface (Laventie *et al.*, 2019) or in biofilms (Manner *et al.*, 2023), which was dependent on heterogeneous presence of single enzymes or regulators.

To better define the role of NbdA in the cell, individual cells should preferably be looked at than whole cultures, to find either the local function, or the function in a subpopulation. To study the influence of NbdA on c-di-GMP levels in a spatiotemporal manner in single cells, the fluorescent reporter gene strain using the *cdrA* promoter could be used (Rybtke *et al.*, 2012). Identifying the signal or signals that modulate the PDE activity of NbdA is key, as well as identification of the conditions, impact, and outcomes for the interaction with other proteins. For instance, determination whether the interaction of NbdA and SadC influences the activity of one of the proteins could provide further insights in the c-di-GMP network of *P. aeruginosa*. Additionally, discovery of the mechanisms by which NbdA influences flagella behaviours or T4P formation could shed further light on the function of NbdA. The potential role of NbdA in cell growth and division through the MHYT domain could also be further explored. The findings on NbdA support the model of complex but highly specific c-di-GMP signalling in *P. aeruginosa* which is achieved through well-defined protein-protein interactions, localisation, and enzymatic activity.

5 Summary

Membrane proteins exert a multitude of essential functions in the cell, that frequently require interaction partners. In particular, for signalling with the second messenger c-di-GMP, protein-protein interactions are considered crucial. Also, in *P. aeruginosa* - a model organism for biofilm formation and infection - the majority of c-di-GMP synthesizing or degrading enzymes are membrane proteins. In the first part of this thesis, membrane proteins in *P. aeruginosa* PAO1 were investigated in a global approach. A native membrane-protein library was created through the formation of native nanodiscs by using amphiphilic polymers. The library was characterized by testing for reproducible and stable extraction of membrane proteins, coverage of the membrane proteome, and the capability to detect protein–protein interactions within a lipid-bilayer environment as well as membrane-bound protein complexes. In addition, membrane-associated proteins involved in c-di-GMP signalling and their interaction partners were investigated in more detail. To this end, a set of more than 20 described protein complexes was used to validate global analyses for the prediction of novel protein-protein interactions. Although elution profiles indicated preservation of the membrane complexes, the dataset was not feasible for protein interaction prediction.

In the second part of the thesis, the membrane-integrated phosphodiesterase NbdA was investigated for its role in the c-di-GMP network. The current model for c-di-GMP signalling suggests the organisation of local signalling supermodules alongside global factors for specific functions in the cell. Thus, the protein NbdA was tested for protein-protein interaction partners in *P. aeruginosa*, either by a pulldown assay following mass spectrometry for novel candidate identification, or by bacterial adenylate cyclase two hybrid (B2H) assay for candidate verification. Out of more than 400 novel candidate proteins, five candidates were selected for further validation. The interaction with four proteins, PilB, SadC, CzcR and PA4200 was confirmed in a B2H assay. Moreover, the influence of NbdA on the global c-di-GMP level was tested. Therefore, either a markerless *nbdA* deletion mutant or overexpression strains were tested. To find out more about the role of the individual domains of NbdA, also global c-di-GMP levels of protein variant overproduction mutants was assayed. Although overexpression of full-length *nbdA* resulted in reduced global c-di-GMP levels indicating a PDE activity *in vivo*, the overproduction of truncated protein variants of NbdA resulted in unexpected c-di-GMP levels. In previous studies a possible role of the MHYT domain in cell elongation as well as growth on solid media was observed. To further test for the specificity of these observations, other MHYT domain containing proteins were tested for similar phenotypes in *P. aeruginosa*. Indeed, the phenotypes were specific for the MHYT domain of NbdA. Previous studies suggested an influence of NbdA overexpression on type IV pili (T4P), thus pili formation was tested in a phage assay and by atomic force microscopy (AFM). Further, the co-localisation of NbdA with pili components was tested by confocal laser scanning microscopy (CLSM) to determine whether NbdA is located at the piliated pole. The findings on NbdA support the model of complex but highly specific c-di-GMP signalling in *P. aeruginosa*.

6 Zusammenfassung

Membranproteine üben in der Zelle eine Vielzahl wichtiger Funktionen aus, häufig mithilfe von Interaktionspartnern. Insbesondere für die Signalübertragung mit dem Botenstoff c-di-GMP sind Protein-Protein-Interaktionen entscheidend. Auch in *P. aeruginosa* - ein Modellorganismus für Biofilmbildung und Infektion - sind die meisten c-di-GMP synthetisierenden oder abbauenden Enzyme Membranproteine. Im ersten Teil dieser Arbeit wurden Membranproteine in *P. aeruginosa* PAO1 in einem globalen Ansatz untersucht. Eine Bibliothek nativer Membranproteine in Nanodiscs wurde unter Verwendung amphiphiler Polymere erstellt. Die Protein-Bibliothek wurde auf Reproduzierbarkeit, stabile Extraktion von Membranproteinen, Umfang des Membranproteoms und die Fähigkeit zum Nachweis von Protein-Protein-Interaktionen getestet. Darüber hinaus wurden membranassoziierte Proteine, die an der c-di-GMP-Signalübertragung beteiligt sind, und ihre Interaktionspartner genauer untersucht. Außerdem wurde ein Satz von mehr als 20 beschriebenen Proteinkomplexen verwendet, um globale Analysen für die Vorhersage neuer Protein-Protein-Wechselwirkungen zu validieren. Obwohl die Elutionsprofile auf den Erhalt der Membrankomplexe hindeuteten, war der Datensatz für die Vorhersage von neuen Proteininteraktionen nicht geeignet.

Im zweiten Teil der Arbeit wurde die membranintegrierte Phosphodiesterase NbdA auf ihre Rolle im c-di-GMP-Netzwerk untersucht. Im aktuellen Modell sind c-di-GMP-Signalproteine in lokalen Supermodulen organisiert, sodass eine spezifische Funktion in der Zelle möglich ist. Daher wurde das Protein NbdA auf Protein-Protein-Interaktionspartner in *P. aeruginosa* getestet. Hierzu wurde ein Pulldown-Assay in Verbindung mit Massenspektrometrie zur Identifizierung neuer Kandidaten ausgeführt. Anschließend wurden Kandidaten in einem *bacterial adenylate cyclase two hybrid*-Assay (B2H) verifiziert. Aus mehr als 400 neuen Kandidatenproteinen wurden fünf Kandidaten für die weitere Validierung ausgewählt. Die Interaktion mit den vier Proteinen, PilB, SadC, CzcR und PA4200 wurde in einem B2H-Assay bestätigt. Darüber hinaus wurde der Einfluss von NbdA auf den globalen c-di-GMP-Spiegel getestet. Die Überexpression von *nbdA* führte zu verringerten globalen c-di-GMP-Spiegeln, was auf eine PDE-Aktivität *in vivo* hinweist. Jedoch wurden bei der Überproduktion verkürzter NbdA-Varianten unerwartete c-di-GMP-Spiegel beobachtet. In vorangegangenen Studien wurde bei einer Überproduktion der MHYT-Domäne eine veränderten Zellmorphologie sowie ein gestörtes Wachstum auf festen Medien beobachtet. In dieser Arbeit wurde gezeigt, dass die Phänotypen spezifisch für die MHYT-Domäne von NbdA waren, da andere MHYT-Domänen enthaltende Proteine diese Phänotypen nicht aufwiesen. Vorangegangende Studien deuteten auf einen Einfluss der NbdA-Überexpression auf Typ IV Pili (T4P) hin, weshalb die Pili-Bildung in einem Phagenassay und durch Rasterkraftmikroskopie (AFM) getestet wurde. Darüber hinaus wurde die Co-Lokalisation von NbdA mit Pili-Komponenten durch konfokale Laser-Scanning-Mikroskopie (CLSM) getestet, um festzustellen, ob sich NbdA am Pili-Pol befindet. Die Ergebnisse zu NbdA stützen das Modell der komplexen, aber hochspezifischen c-di-GMP-Signalübertragung in *P. aeruginosa*.

7 References

Abel, S., Bucher, T., Nicollier, M., Hug, I., Kaever, V., Abel Zur Wiesch, P., and Jenal, U. (2013). Bi-modal distribution of the second messenger c-di-GMP controls cell fate and asymmetry during the *Caulobacter* cell cycle. *PLoS Genet, 9*(9), e1003744.

Agbadaola, M. T. (2023). Polymer-based nanodiscs for the purification and characterisation of membrane proteins in lipid bilayers. (PhD), University of Ibadan, Ibadan, Nigeria.

Ahmad, I., Lamprokostopoulou, A., Le Guyon, S., Streck, E., Barthel, M., Peters, V., Hardt, W. D., and Römling, U. (2011). Complex c-di-GMP signaling networks mediate transition between virulence properties and biofilm formation in *Salmonella enterica* serovar Typhimurium. *PLoS One, 6*(12), e28351.

Ahn, V. E., Faull, K. F., Whitelegge, J. P., Fluharty, A. L., and Privé, G. G. (2003). Crystal structure of saposin B reveals a dimeric shell for lipid binding. *Proc Natl Acad Sci U S A, 100*(1), 38-43.

Alami, M., Dalal, K., Lelj-Garolla, B., Sligar, S. G., and Duong, F. (2007). Nanodiscs unravel the interaction between the SecYEG channel and its cytosolic partner SecA. *Embo j, 26*(8), 1995-2004.

Aldridge, P., Paul, R., Goymer, P., Rainey, P., and Jenal, U. (2003). Role of the GGDEF regulator PleD in polar development of *Caulobacter crescentus*. *Mol Microbiol, 47*(6), 1695-1708.

Almblad, H., Randall, T. E., Liu, F., Leblanc, K., Groves, R. A., Kittichotirat, W., Winsor, G. L., Fournier, N., Au, E., Groizeleau, J., Rich, J. D., Lou, Y., Granton, E., Jennings, L. K., Singletary, L. A., Winstone, T. M. L., Good, N. M., Bumgarner, R. E., Hynes, M. F., Singh, M., Stietz, M. S., Brinkman, F. S. L., Kumar, A., Brassinga, A. K. C., Parsek, M. R., Tseng, B. S., Lewis, I. A., Yipp, B. G., MacCallum, J. L., and Harrison, J. J. (2021). Bacterial cyclic diguanylate signaling networks sense temperature. *Nat Commun, 12*(1), 1986.

Amikam, D., and Galperin, M. Y. (2006). PilZ domain is part of the bacterial c-di-GMP binding protein. *Bioinformatics, 22*(1), 3-6.

An, S., Wu, J., and Zhang, L. H. (2010). Modulation of *Pseudomonas aeruginosa* biofilm dispersal by a cyclic-di-GMP phosphodiesterase with a putative hypoxia-sensing domain. *Appl Environ Microbiol, 76*(24), 8160-8173.

Armbruster, C. R., Lee, C. K., Parker-Gilham, J., de Anda, J., Xia, A., Zhao, K., Murakami, K., Tseng, B. S., Hoffman, L. R., Jin, F., Harwood, C. S., Wong, G. C., and Parsek, M. R. (2019). Heterogeneity in surface sensing suggests a division of labor in *Pseudomonas aeruginosa* populations. *Elife, 8*.

Arora, S. K., Ritchings, B. W., Almira, E. C., Lory, S., and Ramphal, R. (1997). A transcriptional activator, FleQ, regulates mucin adhesion and flagellar gene expression in *Pseudomonas aeruginosa* in a cascade manner. *J Bacteriol, 179*(17), 5574-5581.

Assmann, S. M. (1995). Cyclic AMP as a second messenger in higher plants (Status and Future Prospects). *Plant Physiol, 108*(3), 885-889.

Autzen, H. E., Julius, D., and Cheng, Y. (2019). Membrane mimetic systems in CryoEM: keeping membrane proteins in their native environment. *Curr Opin Struct Biol, 58*, 259-268.

Ayers, M., Sampaleanu, L. M., Tammam, S., Koo, J., Harvey, H., Howell, P. L., and Burrows, L. L. (2009). PilM/N/O/P proteins form an inner membrane complex that affects the stability of the *Pseudomonas aeruginosa* type IV pilus secretin. *J Mol Biol, 394*(1), 128-142.

Bähre, H., and Kaever, V. (2017). Identification and quantification of cyclic di-guanosine monophosphate and its linear metabolites by reversed-phase LC-MS/MS. *Methods Mol Biol, 1657*, 45-58.

Baker, A. E., Diepold, A., Kuchma, S. L., Scott, J. E., Ha, D. G., Orazi, G., Armitage, J. P., and O'Toole, G. A. (2016). PilZ domain protein FlgZ mediates cyclic di-GMP-dependent swarming motility control in *Pseudomonas aeruginosa*. *J Bacteriol, 198*(13), 1837-1846.

Baker, A. E., Webster, S. S., Diepold, A., Kuchma, S. L., Bordeleau, E., Armitage, J. P., and O'Toole, G. A. (2019). Flagellar stators stimulate c-di-GMP production by *Pseudomonas aeruginosa*. *J Bacteriol, 201*(18).

Banerjee, P., Sahoo, P. K., Sheenu, Adhikary, A., Ruhal, R., and Jain, D. (2021). Molecular and structural facets of c-di-GMP signalling associated with biofilm formation in *Pseudomonas aeruginosa*. *Mol Aspects Med, 81*, 101001.

Barniol-Xicota, M., and Verhelst, S. H. L. (2018). Stable and functional rhomboid proteases in lipid nanodiscs by using diisobutylene/maleic acid copolymers. *J Am Chem Soc, 140*(44), 14557-14561.

Barraud, N., Hassett, D. J., Hwang, S. H., Rice, S. A., Kjelleberg, S., and Webb, J. S. (2006). Involvement of nitric oxide in biofilm dispersal of *Pseudomonas aeruginosa*. *J Bacteriol, 188*(21), 7344-7353.

Barth, H. G., Boyes, B. E., and Jackson, C. (1994). Size exclusion chromatography. *Anal Chem, 66*(12), 595r-620r.

Battesti, A., and Bouveret, E. (2012). The bacterial two-hybrid system based on adenylate cyclase reconstitution in *Escherichia coli*. *Methods, 58*(4), 325-334.

Bayburt, T. H., Grinkova, Y. V., and Sligar, S. G. (2002). Self-assembly of discoidal phospholipid bilayer nanoparticles with membrane scaffold proteins. *Nano letters, 2*(8), 853-856.

Bayburt, T. H., Grinkova, Y. V., and Sligar, S. G. (2006). Assembly of single bacteriorhodopsin trimers in bilayer nanodiscs. *Arch Biochem Biophys, 450*(2), 215-222.

Bedrunka, P., and Graumann, P. L. (2017). New functions and subcellular localization patterns of c-di-GMP components (GGDEF domain proteins) in *B. subtilis*. *Front Microbiol, 8*, 794.

Beganovic, S. (2018). Investigating the protein interaction network responsible for nitric oxide induced biofilm dispersal in *Pseudomonas aeruginosa*. (Master thesis), RPTU Kaiserslautern.

Benach, J., Swaminathan, S. S., Tamayo, R., Handelman, S. K., Folta-Stogniew, E., Ramos, J. E., Forouhar, F., Neely, H., Seetharaman, J., Camilli, A., and Hunt, J. F. (2007). The structural basis of cyclic diguanylate signal transduction by PilZ domains. *Embo j, 26*(24), 5153-5166.

Bense, S., Witte, J., Preuße, M., Koska, M., Pezoldt, L., Dröge, A., Hartmann, O., Müsken, M., Schulze, J., Fiebig, T., Bähre, H., Felgner, S., Pich, A., and Häussler, S. (2022). *Pseudomonas aeruginosa* post-translational responses to elevated c-di-GMP levels. *Mol Microbiol, 117*(5), 1213-1226.

Berger, S., Cabrera-Orefice, A., Jetten, M. S. M., Brandt, U., and Welte, C. U. (2021). Investigation of central energy metabolism-related protein complexes of ANME-2d methanotrophic archaea by complexome profiling. *Biochim Biophys Acta Bioenerg, 1862*(1), 148308.

Berrisford, J. M., Baradaran, R., and Sazanov, L. A. (2016). Structure of bacterial respiratory complex I. *Biochim Biophys Acta, 1857*(7), 892-901.

Blonder, J., Goshe, M. B., Xiao, W., Camp, D. G., 2nd, Wingerd, M., Davis, R. W., and Smith, R. D. (2004). Global analysis of the membrane subproteome of *Pseudomonas aeruginosa* using liquid chromatography-tandem mass spectrometry. *J Proteome Res, 3*(3), 434-444.

Bloustine, J., Berejnov, V., and Fraden, S. (2003). Measurements of protein-protein interactions by size exclusion chromatography. *Biophys J, 85*(4), 2619-2623.

Boehm, A., Kaiser, M., Li, H., Spangler, C., Kasper, C. A., Ackermann, M., Kaever, V., Sourjik, V., Roth, V., and Jenal, U. (2010). Second messenger-mediated adjustment of bacterial swimming velocity. *Cell, 141*(1), 107-116.

Bordeleau, E., Purcell, E. B., Lafontaine, D. A., Fortier, L. C., Tamayo, R., and Burrus, V. (2015). Cyclic di-GMP riboswitch-regulated type IV pili contribute to aggregation of *Clostridium difficile*. *J Bacteriol, 197*(5), 819-832.

Boyd, C. D., and O'Toole, G. A. (2012). Second messenger regulation of biofilm formation: breakthroughs in understanding c-di-GMP effector systems. *Annu Rev Cell Dev Biol, 28*, 439-462.

Bradley, D. E., and Pitt, T. L. (1974). Pilus-dependence of four *Pseudomonas aeruginosa* bacteriophages with non-contractile tails. *J Gen Virol, 24*(1), 1-15.

Brencic, A., and Lory, S. (2009). Determination of the regulon and identification of novel mRNA targets of *Pseudomonas aeruginosa* RsmA. *Mol Microbiol, 72*(3), 612-632.

Bridges, C. C. (1966). Hierarchical Cluster Analysis. *Psychological Reports, 18*(3), 851-854.

Broillet, M. C., and Firestein, S. (1996). Gaseous second messengers in vertebrate olfaction. *J Neurobiol, 30*(1), 49-57.

Bruhn, H. (2005). A short guided tour through functional and structural features of saposin-like proteins. *Biochem J, 389*(Pt 2), 249-257.

Bruzaud, J., Tarrade, J., Coudreuse, A., Canette, A., Herry, J. M., Taffin de Givenchy, E., Darmanin, T., Guittard, F., Guilbaud, M., and Bellon-Fontaine, M. N. (2015). Flagella but not type IV pili are involved in the initial adhesion of *Pseudomonas aeruginosa* PAO1 to hydrophobic or superhydrophobic surfaces. *Colloids Surf B Biointerfaces, 131*, 59-66.

Budzik, J. M., Rosche, W. A., Rietsch, A., and O'Toole, G. A. (2004). Isolation and characterization of a generalized transducing phage for *Pseudomonas aeruginosa* strains PAO1 and PA14. *J Bacteriol, 186*(10), 3270-3273.

Burrows, L. L. (2012). *Pseudomonas aeruginosa* twitching motility: type IV pili in action. *Annu Rev Microbiol, 66*, 493-520.

Bush, M. J., Tschowri, N., Schlimpert, S., Flärdh, K., and Buttner, M. J. (2015). c-di-GMP signalling and the regulation of developmental transitions in streptomycetes. *Nat Rev Microbiol, 13*(12), 749-760.

Cabeen, M. T., and Jacobs-Wagner, C. (2005). Bacterial cell shape. *Nat Rev Microbiol, 3*(8), 601-610.

Cai, H., Li, L., Slavik, K. M., Huang, J., Yin, T., Ai, X., Hédelin, L., Haas, G., Xiang, Z., Yang, Y., Li, X., Chen, Y., Wei, Z., Deng, H., Chen, D., Jiao, R., Martins, N., Meignin, C., Kranzusch, P. J., and Imler, J. L. (2023). The virus-induced cyclic dinucleotide 2'3'-c-di-GMP mediates STING-dependent antiviral immunity in *Drosophila*. *Immunity, 56*(9), 1991-2005.e1999.

Cao, Z., Livoti, E., Losi, A., and Gärtner, W. (2010). A blue light-inducible phosphodiesterase activity in the cyanobacterium *Synechococcus elongatus*. *Photochem Photobiol, 86*(3), 606-611.

Carlson, M. L., Stacey, R. G., Young, J. W., Wason, I. S., Zhao, Z., Rattray, D. G., Scott, N., Kerr, C. H., Babu, M., Foster, L. J., and Duong Van Hoa, F. (2019). Profiling the *Escherichia coli* membrane protein interactome captured in peptidisc libraries. *Elife, 8*.

Carlson, M. L., Young, J. W., Zhao, Z., Fabre, L., Jun, D., Li, J., Li, J., Dhupar, H. S., Wason, I., Mills, A. T., Beatty, J. T., Klassen, J. S., Rouiller, I., and Duong, F. (2018). The Peptidisc, a simple method for stabilizing membrane proteins in detergent-free solution. *Elife, 7*.

Carter, T., Buensuceso, R. N., Tammam, S., Lamers, R. P., Harvey, H., Howell, P. L., and Burrows, L. L. (2017). The type IVa pilus machinery is recruited to sites of future cell division. *mBio, 8*(1).

Casabona, M. G., Vandenbrouck, Y., Attree, I., and Couté, Y. (2013). Proteomic characterization of *Pseudomonas aeruginosa* PAO1 inner membrane. *Proteomics, 13*(16), 2419-2423.

Chan, C., Paul, R., Samoray, D., Amiot, N. C., Giese, B., Jenal, U., and Schirmer, T. (2004). Structural basis of activity and allosteric control of diguanylate cyclase. *Proc Natl Acad Sci U S A, 101*(49), 17084-17089.

Chandler, C. E., Horspool, A. M., Hill, P. J., Wozniak, D. J., Schertzer, J. W., Rasko, D. A., and Ernst, R. K. (2019). Genomic and phenotypic diversity among ten laboratory isolates of *Pseudomonas aeruginosa* PAO1. *J Bacteriol, 201*(5).

Chatterjee, M., Anju, C. P., Biswas, L., Anil Kumar, V., Gopi Mohan, C., and Biswas, R. (2016). Antibiotic resistance in *Pseudomonas aeruginosa* and alternative therapeutic options. *Int J Med Microbiol, 306*(1), 48-58.

Chen, G., and Liang, H. (2020). A novel c-di-GMP signal system regulates biofilm formation in *Pseudomonas aeruginosa*. *Microb Cell, 7*(6), 160-161.

Chen, G., Zhou, J., Zuo, Y., Huo, W., Peng, J., Li, M., Zhang, Y., Wang, T., Zhang, L., Zhang, L., and Liang, H. (2021). Structural basis for diguanylate cyclase activation by its binding partner in *Pseudomonas aeruginosa*. *Elife, 10*.

Chen, M. W., Kotaka, M., Vonrhein, C., Bricogne, G., Rao, F., Chuah, M. L., Svergun, D., Schneider, G., Liang, Z. X., and Lescar, J. (2012). Structural insights into the regulatory mechanism of the response regulator RocR from *Pseudomonas aeruginosa* in cyclic Di-GMP signaling. *J Bacteriol, 194*(18), 4837-4846.

Chen, S., Cao, H., Xu, Z., Huang, J., Liu, Z., Li, T., Duan, C., Wu, W., Wen, Y., Zhang, L. H., and Xu, Z. (2023). A type I-F CRISPRi system unveils the novel role of CzcR in modulating multidrug resistance of *Pseudomonas aeruginosa*. *Microbiol Spectr, 11*(5), e0112323.

Chen, Z. A., Jawhari, A., Fischer, L., Buchen, C., Tahir, S., Kamenski, T., Rasmussen, M., Lariviere, L., Bukowski-Wills, J. C., Nilges, M., Cramer, P., and Rappsilber, J. (2010). Architecture of the RNA polymerase II-TFIIF complex revealed by cross-linking and mass spectrometry. *Embo j, 29*(4), 717-726.

Chiang, P., Habash, M., and Burrows, L. L. (2005). Disparate subcellular localization patterns of *Pseudomonas aeruginosa* Type IV pilus ATPases involved in twitching motility. *J Bacteriol, 187*(3), 829-839.

Choi, D. S., Kim, D. K., Choi, S. J., Lee, J., Choi, J. P., Rho, S., Park, S. H., Kim, Y. K., Hwang, D., and Gho, Y. S. (2011). Proteomic analysis of outer membrane vesicles derived from *Pseudomonas aeruginosa*. *Proteomics, 11*(16), 3424-3429.

Christen, B., Christen, M., Paul, R., Schmid, F., Folcher, M., Jenoe, P., Meuwly, M., and Jenal, U. (2006). Allosteric control of cyclic di-GMP signaling. *J Biol Chem, 281*(42), 32015-32024.

Christen, M., Christen, B., Folcher, M., Schauerte, A., and Jenal, U. (2005). Identification and characterization of a cyclic di-GMP-specific phosphodiesterase and its allosteric control by GTP. *J Biol Chem, 280*(35), 30829-30837.

Christen, M., Kulasekara, H. D., Christen, B., Kulasekara, B. R., Hoffman, L. R., and Miller, S. I. (2010). Asymmetrical distribution of the second messenger c-di-GMP upon bacterial cell division. *Science, 328*(5983), 1295-1297.

Claessen, D., Emmins, R., Hamoen, L. W., Daniel, R. A., Errington, J., and Edwards, D. H. (2008). Control of the cell elongation-division cycle by shuttling of PBP1 protein in *Bacillus subtilis*. *Mol Microbiol, 68*(4), 1029-1046.

Comolli, J. C., and Donohue, T. J. (2004). Differences in two *Pseudomonas aeruginosa* cbb3 cytochrome oxidases. *Mol Microbiol, 51*(4), 1193-1203.

Costa, T. R., Felisberto-Rodrigues, C., Meir, A., Prevost, M. S., Redzej, A., Trokter, M., and Waksman, G. (2015). Secretion systems in Gram-negative bacteria: structural and mechanistic insights. *Nat Rev Microbiol, 13*(6), 343-359.

Crone, S., Vives-Flórez, M., Kvich, L., Saunders, A. M., Malone, M., Nicolaisen, M. H., Martínez-García, E., Rojas-Acosta, C., Catalina Gomez-Puerto, M., Calum, H., Whiteley, M., Kolter, R., and Bjarnsholt, T. (2020). The environmental occurrence of *Pseudomonas aeruginosa*. *Apmis, 128*(3), 220-231.

Dahlstrom, K. M., Collins, A. J., Doing, G., Taroni, J. N., Gauvin, T. J., Greene, C. S., Hogan, D. A., and O'Toole, G. A. (2018). A multimodal strategy used by a large c-di-GMP network. *J Bacteriol, 200*(8).

Danielczak, B., Rasche, M., Lenz, J., Pérez Patallo, E., Weyrauch, S., Mahler, F., Agbadaola, M. T., Meister, A., Babalola, J. O., Vargas, C., Kolar, C., and Keller, S. (2022). A bioinspired glycopolymer for capturing membrane proteins in native-like lipid-bilayer nanodiscs. *Nanoscale, 14*(5), 1855-1867.

Dayton, H., Smiley, M. K., Forouhar, F., Harrison, J. J., Price-Whelan, A., and Dietrich, L. E. P. (2020). Sensory domains that control cyclic di-GMP-modulating proteins: A critical frontier in bacterial signal transduction. In S. H. Chou, N. Guiliani, V. Lee, & U. Römling (Eds.), *Microbial cyclic di-nucleotide signaling*: *Springer, Cham*.

de Almeida, N. M., Wessels, H. J., de Graaf, R. M., Ferousi, C., Jetten, M. S., Keltjens, J. T., and Kartal, B. (2016). Membrane-bound electron transport systems of an anammox bacterium: A complexome analysis. *Biochim Biophys Acta, 1857*(10), 1694-1704.

de Kievit, T. R. (2009). Quorum sensing in *Pseudomonas aeruginosa* biofilms. *Environ Microbiol, 11*(2), 279-288.

de Lorenzo, V., and Timmis, K. N. (1994). Analysis and construction of stable phenotypes in gram-negative bacteria with Tn*5*- and Tn*10*-derived minitransposons. *Methods Enzymol, 235*, 386-405.

Del Medico, L., Cerletti, D., Schächle, P., Christen, M., and Christen, B. (2020). The type IV pilin PilA couples surface attachment and cell-cycle initiation in *Caulobacter crescentus*. *Proc Natl Acad Sci U S A, 117*(17), 9546-9553.

Denisov, I. G., Grinkova, Y. V., Lazarides, A. A., and Sligar, S. G. (2004). Directed self-assembly of monodisperse phospholipid bilayer Nanodiscs with controlled size. *J Am Chem Soc, 126*(11), 3477-3487.

Diehl, F. F., Miettinen, T. P., Elbashir, R., Nabel, C. S., Darnell, A. M., Do, B. T., Manalis, S. R., Lewis, C. A., and Vander Heiden, M. G. (2022). Nucleotide imbalance decouples cell growth from cell proliferation. *Nat Cell Biol, 24*(8), 1252-1264.

Dieppois, G., Ducret, V., Caille, O., and Perron, K. (2012). The transcriptional regulator CzcR modulates antibiotic resistance and quorum sensing in *Pseudomonas aeruginosa*. *PLoS One, 7*(5), e38148.

Diggle, S. P., and Whiteley, M. (2020). Microbe Profile: *Pseudomonas aeruginosa*: opportunistic pathogen and lab rat. *Microbiology (Reading), 166*(1), 30-33.

Dilworth, M. V., Findlay, H. E., and Booth, P. J. (2021). Detergent-free purification and reconstitution of functional human serotonin transporter (SERT) using diisobutylene maleic acid (DIBMA) copolymer. *Biochim Biophys Acta Biomembr, 1863*(7), 183602.

Donlan, R. M., and Costerton, J. W. (2002). Biofilms: survival mechanisms of clinically relevant microorganisms. *Clin Microbiol Rev, 15*(2), 167-193.

Dörr, J. M., Koorengevel, M. C., Schäfer, M., Prokofyev, A. V., Scheidelaar, S., van der Cruijsen, E. A., Dafforn, T. R., Baldus, M., and Killian, J. A. (2014). Detergent-free isolation, characterization, and functional reconstitution of a tetrameric K+ channel: the power of native nanodiscs. *Proc Natl Acad Sci U S A, 111*(52), 18607-18612.

Duerig, A., Abel, S., Folcher, M., Nicollier, M., Schwede, T., Amiot, N., Giese, B., and Jenal, U. (2009). Second messenger-mediated spatiotemporal control of protein degradation regulates bacterial cell cycle progression. *Genes Dev, 23*(1), 93-104.

Dunn, N. W., and Holloway, B. W. (1971). Pleiotrophy of *p*-fluorophenylalanine-resistant and antibiotic hypersensitive mutants of *Pseudomonas aeruginosa*. *Genet Res, 18*(2), 185-197.

Düvel, J., Bertinetti, D., Möller, S., Schwede, F., Morr, M., Wissing, J., Radamm, L., Zimmermann, B., Genieser, H. G., Jänsch, L., Herberg, F. W., and Häussler, S. (2012). A chemical proteomics approach to identify c-di-GMP binding proteins in *Pseudomonas aeruginosa*. *J Microbiol Methods, 88*(2), 229-236.

Egan, A. J., and Vollmer, W. (2013). The physiology of bacterial cell division. *Ann N Y Acad Sci, 1277*, 8-28.

Egli, M., Gessner, R. V., Williams, L. D., Quigley, G. J., van der Marel, G. A., van Boom, J. H., Rich, A., and Frederick, C. A. (1990). Atomic-resolution structure of the cellulose synthase regulator cyclic diguanylic acid. *Proc Natl Acad Sci U S A, 87*(8), 3235-3239.

Eilers, K., Kuok Hoong Yam, J., Morton, R., Mei Hui Yong, A., Brizuela, J., Hadjicharalambous, C., Liu, X., Givskov, M., Rice, S. A., and Filloux, A. (2022). Phenotypic and integrated analysis of a comprehensive *Pseudomonas aeruginosa* PAO1 library of mutants lacking cyclic-di-GMP-related genes. *Front Microbiol, 13*, 949597.

Ellison, C. K., Kan, J., Dillard, R. S., Kysela, D. T., Ducret, A., Berne, C., Hampton, C. M., Ke, Z., Wright, E. R., Biais, N., Dalia, A. B., and Brun, Y. V. (2017). Obstruction of pilus retraction stimulates bacterial surface sensing. *Science, 358*(6362), 535-538.

Enomoto, G., Wallner, T., and Wilde, A. (2023). Control of light-dependent behaviour in cyanobacteria by the second messenger cyclic di-GMP. *Microlife, 4*, uqad019.

Eytan, G. D. (1982). Use of liposomes for reconstitution of biological functions. *Biochim Biophys Acta, 694*(2), 185-202.

Fang, X., and Gomelsky, M. (2010). A post-translational, c-di-GMP-dependent mechanism regulating flagellar motility. *Mol Microbiol, 76*(5), 1295-1305.

Feirer, N., Xu, J., Allen, K. D., Koestler, B. J., Bruger, E. L., Waters, C. M., White, R. H., and Fuqua, C. (2015). A Pterin-dependent signaling pathway regulates a dual-function diguanylate cyclase-phosphodiesterase controlling surface attachment in *Agrobacterium tumefaciens*. *mBio, 6*(4), e00156.

Ferreira, R. B., Antunes, L. C., Greenberg, E. P., and McCarter, L. L. (2008). *Vibrio parahaemolyticus* ScrC modulates cyclic dimeric GMP regulation of gene expression relevant to growth on surfaces. *J Bacteriol, 190*(3), 851-860.

Flemming, H. C., Wingender, J., Szewzyk, U., Steinberg, P., Rice, S. A., and Kjelleberg, S. (2016). Biofilms: an emergent form of bacterial life. *Nat Rev Microbiol, 14*(9), 563-575.

Foletti, C., Kramer, R. A., Mauser, H., Jenal, U., Bleicher, K. H., and Wennemers, H. (2018). Functionalized proline-rich peptides bind the bacterial second messenger c-di-GMP. *Angew Chem Int Ed Engl, 57*(26), 7729-7733.

Frangipani, E., Slaveykova, V. I., Reimmann, C., and Haas, D. (2008). Adaptation of aerobically growing *Pseudomonas aeruginosa* to copper starvation. *J Bacteriol, 190*(20), 6706-6717.

Frauenfeld, J., Löving, R., Armache, J. P., Sonnen, A. F., Guettou, F., Moberg, P., Zhu, L., Jegerschöld, C., Flayhan, A., Briggs, J. A., Garoff, H., Löw, C., Cheng, Y., and

Nordlund, P. (2016). A saposin-lipoprotein nanoparticle system for membrane proteins. *Nat Methods, 13*(4), 345-351.

Gabel, C. V., and Berg, H. C. (2003). The speed of the flagellar rotary motor of *Escherichia coli varies* linearly with protonmotive force. *Proc Natl Acad Sci U S A, 100*(15), 8748-8751.

Galperin, M. Y., and Chou, S. H. (2022). Sequence Conservation, Domain Architectures, and Phylogenetic Distribution of the HD-GYP Type c-di-GMP Phosphodiesterases. *J Bacteriol, 204*(4), e0056121.

Galperin, M. Y., Gaidenko, T. A., Mulkidjanian, A. Y., Nakano, M., and Price, C. W. (2001). MHYT, a new integral membrane sensor domain. *FEMS Microbiol Lett, 205*(1), 17-23.

Gambello, M. J., Kaye, S., and Iglewski, B. H. (1993). LasR of *Pseudomonas aeruginosa* is a transcriptional activator of the alkaline protease gene (*apr*) and an enhancer of exotoxin A expression. *Infect Immun, 61*(4), 1180-1184.

Gao, X., Mukherjee, S., Matthews, P. M., Hammad, L. A., Kearns, D. B., and Dann, C. E., 3rd. (2013). Functional characterization of core components of the *Bacillus subtilis* cyclic-di-GMP signaling pathway. *J Bacteriol, 195*(21), 4782-4792.

Gerbracht, K. (2021). Transcriptional and posttranscriptional regulation of the c-di-GMP modulating phosphodiesterase NbdA of *Pseudomonas aeruginosa*. (PhD), RPTU TU Kaiserslautern.

Giacalone, D., Smith, T. J., Collins, A. J., Sondermann, H., Koziol, L. J., and O'Toole, G. A. (2018). Ligand-mediated biofilm formation via enhanced physical interaction between a diguanylate cyclase and its receptor. *mBio, 9*(4).

Giardina, G., Paiardini, A., Fernicola, S., Franceschini, S., Rinaldo, S., Stelitano, V., and Cutruzzolà, F. (2013). Investigating the allosteric regulation of YfiN from *Pseudomonas aeruginosa*: clues from the structure of the catalytic domain. *PLoS One, 8*(11), e81324.

Gibson, D. G., Young, L., Chuang, R. Y., Venter, J. C., Hutchison, C. A., 3rd, and Smith, H. O. (2009). Enzymatic assembly of DNA molecules up to several hundred kilobases. *Nat Methods, 6*(5), 343-345.

Gilbert, K. B., Kim, T. H., Gupta, R., Greenberg, E. P., and Schuster, M. (2009). Global position analysis of the *Pseudomonas aeruginosa* quorum-sensing transcription factor LasR. *Mol Microbiol, 73*(6), 1072-1085.

Glueck, D., Grethen, A., Das, M., Mmeka, O. P., Patallo, E. P., Meister, A., Rajender, R., Kins, S., Räschle, M., Victor, J., Chu, C., Etzkorn, M., Köck, Z., Bernhard, F., Babalola, J. O., Vargas, C., and Keller, S. (2022). Electroneutral polymer nanodiscs enable interference-free probing of membrane proteins in a lipid-bilayer environment. *Small, 18*(47), e2202492.

Gogtay, N. J., and Thatte, U. M. (2017). Principles of Correlation Analysis. *J Assoc Physicians India, 65*(3), 78-81.

Gomelsky, M. (2011). cAMP, c-di-GMP, c-di-AMP and now cGMP: bacteria use them all! *Mol Microbiol, 79*(3), 562-565.

Gomez, J. B., and Waters, C. M. (2023). Switching on cyclic di-GMP heterogeneity in *Pseudomonas aeruginosa* biofilms. *Nat Microbiol, 8*(8), 1380-1381.

Granseth, E., Daley, D. O., Rapp, M., Melén, K., and von Heijne, G. (2005). Experimentally constrained topology models for 51,208 bacterial inner membrane proteins. *J Mol Biol, 352*(3), 489-494.

Grethen, A., Oluwole, A. O., Danielczak, B., Vargas, C., and Keller, S. (2017). Thermodynamics of nanodisc formation mediated by styrene/maleic acid (2:1) copolymer. *Sci Rep, 7*(1), 11517.

Gubellini, F., Verdon, G., Karpowich, N. K., Luff, J. D., Boël, G., Gauthier, N., Handelman, S. K., Ades, S. E., and Hunt, J. F. (2011). Physiological response to membrane protein overexpression in *E. coli*. *Mol Cell Proteomics, 10*(10), M111.007930.

Guérin, A., Sulaeman, S., Coquet, L., Ménard, A., Barloy-Hubler, F., Dé, E., and Tresse, O. (2020). Membrane proteocomplexome of *Campylobacter jejuni* using 2-D Blue Native/SDS-PAGE combined to bioinformatics analysis. *Front Microbiol, 11*, 530906.

Gür, M., Erdmann, J., Will, A., Liang, Z., Andersen, J. B., Tolker-Nielsen, T., and Häussler, S. (2023). Challenges in using transcriptome data to study the c-di-GMP signaling network in *Pseudomonas aeruginosa* clinical isolates. *FEMS Microbes, 4*, xtad012.

Güvener, Z. T., and Harwood, C. S. (2007). Subcellular location characteristics of the *Pseudomonas aeruginosa* GGDEF protein, WspR, indicate that it produces cyclic-di-GMP in response to growth on surfaces. *Mol Microbiol, 66*(6), 1459-1473.

Guzzo, C. R., Salinas, R. K., Andrade, M. O., and Farah, C. S. (2009). PilZ protein structure and interactions with PilB and the FimX EAL domain: implications for control of type IV pilus biogenesis. *J Mol Biol, 393*(4), 848-866.

Ha, D. G., and O'Toole, G. A. (2015). c-di-GMP and its effects on biofilm formation and dispersion: a *Pseudomonas aeruginosa* review. *Microbiol Spectr, 3*(2), Mb-0003-2014.

Hall, C. L., and Lee, V. T. (2018). Cyclic-di-GMP regulation of virulence in bacterial pathogens. *Wiley Interdiscip Rev RNA, 9*(1).

Hancock, R. E., and Speert, D. P. (2000). Antibiotic resistance in *Pseudomonas aeruginosa*: mechanisms and impact on treatment. *Drug Resist Updat, 3*(4), 247-255.

Hay, I. D., Remminghorst, U., and Rehm, B. H. (2009). MucR, a novel membrane-associated regulator of alginate biosynthesis in *Pseudomonas aeruginosa*. *Appl Environ Microbiol, 75*(4), 1110-1120.

Hazelbauer, G. L. (1988). The bacterial chemosensory system. *Can J Microbiol, 34*(4), 466-474.

Hedin, L. E., Illergård, K., and Elofsson, A. (2011). An introduction to membrane proteins. *J Proteome Res, 10*(8), 3324-3331.

Heeb, S., Blumer, C., and Haas, D. (2002). Regulatory RNA as mediator in GacA/RsmA-dependent global control of exoproduct formation in *Pseudomonas fluorescens* CHA0. *J Bacteriol, 184*(4), 1046-1056.

Heide, H., Bleier, L., Steger, M., Ackermann, J., Dröse, S., Schwamb, B., Zörnig, M., Reichert, A. S., Koch, I., Wittig, I., and Brandt, U. (2012). Complexome profiling identifies TMEM126B as a component of the mitochondrial complex I assembly complex. *Cell Metab, 16*(4), 538-549.

Henderson, R., and Unwin, P. N. (1975). Three-dimensional model of purple membrane obtained by electron microscopy. *Nature, 257*(5521), 28-32.

Hengge, R. (2009). Principles of c-di-GMP signalling in bacteria. *Nat Rev Microbiol, 7*(4), 263-273.

Hengge, R. (2016). Trigger phosphodiesterases as a novel class of c-di-GMP effector proteins. *Philos Trans R Soc Lond B Biol Sci, 371*(1707).

Hengge, R. (2020). Linking bacterial growth, survival, and multicellularity - small signaling molecules as triggers and drivers. *Curr Opin Microbiol, 55*, 57-66.

Hengge, R. (2021). High-specificity local and global c-di-GMP signaling. *Trends Microbiol, 29*(11), 993-1003.

Hickman, J. W., and Harwood, C. S. (2008). Identification of FleQ from *Pseudomonas aeruginosa* as a c-di-GMP-responsive transcription factor. *Mol Microbiol, 69*(2), 376-389.

Hickman, J. W., Tifrea, D. F., and Harwood, C. S. (2005). A chemosensory system that regulates biofilm formation through modulation of cyclic diguanylate levels. *Proc Natl Acad Sci U S A, 102*(40), 14422-14427.

Hille, R., Hall, J., and Basu, P. (2014). The mononuclear molybdenum enzymes. *Chem Rev, 114*(7), 3963-4038.

Hmelo, L. R., Borlee, B. R., Almblad, H., Love, M. E., Randall, T. E., Tseng, B. S., Lin, C., Irie, Y., Storek, K. M., Yang, J. J., Siehnel, R. J., Howell, P. L., Singh, P. K., Tolker-Nielsen, T., Parsek, M. R., Schweizer, H. P., and Harrison, J. J. (2015). Precision-engineering the *Pseudomonas aeruginosa* genome with two-step allelic exchange. *Nat Protoc, 10*(11), 1820-1841.

Hollenstein, K., Frei, D. C., and Locher, K. P. (2007). Structure of an ABC transporter in complex with its binding protein. *Nature, 446*(7132), 213-216.

Holloway, B. W. (1955). Genetic recombination in *Pseudomonas aeruginosa*. *J Gen Microbiol, 13*(3), 572-581.

Hou, M., Huang, J., Jia, T., Guan, Y., Yang, F., Zhou, H., Huang, P., Wang, J., Yang, L., and Dai, L. (2023). Deep profiling of the proteome dynamics of *Pseudomonas aeruginosa* reference strain PAO1 under different growth conditions. *J Proteome Res, 22*(6), 1747-1761.

Hu, J. (2021). Toward unzipping the ZIP metal transporters: structure, evolution, and implications on drug discovery against cancer. *Febs j, 288*(20), 5805-5825.

Huang, B., Whitchurch, C. B., and Mattick, J. S. (2003). FimX, a multidomain protein connecting environmental signals to twitching motility in *Pseudomonas aeruginosa*. *J Bacteriol, 185*(24), 7068-7076.

Hwang, Y., and Harshey, R. M. (2023). A second role for the second messenger cyclic-di-GMP in *E. coli*: Arresting cell growth by altering metabolic flow. *mBio, 14*(2), e0061923.

Iadanza, M. G., Higgins, A. J., Schiffrin, B., Calabrese, A. N., Brockwell, D. J., Ashcroft, A. E., Radford, S. E., and Ranson, N. A. (2016). Lateral opening in the intact β-barrel assembly machinery captured by cryo-EM. *Nat Commun, 7*, 12865.

Jaeger, K. E., Dijkstra, B. W., and Reetz, M. T. (1999). Bacterial biocatalysts: molecular biology, three-dimensional structures, and biotechnological applications of lipases. *Annu Rev Microbiol, 53*, 315-351.

Jain, R., Behrens, A. J., Kaever, V., and Kazmierczak, B. I. (2012). Type IV pilus assembly in *Pseudomonas aeruginosa* over a broad range of cyclic di-GMP concentrations. *J Bacteriol, 194*(16), 4285-4294.

Jain, R., Sliusarenko, O., and Kazmierczak, B. I. (2017). Interaction of the cyclic-di-GMP binding protein FimX and the Type 4 pilus assembly ATPase promotes pilus assembly. *PLoS Pathog, 13*(8), e1006594.

Jakovljevic, V., Leonardy, S., Hoppert, M., and Søgaard-Andersen, L. (2008). PilB and PilT are ATPases acting antagonistically in type IV pilus function in *Myxococcus xanthus*. *J Bacteriol, 190*(7), 2411-2421.

Janson, K., Kyrilis, F. L., Tüting, C., Alfes, M., Das, M., Träger, T. K., Schmidt, C., Hamdi, F., Vargas, C., Keller, S., Meister, A., and Kastritis, P. L. (2022). Cryo-electron microscopy snapshots of eukaryotic membrane proteins in native lipid-bilayer nanodiscs. *Biomacromolecules*.

Jesorka, A., and Orwar, O. (2008). Liposomes: technologies and analytical applications. *Annu Rev Anal Chem (Palo Alto Calif), 1*, 801-832.

Jo, J., Cortez, K. L., Cornell, W. C., Price-Whelan, A., and Dietrich, L. E. (2017). An orphan cbb(3)-type cytochrome oxidase subunit supports *Pseudomonas aeruginosa* biofilm growth and virulence. *Elife, 6*.

Jodaitis, L., van Oene, T., and Martens, C. (2021). Assessing the role of lipids in the molecular mechanism of membrane proteins. *Int J Mol Sci, 22*(14).

Jones, C. J., Newsom, D., Kelly, B., Irie, Y., Jennings, L. K., Xu, B., Limoli, D. H., Harrison, J. J., Parsek, M. R., White, P., and Wozniak, D. J. (2014). ChIP-Seq and RNA-Seq reveal an

AmrZ-mediated mechanism for cyclic di-GMP synthesis and biofilm development by *Pseudomonas aeruginosa*. *PLoS Pathog, 10*(3), e1003984.

Jumper, J., Evans, R., Pritzel, A., Green, T., Figurnov, M., Ronneberger, O., Tunyasuvunakool, K., Bates, R., Žídek, A., Potapenko, A., Bridgland, A., Meyer, C., Kohl, S. A. A., Ballard, A. J., Cowie, A., Romera-Paredes, B., Nikolov, S., Jain, R., Adler, J., Back, T., Petersen, S., Reiman, D., Clancy, E., Zielinski, M., Steinegger, M., Pacholska, M., Berghammer, T., Bodenstein, S., Silver, D., Vinyals, O., Senior, A. W., Kavukcuoglu, K., Kohli, P., and Hassabis, D. (2021). Highly accurate protein structure prediction with AlphaFold. *Nature, 596*(7873), 583-589.

Junkermeier, E. H., and Hengge, R. (2023). Local signaling enhances output specificity of bacterial c-di-GMP signaling networks. *Microlife, 4*, uqad026.

Karaolis, D. K., Rashid, M. H., Chythanya, R., Luo, W., Hyodo, M., and Hayakawa, Y. (2005). c-di-GMP (3'-5'-cyclic diguanylic acid) inhibits *Staphylococcus aureus* cell-cell interactions and biofilm formation. *Antimicrob Agents Chemother, 49*(3), 1029-1038.

Karcher, M. L. (2021). Regulation der Synthese der c-di-GMP spezifischen Phosphodiesterase NbdA aus *Pseudomonas aeruginosa*. (Master thesis), RPTU, Kaiserslautern.

Karimova, G., Pidoux, J., Ullmann, A., and Ladant, D. (1998). A bacterial two-hybrid system based on a reconstituted signal transduction pathway. *Proc Natl Acad Sci U S A, 95*(10), 5752-5756.

Karimova, G., Ullmann, A., and Ladant, D. (2001). Protein-protein interaction between *Bacillus stearothermophilus* tyrosyl-tRNA synthetase subdomains revealed by a bacterial two-hybrid system. *J Mol Microbiol Biotechnol, 3*(1), 73-82.

Kawakami, T., Kuroki, M., Ishii, M., Igarashi, Y., and Arai, H. (2010). Differential expression of multiple terminal oxidases for aerobic respiration in *Pseudomonas aeruginosa*. *Environ Microbiol, 12*(6), 1399-1412.

Kerby, R. L., Youn, H., and Roberts, G. P. (2008). RcoM: a new single-component transcriptional regulator of CO metabolism in bacteria. *J Bacteriol, 190*(9), 3336-3343.

Keren, I., Kaldalu, N., Spoering, A., Wang, Y., and Lewis, K. (2004). Persister cells and tolerance to antimicrobials. *FEMS Microbiol Lett, 230*(1), 13-18.

Kerwin, J. F., Jr., Lancaster, J. R., Jr., and Feldman, P. L. (1995). Nitric oxide: a new paradigm for second messengers. *J Med Chem, 38*(22), 4343-4362.

King, C., Stoneman, M., Raicu, V., and Hristova, K. (2016). Fully quantified spectral imaging reveals *in vivo* membrane protein interactions. *Integr Biol (Camb), 8*(2), 216-229.

Klockgether, J., Munder, A., Neugebauer, J., Davenport, C. F., Stanke, F., Larbig, K. D., Heeb, S., Schöck, U., Pohl, T. M., Wiehlmann, L., and Tümmler, B. (2010). Genome diversity of *Pseudomonas aeruginosa* PAO1 laboratory strains. *J Bacteriol, 192*(4), 1113-1121.

Knowles, T. J., Finka, R., Smith, C., Lin, Y. P., Dafforn, T., and Overduin, M. (2009). Membrane proteins solubilized intact in lipid containing nanoparticles bounded by styrene maleic acid copolymer. *J Am Chem Soc, 131*(22), 7484-7485.

Koch, M. D., Black, M. E., Han, E., Shaevitz, J. W., and Gitai, Z. (2022). *Pseudomonas aeruginosa* distinguishes surfaces by stiffness using retraction of type IV pili. *Proc Natl Acad Sci U S A, 119*(20), e2119434119.

Koch, M. D., Fei, C., Wingreen, N. S., Shaevitz, J. W., and Gitai, Z. (2021). Competitive binding of independent extension and retraction motors explains the quantitative dynamics of type IV pili. *Proc Natl Acad Sci U S A, 118*(8).

Komar, J., Alvira, S., Schulze, R. J., Martin, R., Lycklama, A. N. J. A., Lee, S. C., Dafforn, T. R., Deckers-Hebestreit, G., Berger, I., Schaffitzel, C., and Collinson, I. (2016). Membrane

protein insertion and assembly by the bacterial holo-translocon SecYEG-SecDF-YajC-YidC. *Biochem J, 473*(19), 3341-3354.

König, B., Jaeger, K. E., Sage, A. E., Vasil, M. L., and König, W. (1996). Role of *Pseudomonas aeruginosa* lipase in inflammatory mediator release from human inflammatory effector cells (platelets, granulocytes, and monocytes). *Infect Immun, 64*(8), 3252-3258.

Krasteva, P. V., Giglio, K. M., and Sondermann, H. (2012). Sensing the messenger: the diverse ways that bacteria signal through c-di-GMP. *Protein Sci, 21*(7), 929-948.

Krey, J. F., Wilmarth, P. A., Shin, J. B., Klimek, J., Sherman, N. E., Jeffery, E. D., Choi, D., David, L. L., and Barr-Gillespie, P. G. (2014). Accurate label-free protein quantitation with high- and low-resolution mass spectrometers. *J Proteome Res, 13*(2), 1034-1044.

Kuchma, S. L., Ballok, A. E., Merritt, J. H., Hammond, J. H., Lu, W., Rabinowitz, J. D., and O'Toole, G. A. (2010). Cyclic-di-GMP-mediated repression of swarming motility by *Pseudomonas aeruginosa*: the *pilY*1 gene and its impact on surface-associated behaviors. *J Bacteriol, 192*(12), 2950-2964.

Kuchma, S. L., Brothers, K. M., Merritt, J. H., Liberati, N. T., Ausubel, F. M., and O'Toole, G. A. (2007). BifA, a cyclic-di-GMP phosphodiesterase, inversely regulates biofilm formation and swarming motility by *Pseudomonas aeruginosa* PA14. *J Bacteriol, 189*(22), 8165-8178.

Kuchma, S. L., Connolly, J. P., and O'Toole, G. A. (2005). A three-component regulatory system regulates biofilm maturation and type III secretion in *Pseudomonas aeruginosa*. *J Bacteriol, 187*(4), 1441-1454.

Kuchma, S. L., Griffin, E. F., and O'Toole, G. A. (2012). Minor pilins of the type IV pilus system participate in the negative regulation of swarming motility. *J Bacteriol, 194*(19), 5388-5403.

Kühn, M. J., Macmillan, H., Talà, L., Inclan, Y., Patino, R., Pierrat, X., Al-Mayyah, Z., Engel, J. N., and Persat, A. (2023). Two antagonistic response regulators control *Pseudomonas aeruginosa* polarization during mechanotaxis. *Embo j, 42*(7), e112165.

Kühn, M. J., Talà, L., Inclan, Y. F., Patino, R., Pierrat, X., Vos, I., Al-Mayyah, Z., Macmillan, H., Negrete, J., Jr., Engel, J. N., and Persat, A. (2021). Mechanotaxis directs *Pseudomonas aeruginosa* twitching motility. *Proc Natl Acad Sci U S A, 118*(30).

Kukavica-Ibrulj, I., Sanschagrin, F., Peterson, A., Whiteley, M., Boyle, B., MacKay, J., and Levesque, R. C. (2008). Functional genomics of PycR, a LysR family transcriptional regulator essential for maintenance of *Pseudomonas aeruginosa* in the rat lung. *Microbiology (Reading), 154*(Pt 7), 2106-2118.

Kulasakara, H., Lee, V., Brencic, A., Liberati, N., Urbach, J., Miyata, S., Lee, D. G., Neely, A. N., Hyodo, M., Hayakawa, Y., Ausubel, F. M., and Lory, S. (2006). Analysis of *Pseudomonas aeruginosa* diguanylate cyclases and phosphodiesterases reveals a role for bis-(3'-5')-cyclic-GMP in virulence. *Proc Natl Acad Sci U S A, 103*(8), 2839-2844.

Kumari, H., Murugapiran, S. K., Balasubramanian, D., Schneper, L., Merighi, M., Sarracino, D., Lory, S., and Mathee, K. (2014). LTQ-XL mass spectrometry proteome analysis expands the *Pseudomonas aeruginosa* AmpR regulon to include cyclic di-GMP phosphodiesterases and phosphoproteins, and identifies novel open reading frames. *J Proteomics, 96*, 328-342.

Kunji, E. R., Harding, M., Butler, P. J., and Akamine, P. (2008). Determination of the molecular mass and dimensions of membrane proteins by size exclusion chromatography. *Methods, 46*(2), 62-72.

Kunz, S., and Graumann, P. L. (2020). Spatial organization enhances versatility and specificity in cyclic di-GMP signaling. *Biol Chem, 401*(12), 1323-1334.

Laloux, G., and Jacobs-Wagner, C. (2014). How do bacteria localize proteins to the cell pole? *J Cell Sci, 127*(Pt 1), 11-19.

Lamprokostopoulou, A., Monteiro, C., Rhen, M., and Römling, U. (2010). Cyclic di-GMP signalling controls virulence properties of *Salmonella enterica* serovar Typhimurium at the mucosal lining. *Environ Microbiol, 12*(1), 40-53.

Laventie, B. J., Sangermani, M., Estermann, F., Manfredi, P., Planes, R., Hug, I., Jaeger, T., Meunier, E., Broz, P., and Jenal, U. (2019). A surface-induced asymmetric program promotes tissue colonization by *Pseudomonas aeruginosa*. *Cell Host Microbe, 25*(1), 140-152.e146.

Lee, E. Y., Choi, D. S., Kim, K. P., and Gho, Y. S. (2008). Proteomics in gram-negative bacterial outer membrane vesicles. *Mass Spectrom Rev, 27*(6), 535-555.

Lee, P. A., Tullman-Ercek, D., and Georgiou, G. (2006). The bacterial twin-arginine translocation pathway. *Annu Rev Microbiol, 60*, 373-395.

Levi, A., and Jenal, U. (2006). Holdfast formation in motile swarmer cells optimizes surface attachment during *Caulobacter crescentus* development. *J Bacteriol, 188*(14), 5315-5318.

Lewis, K. (2007). Persister cells, dormancy and infectious disease. *Nat Rev Microbiol, 5*(1), 48-56.

Lewis, K. A., Baker, A. E., Chen, A. I., Harty, C. E., Kuchma, S. L., O'Toole, G. A., and Hogan, D. A. (2019). Ethanol decreases *Pseudomonas aeruginosa* flagellar motility through the regulation of flagellar stators. *J Bacteriol, 201*(18).

Li, Y., Heine, S., Entian, M., Sauer, K., and Frankenberg-Dinkel, N. (2013). NO-induced biofilm dispersion in *Pseudomonas aeruginosa* is mediated by an MHYT domain-coupled phosphodiesterase. *J Bacteriol, 195*(16), 3531-3542.

Lichtenberg, D., Robson, R. J., and Dennis, E. A. (1983). Solubilization of phospholipids by detergents. Structural and kinetic aspects. *Biochim Biophys Acta, 737*(2), 285-304.

Lin Chua, S., Liu, Y., Li, Y., Jun Ting, H., Kohli, G. S., Cai, Z., Suwanchaikasem, P., Kau Kit Goh, K., Pin Ng, S., Tolker-Nielsen, T., Yang, L., and Givskov, M. (2017). Reduced intracellular c-di-GMP content increases expression of quorum sensing-regulated genes in *Pseudomonas aeruginosa*. *Front Cell Infect Microbiol, 7*, 451.

Lin, J., Cheng, J., Chen, K., Guo, C., Zhang, W., Yang, X., Ding, W., Ma, L., Wang, Y., and Shen, X. (2015). The *icmF*3 locus is involved in multiple adaptation- and virulence-related characteristics in *Pseudomonas aeruginosa* PAO1. *Front Cell Infect Microbiol, 5*, 70.

Lin, Y. H., Xu, J. L., Hu, J., Wang, L. H., Ong, S. L., Leadbetter, J. R., and Zhang, L. H. (2003). Acyl-homoserine lactone acylase from *Ralstonia* strain XJ12B represents a novel and potent class of quorum-quenching enzymes. *Mol Microbiol, 47*(3), 849-860.

Lindenberg, S., Klauck, G., Pesavento, C., Klauck, E., and Hengge, R. (2013). The EAL domain protein YciR acts as a trigger enzyme in a c-di-GMP signalling cascade in *E. coli* biofilm control. *Embo j, 32*(14), 2001-2014.

Little, A. S., Okkotsu, Y., Reinhart, A. A., Damron, F. H., Barbier, M., Barrett, B., Oglesby-Sherrouse, A. G., Goldberg, J. B., Cody, W. L., Schurr, M. J., Vasil, M. L., and Schurr, M. J. (2018). *Pseudomonas aeruginosa* AlgR phosphorylation status differentially regulates pyocyanin and pyoverdine production. *mBio, 9*(1).

Liu, S., Xu, A., Xie, B., Xin, F., Dong, W., Zhou, J., and Jiang, M. (2022a). Priority changes between biofilm exopolysaccharides synthesis and rhamnolipids production are mediated by a c-di-GMP-specific phosphodiesterase NbdA in *Pseudomonas aeruginosa*. *iScience, 25*(12), 105531.

Liu, Z., Xu, Z., Chen, S., Huang, J., Li, T., Duan, C., Zhang, L. H., and Xu, Z. (2022b). CzcR is essential for swimming motility in *Pseudomonas aeruginosa* during zinc stress. *Microbiol Spectr, 10*(6), e0284622.

Long, Y., Fu, W., Li, S., Ren, H., Li, M., Liu, C., Zhang, B., Xia, Y., Fan, Z., Xu, C., Liu, J., Jin, Y., Bai, F., Cheng, Z., Liu, X., Jin, S., and Wu, W. (2019). Identification of novel genes

that promote persister formation by repressing transcription and cell division in *Pseudomonas aeruginosa*. *J Antimicrob Chemother, 74*(9), 2575-2587.

Lori, C., Ozaki, S., Steiner, S., Böhm, R., Abel, S., Dubey, B. N., Schirmer, T., Hiller, S., and Jenal, U. (2015). Cyclic di-GMP acts as a cell cycle oscillator to drive chromosome replication. *Nature, 523*(7559), 236-239.

Lovering, A. L., Capeness, M. J., Lambert, C., Hobley, L., and Sockett, R. E. (2011). The structure of an unconventional HD-GYP protein from *Bdellovibrio* reveals the roles of conserved residues in this class of cyclic-di-GMP phosphodiesterases. *mBio, 2*(5).

Lu, S., Giuliani, M., Harvey, H., Burrows, L. L., Wickham, R. A., and Dutcher, J. R. (2015). Nanoscale pulling of type IV pili reveals their flexibility and adhesion to surfaces over extended lengths of the pili. *Biophys J, 108*(12), 2865-2875.

Luirink, J., von Heijne, G., Houben, E., and de Gier, J. W. (2005). Biogenesis of inner membrane proteins in *Escherichia coli*. *Annu Rev Microbiol, 59*, 329-355.

Ma, Q., Zhai, Y., Schneider, J. C., Ramseier, T. M., and Saier, M. H., Jr. (2003). Protein secretion systems of *Pseudomonas aeruginosa* and *P. fluorescens*. *Biochim Biophys Acta, 1611*(1-2), 223-233.

Magnowska, Z., Hartmann, I., Jänsch, L., and Jahn, D. (2014). Membrane proteomics of *Pseudomonas aeruginosa*. *Methods Mol Biol, 1149*, 213-224.

Mahler, F., Meister, A., Vargas, C., Durand, G., and Keller, S. (2021). Self-assembly of protein-containing lipid-bilayer nanodiscs from small-molecule amphiphiles. *Small, 17*(49), e2103603.

Majeed, S., Ahmad, A. B., Sehar, U., and Georgieva, E. R. (2021). Lipid membrane mimetics in functional and structural studies of integral membrane proteins. *Membranes (Basel), 11*(9).

Malone, J. G., Jaeger, T., Manfredi, P., Dötsch, A., Blanka, A., Bos, R., Cornelis, G. R., Häussler, S., and Jenal, U. (2012). The YfiBNR signal transduction mechanism reveals novel targets for the evolution of persistent *Pseudomonas aeruginosa* in cystic fibrosis airways. *PLoS Pathog, 8*(6), e1002760.

Manner, C., Dias Teixeira, R., Saha, D., Kaczmarczyk, A., Zemp, R., Wyss, F., Jaeger, T., Laventie, B. J., Boyer, S., Malone, J. G., Qvortrup, K., Andersen, J. B., Givskov, M., Tolker-Nielsen, T., Hiller, S., Drescher, K., and Jenal, U. (2023). A genetic switch controls *Pseudomonas aeruginosa* surface colonization. *Nat Microbiol, 8*(8), 1520-1533.

Mattick, J. S. (2002). Type IV pili and twitching motility. *Annu Rev Microbiol, 56*, 289-314.

Mattingly, A. E., Kamatkar, N. G., Morales-Soto, N., Borlee, B. R., and Shrout, J. D. (2018). Multiple environmental factors influence the importance of the phosphodiesterase DipA upon *Pseudomonas aeruginosa* Swarming. *Appl Environ Microbiol, 84*(7).

McCarthy, R. R., Mazon-Moya, M. J., Moscoso, J. A., Hao, Y., Lam, J. S., Bordi, C., Mostowy, S., and Filloux, A. (2017). Cyclic-di-GMP regulates lipopolysaccharide modification and contributes to *Pseudomonas aeruginosa* immune evasion. *Nat Microbiol, 2*, 17027.

McCormack, J. G., and Denton, R. M. (1986). Ca^{2+} as a second messenger within mitochondria of the heart and other tissues. *Trends Biochem Sci, 11*, 258-262.

Meiresonne, N. Y., Consoli, E., Mertens, L. M. Y., Chertkova, A. O., Goedhart, J., and den Blaauwen, T. (2019). Superfolder mTurquoise2^{ox} optimized for the bacterial periplasm allows high efficiency *in vivo* FRET of cell division antibiotic targets. *Mol Microbiol, 111*(4), 1025-1038.

Merritt, J. H., Brothers, K. M., Kuchma, S. L., and O'Toole, G. A. (2007). SadC reciprocally influences biofilm formation and swarming motility via modulation of exopolysaccharide production and flagellar function. *J Bacteriol, 189*(22), 8154-8164.

Merritt, J. H., Ha, D. G., Cowles, K. N., Lu, W., Morales, D. K., Rabinowitz, J., Gitai, Z., and O'Toole, G. A. (2010). Specific control of *Pseudomonas aeruginosa* surface-associated behaviors by two c-di-GMP diguanylate cyclases. *mBio, 1*(4).

Mhatre, E., Snyder, D. J., Sileo, E., Turner, C. B., Buskirk, S. W., Fernandez, N. L., Neiditch, M. B., Waters, C. M., and Cooper, V. S. (2020). One gene, multiple ecological strategies: A biofilm regulator is a capacitor for sustainable diversity. *Proc Natl Acad Sci U S A, 117*(35), 21647-21657.

Mierzejewska, K., Siwek, W., Czapinska, H., Kaus-Drobek, M., Radlinska, M., Skowronek, K., Bujnicki, J. M., Dadlez, M., and Bochtler, M. (2014). Structural basis of the methylation specificity of R.DpnI. *Nucleic Acids Res, 42*(13), 8745-8754.

Miller, K. E., Kim, Y., Huh, W. K., and Park, H. O. (2015). Bimolecular fluorescence complementation (BiFC) analysis: Advances and recent applications for genome-ide interaction studies. *J Mol Biol, 427*(11), 2039-2055.

Miner, K. D., and Kurtz, D. M., Jr. (2016). Active site metal occupancy and cyclic di-GMP phosphodiesterase activity of *Thermotoga maritima* HD-GYP. *Biochemistry, 55*(6), 970-979.

Mitra, S. D., Afonina, I., and Kline, K. A. (2016). Right place, right time: Focalization of membrane proteins in Gram-positive bacteria. *Trends Microbiol, 24*(8), 611-621.

Monson, E. K., Weinstein, M., Ditta, G. S., and Helinski, D. R. (1992). The FixL protein of Rhizobium meliloti can be separated into a heme-binding oxygen-sensing domain and a functional C-terminal kinase domain. *Proc Natl Acad Sci U S A, 89*(10), 4280-4284.

Moreau, P., Diggle, S. P., and Friman, V. P. (2017). Bacterial cell-to-cell signaling promotes the evolution of resistance to parasitic bacteriophages. *Ecol Evol, 7*(6), 1936-1941.

Morgan, J. L., McNamara, J. T., and Zimmer, J. (2014). Mechanism of activation of bacterial cellulose synthase by cyclic di-GMP. *Nat Struct Mol Biol, 21*(5), 489-496.

Moscoso, J. A., Jaeger, T., Valentini, M., Hui, K., Jenal, U., and Filloux, A. (2014). The diguanylate cyclase SadC is a central player in Gac/Rsm-mediated biofilm formation in *Pseudomonas aeruginosa*. *J Bacteriol, 196*(23), 4081-4088.

Motta, S., Vecchietti, D., Martorana, A. M., Brunetti, P., Bertoni, G., Polissi, A., Mauri, P., and Di Silvestre, D. (2020). The landscape of *Pseudomonas aeruginosa* membrane-associated proteins. *Cells, 9*(11).

Mulcahy, L. R., Burns, J. L., Lory, S., and Lewis, K. (2010). Emergence of *Pseudomonas aeruginosa* strains producing high levels of persister cells in patients with cystic fibrosis. *J Bacteriol, 192*(23), 6191-6199.

Müller, D. J., and Engel, A. (2007). Atomic force microscopy and spectroscopy of native membrane proteins. *Nat Protoc, 2*(9), 2191-2197.

Müller, M., Koch, H. G., Beck, K., and Schäfer, U. (2001). Protein traffic in bacteria: multiple routes from the ribosome to and across the membrane. *Prog Nucleic Acid Res Mol Biol, 66*, 107-157.

Murray, R. G. E., Brenner, D. J., Colwell, R. R., de Vos, P., Goodfellow, M., Grimont, P. A. D., Pfennig, N., Stackebrandt, E., and Zavarzin, G. A. (1990). Report of the ad hoc committee on approaches to taxonomy within the Proteobacteria. *Int J Syst Bacteriol, 40*(2), 213-215.

Narulita, E., Addy, H. S., Kawasaki, T., Fujie, M., and Yamada, T. (2016). The involvement of the PilQ secretin of type IV pili in phage infection in *Ralstonia solanacearum*. *Biochem Biophys Res Commun, 469*(4), 868-872.

Newell, P. D., Boyd, C. D., Sondermann, H., and O'Toole, G. A. (2011). A c-di-GMP effector system controls cell adhesion by inside-out signaling and surface protein cleavage. *PLoS Biol, 9*(2), e1000587.

Newell, P. D., Monds, R. D., and O'Toole, G. A. (2009). LapD is a bis-(3',5')-cyclic dimeric GMP-binding protein that regulates surface attachment by *Pseudomonas fluorescens* Pf0-1. *Proc Natl Acad Sci U S A, 106*(9), 3461-3466.

Nicastro, G. G., Kaihami, G. H., Pulschen, A. A., Hernandez-Montelongo, J., Boechat, A. L., de Oliveira Pereira, T., Rosa, C. G. T., Stefanello, E., Colepicolo, P., Bordi, C., and Baldini, R. L. (2020). c-di-GMP-related phenotypes are modulated by the interaction between a diguanylate cyclase and a polar hub protein. *Sci Rep, 10*(1), 3077.

Nicolas, P., Mäder, U., Dervyn, E., Rochat, T., Leduc, A., Pigeonneau, N., Bidnenko, E., Marchadier, E., Hoebeke, M., Aymerich, S., Becher, D., Bisicchia, P., Botella, E., Delumeau, O., Doherty, G., Denham, E. L., Fogg, M. J., Fromion, V., Goelzer, A., Hansen, A., Härtig, E., Harwood, C. R., Homuth, G., Jarmer, H., Jules, M., Klipp, E., Le Chat, L., Lecointe, F., Lewis, P., Liebermeister, W., March, A., Mars, R. A., Nannapaneni, P., Noone, D., Pohl, S., Rinn, B., Rügheimer, F., Sappa, P. K., Samson, F., Schaffer, M., Schwikowski, B., Steil, L., Stülke, J., Wiegert, T., Devine, K. M., Wilkinson, A. J., van Dijl, J. M., Hecker, M., Völker, U., Bessières, P., and Noirot, P. (2012). Condition-dependent transcriptome reveals high-level regulatory architecture in *Bacillus subtilis*. *Science, 335*(6072), 1103-1106.

Nikolskaya, A. N., and Galperin, M. Y. (2002). A novel type of conserved DNA-binding domain in the transcriptional regulators of the AlgR/AgrA/LytR family. *Nucleic Acids Res, 30*(11), 2453-2459.

Nouwens, A. S., Cordwell, S. J., Larsen, M. R., Molloy, M. P., Gillings, M., Willcox, M. D., and Walsh, B. J. (2000). Complementing genomics with proteomics: the membrane subproteome of *Pseudomonas aeruginosa* PAO1. *Electrophoresis, 21*(17), 3797-3809.

O'Neal, L., Baraquet, C., Suo, Z., Dreifus, J. E., Peng, Y., Raivio, T. L., Wozniak, D. J., Harwood, C. S., and Parsek, M. R. (2022). The Wsp system of *Pseudomonas aeruginosa* links surface sensing and cell envelope stress. *Proc Natl Acad Sci U S A, 119*(18), e2117633119.

Ogasawara, H., Yamamoto, K., and Ishihama, A. (2010). Regulatory role of MlrA in transcription activation of *csgD*, the master regulator of biofilm formation in *Escherichia coli*. *FEMS Microbiol Lett, 312*(2), 160-168.

Okegbe, C., Fields, B. L., Cole, S. J., Beierschmitt, C., Morgan, C. J., Price-Whelan, A., Stewart, R. C., Lee, V. T., and Dietrich, L. E. P. (2017). Electron-shuttling antibiotics structure bacterial communities by modulating cellular levels of c-di-GMP. *Proc Natl Acad Sci U S A, 114*(26), E5236-e5245.

Oluwole, A. O., Klingler, J., Danielczak, B., Babalola, J. O., Vargas, C., Pabst, G., and Keller, S. (2017). Formation of lipid-bilayer nanodiscs by diisobutylene/maleic acid (DIBMA) copolymer. *Langmuir, 33*(50), 14378-14388.

Ouellette, S. P., Karimova, G., Davi, M., and Ladant, D. (2017). Analysis of membrane protein interactions with a bacterial adenylate cyclase-based two-hybrid (BACTH) technique. *Curr Protoc Mol Biol, 118*, 20.12.21-20.12.24.

Overduin, M., and Esmaili, M. (2019). Structures and interactions of transmembrane targets in native nanodiscs. *SLAS Discov, 24*(10), 943-952.

Padan, E. (2009). Bacterial Membrane Transport: Organization of Membrane Activities *Encyclopedia of Life Sciences*.

Pang, Z., Raudonis, R., Glick, B. R., Lin, T. J., and Cheng, Z. (2019). Antibiotic resistance in *Pseudomonas aeruginosa*: mechanisms and alternative therapeutic strategies. *Biotechnol Adv, 37*(1), 177-192.

Pasqua, M., Visaggio, D., Lo Sciuto, A., Genah, S., Banin, E., Visca, P., and Imperi, F. (2017). Ferric uptake regulator Fur is conditionally essential in *Pseudomonas aeruginosa*. *J Bacteriol, 199*(22).

Pelicic, V. (2023). Mechanism of assembly of type 4 filaments: everything you always wanted to know (but were afraid to ask). *Microbiology (Reading), 169*(3).

Pelicic, V., Reyrat, J. M., and Gicquel, B. (1996). Expression of the *Bacillus subtilis sacB* gene confers sucrose sensitivity on mycobacteria. *J Bacteriol, 178*(4), 1197-1199.

Pellequer, J. L., Wager-Smith, K. A., Kay, S. A., and Getzoff, E. D. (1998). Photoactive yellow protein: a structural prototype for the three-dimensional fold of the PAS domain superfamily. *Proc Natl Acad Sci U S A, 95*(11), 5884-5890.

Peng, X., Xu, C., Ren, H., Lin, X., Wu, L., and Wang, S. (2005). Proteomic analysis of the sarcosine-insoluble outer membrane fraction of *Pseudomonas aeruginosa* responding to ampicilin, kanamycin, and tetracycline resistance. *J Proteome Res, 4*(6), 2257-2265.

Perinbam, K., Chacko, J. V., Kannan, A., Digman, M. A., and Siryaporn, A. (2020). A shift in central metabolism accompanies virulence activation in *Pseudomonas aeruginosa*. *mBio, 11*(2).

Perron, K., Caille, O., Rossier, C., Van Delden, C., Dumas, J. L., and Köhler, T. (2004). CzcR-CzcS, a two-component system involved in heavy metal and carbapenem resistance in *Pseudomonas aeruginosa*. *J Biol Chem, 279*(10), 8761-8768.

Pertl-Obermeyer, H., and Obermeyer, G. (2020). *In vivo* cross-linking to analyze transient protein-protein interactions. *Methods Mol Biol, 2139*, 273-287.

Piersimoni, L., Kastritis, P. L., Arlt, C., and Sinz, A. (2022). Cross-linking mass spectrometry for investigating protein conformations and protein-protein interactions─A method for all seasons. *Chem Rev, 122*(8), 7500-7531.

Pollock, N. L., Lee, S. C., Patel, J. H., Gulamhussein, A. A., and Rothnie, A. J. (2018). Structure and function of membrane proteins encapsulated in a polymer-bound lipid bilayer. *Biochim Biophys Acta Biomembr, 1860*(4), 809-817.

Pollock, N. L., Lloyd, J., Montinaro, C., Rai, M., and Dafforn, T. R. (2022). Conformational trapping of an ABC transporter in polymer lipid nanoparticles. *Biochem J, 479*(2), 145-159.

Potvin, E., Sanschagrin, F., and Levesque, R. C. (2008). Sigma factors in *Pseudomonas aeruginosa*. *FEMS Microbiol Rev, 32*(1), 38-55.

Qiu, D., Damron, F. H., Mima, T., Schweizer, H. P., and Yu, H. D. (2008). P_{BAD}-based shuttle vectors for functional analysis of toxic and highly regulated genes in *Pseudomonas* and *Burkholderia* spp. and other bacteria. *Appl Environ Microbiol, 74*(23), 7422-7426.

Randall, T. E., Eckartt, K., Kakumanu, S., Price-Whelan, A., Dietrich, L. E. P., and Harrison, J. J. (2022). Sensory perception in bacterial cyclic diguanylate signal transduction. *J Bacteriol, 204*(2), e0043321.

Rao, F., Yang, Y., Qi, Y., and Liang, Z. X. (2008). Catalytic mechanism of cyclic di-GMP-specific phosphodiesterase: a study of the EAL domain-containing RocR from *Pseudomonas aeruginosa*. *J Bacteriol, 190*(10), 3622-3631.

Rappsilber, J., Mann, M., and Ishihama, Y. (2007). Protocol for micro-purification, enrichment, pre-fractionation and storage of peptides for proteomics using StageTips. *Nat Protoc, 2*(8), 1896-1906.

Rasamiravaka, T., Labtani, Q., Duez, P., and El Jaziri, M. (2015). The formation of biofilms by *Pseudomonas aeruginosa*: a review of the natural and synthetic compounds interfering with control mechanisms. *Biomed Res Int, 2015*, 759348.

Rasmussen, S. G., Choi, H. J., Fung, J. J., Pardon, E., Casarosa, P., Chae, P. S., Devree, B. T., Rosenbaum, D. M., Thian, F. S., Kobilka, T. S., Schnapp, A., Konetzki, I., Sunahara, R. K., Gellman, S. H., Pautsch, A., Steyaert, J., Weis, W. I., and Kobilka, B. K. (2011). Structure of a nanobody-stabilized active state of the β(2) adrenoceptor. *Nature, 469*(7329), 175-180.

Rehner, J. (2020). The role of the MHYT-domain for the function of the phosphodiesterase NbdA in *Pseudomonas aeruginosa* PAO1. (Master thesis), RPTU Kaiserslautern.

Richter, A. M., Possling, A., Malysheva, N., Yousef, K. P., Herbst, S., von Kleist, M., and Hengge, R. (2020). Local c-di-GMP signaling in the control of synthesis of the *E. coli* biofilm exopolysaccharide pEtN-cellulose. *J Mol Biol, 432*(16), 4576-4595.

Rick, T., Kreiling, V., Höing, A., Fiedler, S., Glatter, T., Steinchen, W., Hochberg, G., Bähre, H., Seifert, R., Bange, G., Knauer, S. K., Graumann, P. L., and Thormann, K. M. (2022). GGDEF domain as spatial on-switch for a phosphodiesterase by interaction with landmark protein HubP. *NPJ Biofilms Microbiomes, 8*(1), 35.

Rietsch, A., Vallet-Gely, I., Dove, S. L., and Mekalanos, J. J. (2005). ExsE, a secreted regulator of type III secretion genes in *Pseudomonas aeruginosa*. *Proc Natl Acad Sci U S A, 102*(22), 8006-8011.

Römling, U., Gomelsky, M., and Galperin, M. Y. (2005). C-di-GMP: the dawning of a novel bacterial signalling system. *Mol Microbiol, 57*(3), 629-639.

Rosenau, F., Isenhardt, S., Gdynia, A., Tielker, D., Schmidt, E., Tielen, P., Schobert, M., Jahn, D., Wilhelm, S., and Jaeger, K. E. (2010). Lipase LipC affects motility, biofilm formation and rhamnolipid production in *Pseudomonas aeruginosa*. *FEMS Microbiol Lett, 309*(1), 25-34.

Ross, P., Weinhouse, H., Aloni, Y., Michaeli, D., Weinberger-Ohana, P., Mayer, R., Braun, S., de Vroom, E., van der Marel, G. A., van Boom, J. H., and Benziman, M. (1987). Regulation of cellulose synthesis in *Acetobacter xylinum* by cyclic diguanylic acid. *Nature, 325*(6101), 279-281.

Rossi, E., Motta, S., Aliverti, A., Cossu, F., Gourlay, L., Mauri, P., and Landini, P. (2017). Cellulose production is coupled to sensing of the pyrimidine biosynthetic pathway via c-di-GMP production by the DgcQ protein of *Escherichia coli*. *Environ Microbiol, 19*(11), 4551-4563.

Roy, A. B., Petrova, O. E., and Sauer, K. (2012). The phosphodiesterase DipA (PA5017) is essential for *Pseudomonas aeruginosa* biofilm dispersion. *J Bacteriol, 194*(11), 2904-2915.

Rüger, M. (2019). Die Funktion der c-di-GMP modulierenden Membranproteine NbdA und MucR in *Pseudomonas aeruginosa*. (PhD), RPTU Kaiserslautern.

Rybtke, M. T., Borlee, B. R., Murakami, K., Irie, Y., Hentzer, M., Nielsen, T. E., Givskov, M., Parsek, M. R., and Tolker-Nielsen, T. (2012). Fluorescence-based reporter for gauging cyclic di-GMP levels in *Pseudomonas aeruginosa*. *Appl Environ Microbiol, 78*(15), 5060-5069.

Sachs, J. N., and Engelman, D. M. (2006). Introduction to the membrane protein reviews: the interplay of structure, dynamics, and environment in membrane protein function. *Annu Rev Biochem, 75*, 707-712.

Sarenko, O., Klauck, G., Wilke, F. M., Pfiffer, V., Richter, A. M., Herbst, S., Kaever, V., and Hengge, R. (2017). More than enzymes that make or break cyclic di-GMP-local signaling in the interactome of GGDEF/EAL domain proteins of *Escherichia coli*. *mBio, 8*(5).

Sauer, K., Camper, A. K., Ehrlich, G. D., Costerton, J. W., and Davies, D. G. (2002). *Pseudomonas aeruginosa* displays multiple phenotypes during development as a biofilm. *J Bacteriol, 184*(4), 1140-1154.

Sauer, K., Cullen, M. C., Rickard, A. H., Zeef, L. A., Davies, D. G., and Gilbert, P. (2004). Characterization of nutrient-induced dispersion in *Pseudomonas aeruginosa* PAO1 biofilm. *J Bacteriol, 186*(21), 7312-7326.

Sauer, K., Stoodley, P., Goeres, D. M., Hall-Stoodley, L., Burmølle, M., Stewart, P. S., and Bjarnsholt, T. (2022). The biofilm life cycle: expanding the conceptual model of biofilm formation. *Nat Rev Microbiol, 20*(10), 608-620.

Sawczyc, H., Heit, S., and Watts, A. (2023). A comparative characterisation of commercially available lipid-polymer nanoparticles formed from model membranes. *Eur Biophys J, 52*(1-2), 39-51.

Scherhag, A. (2019). Charakterisierung der putativen Phosphodiesterase NbdA aus *Pseudomonas aeruginosa*. (Master thesis), RPTU Kaiserslautern.

Scherhag, A., Räschle, M., Unbehend, N., Venn, B., Glueck, D., Mühlhaus, T., Keller, S., Pérez Patallo, E., Zehner, S., and Frankenberg-Dinkel, N. (2023). Characterization of a soluble library of the *Pseudomonas aeruginosa* PAO1 membrane proteome with emphasis on c-di-GMP turnover enzymes. *Microlife, 4*, uqad028.

Schirmer, T. (2016). C-di-GMP synthesis: structural aspects of evolution, catalysis and regulation. *J Mol Biol, 428*(19), 3683-3701.

Schirmer, T., and Jenal, U. (2009). Structural and mechanistic determinants of c-di-GMP signalling. *Nat Rev Microbiol, 7*(10), 724-735.

Schmidt, A., Hammerbacher, A. S., Bastian, M., Nieken, K. J., Klockgether, J., Merighi, M., Lapouge, K., Poschgan, C., Kölle, J., Acharya, K. R., Ulrich, M., Tümmler, B., Unden, G., Kaever, V., Lory, S., Haas, D., Schwarz, S., and Döring, G. (2016). Oxygen-dependent regulation of c-di-GMP synthesis by SadC controls alginate production in *Pseudomonas aeruginosa*. *Environ Microbiol, 18*(10), 3390-3402.

Schmidt, A. K., Fitzpatrick, A. D., Schwartzkopf, C. M., Faith, D. R., Jennings, L. K., Coluccio, A., Hunt, D. J., Michaels, L. A., Hargil, A., Chen, Q., Bollyky, P. L., Dorward, D. W., Wachter, J., Rosa, P. A., Maxwell, K. L., and Secor, P. R. (2022). A filamentous bacteriophage protein inhibits Type IV Pili to prevent superinfection of *Pseudomonas aeruginosa*. *mBio, 13*(1), e0244121.

Schmidt, T. G. M., Eichinger, A., Schneider, M., Bonet, L., Carl, U., Karthaus, D., Theobald, I., and Skerra, A. (2021). The role of changing loop conformations in streptavidin versions engineered for high-affinity binding of the Strep-tag II peptide. *J Mol Biol, 433*(9), 166893.

Schneider, J., Yepes, A., Garcia-Betancur, J. C., Westedt, I., Mielich, B., and López, D. (2012). Streptomycin-induced expression in *Bacillus subtilis* of YtnP, a lactonase-homologous protein that inhibits development and streptomycin production in *Streptomyces griseus*. *Appl Environ Microbiol, 78*(2), 599-603.

Schwanhäusser, B., Busse, D., Li, N., Dittmar, G., Schuchhardt, J., Wolf, J., Chen, W., and Selbach, M. (2011). Global quantification of mammalian gene expression control. *Nature, 473*(7347), 337-342.

Senkler, J., Senkler, M., Eubel, H., Hildebrandt, T., Lengwenus, C., Schertl, P., Schwarzländer, M., Wagner, S., Wittig, I., and Braun, H. P. (2017). The mitochondrial complexome of *Arabidopsis thaliana*. *Plant J, 89*(6), 1079-1092.

Shah, M., Taylor, V. L., Bona, D., Tsao, Y., Stanley, S. Y., Pimentel-Elardo, S. M., McCallum, M., Bondy-Denomy, J., Howell, P. L., Nodwell, J. R., Davidson, A. R., Moraes, T. F., and Maxwell, K. L. (2021). A phage-encoded anti-activator inhibits quorum sensing in *Pseudomonas aeruginosa*. *Mol Cell, 81*(3), 571-583.e576.

Shenoy, A. R., and Visweswariah, S. S. (2003). Site-directed mutagenesis using a single mutagenic oligonucleotide and DpnI digestion of template DNA. *Anal Biochem, 319*(2), 335-336.

Sintim, H. O., Smith, J. A., Wang, J., Nakayama, S., and Yan, L. (2010). Paradigm shift in discovering next-generation anti-infective agents: targeting quorum sensing, c-di-GMP signaling and biofilm formation in bacteria with small molecules. *Future Med Chem, 2*(6), 1005-1035.

Sinz, A. (2010). Investigation of protein-protein interactions in living cells by chemical crosslinking and mass spectrometry. *Anal Bioanal Chem, 397*(8), 3433-3440.

Sio, C. F., Otten, L. G., Cool, R. H., Diggle, S. P., Braun, P. G., Bos, R., Daykin, M., Cámara, M., Williams, P., and Quax, W. J. (2006). Quorum quenching by an N-acyl-homoserine lactone acylase from *Pseudomonas aeruginosa* PAO1. *Infect Immun, 74*(3), 1673-1682.

Skerra, A., and Schmidt, T. G. (2000). Use of the Strep-Tag and streptavidin for detection and purification of recombinant proteins. *Methods Enzymol, 326*, 271-304.

Skotnicka, D., Petters, T., Heering, J., Hoppert, M., Kaever, V., and Søgaard-Andersen, L. (2015). Cyclic di-GMP regulates type IV pilus-dependent motility in *Myxococcus xanthus*. *J Bacteriol, 198*(1), 77-90.

Smith, K. D., Shanahan, C. A., Moore, E. L., Simon, A. C., and Strobel, S. A. (2011). Structural basis of differential ligand recognition by two classes of bis-(3'-5')-cyclic dimeric guanosine monophosphate-binding riboswitches. *Proc Natl Acad Sci U S A, 108*(19), 7757-7762.

Sobti, M., Walshe, J. L., Wu, D., Ishmukhametov, R., Zeng, Y. C., Robinson, C. V., Berry, R. M., and Stewart, A. G. (2020). Cryo-EM structures provide insight into how *E. coli* F(1)F(o) ATP synthase accommodates symmetry mismatch. *Nat Commun, 11*(1), 2615.

Sommerfeldt, N., Possling, A., Becker, G., Pesavento, C., Tschowri, N., and Hengge, R. (2009). Gene expression patterns and differential input into curli fimbriae regulation of all GGDEF/EAL domain proteins in *Escherichia coli*. *Microbiology (Reading), 155*(Pt 4), 1318-1331.

Sondermann, H., Shikuma, N. J., and Yildiz, F. H. (2012). You've come a long way: c-di-GMP signaling. *Curr Opin Microbiol, 15*(2), 140-146.

Sowa, S. T., Vela-Rodríguez, C., Galera-Prat, A., Cázares-Olivera, M., Prunskaite-Hyyryläinen, R., Ignatev, A., and Lehtiö, L. (2020). A FRET-based high-throughput screening platform for the discovery of chemical probes targeting the scaffolding functions of human tankyrases. *Sci Rep, 10*(1), 12357.

Spagnolo, A. M., Sartini, M., and Cristina, M. L. (2021). *Pseudomonas aeruginosa* in the healthcare facility setting. *Reviews and Research in Medical Microbiology, 32*(3), 169-175.

Spangler, C., Böhm, A., Jenal, U., Seifert, R., and Kaever, V. (2010). A liquid chromatography-coupled tandem mass spectrometry method for quantitation of cyclic di-guanosine monophosphate. *J Microbiol Methods, 81*(3), 226-231.

Spaniol, B., Lang, J., Venn, B., Schake, L., Sommer, F., Mustas, M., Geimer, S., Wollman, F. A., Choquet, Y., Mühlhaus, T., and Schroda, M. (2022). Complexome profiling on the *Chlamydomonas lpa*2 mutant reveals insights into PSII biogenesis and new PSII associated proteins. *J Exp Bot, 73*(1), 245-262.

Srivastava, D., and Waters, C. M. (2012). A tangled web: regulatory connections between quorum sensing and cyclic di-GMP. *J Bacteriol, 194*(17), 4485-4493.

St Croix, C. M., Shand, S. H., and Watkins, S. C. (2005). Confocal microscopy: comparisons, applications, and problems. *Biotechniques, 39*(6 Suppl), S2-5.

Stanier, R. Y., Palleroni, N. J., and Doudoroff, M. (1966). The aerobic pseudomonads: a taxonomic study. *J Gen Microbiol, 43*(2), 159-271.

Stehr, F., Kretschmar, M., Kröger, C., Hube, B., and Schäfer, M. (2003). Microbial lipases as virulence factors. *Journal of Molecular Catalysis B: Enzymatic, 22*(5-6), 347-355.

Steiner, S., Lori, C., Boehm, A., and Jenal, U. (2013). Allosteric activation of exopolysaccharide synthesis through cyclic di-GMP-stimulated protein-protein interaction. *Embo j, 32*(3), 354-368.

Stelitano, V., Giardina, G., Paiardini, A., Castiglione, N., Cutruzzolà, F., and Rinaldo, S. (2013). C-di-GMP hydrolysis by *Pseudomonas aeruginosa* HD-GYP phosphodiesterases: analysis of the reaction mechanism and novel roles for pGpG. *PLoS One, 8*(9), e74920.

Stover, C. K., Pham, X. Q., Erwin, A. L., Mizoguchi, S. D., Warrener, P., Hickey, M. J., Brinkman, F. S., Hufnagle, W. O., Kowalik, D. J., Lagrou, M., Garber, R. L., Goltry, L., Tolentino, E., Westbrock-Wadman, S., Yuan, Y., Brody, L. L., Coulter, S. N., Folger, K. R., Kas, A., Larbig, K., Lim, R., Smith, K., Spencer, D., Wong, G. K., Wu, Z., Paulsen, I. T., Reizer, J., Saier, M. H., Hancock, R. E., Lory, S., and Olson, M. V. (2000). Complete genome sequence of *Pseudomonas aeruginosa* PAO1, an opportunistic pathogen. *Nature, 406*(6799), 959-964.

Studier, F. W., and Moffatt, B. A. (1986). Use of bacteriophage T7 RNA polymerase to direct selective high-level expression of cloned genes. *J Mol Biol, 189*(1), 113-130.

Sudarsan, N., Lee, E. R., Weinberg, Z., Moy, R. H., Kim, J. N., Link, K. H., and Breaker, R. R. (2008). Riboswitches in eubacteria sense the second messenger cyclic di-GMP. *Science, 321*(5887), 411-413.

Sun, C., Benlekbir, S., Venkatakrishnan, P., Wang, Y., Hong, S., Hosler, J., Tajkhorshid, E., Rubinstein, J. L., and Gennis, R. B. (2018). Structure of the alternative complex III in a supercomplex with cytochrome oxidase. *Nature, 557*(7703), 123-126.

Sutherland, I. W. (2001). The biofilm matrix-an immobilized but dynamic microbial environment. *Trends Microbiol, 9*(5), 222-227.

Swainsbury, D. J., Scheidelaar, S., van Grondelle, R., Killian, J. A., and Jones, M. R. (2014). Bacterial reaction centers purified with styrene maleic acid copolymer retain native membrane functional properties and display enhanced stability. *Angew Chem Int Ed Engl, 53*(44), 11803-11807.

Sydor, A. M., Czymmek, K. J., Puchner, E. M., and Mennella, V. (2015). Super-Resolution microscopy: From single molecules to supramolecular assemblies. *Trends Cell Biol, 25*(12), 730-748.

Tammam, S., Sampaleanu, L. M., Koo, J., Manoharan, K., Daubaras, M., Burrows, L. L., and Howell, P. L. (2013). PilMNOPQ from the *Pseudomonas aeruginosa* type IV pilus system form a transenvelope protein interaction network that interacts with PilA. *J Bacteriol, 195*(10), 2126-2135.

Tchigvintsev, A., Xu, X., Singer, A., Chang, C., Brown, G., Proudfoot, M., Cui, H., Flick, R., Anderson, W. F., Joachimiak, A., Galperin, M. Y., Savchenko, A., and Yakunin, A. F. (2010). Structural insight into the mechanism of c-di-GMP hydrolysis by EAL domain phosphodiesterases. *J Mol Biol, 402*(3), 524-538.

Thoma, J., and Burmann, B. M. (2020). Fake it 'till you make it-The pursuit of suitable membrane mimetics for membrane protein biophysics. *Int J Mol Sci, 22*(1).

Tielen, P., Rosenau, F., Wilhelm, S., Jaeger, K. E., Flemming, H. C., and Wingender, J. (2010). Extracellular enzymes affect biofilm formation of mucoid *Pseudomonas aeruginosa*. *Microbiology (Reading), 156*(Pt 7), 2239-2252.

Tischler, A. D., and Camilli, A. (2004). Cyclic diguanylate (c-di-GMP) regulates *Vibrio cholerae* biofilm formation. *Mol Microbiol, 53*(3), 857-869.

Tunuguntla, R., Bangar, M., Kim, K., Stroeve, P., Ajo-Franklin, C. M., and Noy, A. (2013). Lipid bilayer composition can influence the orientation of proteorhodopsin in artificial membranes. *Biophys J, 105*(6), 1388-1396.

Turner, L. R., Lara, J. C., Nunn, D. N., and Lory, S. (1993). Mutations in the consensus ATP-binding sites of XcpR and PilB eliminate extracellular protein secretion and pilus biogenesis in *Pseudomonas aeruginosa*. *J Bacteriol, 175*(16), 4962-4969.

Tusher, V. G., Tibshirani, R., and Chu, G. (2001). Significance analysis of microarrays applied to the ionizing radiation response. *Proc Natl Acad Sci U S A, 98*(9), 5116-5121.

Tyanova, S., Temu, T., Sinitcyn, P., Carlson, A., Hein, M. Y., Geiger, T., Mann, M., and Cox, J. (2016). The Perseus computational platform for comprehensive analysis of (prote)omics data. *Nat Methods, 13*(9), 731-740.

Ueda, A., and Wood, T. K. (2009). Connecting quorum sensing, c-di-GMP, Pel polysaccharide, and biofilm formation in *Pseudomonas aeruginosa* through tyrosine phosphatase TpbA (PA3885). *PLoS Pathog, 5*(6), e1000483.

Ueta, T., Kojima, K., Hino, T., Shibata, M., Nagano, S., and Sudo, Y. (2020). Applicability of styrene-maleic acid copolymer for two microbial rhodopsins, RxR and HsSRI. *Biophys J, 119*(9), 1760-1770.

Unbehend, N. (2022). Untersuchung der Interaktionspartner von NbdA aus *Pseudomonas aeruginosa* PAO1 mit Hilfe des bakteriellen two-hybrid-systems. (Bachelor thesis), RPTU, Kaiserslautern.

Valent, Q. A., Scotti, P. A., High, S., de Gier, J. W., von Heijne, G., Lentzen, G., Wintermeyer, W., Oudega, B., and Luirink, J. (1998). The *Escherichia coli* SRP and SecB targeting pathways converge at the translocon. *Embo j, 17*(9), 2504-2512.

Valentini, M., and Filloux, A. (2016a). Biofilms and cyclic di-GMP (c-di-GMP) signaling: lessons from *Pseudomonas aeruginosa* and other bacteria. *J Biol Chem, 291*(24), 12547-12555.

Valentini, M., Laventie, B. J., Moscoso, J., Jenal, U., and Filloux, A. (2016b). The diguanylate cyclase HsbD intersects with the HptB regulatory cascade to control *Pseudomonas aeruginosa* biofilm and motility. *PLoS Genet, 12*(10), e1006354.

Van Strien, J., Guerrero-Castillo, S., Chatzispyrou, I. A., Houtkooper, R. H., Brandt, U., and Huynen, M. A. (2019). COmplexome Profiling ALignment (COPAL) reveals remodeling of mitochondrial protein complexes in Barth syndrome. *Bioinformatics, 35*(17), 3083-3091.

Versantvoort, W., Guerrero-Castillo, S., Wessels, H., van Niftrik, L., Jetten, M. S. M., Brandt, U., Reimann, J., and Kartal, B. (2019). Complexome analysis of the nitrite-dependent methanotroph *Methylomirabilis lanthanidiphila*. *Biochim Biophys Acta Bioenerg, 1860*(9), 734-744.

Viruega-Góngora, V. I., Acatitla-Jácome, I. S., Zamorano-Sánchez, D., Reyes-Carmona, S. R., Xiqui-Vázquez, M. L., Baca, B. E., and Ramírez-Mata, A. (2022). The GGDEF-EAL protein CdgB from *Azospirillum baldaniorum* Sp245, is a dual function enzyme with potential polar localization. *PLoS One, 17*(11), e0278036.

Vold, R. R., Prosser, R. S., and Deese, A. J. (1997). Isotropic solutions of phospholipid bicelles: a new membrane mimetic for high-resolution NMR studies of polypeptides. *J Biomol NMR, 9*(3), 329-335.

Wagner, S., Baars, L., Ytterberg, A. J., Klussmeier, A., Wagner, C. S., Nord, O., Nygren, P. A., van Wijk, K. J., and de Gier, J. W. (2007). Consequences of membrane protein overexpression in *Escherichia coli*. *Mol Cell Proteomics, 6*(9), 1527-1550.

Waldron, E. J., Snyder, D., Fernandez, N. L., Sileo, E., Inoyama, D., Freundlich, J. S., Waters, C. M., Cooper, V. S., and Neiditch, M. B. (2019). Structural basis of DSF recognition by its receptor RpfR and its regulatory interaction with the DSF synthase RpfF. *PLoS Biol, 17*(2), e3000123.

Walian, P. J., Allen, S., Shatsky, M., Zeng, L., Szakal, E. D., Liu, H., Hall, S. C., Fisher, S. J., Lam, B. R., Singer, M. E., Geller, J. T., Brenner, S. E., Chandonia, J. M., Hazen, T. C., Witkowska, H. E., Biggin, M. D., and Jap, B. K. (2012). High-throughput isolation and characterization of untagged membrane protein complexes: outer membrane complexes of *Desulfovibrio vulgaris*. *J Proteome Res, 11*(12), 5720-5735.

Wang, B. X., Cady, K. C., Oyarce, G. C., Ribbeck, K., and Laub, M. T. (2021). Two-component signaling systems regulate diverse virulence-associated traits in *Pseudomonas aeruginosa*. *Appl Environ Microbiol, 87*(11).

Wang, D., Chen, W., Huang, S., He, Y., Liu, X., Hu, Q., Wei, T., Sang, H., Gan, J., and Chen, H. (2017). Structural basis of Zn(II) induced metal detoxification and antibiotic resistance by histidine kinase CzcS in *Pseudomonas aeruginosa*. *PLoS Pathog, 13*(7), e1006533.

Wang, Y., Fan, H., and Tong, Y. (2023). Unveil the secret of the bacteria and phage arms race. *Int J Mol Sci, 24*(5).

Wang, Y., Hay, I. D., Rehman, Z. U., and Rehm, B. H. (2015a). Membrane-anchored MucR mediates nitrate-dependent regulation of alginate production in *Pseudomonas aeruginosa*. *Appl Microbiol Biotechnol, 99*(17), 7253-7265.

Wang, Z., and Celis, E. (2015b). STING activator c-di-GMP enhances the anti-tumor effects of peptide vaccines in melanoma-bearing mice. *Cancer Immunol Immunother, 64*(8), 1057-1066.

Watnick, P., and Kolter, R. (2000). Biofilm, city of microbes. *J Bacteriol, 182*(10), 2675-2679.

Weber, H., Pesavento, C., Possling, A., Tischendorf, G., and Hengge, R. (2006). Cyclic-di-GMP-mediated signalling within the sigma network of *Escherichia coli*. *Mol Microbiol, 62*(4), 1014-1034.

Webster, S. S., Lee, C. K., Schmidt, W. C., Wong, G. C. L., and O'Toole, G. A. (2021). Interaction between the type 4 pili machinery and a diguanylate cyclase fine-tune c-di-GMP levels during early biofilm formation. *Proc Natl Acad Sci U S A, 118*(26).

Webster, S. S., Mathelié-Guinlet, M., Verissimo, A. F., Schultz, D., Viljoen, A., Lee, C. K., Schmidt, W. C., Wong, G. C. L., Dufrêne, Y. F., and O'Toole, G. A. (2022). Force-induced changes of PilY1 drive surface sensing by *Pseudomonas aeruginosa*. *mBio, 13*(1), e0375421.

Wessels, H. J., Vogel, R. O., van den Heuvel, L., Smeitink, J. A., Rodenburg, R. J., Nijtmans, L. G., and Farhoud, M. H. (2009). LC-MS/MS as an alternative for SDS-PAGE in blue native analysis of protein complexes. *Proteomics, 9*(17), 4221-4228.

Whitchurch, C. B., Hobbs, M., Livingston, S. P., Krishnapillai, V., and Mattick, J. S. (1991). Characterisation of a *Pseudomonas aeruginosa* twitching motility gene and evidence for a specialised protein export system widespread in eubacteria. *Gene, 101*(1), 33-44.

Whitfield, G. B., Marmont, L. S., Ostaszewski, A., Rich, J. D., Whitney, J. C., Parsek, M. R., Harrison, J. J., and Howell, P. L. (2020). Pel Polysaccharide Biosynthesis Requires an Inner Membrane Complex Comprised of PelD, PelE, PelF, and PelG. *J Bacteriol, 202*(8).

Wigren, E., Liang, Z. X., and Römling, U. (2014). Finally! The structural secrets of a HD-GYP phosphodiesterase revealed. *Mol Microbiol, 91*(1), 1-5.

Wilmaerts, D., Windels, E. M., Verstraeten, N., and Michiels, J. (2019). General mechanisms leading to persister formation and awakening. *Trends Genet, 35*(6), 401-411.

Winsor, G. L., Griffiths, E. J., Lo, R., Dhillon, B. K., Shay, J. A., and Brinkman, F. S. (2016). Enhanced annotations and features for comparing thousands of *Pseudomonas* genomes in the *Pseudomonas* genome database. *Nucleic Acids Res, 44*(D1), D646-653.

Wright, T. A., Jiang, L., Park, J. J., Anderson, W. A., Chen, G., Hallberg, Z. F., Nan, B., and Hammond, M. C. (2020). Second messengers and divergent HD-GYP phosphodiesterases regulate 3',3'-cGAMP signaling. *Mol Microbiol, 113*(1), 222-236.

Xie, K., and Dalbey, R. E. (2008). Inserting proteins into the bacterial cytoplasmic membrane using the Sec and YidC translocases. *Nat Rev Microbiol, 6*(3), 234-244.

Xin, L., Zeng, Y., Sheng, S., Chea, R. A., Liu, Q., Li, H. Y., Yang, L., Xu, L., Chiam, K. H., and Liang, Z. X. (2019). Regulation of flagellar motor switching by c-di-GMP phosphodiesterases in *Pseudomonas aeruginosa*. *J Biol Chem, 294*(37), 13789-13799.

Xing, S., Wallmeroth, N., Berendzen, K. W., and Grefen, C. (2016). Techniques for the analysis of protein-protein interactions *in vivo*. *Plant Physiol, 171*(2), 727-758.

Xu, G., Zhou, L., Qian, G., and Liu, F. (2022). Diguanylate cyclase and phosphodiesterase interact to maintain the specificity of cyclic di-GMP signaling in the regulation of antibiotic synthesis in *Lysobacter enzymogenes*. *Appl Environ Microbiol, 88*(2), e0189521.

Xu, K., Zhang, M., Zhao, Q., Yu, F., Guo, H., Wang, C., He, F., Ding, J., and Zhang, P. (2013). Crystal structure of a folate energy-coupling factor transporter from *Lactobacillus brevis*. *Nature, 497*(7448), 268-271.

Xu, L., Xin, L., Zeng, Y., Yam, J. K., Ding, Y., Venkataramani, P., Cheang, Q. W., Yang, X., Tang, X., Zhang, L. H., Chiam, K. H., Yang, L., and Liang, Z. X. (2016). A cyclic di-GMP-binding adaptor protein interacts with a chemotaxis methyltransferase to control flagellar motor switching. *Sci Signal, 9*(450), ra102.

Yang, Z., Wang, C., Zhou, Q., An, J., Hildebrandt, E., Aleksandrov, L. A., Kappes, J. C., DeLucas, L. J., Riordan, J. R., Urbatsch, I. L., Hunt, J. F., and Brouillette, C. G. (2014). Membrane protein stability can be compromised by detergent interactions with the extramembranous soluble domains. *Protein Sci, 23*(6), 769-789.

Yu, C., and Huang, L. (2018). Cross-linking mass spectrometry: An emerging technology for interactomics and structural biology. *Anal Chem, 90*(1), 144-165.

Zemke, A. C., D'Amico, E. J., Snell, E. C., Torres, A. M., Kasturiarachi, N., and Bomberger, J. M. (2020). Dispersal of epithelium-associated *Pseudomonas aeruginosa* biofilms. *mSphere, 5*(4).

Zhang, S., Wang, J., Fan, Y., Meng, W., Qian, C., Liu, P., Wei, Y., Yuan, C., Du, Y., and Yin, Z. (2022). YciR, a specific 3'-phosphodiesterase, plays a role in the pathogenesis of uropathogenic *Escherichia coli* CFT073. *Front Microbiol, 13*, 910906.

Zhang, Z., Kim, S., Gaffney, B. L., and Jones, R. A. (2006). Polymorphism of the signaling molecule c-di-GMP. *J Am Chem Soc, 128*(21), 7015-7024.

Zhang, Z., Liu, J., Xiao, M., Zhang, Q., Liu, Z., Liu, M., Zhang, P., and Zeng, Y. (2023). Peptide nanotube loaded with a STING agonist, c-di-GMP, enhance cancer immunotherapy against melanoma. *Nano Res, 16*(4), 5206-5215.

Zogaj, X., Bokranz, W., Nimtz, M., and Römling, U. (2003). Production of cellulose and curli fimbriae by members of the family *Enterobacteriaceae* isolated from the human gastrointestinal tract. *Infect Immun, 71*(7), 4151-4158.

Appendix

Table A1: Fraction volumes in the proteome library

Table A1: Fraction sizes in Complexome "✓" = measured in MS, "-" = not measured in MS. Elution volume states the start elution volume of the fraction.

Elution volume [ml]	Fraction number	Fraction size [ml]	replicate 1	replicate 2	replicate 3
8.22	-2	1	-	✓	✓
9.22	-1	1	-	✓	✓
10.22	1	0.5	✓	✓	✓
10.72	2	0.5	✓	✓	✓
11.22	3	0.25	✓	✓	✓
11.47	4	0.25	✓	✓	✓
11.72	5	0.25	✓	✓	✓
11.97	6	0.25	✓	✓	✓
12.22	7	0.25	✓	✓	✓
12.47	8	0.25	✓	✓	✓
12.72	9	0.25	✓	✓	✓
12.97	10	0.25	✓	✓	✓
13.22	11	0.25	✓	✓	✓
13.47	12	0.25	✓	✓	✓
13.72	13	0.25	✓	✓	✓
13.97	14	0.25	✓	✓	✓
14.22	15	0.25	✓	✓	✓
14.47	16	0.25	✓	✓	✓
14.72	17	0.25	✓	✓	✓
14.97	18	0.25	✓	✓	✓
15.22	19	0.25	✓	✓	✓
15.47	20	0.25	✓	✓	✓
15.72	21	0.25	✓	✓	✓
15.97	22	0.25	✓	✓	✓
16.22	23	0.25	✓	✓	✓
16.47	24	0.25	✓	✓	✓
16.72	25	0.25	✓	✓	✓
16.97	26	0.25	✓	✓	✓
17.22	27	0.5	-	✓	✓
17.72	28	0.5	-	✓	✓
18.22	29	0.5	-	✓	✓
18.72	30	0.5	-	✓	✓
19.22	31	0.5	-	✓	✓
19.72	32	0.5	-	✓	✓
20.22	33	0.5	-	✓	✓
20.72	34	0.5	-	✓	✓
21.22	35	0.5	-	✓	✓
21.72	36	0.5	-	✓	✓
22.22	37	0.5	-	✓	✓
22.72	38	0.5	-	✓	✓
23.22					

Table A2 Described membrane complexes

Table A2 Described membrane complexes. The complexes were tested for co-elution, correlation, and clustering. Locus Tag and Gene name obtained from Pseudomonas Genome DB (Winsor *et al.*, 2016), (-) not in database, (*) = associated to the complex, T4P = type IV pili, T2SS = type II secretion system, T6SS = Type VI secretion system.

Complex	Locus Tag	Gene name
ABC transporter triBC	PA0156	*triA*
	PA0157	*triB*
	PA0158	*triC*
ABC-like transporter substrate binding	PA0888	*aotJ* *
ABC-like transporter	PA0889	*aotQ*
	PA0890	*aotM*
	PA0892	*aotP*
ATP synthase (complex V)	PA5559	*atpE*
	PA5558	*atpF*
	PA5560	*atpB*
	PA5555	*atpG*
	PA5553	*atpC*
	PA5557	*atpH*
	PA5554	*atpD*
	PA5556	*atpA*
branched-chain amino acid transport	PA1070	*braG*
	PA1071	*braF*
	PA1072	*braE*
	PA1073	*braD*
	PA1074	*braC*
cytochrome bc1 (complex III)	PA4430	-
	PA4431	-
	PA4429	-
cytochrome oxidase cbb3.1 (complex IV)	PA1552	*ccoP1*
	PA1553	*ccoO1*
	PA1554	*ccoN1*
	PA4133	*ccoN;fixN;cytN**
	PA0105	*coxB**
	PA1555	*ccoP2*
	PA1555.1	*ccoQ2*
	PA1556	*ccoO2*
	PA1557	*ccoN2*
flagella motor	PA1101	*fliF*
	PA1444	*fliN*
	PA1102	*fliG*
	PA1443	*fliM*
flagella stator	PA4953	*motB*
	PA4954	*motA*
FtsQLB cell division	PA4419	*ftsL*
	PA4409	*ftsQ*
	-	*ftsB*
LptBFGC system	PA3828	*lptF*
	PA4459	*lptC*

	PA4461	*lptB*
macroglobulin	PA4488	*magE*
	PA4491	*magB*
	PA4487	*magF*
	PA4489	*magD*
	PA4492	*magA*
MexAB-OprM efflux pump	PA0427	*oprM*
	PA0426	*mexB*
	PA0425	*mexA*
minCD-ftsz cell division	PA3243	*minC*
	PA3244	*minD*
	PA4407	*ftsZ*
NADH dehydrogenase (complex I)	PA2649	*nuoN*
	PA2643	*nuoH*
	PA2647	*nuoL*
	PA2637	*nuoA*
	PA2648	*nuoM*
	PA2645	*nuoJ*
	PA2644	*nuoI*
	PA2641	*nuoF*
	PA2638	*nuoB*
	PA2640	*nuoE*
	PA2642	*nuoG*
	PA2639	*nuoD*
NarGHI	PA3875	*narG*
	PA3874	*narH*
	PA3872	*narI*
NorCB	PA0524	*norB*
	PA0523	*norC*
SEC-SRP	PA4243	*secY*
	PA3821	*secD*
	PA0373	*ftsY*
	PA3820	*secF*
	PA5568	*yidC*
	PA4403	*secA*
	PA3822	*yajC*
	PA4747	*secG*
	PA5128	*secB*
succinat dehydrogenase (complex II)	PA1582	*sdhD*
	PA1581	*sdhC*
	PA1583	*sdhA*
	PA1584	*sdhB*
T2SS-XcpRSYZ-P	PA3102	*xcpS*
	PA3103	*xcpR*
	PA3096	*xcpY*
	PA3104	*xcpP*
	PA3095	*xcpZ*
T2SS-XcpVWX	PA3098	*xcpW*
	PA3097	*xcpX*
	PA3099	*xcpV*

T4P assembly	PA5044	*pilM*
	PA5043	*pilN*
	PA5042	*pilO*
	PA5041	*pilP*
	PA4525	*pilA*
T4P motor	PA4526	*pilB*
	PA0395	*pilT*
	PA0396	*pilU*
T6SS	PA0077	*icmF1*
	PA0078	*tssL1*
	PA0090	*clpV1*
	PA0085	*hcp1**
	PA0080	*tssJ1**
T6SS -Reg	PA0081	*fha1*
	PA0075	*pppA*
	PA0074	*ppkA*
TatABC	PA5070	*tatC*
	PA5069	*tatB*
	PA5068	*tatA*
Transporter DppBCDF	PA4503	*dppB*
	PA4504	*dppC*
	PA4505	*dppD*
	PA4506	*dppF*
Transporter DppBCDF substrate binding	PA4496	*dppA1**

Table A3 Identified GGDEF/EAL/HD-GYP domain proteins and c-di-GMP effectors

Table A3: Proteins involved in c-di-GMP signalling. Identified proteins with GGDEF/EAL/HD-GYP domains and c-di-GMP effectors. Predicted localisation of the proteins taken from Pseudomonas Genome DB (Winsor *et al.* 2016), where only highest confidence class was considered. CM = cytoplasmic membrane, C = cytoplasmic. Additional domains and activity from Valentini *et al.*, 2016a. List of described c-di-GMP effectors from Valentini *et al.*, 2016a, and Banerjee *et al.*, 2021.

	Locus Tag	Name	additional domains	identified in replicate	localisation	activity
GGDEF domain containing						
1	PA0290	-	PAS	BC	cm	ND
2	PA0847	-	TM, Chase4, HAMP, PAS	ABC	cm	DGC
3	PA1107	RoeA	TM	C	cm	DGC
4	PA1120	YfiN,TtpbB	HAMP	ABC	cm	DGC
5	PA1851	-	TM	B	cm	ND
6	PA2771	Dcsbis	GAF	BC	cm	ND
7	PA2870	-	TM	BC	cm	DGC
8	PA3343	HsbD	TM	ABC	cm	DGC
9	PA3702	WspR	Rec	ABC	c	DGC
10	PA4332	SadC	TM	C	cm	DGC
11	PA4843	AcbA, GcbA	Rec	AC	c	DGC
12	PA4929	NicD	7TMR_DISM	AC	cm	DGC

13	PA5487	DgcP		ABC	c	DGC
GGDEF-EAL domain containing						
14	PA0285	-	TM, PAS	ABC	cm	ND
15	PA0575	RmcA	PBPb, TM, PAS	AC	cm	ND
16	PA0861	RbdA	TM, PAS	ABC	cm	PDE
17	PA1181	-	MASE, PAS	ABC	cm	ND
18	PA1433	LapD	HAMP	ABC	cm	-
19	PA2072	-	Chase4, TM, PAS	ABC	cm	PDE
20	PA2567	-	GAF	ABC	cm	PDE
21	PA3311	NbdA	TM, MHYT	ABC	cm	PDE
22	PA4367	BifA	TM	ABC	cm	PDE
23	PA4601	MorA	TM, PAS	C	cm	ND
24	PA4959	FimX	PAS	ABC	cm	-
25	PA5017	DipA	PAS, GAF	B	cm	PDE
EAL domain containing						
26	PA2818	Arr	TM	ABC	cm	PDE
27	PA3825	-	-	ABC	cm	PDE
HD-GYP domain						
28	PA2572	-	Rec	ABC	c	-
29	PA4781	-	Rec	ABC	c	PDE
Effector proteins						
	PA1097	FleQ	Unknown	ABC	c	
	PA2799	-	PilZ domain	B	c	
	PA2960	PilZ	PilZ domain	ABC	u	
	PA2989	-	PilZ domain	ABC	c	
	PA3353	FlgZ	PilZ domain	ABC	c	
	PA4608	MapZ	PilZ domain	ABC	c	
	PA4878	BrlR	Unknown	BC	c	
	PA4958	FimW	Unknown	ABC	c	
	PA5346	SadB	Unknown	ABC	c	

Table A4: significant enriched proteins identified in NbdA pulldown

Table A4: Locus tag and name derived from the Pseudomonas Genome DB (Winsor *et al.*, 2016). Highly significant FDR < 0.01 (red), significance level FDR < 0.05 (orange). The tested proteins were highlighted bold.

Locus Tag	Name	*p*-value	Fold change	Highly significant	localisation
PA3579		2.84	6.45	+	c
PA4200		**5.41**	**5.40**	**+**	**c**
PA3311	***nbdA***	**6.29**	**5.05**	**+**	**cm**
PA1430	*lasR*	4.67	4.89	+	c
PA2523	***czcR***	**6.96**	**4.83**	**+**	**c**
PA3913	*yhbU*	6.34	4.75	+	c
PA3277		5.84	4.73	+	c
PA0341	*lgt*	4.50	4.51	+	cm
PA4967	*parE*	5.88	4.32	+	c

PA2462		5.54	3.90	+	omv
PA3725	*recJ*	4.07	3.83	+	c
PA5446		4.45	3.82	+	u
PA1462		5.19	3.71	+	cm
PA2728		2.75	3.52	+	c
PA3042		1.68	3.38	+	u
PA1041		1.76	3.34	+	om
PA5095		1.48	3.29	+	cm
PA3314		5.78	3.26	+	cm
PA3477	*rhlR*	6.01	3.22	+	c
PA0998	*pqsC*	7.22	3.21	+	c
PA2648	*nuoM*	5.51	3.18	+	cm
PA2707		4.64	3.17	+	c
PA1009		3.99	3.16	+	c
PA4931	*dnaB*	5.39	3.12	+	c
PA5093		2.70	3.11	+	c
PA0336	*rppH*	3.05	3.07	+	c
PA5365	*phoU*	6.65	3.05	+	c
PA1897		3.29	3.04	+	cm
PA1003	*mvfR*	2.03	3.01	+	cm
PA5504		1.54	2.99	+	cm
PA0967	*ruvB*	7.37	2.98	+	c
PA2762		1.30	2.96	+	u
PA2727		2.93	2.96	+	c
PA0352	*yicE*	3.99	2.95	+	cm
PA4666	*hemA*	3.12	2.95	+	c
PA0995	*ogt*	2.78	2.93	+	c
PA5279		4.04	2.92	+	c
PA3708	*wspA*	2.59	2.91	+	omv
PA5042	*pilO*	1.55	2.91	+	cm
PA4438	*yhcM*	2.30	2.89	+	c
PA3151	*hisF2*	1.74	2.86	+	c
PA1361	*norM*	1.60	2.84	+	cm
PA5563	*soj*	3.77	2.84	+	cm
PA2754		8.05	2.83	+	u
PA4224	*pchG*	3.33	2.83	+	c
PA4361		3.37	2.81	+	c
PA2402	*pvdI*	5.34	2.79	+	u
PA4555	*pilY2*	4.41	2.78	+	u
PA4145		4.23	2.78	+	c
PA1663	*sfa2*	4.42	2.77	+	c
PA5094		2.41	2.77	+	cm
PA2637	*nuoA*	0.90	2.76	+	cm
PA4811	*fdnH*	5.30	2.76	+	p
PA1373	*fabF2*	3.40	2.75	+	c
PA2573		0.75	2.72	+	om
PA2969	*plsX*	4.13	2.72	+	c
PA3153	*wzx*	1.45	2.71	+	cm
PA4609	*radA*	5.28	2.68	+	u
PA2983		2.10	2.65	+	omv
PA3826		4.21	2.61	+	cm
PA2725		3.08	2.61	+	c
PA5299		4.45	2.60	+	c
PA2438		1.43	2.60	+	u
PA0363	*coaD*	2.37	2.60	+	c
PA4408	*ftsA*	6.03	2.60	+	c
PA5512	*mifS*	1.51	2.58	+	cm
PA2231	*pslA*	3.83	2.55	+	cm
PA5340		1.62	2.55	+	u
PA0374	*ftsE*	1.97	2.54	+	cm
PA3696		3.34	2.53	+	u
PA2453		1.51	2.53	+	omv

PA3933	*betT3*	1.80	2.50	+	cm
PA2824	*sagS*	2.48	2.49	+	c
PA0415	*chpC*	5.23	2.48	+	u
PA4187	*yaaU*	1.68	2.47	+	cm
PA4954	*motA*	1.44	2.47	+	cm
PA1636	*kdpD*	1.07	2.46	+	cm
PA1532	*dnaX*	4.51	2.44	+	c
PA3485	*tsi3*	4.73	2.43	+	u
PA2629	*purB*	1.11	2.41	+	c
PA0090	*clpV1*	6.28	2.41	+	c
PA4385	*groEL*	3.76	2.40	+	omv
PA3365	*amiB*	4.40	2.40	+	c
PA5468		1.37	2.39	+	cm
PA5367	*pstA*	1.34	2.39	+	cm
PA2857		2.66	2.38	+	cm
PA4999	*waaL*	4.67	2.37	+	cm
PA0778	icp	3.46	2.37	+	u
PA0889	aotQ	1.48	2.37	+	cm
PA3189	gltF	3.39	2.37	+	cm
PA4214; PA1903	phzE1; phzE2	3.52	2.36	+	-
PA4503	dppB	1.22	2.36	+	omv
PA4946	mutL	5.94	2.36	+	c
PA5036	*gltB*	4.00	2.35	+	c
PA0575	*rmcA*	2.53	2.35	+	cm
PA3724	*lasB*	3.13	2.34	+	e
PA3838		1.32	2.33	+	omv
PA5313	*gabT2*	2.62	2.32	+	c
PA0524	*norB*	2.07	2.31	+	cm
PA4528	*pilD*	1.09	2.31	+	cm
PA0304	*spuH*	1.52	2.30	+	cm
PA5379	*sdaB*	2.34	2.30	+	c
PA0392	*yggT*	1.37	2.30	+	cm
PA1277	*cobQ*	3.20	2.29	+	c
PA1097	***fleQ***	**6.22**	**2.29**	**+**	**c**
PA5056	*phaC1*	2.56	2.27	+	c
PA2966	*acpP*	0.97	2.26	+	c
PA1045		4.18	2.26	+	c
PA2555		3.71	2.25	+	c
PA0281	*cysW*	3.24	2.24	+	cm
PA0303	*spuG*	1.28	2.24	+	cm
PA0267		4.12	2.23	+	c
PA4812	*fdnG*	2.87	2.22	+	omv
PA0345		1.68	2.22	+	cm
PA4444	*mltB1*	4.39	2.21	+	cm
PA2823		3.89	2.21	+	c
PA5002	*dnpA*	1.05	2.21	+	c
PA5000	*wapR*	3.53	2.20	+	cm
PA0396	*pilU*	3.25	2.20	+	c
PA0337	*ptsP*	4.42	2.18	+	c
PA3263	*yaiD*	4.30	2.17	+	p
PA3802	*hisS*	2.25	2.16	+	c
PA1246	*aprD*	2.13	2.15	+	cm
PA4321		1.39	2.14	+	u
PA1889		1.52	2.13	+	u
PA5252	*yheS*	3.21	2.13	+	c
PA5121		1.59	2.13	+	cm
PA0105	*coxB*	2.49	2.12	+	cm
PA4455	*yrbE*	1.55	2.11	+	omv
PA5022	*aefA*	2.60	2.10	+	omv
PA3643	*lpxB*	1.24	2.10	+	c
PA2651		1.25	2.09	+	cm
PA1667	*hsiJ2*	2.19	2.09	+	c

PA5529		3.64	2.09	+	cm
PA2627	*ycfC*	1.29	2.08	+	u
PA3141	*wbpM*	1.79	2.08	+	omv
PA0399		3.45	2.08	+	c
PA2810	*copS*	2.64	2.08	+	cm
PA2449	*gcsR*	2.92	2.07	+	c
PA4787		4.34	2.05	+	c
PA3875	*narG*	2.93	2.05	+	omv
PA1428	*yjaB*	4.09	2.05	+	c
PA3071		3.66	2.04	+	c
PA2234	*pslD*	2.60	2.04	+	omv
PA2435		1.67	2.00	+	cm
PA3813	*iscU*	3.62	1.99	+	c
PA1126		4.69	1.98	+	cm
PA3346	*hsbR*	3.64	1.96	+	c
PA0877		2.40	1.95	+	c
PA5353	*glcF*	2.14	1.95	+	cm
PA5208		3.59	1.94	+	c
PA3161	*himD*	3.46	1.93	+	c
PA3271		2.12	1.93	+	omv
PA0176	*aer2; mcpB*	3.48	1.92	+	c
PA4505	*dppD*	2.59	1.92	+	omv
PA2996	*nqrD*	2.80	1.91	+	cm
PA4526	***pilB***	**3.01**	**1.88**	**+**	**c**
PA2329		3.02	1.87	+	cm
PA5323	*argB*	3.72	1.87	+	c
PA4234	*uvrA*	6.01	1.87	+	c
PA3746	*ffh*	4.69	1.86	+	cm
PA5438		4.08	1.78	+	c
PA4233	*yajR*	3.89	1.77	+	omv
PA2542	*ytfN*	0.79	2.15		om
PA1959	*bacA*	1.17	2.07		cm
PA5370		0.72	2.04		cm
PA4492	*magA*	0.72	2.04		cm
PA3676	*mexK*	1.17	1.97		cm
PA0920		1.41	1.93		cm
PA2478	*dsbD2; dipZ2*	0.94	1.93		cm
PA0913	*mgtE*	1.21	1.92		omv
PA0020	*tsaP*	1.63	1.92		u
PA1057	*shaD*	1.42	1.92		u
PA1072	*braE*	0.84	1.89		cm
PA2237	*pslG*	1.25	1.88		cm
PA0280	*cysA*	1.03	1.87		cm
PA0307		1.61	1.86		u
PA1611		1.66	1.85		c
PA5194		0.82	1.84		cm
PA2604	*yccA*	1.64	1.84		cm
PA1222	*mltA*	1.60	1.84		om
PA4807	*selB*	2.18	1.84		c
PA2583		1.73	1.83		cm
PA4564	*creA*	0.91	1.83		u
PA1615		0.96	1.82		cm
PA2323	*gapN*	2.92	1.81		c
PA0861	*rbdA*	2.13	1.81		cm
PA3211		1.32	1.81		cm
PA3000	*aroP1*	1.23	1.80		cm
PA5170	*arcD*	1.26	1.80		cm
PA0560	*ygjP*	2.15	1.80		c
PA1446	*fliP*	1.10	1.80		cm
PA4725	*cbrA*	1.62	1.79		cm
PA1207	*kefB*	1.59	1.79		cm
PA4218	*ampP*	0.58	1.78		cm

PA4332	***sadC***	**1.24**	**1.78**	**cm**
PA2382	*lldA*	2.76	1.78	c
PA4278		1.02	1.78	u
PA5025	*metY*	1.64	1.78	c
PA5345	*recG*	2.05	1.77	c
PA4684		1.68	1.75	c
PA4197	*bfiS*	3.33	1.75	cm
PA3363	*amiR*	4.42	1.75	c
PA0771	*era*	1.27	1.74	cm
PA2620	*clpA*	4.19	1.74	c
PA1341	*aatQ*	0.59	1.73	cm
PA1822	*fimL*	3.68	1.73	c
PA0487	*modR;modE*	4.15	1.72	c
PA4175	*piv*	1.77	1.72	e
PA5108		0.59	1.71	u
PA4770	*lldP*	1.87	1.71	cm
PA5358	*ubiA*	1.18	1.71	cm
PA4219	*ampO*	0.86	1.71	cm
PA4398		1.75	1.70	cm
PA4583	*rtcB*	2.53	1.70	c
PA0004	*gyrB*	5.91	1.70	c
PA0180	*cttP*	1.25	1.69	cm
PA2263	*kguD;yiaE*	2.00	1.69	c
PA5338	*spoT*	4.20	1.68	c
PA3710		2.43	1.68	cm
PA4506	*dppF*	1.97	1.66	omv
PA2491	*mexS*	2.48	1.66	c
PA1044		0.99	1.66	cm
PA1818	*cadA*	2.65	1.66	c
PA5452	*wbpW*	3.22	1.66	c
PA5307		0.87	1.66	u
PA2683	*tdcB*	3.13	1.65	c
PA4614	*mscL*	1.23	1.65	omv
PA1885		2.04	1.65	u
PA2541		1.07	1.65	cm
PA0406	*tonB3*	2.06	1.65	u
PA2789		1.12	1.64	cm
PA2063		1.98	1.64	u
PA1969		1.81	1.64	omv
PA1723	*pscJ*	2.51	1.63	om
PA1161	*rrmA*	2.27	1.63	c
PA0158	*triC*	1.32	1.63	cm
PA1557	*ccoN2*	0.72	1.63	cm
PA1831		2.62	1.62	c
PA0074	*ppkA*	2.45	1.62	omv
PA2611	*cysG*	1.09	1.61	c
PA5296	*rep*	2.23	1.61	c
PA3342		1.97	1.61	c
PA1526		2.76	1.61	c
PA4373		4.11	1.61	cm
PA2097		1.28	1.61	c
PA3819	*ycfJ*	1.25	1.61	u
PA0928	*gacS*	1.35	1.60	cm
PA3026		1.67	1.59	c
PA0534	*pauB1*	1.18	1.59	u
PA5318		2.80	1.59	c
PA1083	*flgH*	1.46	1.59	om
PA0486	*yihE*	1.39	1.59	c
PA4418	*ftsI*	1.40	1.59	cm
PA3147	*wbpJ*	1.30	1.58	omv
PA4016		1.29	1.58	u
PA4604	*yjiA*	2.20	1.58	c

PA2858	*ybbP*	1.49	1.57		cm
PA2647	*nuoL*	0.82	1.57		cm
PA3562	*fruI*	1.80	1.57		c
PA0934	*relA*	3.89	1.57		c
PA1552.1; PA1555.1	*ccoQ1, ccoQ2*	1.41	1.56		-
PA5513	*poxA*	3.58	1.56		c
PA3878	*narX*	2.24	1.56		omv
PA0797		2.38	1.55		c
PA5308	*lrp*	5.10	1.55		c
PA2982		2.75	1.54		u
PA1180	*phoQ*	1.04	1.54		omv
PA4117	*bphP*	3.93	1.54		cm
PA4722		2.32	1.54		c
PA5008	*wapP*	0.79	1.54		c
PA1666	*lip2*	0.96	1.54		u
PA0365	*laoB*	0.78	1.54		cm
PA5510		0.96	1.53		cm
PA1095	*fliS*	3.72	1.53		c
PA4133	*ccoN; fixN; cytN*	0.56	1.53		cm
PA2526	*muxC*	1.27	1.53		cm
PA0595	*lptD*	1.17	1.53		omv
PA0294	*aguR*	4.81	1.52		c
PA1760		3.33	1.52		c
PA5040	*pilQ*	2.82	1.51		omv
PA1745		3.08	1.50		u
PA1031	*yigN*	1.89	1.50		u
PA0390	*metX*	1.75	1.50		c
PA3859		0.49	1.50		u
PA2705		2.83	1.50		c
PA4461	*lptB*	1.96	1.50		omv
PA3764	*yfhD*	1.46	1.49		c
PA0102		2.83	1.49		c
PA4112		1.99	1.49		c
PA0401	*pyrC'; pyrX*	2.10	1.49		c
PA1647		4.47	1.48		cm
PA3876	*narK2*	1.82	1.48		cm
PA0402	*pyrB*	3.18	1.47		c
PA3974	*ladS*	1.85	1.47		cm
PA1947	*rbsA*	2.14	1.47		cm
PA1099	*fleR*	1.67	1.47		c
PA5130	*yibN*	1.50	1.47		omv
PA1454	*fleN*	1.24	1.47		cm
PA4023	*eat*	0.65	1.47		cm
PA2000	*dhcB*	3.01	1.45		c
PA3233		4.08	1.45		c
PA4439	*trpS*	0.72	1.44		c
PA2643	*nuoH*	1.04	1.44		cm
PA4845	*dipZ*	1.73	1.43		cm
PA4481	*mreB*	5.58	1.43		omv
PA4454	*yrbD*	1.21	1.43		omv
PA3099	*xcpV*	0.94	1.43		cm
PA5411	*gbcB*	2.22	1.43		c
PA1064		1.00	1.43		omv
PA1920	*nrdD*	3.83	1.43		c
PA4055	*ribC*	1.77	1.42		c
PA0126		1.19	1.42		omv
PA3617	*recA*	6.60	1.41		omv
PA1679		1.41	1.41		c
PA2220	*oprR*	1.74	1.41		c
PA4413	*ftsW*	1.06	1.41		cm
PA3335		4.18	1.41		c

PA0285		1.78	1.40	cm
PA0001	*dnaA*	3.89	1.40	c
PA3187	*gltK*	3.16	1.39	omv
PA5368	*pstC*	0.97	1.39	cm
PA0357	*mutM*	1.94	1.38	c
PA2709	*cysK*	1.07	1.38	c
PA1755		2.75	1.38	u
PA0600	*agtS*	2.48	1.37	u
PA0413	*chpA*	6.35	1.37	c
PA1640		2.19	1.37	c
PA5366	*pstB*	2.05	1.37	cm
PA5013	*ilvE*	0.89	1.37	c
PA1880		2.57	1.37	cm
PA4942	*hflK*	2.89	1.37	omv
PA0958	*oprD*	2.58	1.37	omv
PA3075		1.80	1.36	u
PA5124	*ntrB*	3.28	1.36	cm
PA0955		2.24	1.36	omv
PA3487	*tle5*	4.64	1.36	p
PA0302	*spuF*	2.66	1.35	omv
PA3958		1.10	1.35	cm
PA5306	*ynbE*	1.80	1.35	u
PA3074		1.70	1.34	cm
PA0545		1.10	1.34	cm
PA1851		0.87	1.33	cm
PA1528	*zipA*	1.60	1.33	omv
PA4319		1.06	1.33	cm
PA5043	*pilN*	2.29	1.32	cm
PA1774	*crfX*	0.90	1.32	u
PA4065		3.19	1.32	cm
PA5248		0.83	1.32	cm
PA0298	*spuB*	2.67	1.31	c
PA5361	*phoR*	1.69	1.31	cm
PA0003	*recF*	4.02	1.31	c
PA1668	*dotU2*	0.60	1.30	c
PA2639	*nuoD*	2.74	1.30	c
PA5041	*pilP*	1.86	1.30	cm
PA5474		0.79	1.29	c
PA1336	*aauS*	1.23	1.29	cm
PA4545	*comL*	3.01	1.29	omv
PA3217	*cyaB*	2.17	1.29	cm
PA3333	*fabH2*	4.55	1.29	c
PA3766		0.77	1.29	cm
PA5012	*waaF*	1.32	1.28	c
PA0715		2.75	1.28	c
PA1460	*motC*	3.19	1.28	cm
PA1273	*cobB*	1.64	1.28	c
PA1158		1.19	1.28	cm
PA3748	*yfjD*	1.28	1.27	cm
PA5064		1.53	1.27	c
PA5239	*rho*	4.47	1.27	c
PA0047		3.24	1.25	u
PA3206	*cpxS*	1.38	1.25	cm
PA1513		1.33	1.25	cm
PA2413	*pvdH*	1.81	1.25	c
PA5291	*betT2*	1.37	1.24	omv
PA4436		2.70	1.24	c
PA5006		1.61	1.24	c
PA3191	*gtrS*	1.52	1.23	cm
PA3640	*dnaE*	3.64	1.23	c
PA2232	*pslB*	4.02	1.23	c
PA3685	*yeaZ*	1.65	1.22	cm

PA3677	*mexJ*	1.20	1.22		cm
PA3704	*wspE*	2.35	1.22		c
PA0838	*btuE*	0.98	1.22		p
PA3728		2.18	1.21		cm
PA1433		1.49	1.21		cm
PA3996	*lis*	1.78	1.20		c
PA0536		1.07	1.20		omv
PA2660		2.91	1.20		c
PA4751	*ftsH*	2.41	1.20		omv
PA1896		2.62	1.19		c
PA4551	*pilV*	2.59	1.19		u
PA2424	*pvdL*	2.68	1.19		u
PA5414		1.43	1.18		omv
PA4003	*pbpA*	1.47	1.18		omv
PA3160	*wzz*	1.78	1.18		omv
PA2955		1.14	1.18		u
PA4953	*motB*	1.77	1.17		cm
PA0080	*tssJ1*	1.80	1.17		omv
PA4941	*hflC*	2.56	1.17		omv
PA5231	*yhiH*	1.49	1.17		cm
PA5568	*yidC*	1.41	1.16		omv
PA0608	*gph*	1.56	1.15		c
PA2999	*nqrA*	3.78	1.15		omv
PA2527	*muxB*	1.92	1.15		cm
PA5560	*atpB*	2.67	1.15		omv
PA2302	*ambE*	4.13	1.14		c
PA5376	*cbcV*	2.64	1.14		cm
PA3138	*uvrB*	1.73	1.13		c
PA2235	*pslE*	2.73	1.13		omv
PA2019	*mexX*	1.97	1.13		cm
PA3491	*rnfC*	3.24	1.13		c
PA0973	*oprL*	3.00	1.12		omv
PA4889		2.08	1.11		u
PA3349		4.56	1.11		c
PA0088	*tssF1*	2.59	1.11		c
PA1806	*fabI*	2.59	1.10		cm
PA4431		4.16	1.09		omv

Table A5 significantly decreased proteins identified in NbdA pulldown

Table A5: Locus tag and name derived from the Pseudomonas Genome DB (Winsor *et al.*, 2016). Highly significant FDR < 0.01, significance level FDR < 0.05.

Locus tag	Name	*p*-value	Fold change	Highly significant	localisation
PA3107	*metZ*	5.02	-1.79	+	c
PA1512; PA5267; PA0263	*hcpA;hcpB;hcpC*	4.93	-1.86	+	-
PA0766	*mucD*	1.93	-1.97	+	p
PA2682	-	4.88	-2.09	+	c
PA4847	*accB*	2.11	-2.24	+	u
PA5142	*hisH1*	4.35	-1.08		c
PA4248	*rplF*	4.25	-1.09		c
PA3647	-	2.46	-1.10		u
PA0329	-	3.66	-1.10		u
PA0579	*rpsU*	2.41	-1.11		c
PA5553	*atpC*	2.73	-1.12		omv
PA2624	*idh*	2.96	-1.13		omv

PA2013	*liuC*	2.58	-1.14		c
PA0972	*tolB*	3.74	-1.14		omv
PA2619	*infA*	2.61	-1.14		c
PA1800	*tig*	2.54	-1.14		omv
PA2553	-	2.96	-1.15		c
PA4402	*argJ*	1.80	-1.15		c
PA4274	*rplK*	2.86	-1.16		omv
PA2950	*fabV*	2.50	-1.16		c
PA3455	-	5.67	-1.16		c
PA2011	*liuE*	1.62	-1.19		c
PA4741	*rpsO*	2.19	-1.19		c
PA3940	-	3.25	-1.21		c
PA1618	*ybdB*	3.91	-1.21		u
PA2667	*mvaU*	2.40	-1.22		c
PA4432	*rpsI*	2.39	-1.23		omv
PA4255	*rpmC*	4.53	-1.23		c
PA2741	*rplT*	2.72	-1.25		omv
PA3742	*rplS*	2.98	-1.26		c
PA4743	*rbfA*	2.68	-1.27		c
PA3257	*algO*	2.97	-1.28		cm
PA4247	*rplR*	3.36	-1.28		c
PA2008	*fahA*	2.07	-1.30		c
PA3266	*capB*	1.14	-1.31		c
PA4315	*mvaT*	1.80	-1.31		c
PA0387	*yggV*	1.51	-1.32		c
PA0856	-	2.10	-1.34		u
PA4695	*ilvH*	2.31	-1.35		c
PA2951	*etfA*	3.35	-1.38		p
PA3745	*rpsP*	2.07	-1.38		c
PA5128	*secB*	1.19	-1.41		omv
PA5348	-	3.01	-1.42		c
PA2513	*antB*	2.74	-1.43		c
PA5197	*rimK*	2.34	-1.44		c
PA0904	*lysC*	4.32	-1.48		c
PA3629	*adhC*	3.78	-1.49		c
PA4565	*proB*	1.68	-1.58		c
PA1400	-	3.71	-1.66		c
PA2891	*atuF*	2.79	-1.67		c
PA1074	*braC*	1.73	-1.71		p
PA3922	-	2.49	-1.76		u
PA1579	-	2.33	-1.85		p

Figure A1 Detection of NbdA

The amino acid sequence of NbdA (new annotation) is shown in **Fig. A1 A**. The majority of peptides identified derived from the GGDEF and the EAL domain. Only one peptide derived from the MHYT domain was identified. Overall, the sequence coverage was 45.8 %. It was also tested if the protein NbdA could be detected when gene expression was under the control of the native promoter. Therefore, a mNeonGreen-His tag was genetically fused to NbdA in the original gene locus (Gerbracht, 2021). In CLSM, the fusion protein NbdA-mNeonGreen-His was detected with clearer foci after a heat shock at 42 °C (Gerbracht, 2021). Therefore, a heat shock was performed on the culture, membranes were isolated and seperated on a SDS-PAGE. NbdA-mNeonGreen-His was not detected in a western blot with His-tag antibodies (**Fig. A1 B**). A positive control however showed a

signal. In addition, a strain carrying Strep-tagged NbdA in the original locus was tested for immunodetection of NbdA. Thus, 100 µg protein from isolated membranes from a stationary phase culture was loaded on each lane. Still, NbdA was not detected (**Fig. A1 C**).

A

```
  1  MDWQGLRFLGESPVDGYVLQNCTYSPSLVALAFLVACLAGYTALDMVERVGNSLSHPRLW
 61  QWIGAFCLGSGIWATHFVAMLAFHAPIALRYDLPITGLSLLIAVAASYLTMYMTARPRFG
121  LLPCLLAACCIGLGIAAMHYTGMAAMRSVATQYYQPSLFALSVLIAIGAAFTALAAVPYL
181  RGRRSARYRYMKLIASLLLAGAIAAMHFTGMAALVLSVPAGTPLELQASADSLRLGWLTG
241  VLASAIAACGIWAAWSEKQRERRLSENSRVNALLNQLDHAHASLRQMARYDSLTGLQNRT
301  AFNEVFVQHLENCRLRGKGLAVMFLDLDHFKRINDSLGHDSGDQLLKIVSERIRSVLRDS
361  DVVARFAGDEFCVLADLTQDHEAHILSQRLMQKMKEPIALDGRTLVMTASVGVSLYPNDG
421  EQCEELLKNAGLALHQSKACGRNNAQFFSRQLLVRATQELQMEEELRQALRDDQLELHYQ
481  PILALADGEVHQLEALVRWRHPTQGLLGPDRFIGLAEANGMIDQLDDWVLRRACRDLRSL
541  HLAGHERLRVAVNCCASNLGRASLVDEVRHALEQAGLAACFLELEVTEDALMYNIDQTIP
601  LLERLRELGVSLSIDDFGTGYSSLAYLRRLPLDALKVDRSFIMDIPASQRDMEIAQAIIA
661  MAQKLHLKVVAEGVETPQQLAFLRENHCELVQGYLFSRPLPLAALEEFLRAYRFDAAPPL
721  RSLNQA
```

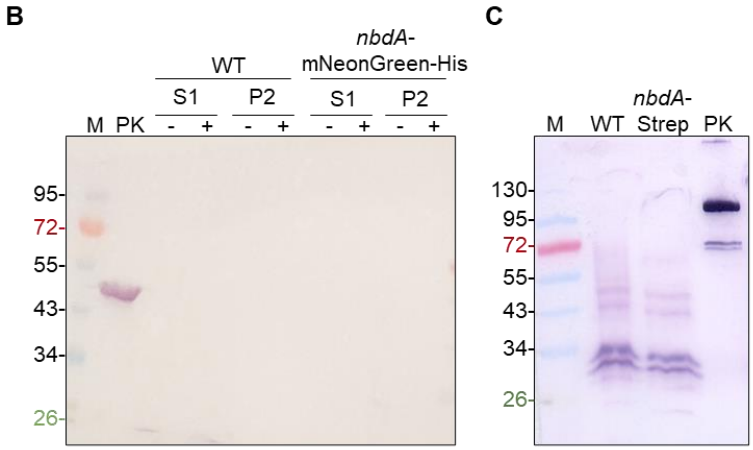

Fig. A1: A: Peptides for NbdA detection in mass spectrometry. Amino acid sequence of NbdA. Regions of detected peptides are highlighted in grey.The MHYT domain is coloured blue, the GGDEF domain green and the EAL domain red. Conserved amino acid motifs are coloured orange. Underlined sequences are predicted transmembrane regions (Galperin *et al.*, 2001). The new annotation of NbdA was used, resulting in a 726 aa protein (Gerbracht, 2021). **B**:**Western blot of a heat shock assay**. M: Colour Prestained Protein Standard, Broad Range (10 - 250 kDa). PK: positive control for the westernblot, PleD (49.6 kDa). WT: PAO1. *nbdA*-nNeonGreen-His: the strain PAO1::*nbdA*-mNeonGreen-His integrated at the native genlocus. S1: protein lysate, supernatant after cell disruption and first centrifugation. P2: membrane fraction, pellet after ultracentrifugation. (-) no heat shock. (+) cultures were heat shocked for 30 min at 42 °C before cell disruption. His-tagged proteins were detected with the 6xHis-H8 antibody (primary) and anti-mouse IgG-AP conjugate (secondary), with a colorimetric reaction. **C**: **Western blot of membrane fraction**. Cultures were grown for 7 h at 37 °C. Cells were harvested and immeadiately shock.frosted in liquid nitrogen. The membranes were isolated, solubilised with detergent and 100 µg protein was loaded in each lane. M: Colour Prestained Protein Standard, Broad Range (10 - 250 kDa). WT: PAO1. *nbdA*-Strep: the strain PAO1::*nbdA*-Strep. PK: positive control, RdmS (115 kDa). Strep-tagged proteins were detected with the Strep-Tacin AP conjugate in a colorimetric reaction.

Identified peptides for NbdA in the proteome of PAO1:

ASLVDEVR; ATQELQMEEELR; ATQELQMEEELRQALR; AYRFDAAPPLR; DMEIAQAIIAMAQK; DSDVVAR; ENHCELVQGYLFSR; EPIALDGR; FAGDEFCVLADLTQDHEAHILSQR; FDAAPPLR; FIGLAEANGMIDQLDDWVLR; FIGLAEANGMIDQLDDWVLRR; GLAVMFLDLDHFK; GLAVMFLDLDHFKR; HPTQGLLGPDR; INDSLGHDSGDQLLK; LPLDALK; LPLDALKVDR; LRELGVSLSIDDFGTGYSSLAYLR; MKEPIALDGR; NAGLALHQSK; NNAQFFSR; PLPLAALEEFLR; RINDSLGHDSGDQLLK; RLPLDALK; RLPLDALKVDR; SFIMDIPASQR; SLHLAGHER; SVLRDSDVVAR; TAFNEVFVQHLENCR; TLVMTASVGVSLYPNDGEQCEELLK; VAVNCCASNLGR; VDRSFIMDIPASQR; VGNSLSHPR; VNALLNQLDHAHASLR; VVAEGVETPQQLAFLR; WRHPTQGLLGPDR; YDSLTGLQNR

Figure A2: Identified proteins in the library

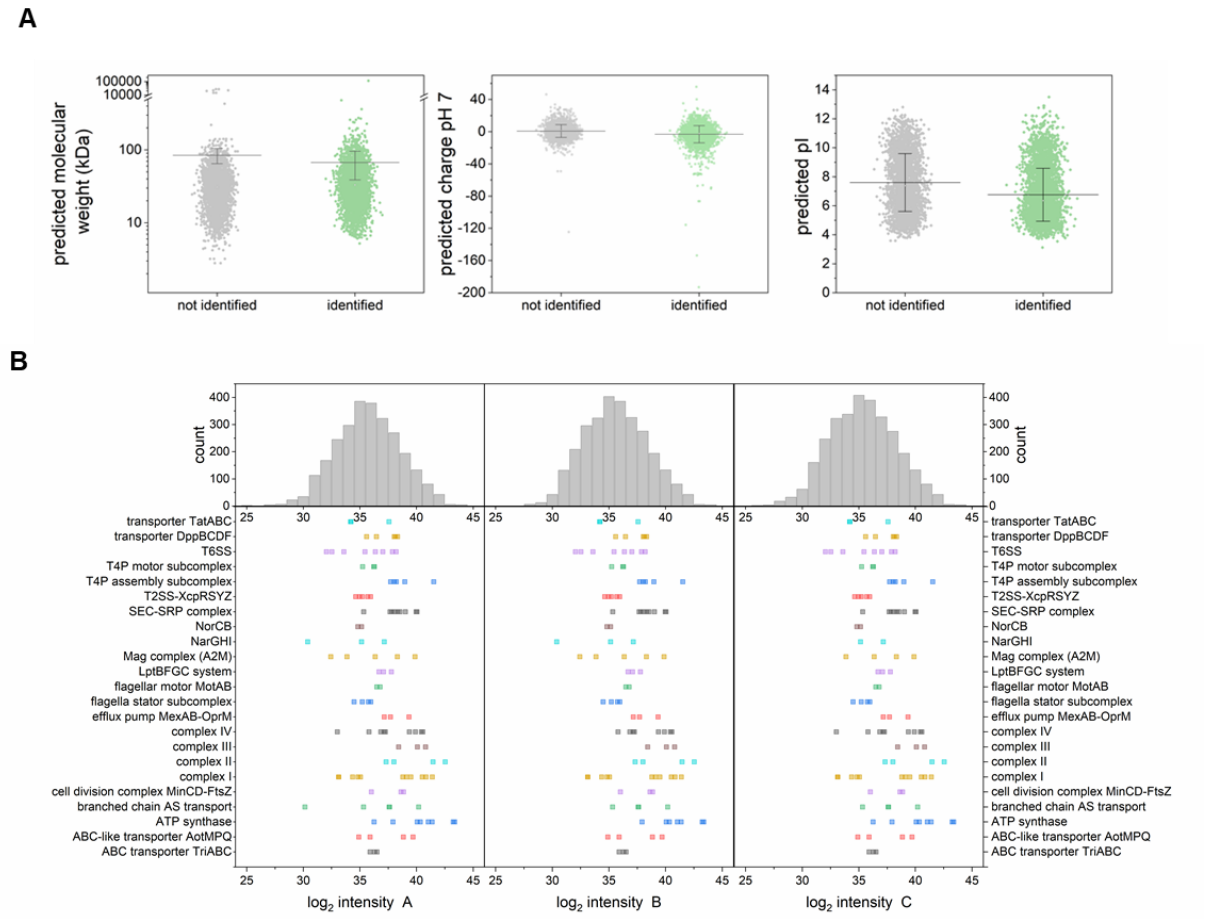

Fig. A2 Identified proteins in the library of membrane proteins from *P. aeruginosa*. **A**: Identified proteins (green) and unidentified proteins (grey) show no difference in prediceted molecular weight (left), predicted charge at pH 7 (middle) or predicted pI (right). Predictions from Pseudomonas genome DB (Winsor *et al.*, 2016). **B**: Intensity measured in MS for proteins belonging to the desribed complexes (lower pannel). Histogram of measured intensity in the three replicates (upper pannel).

Figure A3: MS analysis of the NbdA $_{AGDEF-EAL}$ enzymatic assay (H. Bähre, Hannover)

The samples were prepared as described in section 2.4.15. The HPLC chromatograms of the analysed samples are depicted in section 3.3.4. All samples contained GTP as well as c-di-GMP as substrate. MS analysis was carried out by the H. Bähre lab (ZFA Metabolomics, MHH Hannover). Formation of pGpG was confirmed by mass spectrometry analysis after 2 h and 16 h incubation with manganese ions, as well as after 16 h incubation with magnesium ions.

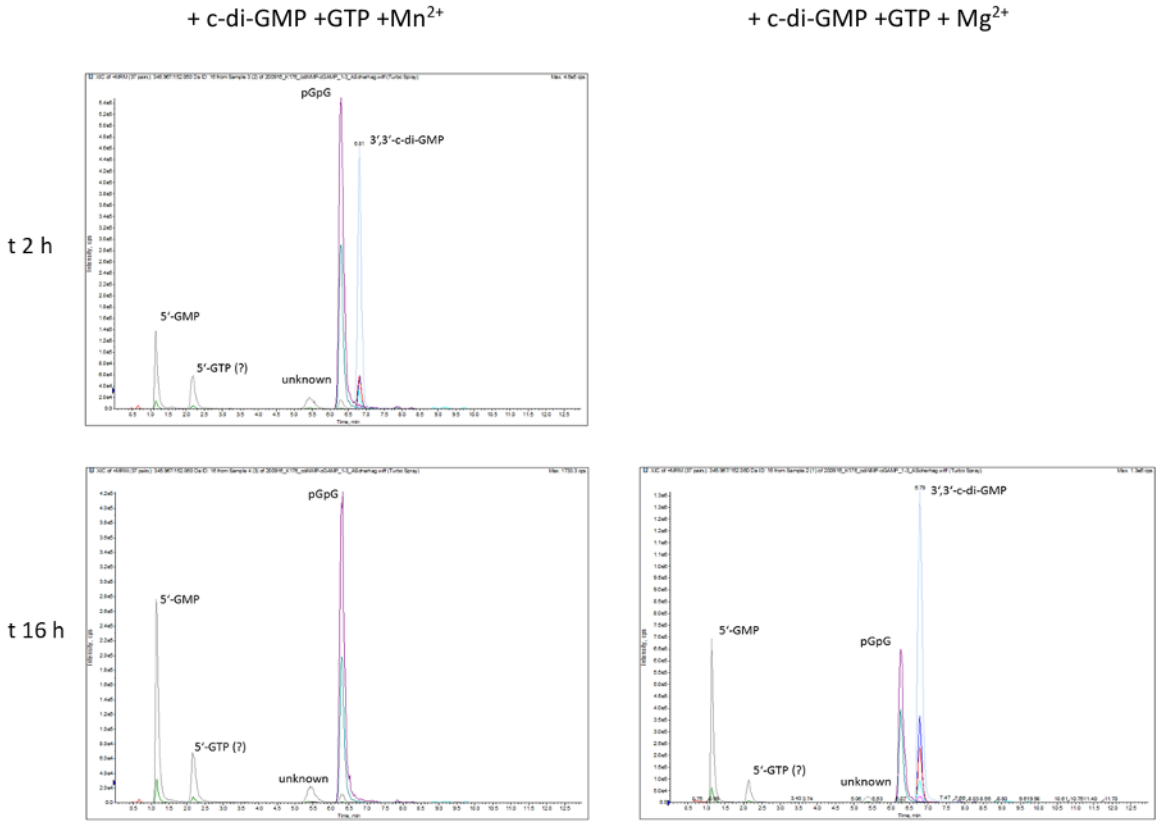

Fig. A3: Mass spectrometry analysis of an enzymatic test oft NbdA$_{cyt}$ with GTP and c-di-GMP. Buffer was supplemented with manganese ions (left pannel) or magnesium ions (right pannel). Reactions were stopped by heat either after 2 h incubation (upper pannel) or after 16 h (lower pannel). Analysis was carried out in the H. Bähre lab (ZFA Metabolomics, MHH Hannover) according to a published protocol (Bähre *et al*., 2017).

Figure A4 Metabolites in WT compared to Δ*nbdA*

Metabolites were measured for the wildtype PAO1 and the *nbdA* deletion mutant from culture extracts. MS measurements for the metabolites was carried out with a TOF mass spectrometer by [redacted]. From the 4 biological replicates, the fold change and *p*-value of the individual buckets (detected metabolites) were depicted in a volcano plot (Fig. A4). There are differences in metabolite levels for some metabolites in WT compared to Δ*nbdA*. From the 4 biological replicates, buckets were annotated with the MetaboScape database. Thereby, 24 Buckets could be identified. Of the identified buckets, one was significantly enriched in the WT

compared to the *nbdA* deletion strain. The identified metabolite is β-Nicotinamide adenine dinucleotide, that was about 3-fold enriched in the WT. However, other components were found to be different in WT and *nbdA* deletion but were not identified. Masses and retention time of these components are listed in Table A6.

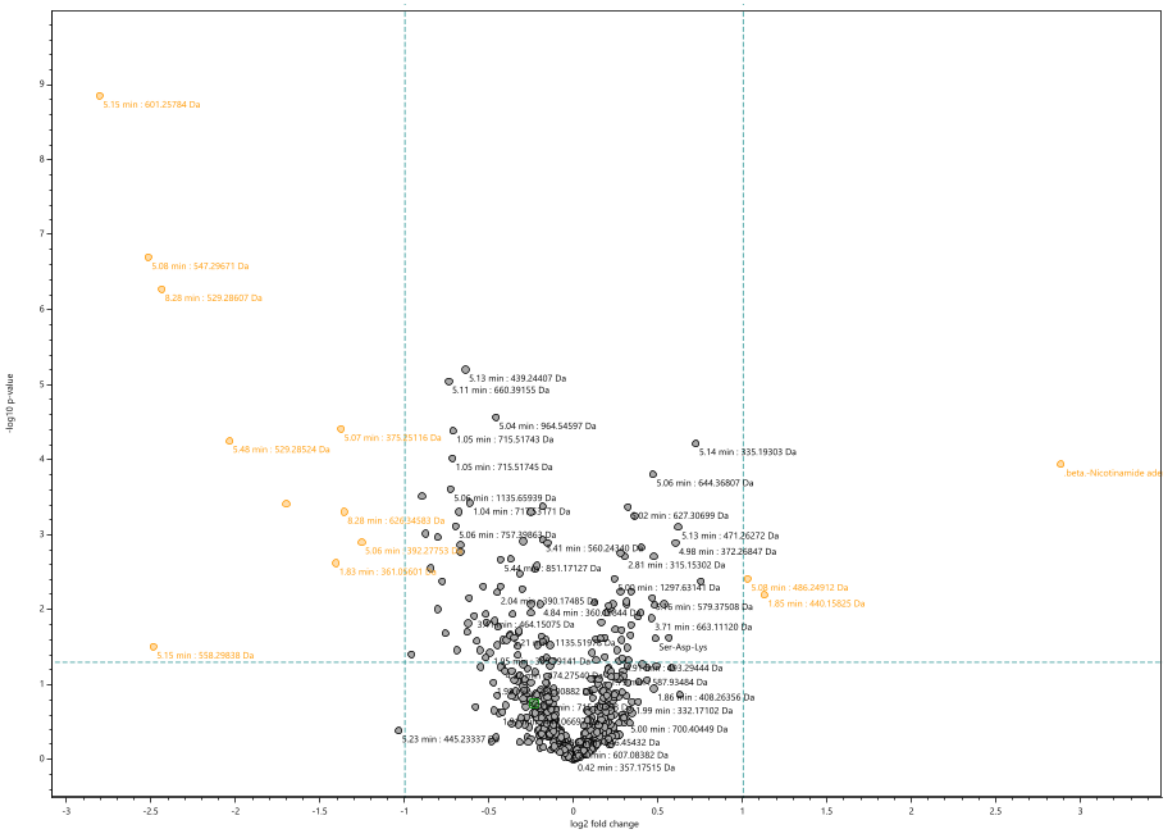

Fig. A4: Volcano plot of metabolite assay ([redacted]). Fold change to the WT is depicted on the x-axis, the *p*-value on the y-axis. Buckets with a positive value are enriched in the WT, with a threshold of > 1 to be considered significant. Buckets with a negative fold change value are enriched in the Δ*nbdA* strain (threshold < -1). Significance level for *p*-values was 0.05. Significant changes in buckets are coloured orange. Masses are noted for the detected but not identified buckets.

Table A6 Metabolites in PAO1 (WT) and Δ*nbdA*. Meatbolites of four replicates for each strain were analysed by mass spectrometry. RT: retention time. FC: fold change. Data obtained from collaboration with [redacted].

RT (min)	Mass (Da).	$\log_2$ FC	- $\log_{10}$ *p*-value	Identified as
Enriched in WT				
4.11	663.11287	2.89	3.97	β-Nicotinamide adenine dinucleotide ($C_{21}H_{27}N_7O_{14}P_2$)
9.08	486.24912	1.01	2.4	-
1.85	440.15825	1.11	2.2	-
Enriched in Δ*nbdA*				
5.15	601.12784	-2.8	8.91	-
5.08	547.29671	-2.52	6.7	-
8.28	529.28607	-2.45	6.28	-
5.48	529.28524	-2.08	4.22	-

5.07	375.25116	-1.39	4.4	-
5.15	558.29838	-2.49	1.5	-
5.06	392.27753	-1.25	2.9	-
1.83	361.06601	-1.4	2.4	-
compond identified, no significant change				
5.08	297.0871	-0.23	0.84	5'-Methylthioadenosine
4.16	347.0621	0.19	0.18	Adenosine 2'-monophosphate
2.76	427.029	-0.25	0.18	Adenosine 3',5'-diphosphate
4.6	347.0621	0.69	0.58	Adenosine monophosphate
4.96	347.0617	0.12	0.16	Adenosine monophosphate
5.02	525.2519	0.05	0.23	Glu Ile Ala His Gly
2.41	360.1628	-0.12	0.17	Glu Val Asn
2.01	257.0997	0.26	0.40	Glycerophosphocholine
2.68	363.0569	0.07	0.22	Guanosine 5'-monophosphate
4.96	339.1888	-0.48	0.42	His Ala Ile
4.95	396.2113	-0.12	0.17	His Gln Leu
4.92	397.197	0.20	1.00	His Glu Leu
4.93	325.1723	0.06	0.24	His Gly Leu
4.93	316.208	-0.13	0.24	Ile Lys Gly
4.89	330.2243	0.10	0.22	Ile-Ala-Lys
4.77	388.2331	0.04	0.50	Leu Lys Glu
5.14	422.1952	0.14	0.34	Phe Ala Trp
5.19	365.2053	-0.27	0.64	Pro His Leu
2.77	385.2321	0.02	0.25	PyroGlu-Lys-Lys
1.9	348.1625	0.55	0.59	Ser-Asp-Lys
4.92	424.0368	-0.11	0.30	Thiamine pyrophosphate
2.96	309.1302	-0.01	0.12	Tyr-Gln
5.03	374.2169	-0.33	0.33	Val Lys Glu

Figure A5: Growth on plates of a NbdA overpruducing strain

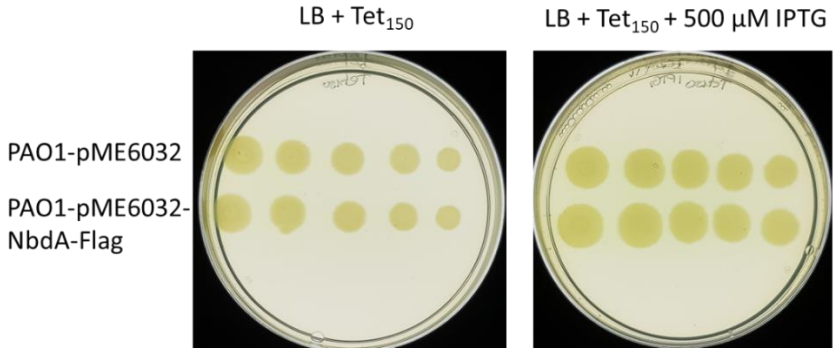

Fig. A5: Growth on plates of a NbdA overexpression in pME6032. The strains PAO1 carrying pASCA07 (pME6032-NbdA-Flag) or the empty vector (pME6032) were testred for growth on plates. Dilution series of 10^0 to 10^{-4} was pipetted in freh LB medium supplemented with tetracyline. 3 µl of each dilution were dropped on LB agar plates containing tetracycline (left) or tetracycline and IPTG (right). Plates were incubated for 24 hours at 37 °C. The experiment was carried out in biological duplicates.

Figure A6: Cell morphology of a NbdA overpruducing strain

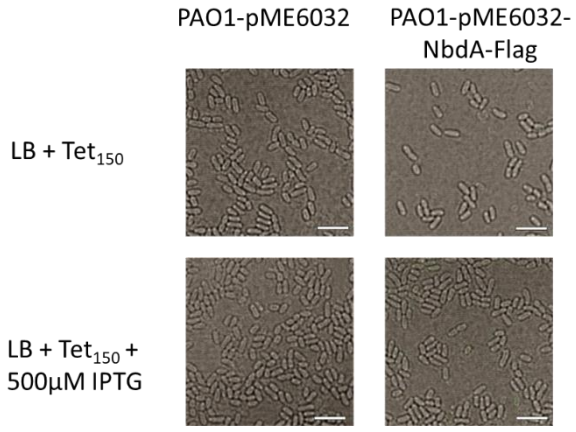

Fig. A6: Cell morphology of a strain overproducing NbdA-Flag encoded on pME6032. The strains PAO1 carrying pASC07 (pME6032-NbdA-Flag) or the empty vector (pME6032) were testred for cell morphology. Cultures were set to an OD_{600} of 0.05 in 200 µl LB supplemented with tetracycline. 96-well plates were incubated for 24 hours at 37 °C shaking in a Tecan plate reader. Cells were immobilised on an agarose pad. Images were taken in a Zeiss LSM 880 by transmitted light microscopy. Scale bar 5 µm.

Figure A7 Properties of Fluorophores

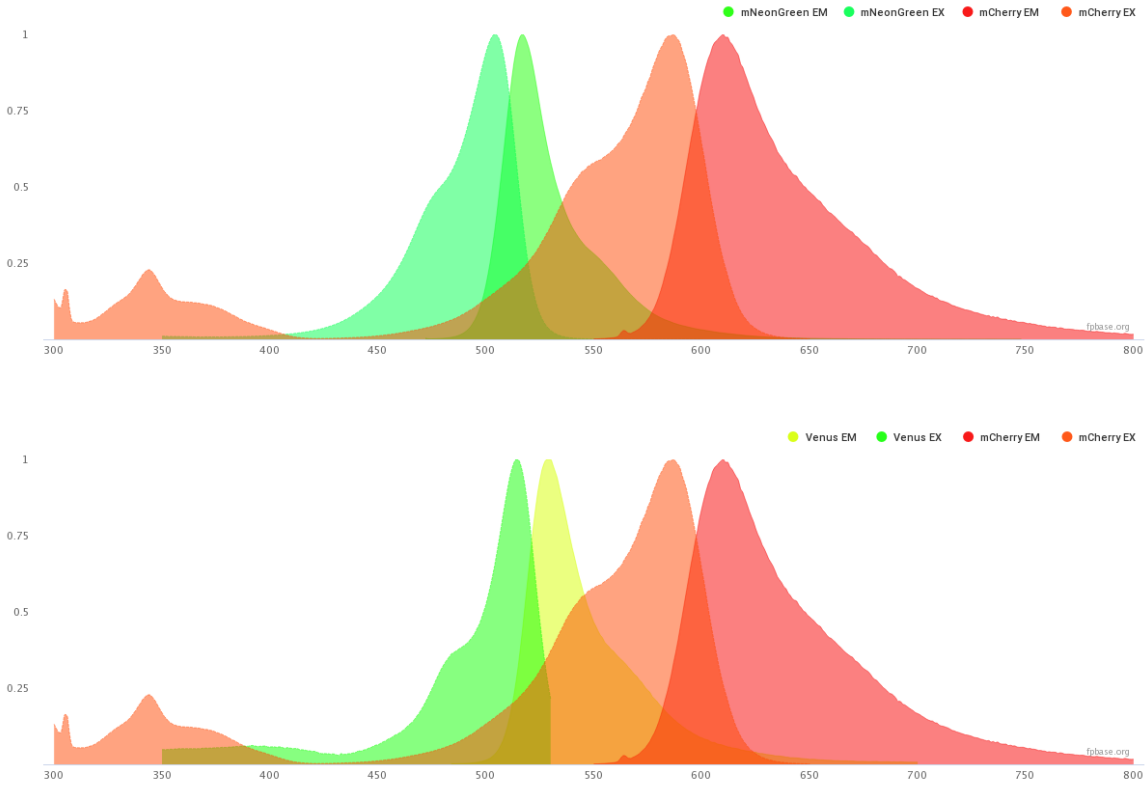

Figure A7 Properties of the flourophores mNeonGreen and Venus with mCherry. Excitation and Emission spectra of mNeonGreen and mCherry (upper pannel) and Venus with mCherry (lower pannel). Spectra were obtained from FPbase.

Figure A8: Protein marker comparison

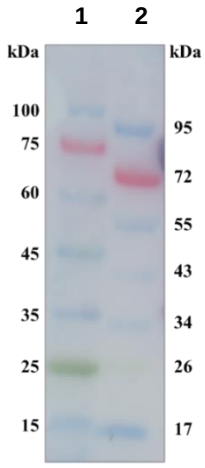

Fig. A2: Protein marker comparison on a 10 % SDS-PAGE. 1: Prestained protein marker by proteintech, 2: Colour Prestained Protein Standard broad range by New England Biolabs.

FORMALIA

Curriculum vitae

Anna Scherhag

Berufserfahrung

10/2019 – 10/2023	Wissenschaftlicher Mitarbeiter mit Ziel der Promotion in der Abteilung Mikrobiologie von Nicole Frankenberg-Dinkel, Rheinland-Pfälzische Technische Universität Kaiserslautern-Landau (RPTU)

Studium und schulische Laufbahn

10/2017 - 09/2019	Studium „Biology“ an der Technischen Universität Kaiserslautern, Vertiefungsrichtung: „Microbial and Plant Biotechnology“ Abschluss: Master of Science (Note: 1,1)
10/2013 - 09/2017	Studium „Biowissenschaften“ an der Technischen Universität Kaiserslautern Abschluss: Bachelor of Science (Note: 1,7)
2004 - 2013	Kurfürst-Balduin-Gymnasium Münstermaifeld Abitur (Note: 2,5)

Konferenzteilnahmen

02/2023	BLAST XVII Meeting (Charlotte NC, online)	
05/2022	SPP 1879 International Symposium 2022 (Berlin)	Poster
02/2022	VAAM-Jahrestagung (Düsseldorf, online)	Poster
05/2021	SPP 1879 Progress Meeting 2021 (online)	Vortrag
09/2020	Biofilms 9 (Karlsruhe, online)	Poster
02/2020	SPP 1879 Progress Meeting 2020 (Göttingen)	Poster
10/2019	Rheinland-Pfalz Symposium (Kaiserslautern)	Vortrag
03/2019	VAAM-Jahrestagung (Mainz)	

Publikation

Scherhag, A., Räschle, M., Unbehend, N., Venn, B., Glück, D., Mühlhaus, T., Keller, S., Pérez Patallo, E., Zehner, S., Frankenberg-Dinkel, N. (2023). „Characterization of a soluble library of the *Pseudomonas aeruginosa* PAO1 membrane proteome with emphasis on c-di-GMP turnover enzymes” *microlife* 4, uqad028.
DOI: https://doi.org/10.1093/femsml/uqad028

Darlegung des Eigenanteils

Name: Anna Scherhag

Titel: Investigation of membrane proteins involved in c di GMP signalling in *P. aeruginosa* with focus on the phosphodiesterase NbdA

Wie in 2.4.14 beschrieben, wurde die massenspektroskopische Identifizierung und Quantifizierung der Proteine von Markus Räschle (AG Storchovà, RPTU) durchgeführt. Dies umfasst auch die Auswertung der MS Daten in MaxQuant und Perseus (Protein Identifizierung, IBAQ-Werte, Berechnung von FC und *p*-value beim Pulldown, cf. 2.7.3). Probenvorbereitung, tryptischer Verdau und Stage tipping wurde in Absprache mit Markus Räschle von mir durchgeführt.
Die in Abbildung 3.17 (Kaptiel 3.3.2), 3.19 (Kapitel 3.3.3), [redacted] gezeigten Daten wurden in Zusammenarbeit mit Hannah Becker und Simone Stegmüller (AG Richling, RPTU) angefertigt. Wie in 2.5.3 beschrieben, wurde die Messung der Nukleotidgehalte lyophilisierter Extrakte mittels Massenspektroskopie von Hannah Becker durchgeführt. Probenvorbereitung, statistische Auswertung und Interpretation der Daten erfolgte im Rahmen dieser Arbeit (siehe auch 2.5.2 und 2.7.1).
Die Abbildung 3.21 C und D in Kapitel 3.3.4, sowie Abbildung A3 enthält Daten, die in Zusammenarbeit mit Heike Bähre (ZFA Metabolomics, Medizinische Hochschule Hannover) gemessen wurden. Probenvorbereitung und Darstellung der Daten erfolgte im Rahmen dieser Arbeit.
Die in Abbildung 3.25 in Kapitel 3.3.7 gezeigten Aufnahmen wurden von Jürgen Seehase (AG Ziegler, RPTU) mittels AFM angefertigt (beschrieben in 2.6.6).
Teile dieser Arbeit wurden bereits im Artikel „Characterization of a soluble library of the *Pseudomonas aeruginosa* PAO1 membrane proteome with emphasis on c-di-GMP turnover enzymes" im Journal *microlife*, Volume 4 (2023) veröffentlicht. Eine Aufstellung der Anteile an der Publikation ist im Kapitel „Beiträge zur Publikation" zu finden.
Die vorliegende Einschätzung über die erbrachte Leistung von Dritten wurde mit den genannten Personen einvernehmlich abgestimmt.

13.02.2024	Anna Scherhag	13.02.2024	Susanne Zehner
(Datum, Unterschrift Doktorand/in)		(Datum, Unterschrift Betreuer/in)	

Darlegung aller benutzten Hilfsmittel und Hilfestellungen

Name: Anna Scherhag

Titel: Investigation of membrane proteins involved in c di GMP signalling in *P. aeruginosa* with focus on the phosphodiesterase NbdA

Die Analyse der Daten erfolgte mit den in Kapitel 2 angegeben Hilfsmitteln und Software. Die Arbeit wurde in Microsoft Word (Version 2309) geschrieben. Referenzen und Literaturverzeichnis wurden mit EndNote eingefügt. Außerdem wurde LEOs Wörterbücher (www.leo.org), DeepL Übersetzer (www.deepl.com/de/translator) und DeepL Write (www.deepl.com/write) benutzt, um den Text sprachlich zu verbessern. Die Arbeit wurde von Susanne Zehner (RPTU) Korrektur gelesen.

13.02.2024 Anna Scherhag

_____

(Datum, Unterschrift Doktorand/in)

Erklärungen lt. § 6 (4) der Promotionsordnung des Fachbereichs Biologie vom 27.11.2018

Ich erkläre wahrheitsgemäß, dass ich die eingereichte Dissertation selbst angefertigt und alle für die Arbeit benutzten Hilfsmittel und Hilfestellungen in der Arbeit angegeben habe. Die Dissertation oder Teile hiervon habe ich bisher nicht als Prüfungsarbeit für eine staatliche oder andere wissenschaftliche Prüfung eingereicht. Ebenso habe ich die gleiche oder eine andere Abhandlung nicht bei einem anderen Fachbereich oder einer anderen Universität als Dissertation eingereicht.

Kaiserslautern, 13.02.2024 Anna Scherhag

_____

(Ort, Datum, Unterschrift)